

University of Texas at Arlington

MavMatrix

Chemistry & Biochemistry Dissertations

Department of Chemistry and Biochemistry

2023

ANALYSIS OF ISOTOPIC ISOMERS BY GAS CHROMATOGRAPHY AND MOLECULAR ROTATIONAL RESONANCE SPECTROSCOPY AND ENANTIOSELECTIVE METHOD DEVELOPMENT BY LIQUID CHROMATOGRAPHY

Saba Aslani

Follow this and additional works at: https://mavmatrix.uta.edu/chemistry_dissertations

 Part of the [Chemistry Commons](#)

Recommended Citation

Aslani, Saba, "ANALYSIS OF ISOTOPIC ISOMERS BY GAS CHROMATOGRAPHY AND MOLECULAR ROTATIONAL RESONANCE SPECTROSCOPY AND ENANTIOSELECTIVE METHOD DEVELOPMENT BY LIQUID CHROMATOGRAPHY" (2023). *Chemistry & Biochemistry Dissertations*. 219.
https://mavmatrix.uta.edu/chemistry_dissertations/219

This Dissertation is brought to you for free and open access by the Department of Chemistry and Biochemistry at MavMatrix. It has been accepted for inclusion in Chemistry & Biochemistry Dissertations by an authorized administrator of MavMatrix. For more information, please contact leah.mccurdy@uta.edu, erica.rousseau@uta.edu, vanessa.garrett@uta.edu.

ANALYSIS OF ISOTOPIC ISOMERS BY GAS CHROMATOGRAPHY AND MOLECULAR
ROTATIONAL RESONANCE SPECTROSCOPY AND ENANTIOSELECTIVE METHOD
DEVELOPMENT BY LIQUID CHROMATOGRAPHY

by

Saba Aslani

DISSERTATION

Submitted in partial fulfillment of the requirements

for the degree of Doctor of Philosophy at

The University of Texas at Arlington

May 2023

Arlington, Texas

Copyright © by Saba Aslani 2023

All Rights Reserved



*I dedicate this dissertation to my parents, Payam Aslani and Fatemeh Bahrami,
for their endless love and support*

Acknowledgements

First, I would like to express my endless gratitude to my advisor, Dr. Daniel W. Armstrong for his guidance during my graduate program. He always motivated me to think outside the box, have innovative ideas, and work smart and hard. I consider myself lucky to be a part of his team and pursue my Ph.D. under his supervision.

I would like to thank my graduate committee members: Dr. Morteza Khaledi, Dr. Carl Lovely, and Dr. Robin Macaluso for their valuable advice, guidance, and time. Also, I thank Dr. Justin Neill and Alexander Mikhonin (BrightSpec Inc.), and Len Sidisky (MilliporeSigma), for their collaboration over the course of my research. I thank Dr. Farooq Wahab for his priceless guidance throughout my research. I genuinely appreciate Dr. JT Lee, for being my mentor during my internship at AZYP. I acknowledge the invaluable assistance from my group members: Dr. Mohsen Talebi, Dr. Abiud Portillo, Dr. Nimisha Thakur, Arzoo Patel, Umang Dhahubhadel, Joshua Putman, Troy Handlovic, Sam Sung, Beth Readell, Dr. Alain Berthod, and Dr. John Lang. I greatly appreciate the assistance of all faculty and staff in the Department of Chemistry and Biochemistry at the University of Texas at Arlington, especially, Anne Ellis and Dr. Roy McDougald for their invaluable help. I deeply thank my parents, Payam and Fatemeh for their unwavering support and encouragement in my life. I am deeply grateful to my friends, Sogand, Negar, Melika, Rony, Saint, Masrour, Soheil, and Mehdi for supporting me in tough times. Finally, I would like to thank Randy, for his boundless love and support.

May 2023

Abstract

ANALYSIS OF ISOTOPIC ISOMERS BY GAS CHROMATOGRAPHY AND MOLECULAR ROTATIONAL RESONANCE SPECTROSCOPY AND ENANTIOSELECTIVE METHOD DEVELOPMENT BY LIQUID CHROMATOGRAPHY

Saba Aslani, PhD

The University of Texas at Arlington, 2023

Supervising Professor: Daniel W. Armstrong

This dissertation focuses on developing improved methods and a better understanding of gas and liquid chromatographic separation of isotopic isomers and enantiomers. The second and third chapters of this thesis discuss analytical determination of isotopic isomers using gas chromatography. Deuterated compounds have found applications in many fields. They are used in drug discovery due to increased stability and bioavailability and reduced toxicity of the deuterated drug molecules. Also, deuterated compounds are used to investigate reaction mechanisms and rate determining steps. One of the methods of synthesizing deuterated compounds is starting from lower molecular weight deuterated building blocks. Therefore, analysis and separation of these small molecular weight analytes is important. Chapter two is the most comprehensive analysis in separation of deuterated compounds using gas chromatography yet reported. It provides the optimum conditions for separation of 46 pairs of deuterated isotopologues after examination of 12 stationary phases of different polarities. Chapter three describes the factors that affect chromatographic retention and isotope effects since the mass difference between deuterated and protiated analytes is not the only contributing factor for such GC separations. The position of

deuterium atom also plays a role in chromatographic isotope effects mainly through inductive and resonance effects. The fourth chapter describes the second-generation (targeted) molecular rotational resonance (MRR) spectroscopy detector for gas chromatography (GC) for increased sensitivity and as the ultimate detector for structural determination and specificity among other GC detectors. Another improved feature of the targeted GC-MRR instrument, was wider molecular weight range and ability to analyze larger molecules (molecular weight range of 46–244 Da). These improvements were possible by incorporation of Fabry–Pérot cavity and supersonic jet which provided immensely efficient cooling. As a result, the limits of detection of targeted MRR detector could be close to those of the classic GC thermal conductivity detector (TCD).

Chapter five investigates enantioselective method development in HPLC and investigates the effect of trace amounts of water in normal phase liquid chromatography (NPLC) enantioselective separations. The presence of adventitious water in NPLC mobile phases has been frowned upon, due to irreproducibility in such analyses. We investigated this phenomenon by adding controlled amounts of water to various NPLC mobile phases. A large group of chiral pharmaceutical compounds were analyzed and investigated. The presence of water resulted in improved efficiency and resolution in most cases and reduced retention for all separations. Some might attribute these results to the polarity of the mobile phase. However, upon more thoroughly investigating the “water effect”, more factors were found to contribute.

Chapter six introduces a new gas chromatography stationary phase which is made from dispersion of metal organic frameworks in ionic liquids. This is the first gas-liquid chromatography stationary phase that was able to provide sufficient retention for permanent gases like CO₂, propane, and butane to separate them from air. Moreover, unique selectivities were observed for different mixtures of alkanes, alcohols, ethers, and ketones.

Table of Contents

Acknowledgements.....	iv
Abstract.....	v
List of Illustrations.....	xi
List of Tables.....	xiv
Chapter 1 Introduction	
1.1 Analysis of isotopologues and isotopomers with GC.....	1
1.1.2 Significance of analysis of low molecular weight deuterated isotopologues.....	2
1.1.3 Normal and inverse isotope effects in GC.....	2
1.2 Gas chromatography- Molecular Rotational Resonance Spectroscopy (GC-MRR).....	3
1.2.1 Broadband GCMRR.....	5
1.2.2 Applications of broadband GC-MRR.....	6
1.2.3 Targeted GC- MRR.....	8
1.3 Ionic liquids and Metal Organic Frameworks in Gas Chromatography.....	9
1.3.1 Ionic liquids as GC stationary phases	9
1.3.2 Metal organic frameworks (MOFs) in GC	12
1.4 Enantioselective method development for HPLC.....	13
1.4.1 Effect of presence of water in enantioseparations	14
1.5 Organization of Dissertation	14
Chapter 2 Evaluation of gas chromatography for the separation of a broad range of isotopic compounds.....	
2.1 Abstract.....	16
2.2 Introduction.....	16
2.3 Materials and methods.....	19
2.3.1 Chemicals and reagents.....	19
2.3.2 GC Columns	19
2.3.3 Derivatization experiments.....	19
2.3.4 Experimental.....	20
2.3.5 Apparatus and instrument.....	20

2.4 Results and discussion.....	20
2.4.1 Stationary phase selection.....	20
2.4.2 Separations of non-deuterated, partially deuterated, and deuterated small molecules (≤170 amu molecular weight)	23
2.4.3 Separation of deuterated drug molecules.....	31
2.4.4 Isotope effects.....	34
2.5 Conclusions.....	37
2.6 Supporting information.....	39
Chapter 3 Effect of position of deuterium substitution on gas chromatographic retention.....	42
3.1 Abstract.....	42
3.2 Introduction.....	43
3.3 Experimental	45
3.3.1 Reagents and materials	45
3.3.2 Derivatization experiments	48
3.3.3 Methods.....	48
3.4 Results and discussion.....	49
3.4.1 Isotope effects.....	49
3.4.2 Effect of the location of deuterium atoms on isotope effects.....	51
3.4.3 Additivity of chromatographic isotope effects.....	54
3.4.4 Factors that affect deuterated analyte-stationary phase interactions.....	58
3.4.5 van't Hoff studies.....	62
3.5 Conclusions.....	64
3.6 Supporting information.....	65
Chapter 4 Enhancing Sensitivity for High Selectivity Gas Chromatography Molecular Rotational Resonance Spectroscopy.....	83
4.1 Abstract	83
4.2 Introduction	84
4.3 Experimental Section	87
4.3.1 Materials.....	87

4.3.2 Microwave Library Spectrum Measurements.....	88
4.3.3 Millimeter-Wave GC-MRR.....	88
4.3.4 Microwave GC-MRR with Supersonic Jet Expansion and Fabry.....	
Perot Cavity (Targeted band GC-MRR)	89
4.3.5 Estimation of Limits of Detection.....	90
4.4 Results & Discussion.....	91
4.4.1 Incorporation of Supersonic Jet Expansion Unit in GC-MRR.....	93
4.4.2 Fabry-Perot Microwave Cavity in Targeted Mode GC-MRR.....	94
4.4.3 Performance Comparison of GC-TCD, Millimeter Wave GC-MRR, and Targeted Band GC-MRR.....	96
4.4.4 Synergistic Effects of Different Carrier and Supersonic Jet Expansion Gases.....	97
4.4.5 GC-MRR of Isomers and Isotopologues.	102
4.5 Conclusions.....	103
4.6 Supporting information.....	105

Chapter 5

A metal organic framework - ionic liquid pseudophase system as a gas chromatography stationary phase

5.1

Abstract.....116

5.2 Introduction.....116

5.3 Materials and Methods.....119

5.3.1 Chemicals and reagents119

5.3.2 GC columns120

5.3.3 Experimental120

5.3.4 Apparatus and instrument120

5.3.5 Synthesis of Ionic liquids.....121

5.3.6 Determination of Behaviors of MOFs in ILs.....122

5.3.7 Partial Specific Volume.....122

5.4 Results and Discussion.....122

5.4.1 The Three Phase Model Theory and Mechanism.....131

5.4.2 Theory.....	133
5.5 Conclusions.....	136
5.7 Supporting information	137

Chapter 6

An examination of the effects of water on normal phase enantioseparations

6.1 Abstract.....	140
6.2 Introduction.....	141
6.3 Material and methods.....	143
6.3.1. Chemicals.....	143
6.3.2 Chromatography.....	143
6.3.3 Spectroscopic measurements	145
6.4 Results and discussion.....	145
6.4.1 The water-hexane-ethanol ternary system.....	145
6.4.2 Water effect on normal phase chiral separations.....	147
6.4.3 Water in NPLC makes enantioseparation possible.....	146
6.4.4 Water effects on normal phase solvent polarity studied by solvatochromism.....	150
6.4.5 How much is water hydrating the stationary phase?	152
6.4.6 Thermodynamic study of water's influence on solute-stationary phase interactions.....	154
6.4.7 Kinetic study of water influence on solute-stationary phase interaction.....	161
6.4.8 Water effects on adsorption isotherms.....	165
6.5 Conclusions	168

Chapter 7

Conclusions	169
Appendix A Publication information.....	170
Appendix B Rights and Permissions.....	171
References.....	175
Biographical information	193

List of illustrations

Figure 1.1 Schematic of the first GC-hyphenated MRR instrument (broadband)	5
Figure 1.2 a) Total GC-MRR chromatogram of five common organic molecules. b) The 24 extracted molecule chromatograms.....	7
Figure 2.1: Columns showing the best chromatographic performance according to the polarity of the compounds.....	28
Figure 2.2 Separations of a) Tetrachloroethane H2 & D2 b) DMF-H7 & D1 c) methamphetamine-H15 & D5 d) L-leucine-5,5,5-H13 and D3.....	28
Figure 2.3. Percent isotope effects on various columns used in this study.....	35
Figure 2.S1: Chemical structures of the solvents analyzed in the study.....	39
Figure 2.S2: Chemical structures of the drugs analyzed in the study.....	40
Figure 3.1 Chromatograms of trifluoroacetylated amphetamine isotopologues.....	51
Figure 3.2 Chromatographic isotope effect, CIE (k_D-k_H for normal CIE and k_D-k_H for inverse CIE) vs. temperature plots for trifluoroacetylated amphetamine isotopologues.....	53
Figure 3.3. CIE vs T plots of benzyl alcohol isotopologues on A) IL-111i stationary phase and B) PDMS-5 stationary phase.....	55
Figure 3.4 The general trend relation between chromatographic isotope effect (CIE) and retention for a pair of isotopomer.....	58
Figure 3.S1 Structure of the analytes.....	65
Figure 3.S2 Isotope effect vs T plots-benzyl alcohol.....	66
Figure 3.S3 Isotope effect vs T-methamphetamine.....	67
Figure 3.S4 Isotope effect vs T plots-toluene.....	68

Figure 3.S5 Isotope effect vs T plots-DMF.....	69
Figure 3.S6 Additivity plots-methamphetamine.....	70
Figure 3.S7 Additivity plots-methamphetamine.....	71
Figure 3.S8 Additivity plots-amphetamine.....	72
Figure 4.1. Depiction of a 3D coordinate system of an asymmetric rotor, 2-chloropyridine, with the origin at the center of mass of the molecule.....	86
Figure 4.2. Simulation of rotational cooling effect on the microwave rotational resonance (MRR) spectra.....	92
Figure 4.3. The interfacing of gas chromatography with a microwave Fabry-Perot cavity using a supersonic jet expansion system (GC-MRR).....	94
Figure 4.4 Effect of various gases in direct MRR and GC-MRR.....	99
Figure 4.5. Illustration of the concept of a (a) total molecular chromatogram and (b) an extracted molecular chromatogram of various deuterated and structural isomers.....	103
Figure 4.S1 Carrier and makeup gas effects on GC-MRR: N ₂ (GC) + Ne (MRR) signal enhancement near the corresponding limits of quantitation (LOQ) for three chemicals.....	112
Figure 4.S2 MRR enables unambiguous discrimination between all listed bromonitrobenzene isomers and isotopologues.	113
Figure 4.S3 Example of MRR specificity over mass spectrometry.....	114
Figure 4.S7 MRR spectra fit utilized in this work. Example of 1-bromo-4-nitrobenzene.....	115
Figure 5.1 Digital microscopic picture of metal ZIF-8 (brown spots) dispersed in DMIM-C9.....	126
Figure 5.2. Chromatograms of separation of alkane and alcohol compounds on two stationary phases.....	127
Figure 5.3. Chromatograms of separation of Rohrschneider compounds and ether compounds on two stationary phases.....	128

Figure 5.4. Chromatograms showing separations of ketone and alkane compounds on two stationary phases.....	129
Figure 5.5. Separation of CO ₂ from air on ZIF-8 DMIMC9 NTf ₂ stationary phase.....	130
Figure 5.6. Separation of butane from air on ZIF-8 DMIMC9 NTf ₂ stationary phase.	131
Figure 5.7. Three-phase model showing the partitioning equilibria of an analyte (red ball) in the IL + MOF system.....	132
Figure 5.8. Plots of equation 6.....	135
Figure 6.1 Ternary phase diagram of the hexane-water-ethanol system at 20°C.	146
Figure 6.2 Effect of water on the separation of three chiral cathinones.	149
Figure 6.3 Water adsorption by the macrocyclic glycopeptide SPP stationary phases exposed to the heptane/ethanol 80:20 v/v solvent containing the indicated amount of water.	153
Figure 6.4 Variation of the water effect expressed in terms of Gibbs energy variation.....	156
Figure 6.5 Effect of water addition to hexane/ethanol 80:20 v/v mobile phase.....	157
Figure 6.6 Evolution of H, the height equivalent to a theoretical plate, with the mobile phase flow rate.	162
Figure 6.7 Six possible solute-stationary phase exchanges as described by Horvath and Lin.....	164
Figure 6.8 Effect of water addition in semi-preparative conditions.	167

List of Tables

Table 1.1 Chemical structures of commercial ionic liquid stationary phases.....	11
Table 2.1 Columns used in the study.....	22
Table 2.2: The resolution of 47 isotopologue pairs on 12 different columns.....	24
Table 2.3 List of the best separations (highest resolution and best peak shapes) achieved for 47 pairs of isotopologues.	32
Table 2.S1 Effect of % of phenyl in the stationary phase on retention times of benzyl alcohol-D5 and benzyl alcohol-D2.	41
Table 2.S2 Effect of % of phenyl in the stationary phase on chromatographic parameters of separation of phenol and phenol-D5.....	41
Table 3.1 List of compounds used in this study.....	46
Table 3.2 Retention orders and ratios of chromatographic isotope effects for each stationary phase.	56
Table 3.3 Comparison of magnitudes of isotope effects on PDMS-5 and IL-111i stationary phases.	57
Table 3.4 van't Hoff parameters calculated for five groups of isotopologues.	63
Table 3.S1 Temperature settings.....	65
Table 3.S2 Inverse isotope effect of amphetamine isotopologues on PDMS5.....	73
Table 3.S3 Inverse isotope effect of methamphetamine isotopologues on PDMS5.....	73
Table 3.S4 Inverse isotope effect of benzyl alcohol isotopologues on PDMS 5.....	74
Table 3.S5 Inverse isotope effect of toluene isotopologues on PDMS 5.....	75
Table 3.S6 Inverse isotope effect of N,N-dimethylformamide isotopologues on PDMS 5.....	76
Table 3.S7 Normal isotope effect of amphetamine isotopologues on IL-111i.....	78

Table 3.S8 Normal isotope effect of methamphetamine isotopologues on IL-111i.....	79
Table 3.9 Normal isotope effect of benzyl alcohol isotopologues on IL-111i.....	80
Table 3.10 Normal isotope effect of toluene isotopologues on IL-111i.....	81
Table 3.11 Normal isotope effect of N, N-dimethylformamide isotopologues on IL-111i.....	82
Table 4.1 A comparison of detection limits.....	100
Table 4.S1 Summary of GC-TCD methods.....	105
Table 4.S2 Millimeter-wave room temperature broadband GC-MRR conditions.....	108
Table 5.1. List of ionic liquids and MOFs with their behavior indicated.....	122
Table 5.S1. Chromatographic parameters for IL and IL + MOF columns for Figure 5.2.....	137
Table 5.S2. Chromatographic parameters for IL and IL + MOF columns for Figure 5. 3.....	138
Table 5.S3. Chromatographic parameters for IL and IL + MOF columns for Figure 5.4.	139
Table 6.1 Solvatochromic data of Nile red in different hexane/ethanol mobile phases.....	151
Table 6.2 Chromatographic retention parameter changes induced by addition of water to mobile phase.....	159

Chapters

Chapter 1 Introduction

1.1 Analysis of Isotopologues and isotopomers with GC

According to IUPAC definitions, isotopologues are molecules that differ only in their isotopic composition. They have the same bonding arrangement of atoms i.e. CH_3OH and CH_2DOH and $\text{CH}_3^{18}\text{OH}$. Isotopomers have the same isotopic composition but have different positions of the isotopes within the molecule i.e. CH_2DOH and CH_3OD or $^{13}\text{CH}_3\text{CN}$ and $\text{CH}_3^{13}\text{CN}$ [1, 2]. In terms of gas chromatography separations, there are difficulties in achieving separations of these molecules due to the fact that these compounds have very similar properties. There have been only a few reports on the separations of a limited number of isotopologues with GC [3-8]. Recently, we reported the most comprehensive study in this field, wherein 46 pairs of isotopologues were evaluated on 12 GC stationary phases of different polarity [9]. A guide was provided for these separations.

1.1.2 Significance of analysis of low molecular weight deuterated isotopologues

Austedo (deutetrabenazine) was the first drug that was approved by food and drug administration in 2017 for treatment of chorea associated with Huntington's disease and for tardive dyskinesias [10]. It was shown to have improved tolerability compared to the non-deuterated version tetrabenazine [11, 12]. The number of deuterated drugs that are under investigation or clinical trial is growing i.e. d6-dextromethorphan/quinidine, BMS-986165, and VX-984 [12]. Deuterated drugs provide more biostability due to stronger C-D bond vs C-H bond which led to various benefits of using the deuterated drugs [13-15]. Lower needed dosage, less

side effects, reduction of toxicity, and increased bio activation are among other benefits of deuterated vs. protiated drugs [12-21]. Lower molecular weight deuterated isotopologues provide the deuterated pool from which the bigger deuterated drugs are synthesized. Even though there are other methods for synthesis of deuterated compounds, use of the deuterated pool is the most prevalent one [12, 22]. Therefore, it is important to be able to analyze and separate the low molecular weight molecules that are starting materials for the synthesis of the larger molecules of medicinal potency. Additionally, deuterated compounds can be utilized in understanding chemical reaction mechanisms through kinetic isotope effects (KIEs) [23]. Deuteration affects reaction rates due to the higher activation energy of CH vs CH bond which leads to deuterium kinetic isotopic effect (DKIE), represented as the ratio of k_H/k_D . Also, DKIEs are used to determine the rate-limiting steps and transition states [23-25].

1.1.3 Normal and inverse isotope effects in GC

In GC, the case in which the heavier isotopologue elutes earlier than the lighter isotopologue is called an inverse isotope effect. This happens due to lower molar volume of the heavier counterpart which results in lower dispersion forces with the stationary phase. Therefore, in stationary phases that have dispersion forces as the main interaction affecting selectivity, inverse isotope effects are observed. The normal isotope effect refers to the case where the heavier isotopologue elutes later than the protiated one. There are few good explanations for this isotope effect other than lower vapor pressure of the deuterated vs the protiated compound [26]. In chapter three we discuss the types of interactions that control isotope effects and lead to normal isotope effects. Factors that affect isotope effects, include the mass difference and the position of deuterium atoms. However, there are only a few studies that discuss the “positional effect” of

deuterium atoms on a molecule and only for a very limited number of analytes [4, 27]. We analyzed toluene, benzyl alcohol, *N, N*-dimethyl formamide, amphetamine, and methamphetamine isotopologue groups on two stationary phases of very different polarities and interaction capabilities to study this effect further. The results are discussed in chapter three [28-34].

1.2 Gas chromatography - Molecular Rotational Resonance Spectroscopy (GC-MRR)

Rotational spectra are obtained by measuring the energies of transitions between quantized rotational states of molecules in the gas phase [35]. In order for a molecule to be detectable by microwave spectroscopy, it should have a permanent electric dipole moment ($\mu \neq 0$) [36]. To induce rotational transitions, molecules interact with the electric vector of microwave radiation via their electric dipole moment. These transitions occur in the microwave region of the electromagnetic spectrum, which spans from 1000 MHz ($\lambda = 30$ cm) to 1 million MHz ($\lambda = 0.3$ mm) [36]. A molecule's quantized rotational energy levels are dependent on their principal moments of inertia (*I*). Hence, the molecular structure, isotopic composition, and various other molecular properties have a significant impact on these energy levels. As a result, these spectra provide a significant amount of structural information, owing to the sensitivity of the rotational energy levels to the molecular properties [36]. By knowing the angular momentum and moments of inertia, the energies of the rotational levels of a molecule can be calculated [37, 38]. Additionally, since the response factor can be calculated accurately for a given molecule, compounds can be identified and quantified without having reference standards [39-42]. Rotational spectroscopy usually achieves a high degree of accuracy in the measurement of

transition frequencies, typically better than one part per million. This high level of accuracy is made possible by the fact that the spectra are typically measured in isolated gas environments which minimizes interference from other molecules. Furthermore, the excited rotational states have longer lifetimes, leading to narrower spectral bands and higher spectroscopic resolution [43, 44]. Therefore, even for isotopomers, which are not easily distinguishable by any other spectroscopic method, unique fingerprints can be achieved. MRR spectroscopy is useful for identifying compounds by calculating the spectra based on their molecular structure or by comparing them to a standard. When using calculated values, the instrument will specifically search for the predicted transitions in the mixture. As a result, even compounds with similar exact masses or isobaric compounds can be differentiated, which is not possible with most of MS techniques. This ability to distinguish between closely related compounds is due to the specificity of the calculated transitions and the unique spectral patterns of each compound [43].

Fourier transform ion cyclotron resonance mass spectrometry (FTICR MS) has a remarkable mass resolution performance, achieving up to $\sim 10^6$ resolution. However, this level of resolution can only be achieved in a high vacuum environment (10^{-9} Torr or lower), and the technique requires a high-field superconducting magnet [45]. This high magnetic field can raise safety concerns and the continuous consumption of liquid helium leads to high operating and maintenance costs [46]. Although other mass analyzers with lower resolution power (10^4 or less) can distinguish between isotopologues, they cannot differentiate isotopomers, leading to complications in mass spectrometry (MS) analysis. Furthermore, isotopomers often have similar fragmentation patterns and cannot be separated by chromatography, adding to the complexity of the analysis [39].

1.2.1 Broadband GC-MRR

The first report of GC hyphenation with MRR detection utilized chirped-pulse Fourier transform microwave (CP-FTMW) spectroscopy and provided great specificity in detection. A chirped pulse is defined as an excitation pulse where the frequency increases or decreases with time, in order to simultaneous excitation of a wide range of molecular spectra [43, 47, 48]. A schematic of the first GC-hyphenated MRR instrument is shown in Fig. 1.

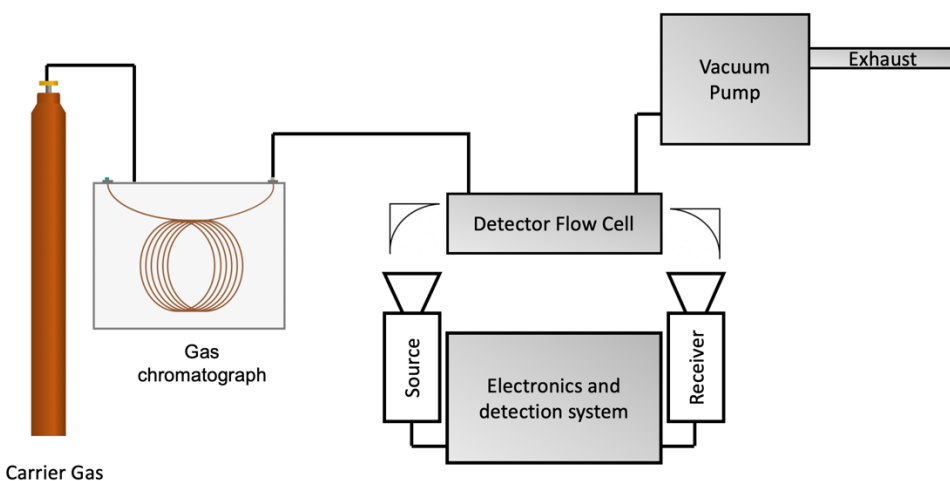


Figure 1.1 Schematic of the first GC-hyphenated MRR instrument (broadband). Reprinted with permission from Ref [49].

To obtain rotational spectra, a low-pressure sample cell (with a pressure of about 10^{-2} torr) is excited with a short pulse (typically 250 ns). The excited molecules emit coherent radiation at their characteristic rotational frequencies through free induction decay (FID) for several microseconds. This radiation is then recorded in the time domain using horn antennae and subsequently Fourier transformed into the frequency domain [43].

1.2.2 Applications of broadband GC-MRR

The broadband GC-MRR instrument was used to separate, identify, and quantify isotopologues and isotopomers, which traditional GC instruments cannot [9, 43]. As depicted in Figure 1.2, two kinds of chromatograms are generated. The first one, shown in Figure 1.2.a, is the total molecule chromatogram (TMC), which is obtained by adding all the observed transitions. Each point on the TMC represents a high-resolution spectrum with broad bandwidth. Figure 1.2.b displays the extracted molecule chromatograms (EMC) of all the isotopically distinct compounds that exist in the mixture. This indicates the selectivity of this technique, because even compounds with identical exact masses that cannot be distinguished by any other GC detectors, can be easily identified since each of them have different rotational transitions due to their distinct moments of inertia.

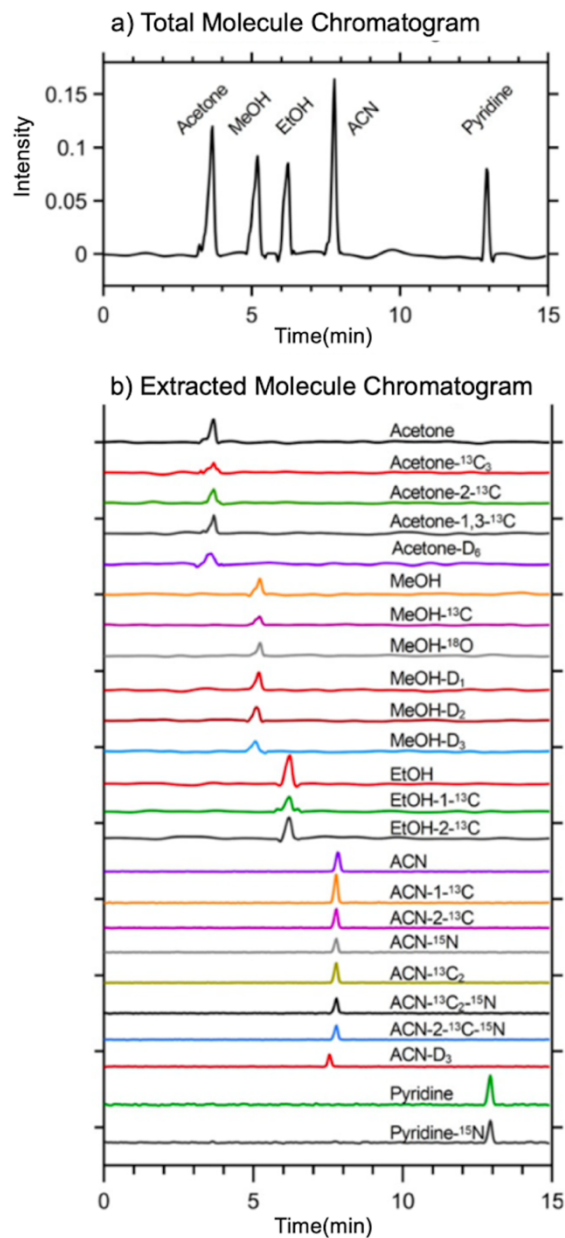


Figure 1.2 a) Total GC-MRR chromatogram of five common organic molecules. b) The 24 extracted molecule chromatograms. Reprinted with permission from Ref. [43].

It is noteworthy that this kind of analysis can be performed quickly, and quantitation of analytes is possible even in complex mixtures with ng amounts of sample. Unlike NMR spectroscopy which is inherently insensitive and less reliable for the analysis of complex mixtures [43]. The GC-MRR method also was utilized for determining the natural isotopic abundances of chlorine and bromine atoms in a mixture of five heterocyclic compounds and bromoethane. This was possible due to the quantitative information provided for all analytes by integrating the peak areas of GC-MRR. Additional information can be found in Ref. [43].

1.2.3 Targeted GC- MRR

The initial GC-MRR suffered from two major limitations: a) a limited range of molecular weight analysis (only compounds with molecular weights under 120 Da could be analyzed), and b) low sensitivity. These limitations were attributed to the broadband excitation source (75-110 GHz), lack of a heated transfer line, and room temperature to 80 °C detector flow cell temperature. The second iteration of the GC-MRR, referred to as the targeted-mode GC-MRR, addressed these limitations by incorporating a nozzle and using a pulsed-jet mechanism to enable spectral cooling of molecules. This allowed for the analysis of larger molecules within the 9-18 GHz frequency range. These improvements resulted in a lower limit of detection for the targeted instrument compared to the broadband instrument [39, 50].

1.3 Ionic liquids and Metal Organic Frameworks in Gas Chromatography

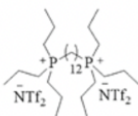
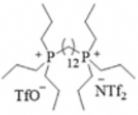
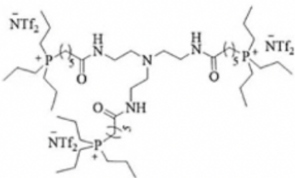
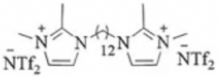

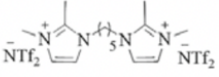
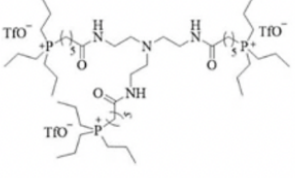
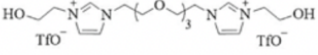
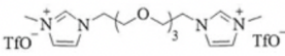
1.3.1 Ionic liquids as GC stationary phases

Ionic liquids (ILs) represent the most recent addition to the broad spectrum of gas chromatography liquid stationary phases. [51-53]. The preferred “multicationic” ionic liquids have broad liquid ranges, low vapor pressures due to strong Columbic interactions, high thermal stabilities, remarkable solvation abilities for different organic solutes, and good wettability of fused silica surfaces. These properties of ionic liquids make them desirable as gas chromatography stationary phases [54, 55]. Furthermore, the characteristics of ionic liquids can be modified by selecting different combinations of cations and anions, allowing for tuning of their properties to suit specific analytical requirements [56-58]. Ionic liquids have a unique behavior characterized by their ability to exhibit both polar and nonpolar interactions, making them highly polar GC stationary phases. This allows for a broad range of selectivity, including the separation of isotopic compounds [9, 51, 59].

To comprehend the characteristics and explore more efficient techniques for manipulating ionic liquids, it is crucial to have knowledge of their structure. The liquid state of ionic liquids at room temperature is attributable to their chemical composition, making it vital to carefully select both the anion and cation to prevent the formation of crystals. Hence, in the creation of ionic liquids, it is necessary to carefully choose or synthesize the constituent ions from a broad range of ion structures while considering the balance between ion-ion interactions and symmetry. As an example, the alkyl chain in the cation must be of sufficient length to lower Coulombic forces and disrupt lattice packing, while avoiding excessive length ($\sim n < 12$), which can raise the melting point despite greater asymmetry. Dispersive interactions tend to increase with the length of non-polar groups, akin to linear alkanes [60]. It was shown that incorporating dicationic and tricationic

ionic liquids in the stationary phases yields enhanced thermal stability, increased viscosity, and superior performance as gas chromatography (GC) stationary phases compared to monocationic ionic liquids [52, 53, 56, 61-63]. The ionic liquids developed by Armstrong and coworkers have been demonstrated to be highly effective as gas chromatography (GC) stationary phases, with several of them being commercially available [51-55]. These stationary phases exhibit outstanding thermal stability and a wide range of possibilities for structural modification. Table 1.1 shows the structure of the commercialized ionic liquids [53, 56, 61-64].

Table 1.1 Chemical structures of commercial ionic liquid stationary phases. Reprinted with permission from Ref [64].

IL column	Temperature limits	IL molecular structure and IUPAC name
SLB-IL59	Subambient to 300 °C	 <p>1,12-Di(triisopropylphosphonium)dodecane bis(trifluoromethanesulfonyl)imide</p>
SLB-ILPAH	Subambient to 300 °C	
SLB-IL60	35–300 °C	
SLB-IL60i	35–280 °C	
SLB-IL61	40–290 °C	 <p>1,12-Di(triisopropylphosphonium)dodecane bis(trifluoromethanesulfonyl)imide trifluoromethanesulfonate</p>
SLB-IL76	Subambient to 270 °C	 <p>Tri(triisopropylphosphoniumhexanamido)triethylamine bis(trifluoromethanesulfonyl)imide</p>
SLB-IL76i	Subambient to 270 °C	
SLB-IL82	50–270 °C	 <p>1,12-Di(2,3-dimethylimidazolium)dodecane bis(trifluoromethanesulfonyl)imide</p>
SLB-IL100	Subambient to 230 °C	 <p>1,9-Di(3-vinylimidazolium)nonane bis(trifluoromethanesulfonyl)imide</p>
SLB-IL111	50–270 °C	 <p>1,5-Di(2,3-dimethylimidazolium)pentane bis(trifluoromethanesulfonyl)imide</p>
SLB-IL111i	50–260 °C	
SLB-ILD3606	50–260 °C	
Watercol 1460	30–260 °C	 <p>Tri(triisopropylphosphoniumhexanamido)triethylamine trifluoromethanesulfonate</p>
Watercol 1910	30–180 °C	 <p>1,11-Di(3-hydroxyethylimidazolium)3,6,9-trioxaundecane trifluoromethanesulfonate</p>
Watercol 1900	30–180 °C	 <p>1,11-Di(3-methylimidazolium)3,6,9-trioxaundecane</p>

1.3.2 Metal organic frameworks (MOFs) in GC

Metal–Organic Frameworks (MOFs) are polymer coordinated compounds composed of metal ions or clusters linked by organic ligands [65]. MOFs can be applicable in a variety of fields due to their large chemical and structural tunability, since there are almost infinite possible combinations of inorganic building units and organic linkers [66]. MOFs can be specifically designed to have desired structural features (pore size, shape, etc.) and functionalities by substitution of metal nodes, selective use of organic ligands and incorporation of functional groups [66]. These features may provide unique recognition effects which can lead to novel selectivities in chromatographic separations.

UiO-66, MIL-100, MIL-101, ZIF7, ZIF-8 are some of MOFs that have great chemical and thermal stabilities and have been used as GC stationary phase and show selectivity for alkanes. However, the separations suffered from low efficiency and loading capability, which is often the case in gas-solid chromatography [67-69]. In order to coat GC capillary columns, very small amounts of stationary phase (MOFs) are required, which allows the use of more expensive materials. Therefore, it allows the use of tailored synthetic materials that provide unique interactions between various analytes to the stationary phases [66]. A stationary phase that could utilize the plethora of interactions provided by ionic liquids and MOFs could be highly beneficial and potentially more widely applicable along with the added benefits from properties of gas-liquid chromatography (GLC) i.e. higher efficiency and loadability. Here, we introduce a novel stationary phase based on colloidal MOFs dispersed in ionic liquids for GLC. We report the first case of permanent gas separation in GLC with separation of CO₂, propane, and butane from air as well as novel selectivities in separation of other analyte groups i.e. alkanes, alcohols, aldehydes, ketones, and ethers.

1.4 Enantioselective method development for HPLC

The development of analytical methods for the determination of stereoisomers of active pharmaceutical ingredients (APIs) has gained higher significance since the public health disaster with the drug, thalidomide [70]. Since different enantiomers of a racemic API may exhibit different pharmacological effects, it is important to separate different stereoisomers which may have different biological properties [71]. Additionally, each isomer is required to be tested for toxicity and pharmacokinetic properties in order to be approved by the Food and Drug Administration (FDA) [72]. Use of “chiral” chromatography has proven to be invaluable for identification and quantitation of chiral compounds [73-75]. Resolution of chiral compounds in liquid chromatography can be based on indirect methods in which the compound has to be derivatized prior to analysis [76]. Another way of chiral recognition is through chiral selectors being added to the mobile phase [77] or the stationary phase [78]. Chiral stationary phases based on macrocyclic glycopeptides have proven to be effective in separating a diverse range of acidic, basic, and neutral compounds due to their ability to provide six types of molecular interactions: ionic, hydrogen-bonding, π - π , dipole, hydrophobic, and steric interactions [79]. They also possess multiple inclusion sites that influence selectivity based on the molecular shape of the analyte. The optimization of enantiomer resolution is achieved by changing the mobile phase to utilize the types and relative strengths of the various interactions. Five different LC modes can be used with macrocyclic glycopeptide-based stationary phases. These modes include, reversed phase mode (RPLC), normal phase mode (NPLC), the polar organic mode, and the polar ionic mode (PIM). In NPLC mode the used mobile phases are usually alkanes, like hexane or heptane, mixed with ethanol or propanol [80].

1.4.1 Effect of presence of water in enantioseparations

The presence of unwanted water in mobile phases has been avoided in NPLC since it led to irreproducibility in analyses. There have been a few studies on adding known amounts of water to the mobile phase in order to study the effect and produce more reproducible separations [77, 81, 82]. A study on a wide variety of stationary phases in supercritical fluid chromatography (SFC) showed that NicoShell, TeicoShell, and VancoShell macrocyclic antibiotic phases have been shown to be more affected by water addition [83]. A comprehensive investigation of enantioselective method development for a broad range of enantiomers on various stationary phases for normal phase chiral HPLC is described. We showed that altering the polarity of the mobile phase is not the only nor the main effect of adding the water to the mobile phase.

1.5 Organization of Dissertation

Chapter 2 reports the investigation of separation of 47 isotopologue pairs on twelve different stationary phases of different polarities, which provided a plethora of different interactions for separation of isotopologue pairs. The isotope effects were studied on all stationary phases and the optimum separation conditions for each pair were determined.

In chapter 3, the effect of location of deuterium atoms on isotope effects was investigated by analyzing five groups of isotopologues (each containing different structural iterations with deuterium atoms at different locations) with two GC stationary phases of significantly different polarity. The factors that affect the separation of “isotopic pairs” are discussed.

Chapter 4 introduces a second-generation molecular rotational resonance (MRR) spectroscopy detector that was hyphenated with GC. This chapter describes the improved features of this new MRR detector and how it is more sensitive compared to the first generation MRR. The

limits of detection of first and second-generation MRR detectors were compared to thermal conductivity detector (TCD) as a universal GC detector.

In chapter 5 a new gas-liquid chromatography stationary phase is introduced. Four metal organic frameworks (MOFs) were added to 18 ionic liquids and the combination that provided a good dispersion was used as a novel GLC stationary phase. The ability of this stationary phase for separation of permanent gases as well as different groups of alkanes, alcohols, ethers, and ketones was demonstrated.

Chapter 6 is focused on effect of addition of water to normal phase liquid chromatography stationary phases. The effect of water addition on hydration of stationary phase, polarity of mobile phase, and kinetic and thermodynamic properties of separations was studied.

Chapter 2

Evaluation of gas chromatography for the separation of a broad range of isotopic compounds

2.1 Abstract

The separation of deuterated compounds from their protiated counterparts is essential in areas of drug discovery and development, investigating kinetic isotope effects and quantitative method of non-mass spectrometry-based stable isotope dilution assay (non-MS SIDA). The separations of 47 isotopologue pairs of common compounds and drugs were achieved by gas-liquid chromatography, employing twelve different stationary phases. Polydimethylsiloxane phase, phenyl-substituted polydimethylsiloxane phases, wax phases, ionic liquid phases, and chiral stationary phases, were selected to encompass a wide polarity range and diverse chemical interactions. The best-performing stationary phases are presented for separation of protic-polar, aprotic-dipolar, nonpolar analytes. Overall, the IL111i, SPB-20, and PAG stationary phases were remarkable in their ability to separate the isotopologues. The isotope effect was also evaluated. It was observed that nonpolar stationary phases often exhibit an inverse isotope effect in which heavier isotopic compounds elute earlier than their lighter counterparts. Conversely, polar stationary phases often show a normal isotope effect, while those of intermediate polarities can show both effects depending on the isotopologues. The location of deuterium atoms, however, affects isotopologue retention times. Deuterium substituted aliphatic groups appear to have a greater inverse isotope effect on retention than aromatic substituents.

2.2 Introduction

Deuterated compounds have applications in a number of scientific disciplines, including drug discovery and development, analytical testing, agriculture, and development of new materials

[12, 84-88]. Deuterated compounds have been extensively used for elucidating chemical reaction mechanisms by investigating kinetic isotope effects (KIEs) since the first paper on isotope effects was published in 1947 [23]. The mass difference resulting from the extra neutron in deuterium is sufficient to alter the physicochemical properties of deuterated molecules [28]. Deuterated molecules exhibit different reaction rates as compared to their non-deuterated counterparts because the activation energy for the C-D bond is higher than the C-H bond [25]. This stability difference in deuterated and non-deuterated molecules is manifested as the deuterium kinetic isotopic effect (DKIE) and is represented as the ratio of k_H/k_D . The rate-limiting steps and transition states are determined using KIEs when evaluating reaction mechanisms [23-25].

The incorporation of deuterium into drug molecules has opened new avenues in pharmaceutical studies. The first deuterated drug, deutetrabenazine (Austedo), was approved by the FDA in 2017 to treat Huntington's chorea [89]. Metabolism of the drug is directly impacted by deuterium substitution because of the kinetic isotope effect [84]. The interactions of deuterated molecules with enzymes involved in metabolism are altered and may increase the drug's biological half-life. This, in turn, leads to a reduction of the required drug dose and mitigation of any side effects. In addition to affecting the circulation of drugs in the bloodstream, deuterated drugs have been shown to (a) reduce the formation of unwanted metabolites (formally known as metabolic shunting), (b) stabilize unstable enantiomers in the desired therapeutic stereochemical orientation by minimizing the rapid interconversion of stereoisomers and, (c) increase bioactivation [12]. The pharmacokinetic effects of more than 20 deuterated drugs are currently being scrutinized for their efficacy and safety [12, 88]. In regard to this, separation of deuterated compounds is crucial since they can serve as precursors for the industrial synthesis of deuterated active pharmaceutical ingredients (APIs).

Another exciting application of deuterated compounds is in the field of digital display technology. Organic light-emitting diodes (OLEDs) offer numerous advantages over liquid crystal displays (LCDs) and light-emitting diodes (LEDs) as OLEDs are more flexible, brighter, energy-efficient, and provide larger fields of view [90]. However, the biggest challenge of OLEDs is their limited lifetime. One solution to this problem is provided by deuterated OLEDs, which increased the device lifetime by a factor of 22.5 without altering the performance [91]. Deuterated solvents serve as the source of the deuterium in the synthesis of these next-generation OLEDs. Various other applications of "deuterium swapped molecules" have been reviewed recently [25, 85, 92].

The separation of isotopologues is useful as a quantitative method of stable isotope dilution assay (SIDA). In this method, labeled stable isotopes are used as internal standards owing to their nearly identical physical and chemical properties [93]. This method is prevalent in flavor analysis [94]. After adding the internal standard and achieving equilibration with the analyte of interest, mass spectrometry can be used to distinguish the analyte and the isotopic internal standard. Based on the known amount of the internal standard, the content of the analyte can be determined. However, SIDA using a flame ionization detector (FID) could be an attractive alternative due to the detector's robustness, low cost, and easy availability.

Gas chromatography (GC) with FID is a convenient and efficient method for the separation and quantification of deuterated compounds. The chromatographic separations of two isotopically distinct compounds were reported early on in 1958 [95]. These separations are particularly challenging to achieve owing to the very small mass and boiling point difference of isotopologues. There have been only a few subsequent reports that have shown the separation or partial separation of a very small number of isotopic compounds [4, 8, 96-98]. One study compared isotope effects (normal vs. inverse) of partial separations on a 5% phenyl polydimethylsiloxane column and an

early ionic liquid-based column [7]. To date, there have been no comprehensive studies done to achieve higher resolutions for these difficult and important separations. In this work, 47 pairs of isotopic (hydrogen/deuterium) compounds, from common solvents to more complex drugs, have been separated by employing 12 different GC stationary phases encompassing a broad polarity range. Moreover, this is the first study reporting the separation of various deuterated drugs from their non-deuterated counterparts.

2.3 Materials and methods

2.3.1 Chemicals and reagents

Non-deuterated and deuterated compounds and derivatizing agents were purchased from MilliporeSigma (formerly Sigma-Aldrich, St. Louis, MO). The non-deuterated and deuterated drugs were purchased from Cambridge Isotope Laboratories, Inc. as 1 mg/mL solutions.

2.3.2 GC Columns

GC columns listed in Table 2.1 (PDMS-0, PDMS-5, PDMS-20, PDMS-35, PDMS-50, PAG, Wax, IL60i, IL111i, GTA, β -DEX, B-PH) were provided by MilliporeSigma (Bellefonte, PA, USA)

2.3.3 Derivatization experiments

L-leucine, L-leucic acid, and ibuprofen were derivatized prior to the analysis[99]. First, esterification was done by adding 1 mg of the sample to 1 mL of 3N methanolic hydrochloric acid, and the mixture was heated at 100 °C for 30 minutes, followed by evaporating the solvent using nitrogen gas. Ibuprofen was analyzed after this step in the ester form, whereas L-leucic acid and L-leucine were further trifluoroacetylated before the analysis. For trifluoroacetylation, the esterified form of L-leucic acid and L-leucine were dissolved in 1 mL dichloromethane and then

added to 100 μL of trifluoroacetic anhydride. The mixture was heated at 60 $^{\circ}\text{C}$ for 20 minutes. Afterward, the solvent and excess reagent were evaporated with a stream of nitrogen gas.

2.3.4 Experimental

The samples were prepared in dichloromethane at 1 mg/mL for analysis. If dichloromethane coeluted with the analyte, toluene was used, instead, to dissolve the samples. Drug molecules were purchased as solutions in methanol or acetonitrile. Analysis conditions are as follows: mobile phase: He, split ratio: 100:1, inlet temperature: 250 $^{\circ}\text{C}$, Detector (FID) temperature: 250 $^{\circ}\text{C}$, injection volume: 1 μL , column dimensions: 30 m x 0.25 mm x 0.25 μm . The temperature programs and average velocities are provided in supporting information (Tables S1-S12).

2.3.5 Apparatus and instrument

The gas chromatographic analyses were performed on an Agilent 6850 (Agilent, Palo Alto, CA, USA) gas chromatograph equipped with a flame ionization detector. Helium was used as a carrier gas for all analyses. The detector and injection port temperature were both set at 250 $^{\circ}\text{C}$. An Agilent ChemStation data processing unit was used for processing and storing the chromatograms. Resolutions were calculated using PeakFit (software version 4.12), employing the exponentially modified Gaussian (EMG) model [100].

2.4 Results and discussion

2.4.1 Stationary phase selection

Stationary phase selectivity is the all-important parameter affecting the separation of isotopologues in gas chromatography. Twelve GC stationary phases were selected based on their polarity and different chemical interactions (see *Table 2.1*). Their polarity numbers were derived

from Rohrschneider-McReynolds constants [64, 101]. The polydimethylsiloxane (PDMS) phase was the most nonpolar stationary phase, which primarily relies on Van der Waals interactions for separations. The polarity of PDMS stationary phases can be altered by substituting phenyl functional groups. The phenyl groups add other dimensions of dipole-dipole, dipole-induced dipole, and π - π interactions. Four phenyl-substituted PDMS (polydimethylsiloxane) stationary phases containing 5%, 20%, 35%, and 50% phenyl content were selected to determine the effect of percentage of phenyl substitution on the separation of isotopologue pairs. The greater the percentage of phenyl functional groups on the PDMS, the more polar is the stationary phase (see *Table 2.1*). However, even 50% phenyl polydimethylsiloxane (see *Table 2.1*) cannot be considered a polar stationary phase as compared to others discussed below.

Table 2.1 Columns used in the study.

<i>Commercial Name</i>	<i>Stationary phase composition</i>	<i>Polarity Number*</i>
<i>IL111i</i>	1,5-Di(2,3-dimethylimidazolium) pentane bis(trifluoromethylsulfonyl)imide	111
<i>IL-60i</i>	1,12-Di(triethylphosphonium)dodecane bis(trifluoromethylsulfonyl)imide	60
<i>SupelcoWax10</i>	100% poly(ethyleneglycol)	52
<i>PAG</i>	Poly(alkyleneglycol)	45
<i>SPB-50</i>	Poly (50% diphenyl/50% dimethylsiloxane)	21
<i>SPB-35</i>	Poly (35% diphenyl/65% dimethylsiloxane)	19
<i>SPB-20</i>	Poly (20% diphenyl/80% dimethylsiloxane)	12
<i>SLB-5ms</i>	Poly (5% diphenyl/95% dimethylsiloxane)	6
<i>Equity 1</i>	Poly(dimethylsiloxane)	3
<i>Chiraldex G-TA</i>	CD Type: γ (gamma) Derivative: Dipentyltrifluoroacetyl	31
<i>β-DEX120</i>	CD Type: β (beta) * * 20% permethylated β -CD dissolved in phenyl-containing polydimethylsiloxane (SPB-35) stationary co-phase	19
<i>B-PH</i>	CD Type: β (beta) Derivative: Permethyl-hydroxypropyl	37

* derived from Rohrschneider-McReynolds constants [64, 101]

Traditional polar GC stationary phases are commonly made using polyethylene glycol (PEG), which imparts hydrogen bonding interactions besides dispersive, dipole-dipole, and dipole-induced dipole interactions. Supelcowax 10 was evaluated in this study. Polyalkylene glycol (PAG) is another polar stationary phase that is a copolymer of ethylene and propylene glycol. PAG is, therefore, slightly less polar than PEG. Two ionic liquid-based (IL) stationary phases were selected for evaluating their effectiveness in separating isotopologues. Ionic liquids show excellent performance as GC stationary phases owing to multiple solvation interactions, unusual dual-nature behavior, tunable selectivity through structural modifications, high thermal stabilities, and high

viscosities [51, 55, 64, 102]. In this study, an extremely polar imidazolium-based dicationic IL column (SLB-IL111i) and a moderately polar phosphonium-based dicationic IL column (SLB-IL-60i) were chosen for evaluation [52, 103] (see *Table 2.1*).

Cyclodextrin (CD) based chiral stationary phases were selected to explore their potential in isotopic pair separations. Cyclodextrins are cyclic macromolecules that consist of six or more D(+) glucose units connected through (1-4) glycosidic linkages [104]. One γ -CD, containing eight glucose units (Chiraldex G-TA) and two β -CD, containing seven glucose units (β -DEX, B-PH) columns were screened [105-107]. The interior of the CD cavity is nonpolar due to methylene hydrogens, and the exterior is polar due to its derivatized hydroxyl groups. While the derivatized cyclodextrins themselves are polar, they are often dissolved in a less polar stationary phase matrix such as SPB-35(see *Table 2.1*). Hence, they can have variable intermediate polarities.

2.4.2 Separations of non-deuterated, partially deuterated, and deuterated small molecules (≤ 170 amu molecular weight)

Table 2.2 (compound numbers 1-31) lists the resolutions for the separations of isotopologue pairs for a variety of compounds on 12 different stationary phases. The best separations (highest resolution and best peak shapes) of the 31 low molecular weight isotopologue pairs along with the corresponding chromatographic conditions are given in Table 2.3.

Table 2.2 The resolution of 47 isotopologue pairs on 12 different columns (The optimum condition was used for each mixture and the resolution accuracy is ± 0.05). Conditions: mobile phase: He, split ratio: 100:1, injection volume: 1 μ L, column dimensions: 30 m x 0.25 mm x 0.25 μ m. See Figure 2.S1 of the supporting information for the structures of the compounds.

	<i>Pairs of Isotopologues</i>	<i>Equity 1</i>	<i>SLB-5ms</i>	<i>SPB-20</i>	<i>SPB-35</i>	<i>SPB-50</i>	<i>PAG</i>	<i>Wax</i>	<i>IL 60i</i>	<i>IL 111i</i>	<i>GTA</i>	<i>β-DEX 120</i>	<i>B-PH</i>
1	MeOH & MeOH-2D	X	X	X	X	X	0.50	X	X	X	X	X	X
2	MeOH & MeOH-3D	X	X	X	X	X	0.55	X	X	X	X	X	0.70
3	MeOH-1D & MeOH-3D	X	X	X	X	X	0.50	X	X	X	X	X	X
4	ACN & ACN-D3	X	X	0.70	0.50	1.00	1.70	1.35	0.80	X	1.20	1.15	1.00
5	Chlorobenzene & Chlorobenzene-D5	0.95	0.95	1.25	0.70	0.90	X	X	X	1.10	X	X	X
6	1,2 dichlorobenzene & 1,2 dichlorbenzene-D4	X	X	X	X	X	X	X	X	1.15	X	0.70	X
7	IPA & IPA-D8	X	X	0.60	X	X	1.15	1.20	X	X	0.80	X	X
8	IPA & IPA-D6	X	X	X	X	X	1.45	0.40	X	X	0.65	X	X
9	o-xylene & o-xylene-D10	2.45	2.60	2.70	1.50	1.95	2.00	1.85	X	1.00	X	1.95	1.00
10	DMSO & DMSO-D6	X	X	1.00	0.75	0.90	X	X	0.70	1.20	X	X	X
11	Pyridine & Pyridine - D5	X	X	0.60	X	X	X	X	X	1.45	X	X	X
12	Tetrachloroethane & Tetrachloroethane-D2	0.90	1.10	1.45	1.05	1.20	0.65	X	X	X	X	X	X
13	DMF & DMF-D7	X	X	X	X	0.50	1.15	0.85	1.30	2.70	X	X	1.00
14	DMF & DMF-D1	X	X	X	X	X	1.20	X	0.80	1.45	X	X	1.20
15	DMF-D1 & DMF-D7	X	X	0.65	0.80	0.70	X	X	0.80	1.50	X	X	X
16	Benzene & Benzene-D6	0.90	0.95	1.15	X	X	X	X	X	X	X	X	X
	Pair of Isotopologues	Equity 1	SLB-5ms	SPB-20	SPB-35	SPB-50	PAG	Wax	IL 60i	IL 111i	GT A	β-DEX 120	B-PH

17	Toluene & Toluene-D8	1.50	1.95	2.40	X	0.90	1.10	X	X	0.95	X	1.40	X
18	Acetone & Acetone-D6	X	X	1.00	X	X	0.95	X	X	X	X	1.10	X
19	Chloroform & Chloroform-D	X	X	0.70	X	X	X	X	X	X	X	X	X
20	Nitromethane & Nitromethane-D3	X	X	0.95	X	1.10	1.20	1.10	X	X	X	1.10	X
21	THF & THF-D8	X	X	X	X	X	0.70	0.75	X	0.75	X	1.20	X
22	Phenol & Phenol-D5	0.65	0.80	0.90	0.80	0.80	X	X	X	1.15	X	X	X
23	Benzylalcohol & Benzylalcohol-D7	1.40	1.80	1.45	2.00	1.60	1.75	1.50	X	0.90	1.10	1.50	1.50
24	Benzylalcohol & Benzylalcohol-D5	0.85	1.00	1.00	0.80	0.95	0.70	X	X	1.00	X	0.80	X
25	Benzylalcohol & Benzylalcohol-D2	1.10	1.00	1.40	1.10	1.25	1.35	1.05	X	X	X	0.65	X
26	Benzylalcohol-D7 & Benzylalcohol-D5	1.10	1.00	1.40	1.10	1.20	1.40	0.90	X	X	X	0.95	X
27	Benzylalcohol-D7 & Benzylalcohol-D2	0.60	1.00	1.10	1.10	1.05	0.70	X	X	1.05	X	0.60	X
28	Benzylalcohol-D5 & Benzylalcohol-D2	X	X	X	X	X	0.85	0.85	X	1.20	X	X	X
29	Ethyl Acetate & Ethyl acetate-D8	1.25	1.50	2.40	0.80	0.90	X	1.75	0.60	X	X	1.50	X
30	Cyclohexane & Cyclohexane-D12	1.40	2.55	2.55	X	0.80	0.95	X	X	X	X	1.80	X
31	Hexane & Hexane-D14	1.25	2.55	3.00	X	0.85	0.70	X	X	X	X	X	X
32	Amphetamine & Amphetamine-D5	X	0.70	1.35	1.20	0.95	X	X	X	X	-	-	-
33	MDA & MDA-D5	0.70	1.00	1.40	1.50	1.20	X	X	X	X	-	-	-
34	MDEA & MDEA-D5	0.95	0.95	1.50	1.50	1.20	X	X	X	X	-	-	-
35	MDEA & MDEA-D6	0.95	1.25	1.60	1.75	1.20	X	X	X	X	-	-	-
	Pair of Isotopologues		SLB-5ms	SPB-20	SPB-35	SPB-50	PAG	Wax	IL 60i	IL 111i	GT A	β-DEX 120	B-PH

36	Methamphetamine & Methamphetamine-D8	0.95	1.25	1.80	1.35	1.30	X	X	X	2.45	-	-	-
37	Methamphetamine & Methamphetamine-D5	X	0.75	1.30	1.20	0.95	X	X	0.60	X	-	-	-
38	Methamphetamine-D5 & Methamphetamine-D8	X	X	0.90	0.70	0.65	X	X	X	0.60	-	-	-
39	Methamphetamine-D6 & Methamphetamine-D8	X	X	X	X	X	X	X	X	1.20	-	-	-
40	Methamphetamine-D5 & Methamphetamine-D6	X	X	X	X	X	X	X	X	0.75	-	-	-
41	MDMA & MDMA-D5	0.80	1.35	1.35	1.40	1.20	X	X	X	X	-	-	-
42	Cocaine & Cocaine-D3	X	X	0.95	0.70	X	X	X	X	X	-	-	-
43	Ephedrine & Ephedrine-D3	X	X	1.00	0.65	X	X	X	X	0.70	-	-	-
44	Ibuprofen & Ibuprofen D3	0.70	0.75	0.85	X	0.85	0.80	0.75	X	X	-	-	-
45	Nicotine & Nicotine-D4	X	X	0.60	0.60	X	X	X	X	1.10	-	-	-
46	L-Leucine & L-Leucine D3	0.85	0.95	1.00	0.55	X	1.20	1.05	0.50	X	-	-	-
47	L-Leucic acid & L-Leucic acid D3	0.65	0.80	0.75	X	X	1.10	1.00	X	X	-	-	-

X Resolution less than 0.3 – Not evaluated

It is well known that besides the difference in vapor pressure of two analytes, the nature of the stationary phase plays a vital role in the separation of the isotopologues [8, 96]. The compounds used in this study were roughly divided into three large groups according to their normalized $E_T(30)$ values, (E_N^T), which is a dimensionless number ranging from 0.00 (for TMS as the least polar solvent) to 1.00 (for water as the most polar solvent). The $E_T(30)$ values are derived from the long-wavelength UV/Vis charge-transfer absorption band of the negatively solvatochromic

pyridinium N-phenolate betaine dyes. The three resulting groups are : (a) protic-polar (E_N^T ca. 0.5-1.0), (b) aprotic-dipolar (E_N^T ca. 0.3-0.5), and (c) non-polar (E_N^T ca. 0.0-0.3) [108]. Figure 2.1 shows that three stationary phases, in particular, provided the best separations for the broad range of isotopic compounds in this study. To a first approximation, the principle of "like dissolves like" often holds true in the case of isotopologue separations. This implies that the polar stationary phases were usually more effective in separating polar isotopologues, while nonpolar stationary phases were often suitable for nonpolar analytes. IL111i, the most polar ionic liquid-based stationary phase, showed the best chromatographic performance for polar analytes in contrast with Supelcowax-10, which is otherwise a versatile polar column based upon polyethylene glycol (PEG). The very polar solvents such as dimethyl sulfoxide, dimethylformamide, pyridine, and their deuterated counterparts were exclusively separated on IL111i. A challenging separation of dimethylformamide and dimethylformamide-D1 with just one-unit mass difference was remarkably achieved with IL111i with an excellent resolution of 1.45 (*see Figure 2.2b*). It should be noted again that all columns in this study were only 30 m in length and that higher resolutions can be easily obtained with longer columns (*see Experimental*).

Additionally, the unique and often broad selectivity of IL111i is due to the fact that it is the only stationary phase that interacts with molecules by π - π , dipole-dipole, and dipole-induced dipole interactions in addition to typical hydrogen bonding, dispersive, and acid-base type interactions. Thus, IL111i also provides excellent separations for mid-polar and nonpolar solvents owing to their dual-nature retention behavior [54]. The mid-polarity IL60i was not as effective for the isotopologues in this study, with just a 15% "hit rate".

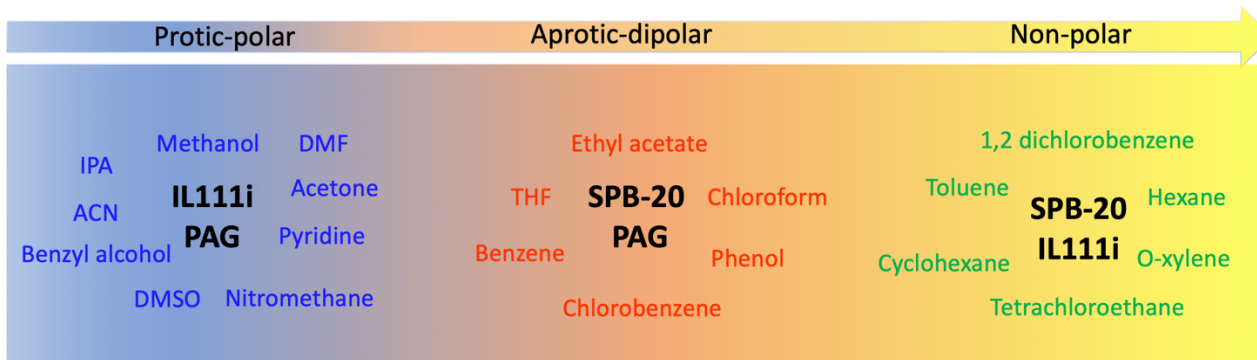


Figure 2.1 Columns showing the best chromatographic performance according to the polarity of the compounds. The analytes have been divided into three categories according to their E_N^T values (a) protic-polar (E_N^T ca. 0.5-1.0), (b) aprotic-dipolar (E_N^T ca. 0.3-0.5), and (c) non-polar (E_N^T ca. 0.0-0.3) [108].

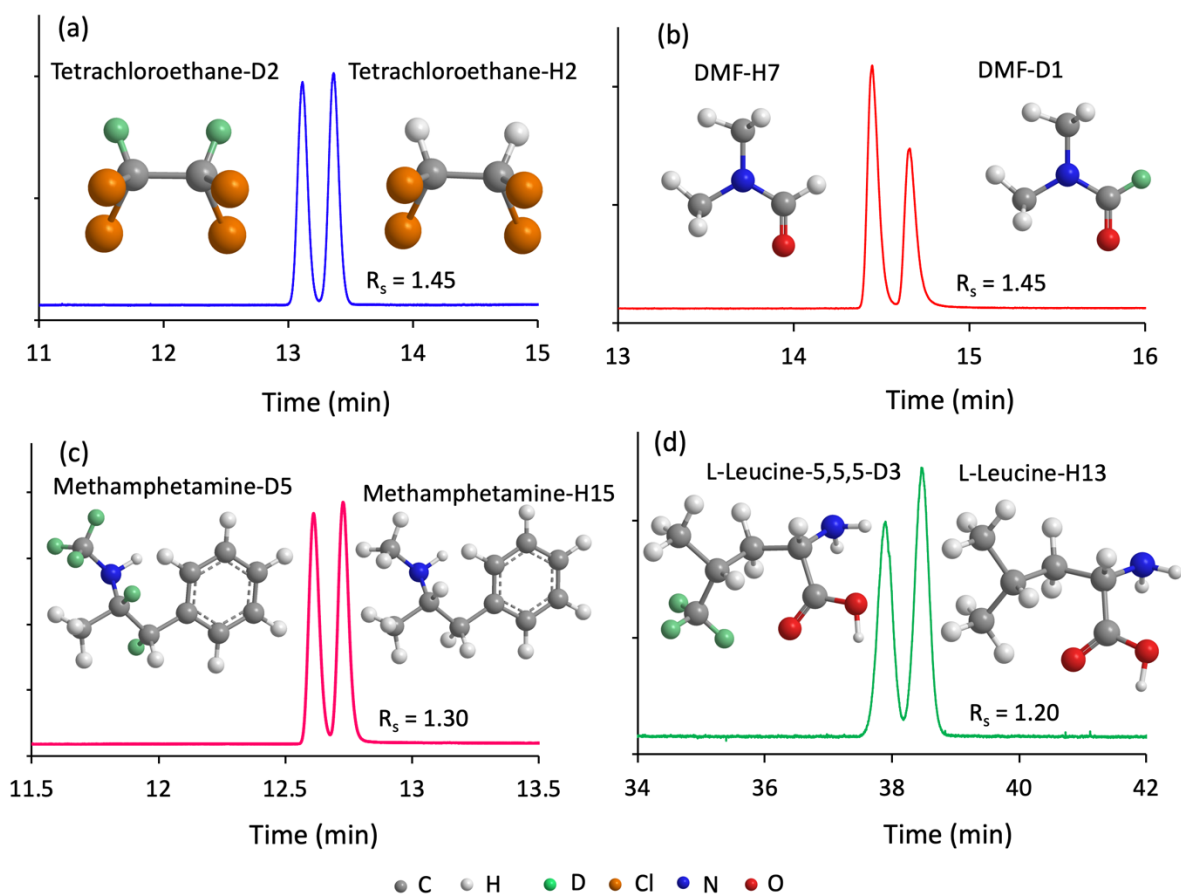


Figure 2.2 Separations of a) Tetrachloroethane H2 & D2 b) DMF-H7 & D1 c) methamphetamine-H15 & D5 d) L-leucine-5,5,5-H13 and D3. Conditions: mobile phase: He, split ratio: 100:1, injection volume: 1 μ L, column dimensions: 30m x 0.25mm x 0.25 μ m. See Table 2.3 for corresponding temperature programs and average velocities.

Interestingly, PAG (a polyalkylene glycol phase) was more effective in separating polar and mid polar compounds as compared to Supelcowax-10 (PEG-based stationary phase). PAG was very useful for the separation of non-deuterated and deuterated alcohols. Note that PAG was the only stationary phase to achieve partial separation of the pairs: methanol and methanol-D2, methanol and methanol-D3, and methanol-D and methanol-D3. Also, isopropyl alcohol and isopropyl alcohol-D6 were effectively separated by PAG with a resolution of 1.45. PDMS stationary phase with 20% phenyl functional groups (SPB-20) also separated mid-polarity compounds effectively. Tetrachloroethane and tetrachloroethane-D2 with a mass difference of two were nicely separated by SPB-20 (see *Figure 2.2a*).

The polydimethylsiloxane stationary phases with phenyl contents ranging from 0 to 50% (Equity-1, SPB-5, SPB-20, SPB-35, and SPB-50) were compared for the separation of isotopologues of compounds 1-31. From Table 2.1, as expected, Equity-1 and SPB-5 with 0% and 5% phenyl content, respectively (hence relatively nonpolar) performed better for nonpolar analytes. Conversely, SPB-35 and SPB-50 being relatively more polar, were more effective in separating mid-polar and polar compounds. Interestingly, SPB-20 was the most effective stationary phase among all the polydimethylsiloxane phases giving the most separation hits (hit rate of 71%) and highest resolutions for isotopologue pairs of these compounds (*Table 2.2*).

For the separation of phenol and phenol-D5, it was observed that increasing the percentage of diphenyl moieties in the stationary phase, increased the retention and selectivity due to stronger π - π interactions; however, resolutions were essentially unchanged because of the consequent

decrease in efficiency. Measured parameters are provided in supporting information (see *Table 2.S14*).

Among the chiral stationary phases, β -DEX was moderately effective in separating isotopologue pairs, whereas the G-TA and B-PH did not perform particularly well. Nonetheless, there were some noteworthy separations achieved by these chiral stationary phases; for instance, tetrahydrofuran and tetrahydrofuran-D8 were separated with the best resolution of 1.20 on β -DEX. Note that β -DEX is prepared by dissolving 20% permethylated β -CD in SPB-35 (a 35% phenyl-containing polydimethylsiloxane stationary co-phase). Consequently, it could be surmised that separations achieved on β -DEX were partially or wholly due to the presence of SPB-35 (see *Table 2.2*). However, on comparing β -DEX and SPB-35, it can be seen that some separations were solely due to interactions with the derivatized β -CD molecule. For example, toluene and toluene-D8, acetone and acetone-D6, cyclohexane and cyclohexane-D12, nitromethane and nitromethane-D3, and tetrahydrofuran and tetrahydrofuran-D8 all separated on the β -DEX column but were not separated on SPB-35. Therefore, either inclusion or external adsorption on the methylated cyclodextrin must play a role in the separations [109]. A previous study on the separation of deuterated compounds from their protiated counterparts using cyclodextrins and crown ethers reported that the size of the inclusion cavity may play a role in separation [110]. However, this study did conclude that cavity size is not the only factor involved in achieving separations and that the cavity environment plays a significant role too [110]. Indeed it appears that the earlier noted external adsorption on the cyclodextrin molecule may be the more important effect [109]. B-PH also was able to achieve a partial separation of methanol and methanol-D3.

2.4.3 Separation of deuterated drug molecules

Sixteen drugs were separated from their fully or partially deuterated counterparts. Table 2.2 (compound numbers 32-48) lists the achieved separations and the corresponding resolutions of the isotopologue pairs on nine different stationary phases. The chiral stationary phases were not evaluated because of their low upper-temperature limits and the high boiling points of the drug molecules. The best separations of the 16 isotopologues pairs along with the corresponding chromatographic conditions are tabulated in Table 2.3 (compound numbers 32-48). A class of central nervous system (CNS) stimulant drugs including amphetamine, 3,4-methylenedioxyamphetamine (MDA) 3,4-methylenedioxy-N-ethylamphetamine (MDEA), methamphetamine, 3,4-methylenedioxymethamphetamine (MDMA), cocaine, and ephedrine were separated from their deuterated counterparts. Except for ephedrine, all others are primarily drugs of abuse and produce an intense high along with effects of euphoria, enhanced sociability, and increased energy [111, 112]. The increase in the abuse of these illicit drugs requires their regular analysis in biological media. Better and reproducible quantification of the drugs using deuterated analogs of the drugs as the internal standards have been reported earlier [113-115]. GC-FID separation of the drug analyte from the deuterated counterpart as an internal standard is an inexpensive and effective alternative to using the mass spectrometer as a detector. Besides the recreational drugs, ibuprofen (non-steroidal anti-inflammatory), nicotine (a stimulant), L-leucine (amino acid and muscle building supplement), and L-leucic acid (a metabolite of leucine and a muscle-building supplement) also were separated from their deuterated analogues. In terms of stationary phase hit rates for this group of analytes, polydimethylsiloxane-containing (with 0%, 5%, 20%, 35%, and 50% phenyl substitution) stationary phases performed better than wax and ionic liquid-based

stationary phases. SPB-20 gave the best separations for these drugs with a hit rate of 81%, followed by SPB-35 (hit rate = 75%) and SPB-50 (hit rate = 56%). However, it should be noted that some of the most difficult separations were exclusively achieved with IL111i; for instance, methamphetamine-D5 & methamphetamine-D6 and methamphetamine-D6 & methamphetamine-D8. Although PAG showed just a hit rate of just 19% for drugs, it alone baseline separated L-leucine (see Figure 2.2d) and L-leucic acid. In total, the results presented in Tables 1 and 2 show that three of the tested stationary phases (i.e., IL-111i, PAG, and SPB-20) are sufficient to achieve the best separations of all tested isotopologue pairs.

Table 2.3 List of the best separations (highest resolution and best peak shapes) achieved for 47 pairs of isotopologues. Conditions: mobile phase: He, split ratio: 100:1, injection volume: 1 μ L, column dimensions: 30m x 0.25mm x 0.25 μ m. See Figure 2.S1 of the supporting information for the structures of the compounds.

	<i>Pair of Isotopologues</i>	<i>Column</i>	<i>Temperature program (°C)</i>	<i>Average velocity (cm/s)</i>	<i>Resolution</i>	<i>Isotope effect</i>
1	MeOH & MeOH-2D	PAG	25 °C	25	0.50	Inverse
2	MeOH & MeOH-3D	B-PH	26 °C	20	0.70	Inverse
3	MeOH-1D & MeOH-3D	PAG	25 °C	25	0.50	Inverse
	Pair of Isotopologues	Column	Temperature program (°C)	Average velocity (cm/s)	Resolution	Isotope effect
4	ACN & ACN-D3	PAG	27-60 °C @ 3 °C/min	30	1.70	Inverse
5	Chlorobenzene & Chlorobenzene-D5	SPB-20	40-100 °C @ 2 °C/min	35	1.30	Inverse
6	1,2 dichlorobenzene & 1,2 dichlorobenzene-D4	IL111i	30-100@ 2 °C/min	25	1.15	Normal
7	IPA & IPA-D8	Supelco Wax10	25 °C	25	1.20	Inverse
8	IPA & IPA-D6	PAG	25 °C	25	1.45	Inverse

9	o-xylene & o-xylene-D10	SPB-20	35-200 °C @ 8°C/min	30	2.70	Inverse
10	DMSO & DMSO-D6	IL111i	70- 170 °C (2 min) @ 8 °C/min	30	1.20	Normal
11	Pyridine & Pyridine-D5	IL111i	40-80 °C (2 min) @ 5°C/min	30	1.45	Normal
12	Tetrachloroethane & Tetrachloroethane-D2	SPB-20	60 °C	30	1.45	Inverse
13	DMF & DMF-D7	IL111i	70-170 °C @ 8°C/min	30	2.70	Normal
14	DMF & DMF-D1	IL111i	70 -150 °C @ 3°C/min	30	1.45	Normal
15	DMF-D1 & DMF-D7	IL111i	80-150 °C @ 5 °C/min	30	1.50	Normal
16	Benzene & Benzene-D6	SPB-20	30 °C	30	1.15	Inverse
17	Toluene & Toluene-D8	SPB-20	30 °C	30	2.40	Inverse
18	Acetone & Acetone-D6	β-DEX 120	25 °C	25	1.10	Inverse
19	Chloroform & Chloroform-D	PDMS-20	24 °C	20	0.70	Inverse
20	Nitromethane & Nitromethane-D3	PAG	40- 70@ 2°C	30	1.20	Inverse
21	THF & THF-D8	β-DEX 120	25 °C	25	1.20	Inverse
22	Phenol & Phenol-D5	IL111i	40-80 °C @ 5 °C /min	30	1.15	Normal
23	Benzylalcohol & Benzylalcohol- D7	SPB-35	60-150 @2 °C /min	25	2.00	Inverse
24	Benzylalcohol & Benzylalcohol- D5	IL111i	60-200 °C @ 2 °C/min	25	1.00	Normal
25	Benzylalcohol & Benzylalcohol- D2	SPB-20	50 °C	30	1.40	Inverse
26	Benzylalcohol-D7 & Benzylalcohol-D5	SPB-20	50 °C	30	1.40	Inverse
27	Benzylalcohol-D7 & Benzylalcohol-D2	IL111i	70 °C	30	0.95	Normal
	Pair of Isotopologues	Column	Temperature program (°C)	Average velocity (cm/s)	Resolution	Isotope effect
28	Benzylalcohol-D5 & Benzylalcohol-D2	IL111i	50-200 °C @1 °C/min	25	1.20	Normal
29	Ethyl Acetate & Ethyl acetate-D8	SPB-20	25 °C	25	2.40	Inverse
30	Cyclohexane & Cyclohexane-D12	SLB-5ms	30-60 °C @2 °C/min	25	2.55	Inverse
31	Hexane & Hexane-D14	SPB-20	25 °C	30	3.00	Inverse

32	Amphetamine & Amphetamine-D5	SPB-20	80-150 °C @3 °C/min	35	1.35	Inverse
33	MDA & MDA-D5 (MDA: 3,4-Methylenedioxy amphetamine)	SPB-35	80-220 °C @3 °C/min	35	1.40	Inverse
34	MDEA & MDEA-D5 (MDEA: 3,4-Methylenedioxy-N- ethylamphetamine)	SPB-35	130 °C	35	1.50	Inverse
35	MDEA & MDEA-D6	SPB-35	100-180 °C @ 2 °C/min	30	1.60	Inverse
36	Methamphetamine & Methamphetamine-D8	SPB-20	100-200 °C @5 °C/min	40	1.80	Inverse
37	Methamphetamine & Methamphetamine-D5	SPB-20	80-200 °C @3 °C/min	30	1.30	Inverse
38	Methamphetamine-D5 & Methamphetamine-D8	SPB-20	80 °C	30	0.90	Inverse
39	Methamphetamine-D6 & Methamphetamine-D8	IL111i	80-200 °C @3 °C/min	25	1.20	Normal
40	Methamphetamine-D5 & Methamphetamine-D6	IL111i	80-200 °C @3 °C/min	25	0.75	Normal
41	MDMA & MDMA-D5 (MDMA: 3,4-Methylenedioxy methamphetamine)	SPB-35	80-200 °C @2 °C/min	35	1.35	Inverse
42	Cocaine & Cocaine-D3	SPB-20	80-200 °C @3 °C/min	30	0.95	Inverse
43	Ephedrine & Ephedrine-D3	SPB-20	80-160 °C @1 °C/min	30	1.00	Inverse
44	Ibuprofen & Ibuprofen D3	SPB-50	150 °C	30	0.85	Inverse
45	Nicotine & Nicotine-D4	IL111i	80-200 °C @5 °C/min	25	1.10	Normal
46	L-Leucine & L-Leucine D3	PAG	100 °C	30	1.20	Inverse
47	L-Leucic acid & L-leucic acid D3	PAG	90 °C	30	1.10	Inverse

2.4.4 Isotope effects

It has been previously reported that heavier molecules (deuterium-labeled) elute earlier than the lighter ones in the case of weakly polar phases like squalane and the Ucon column [8]. This phenomenon is referred to as an inverse isotope effect. The situation where lighter isotopologues elute earlier than heavier ones is referred to as a normal isotope effect and has been

reported in the case of adsorption chromatography (gas-solid chromatography) and polar stationary phases [7, 8, 96].

Table 2.3 lists the isotope effect for each isotopologue pair. Figure 2.3 shows pie charts for the percent of each isotope effect on the 12 different stationary phases employed in this study. IL111i, the most polar stationary phase, showed a normal isotope effect in all cases (total separations = 21). IL60i showed a normal isotope effect in 66% of cases and an inverse isotope effect in 33% of cases (total separations = 9). Supelcowax and PAG columns showed inverse isotope effect in 80 and 92 % cases (Total separations=15 & 25 respectively). The polydimethylsiloxane-based stationary phases viz. Equity-1, SPB-5, SPB-20, SPB-35, SPB-50 exhibited an inverse isotope effect for almost all of the separations achieved on these stationary phases.

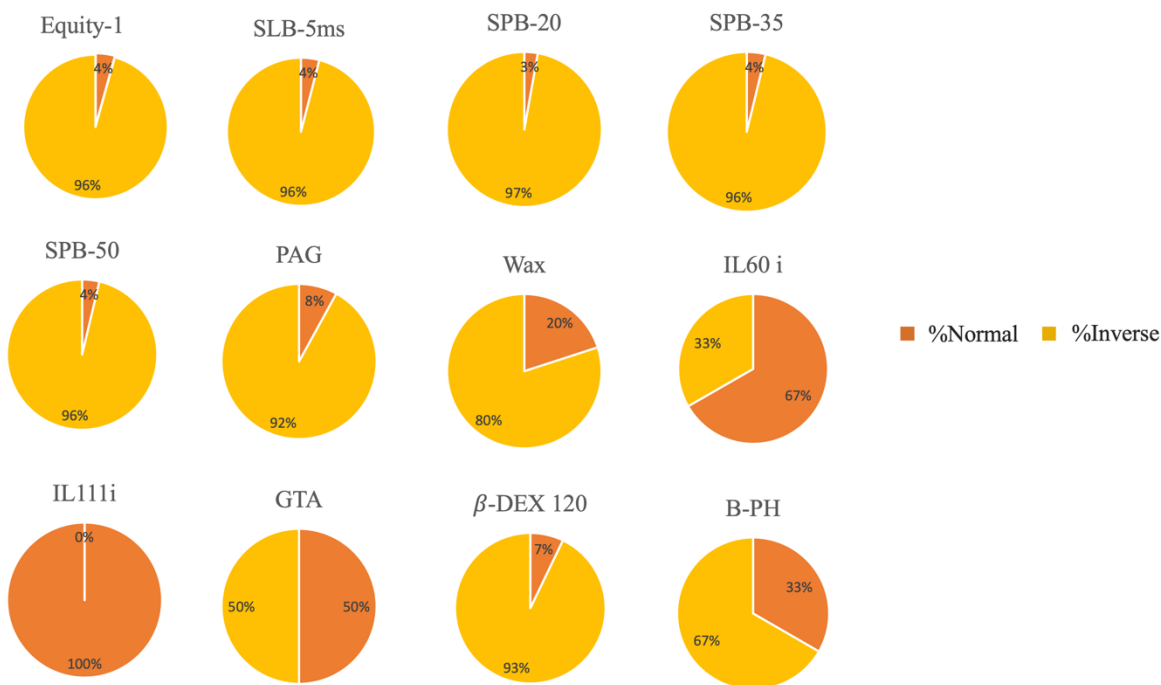


Figure 2.3. Percent isotope effects on various columns used in this study. Normal isotope effect: lighter isotopologues (non-deuterated) elute earlier than heavier (deuterated) isotopologues.

Inverse isotope effect: heavier isotopologues (deuterated) elute before the lighter (non-deuterated) isotopologues.

The fundamental reason for isotope effects lies with the mass difference in H and D atoms, which results in a shorter and stronger C-D bond as compared to a C-H bond [116]. The physical properties like polarity, polarizability, vapor pressure, and molar volumes are consequently different for molecules with different numbers of deuterium atoms. The deuterated (heavier) molecules have a lower molar volume, which manifests itself with lower dispersion forces [26]. In nonpolar or lower polarity stationary phases like the polydimethylsiloxane-based stationary phases used in this study, dispersion forces are predominant and control the separation. Consequently, the more deuterated molecules show less retention as compared to their protiated counterparts (or molecules with fewer deuterium atoms). Retention on the most polar stationary phases is largely a function of dipole-dipole, $n-\pi$, and hydrogen bonding interactions, which predominate over dispersion forces.

As the role of dispersion forces decreases, more normal isotope effects can be seen [7]. IL111i has a short C5 alkyl chain linkage as compared to IL60i, which has a C12 carbon chain linkage. Therefore, dispersion forces are less operative in IL111i, and a normal isotope effect is seen in 100% of the separations. On the other hand, IL60i showed a normal isotope effect in the majority of the cases owing to its polarity along with an inverse isotope effect in few cases (because of the dispersion forces exerted by the alkyl spacer chain). The chiral stationary phases, GTA, B-PH, and β -Dex120, showed 50%, 33%, and 7 % normal isotope effects, respectively. The reason for the dominance of the inverse isotope effect in β -Dex120 is that in this stationary phase, the

chiral moieties are dissolved in a phenyl-containing polydimethylsiloxane co-phase which constitutes a higher percentage of the stationary phase (80%).

A previous study on the effect of deuterium atoms on inverse isotope effect measured retention times of a small group of isotopologues on a 5% diphenyl-containing polydimethylsiloxane stationary phase [4]. This study showed that although the two deuterated ethyl benzenes each have five deuterium atoms, ethylbenzene-D₅_{aliphatic} elutes before ethyl benzene-D₅_{ring}, and they both elute before protiated ethylbenzene. An interesting example in our study that supports this finding involves benzyl alcohol-D₂_{aliphatic} and benzyl alcohol-D₅_{ring} (see Figure 2.S1 of the supporting information for structures). When injected separately, benzyl alcohol-D₂_{aliphatic} elutes before benzyl alcohol-D₅_{ring}, and they both elute before protiated benzyl alcohol. We normally expect the heavier isotope to elute earlier on polydimethylsiloxane-based stationary phases (inverse isotope effect) [26]. This shows that deuterium atoms on the aliphatic chain affect the inverse isotope effect more than those on the aromatic ring. While the difference in retention times of the two compounds is too small to show two resolved peaks (i.e., resolution ~ 0.3), by increasing the percentage of diphenyl moieties in the stationary phase, the two peaks elute slightly further from each other (see supporting information *Table 2.S13* for retention times on PDMS stationary phases). Also, a better resolution of the two peaks is achieved on more polar stationary phases like PAG and WAX (*Table 2.2*).

2.5 Conclusions

Deuterated compounds are finding a number of applications in non-traditional fields such as drug discovery, materials research and development, and analytical testing. Consequently, separations of deuterated compounds are of increasing importance. Among the polydimethylsiloxane stationary phases with phenyl content of 0%, 5%, 20%, 35%, and 50%, it

was observed that the stationary phase containing 20% phenyl content was the best performing of these related stationary phases in terms of having high resolutions with reasonable retention times. Besides polydimethylsiloxane-based stationary phases, an ionic liquid-based stationary phase, IL111i, and one specific polyalkylene glycol stationary phase, PAG performed remarkably well for the separations of deuterated compounds. Stationary phases in the upper polarity range displayed normal isotope effect rather than inverse isotope effect (which is commonly observed for low polarity polydimethylsiloxane-based stationary phases). It is noteworthy that the position of deuterium atoms plays an important role in separation selectivity and can result in unexpected retention orders in the case of the mixture of benzyl alcohol-D5 and benzyl alcohol-D2 on polydimethylsiloxane-based stationary phases. Overall, the best separations for all the studied isotopic compounds could be attained on either the IL111i, the PAG, or the SPB-20.

2.5 Supporting Information

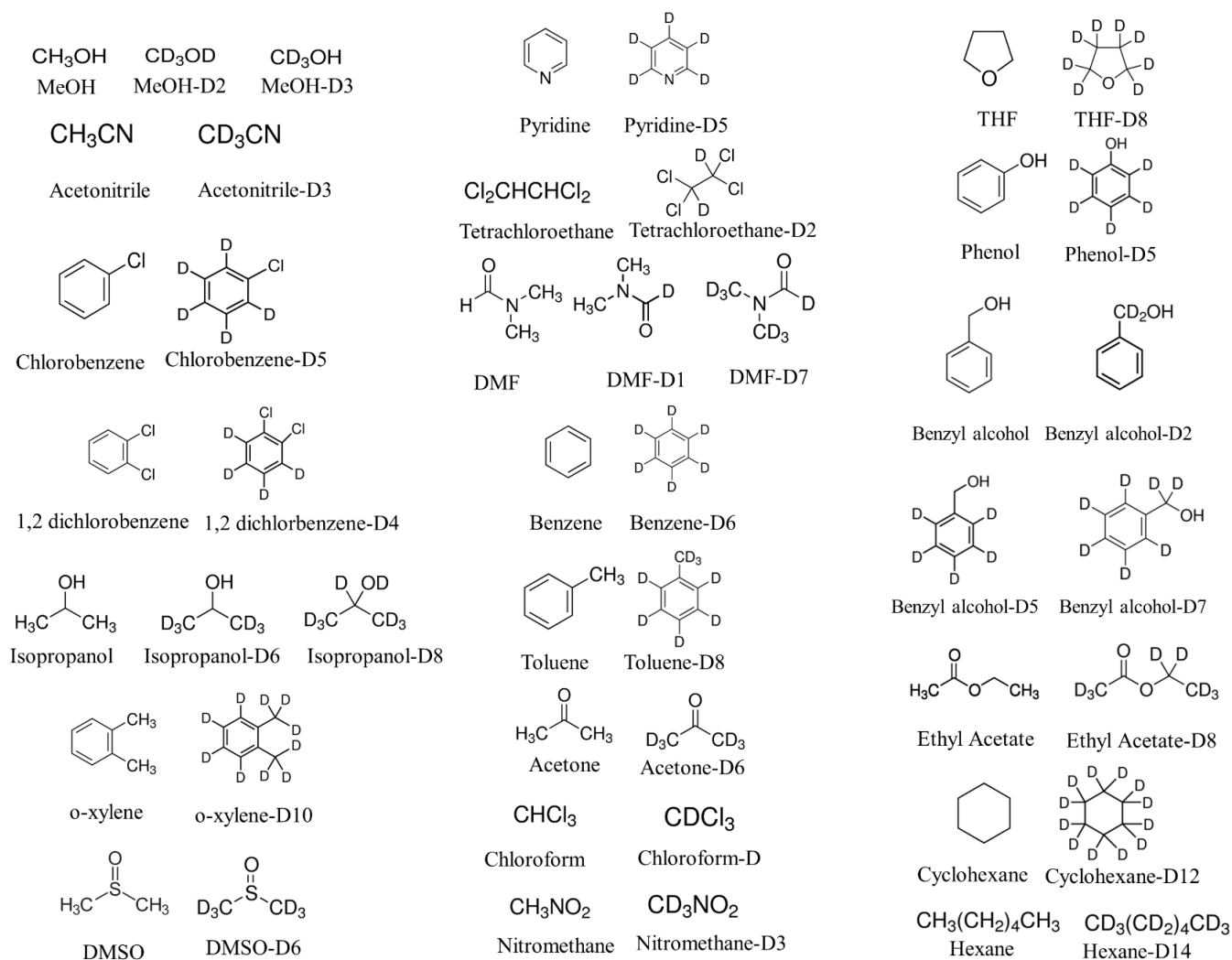


Figure 2.S1: Chemical structures of the solvents analyzed in the study.

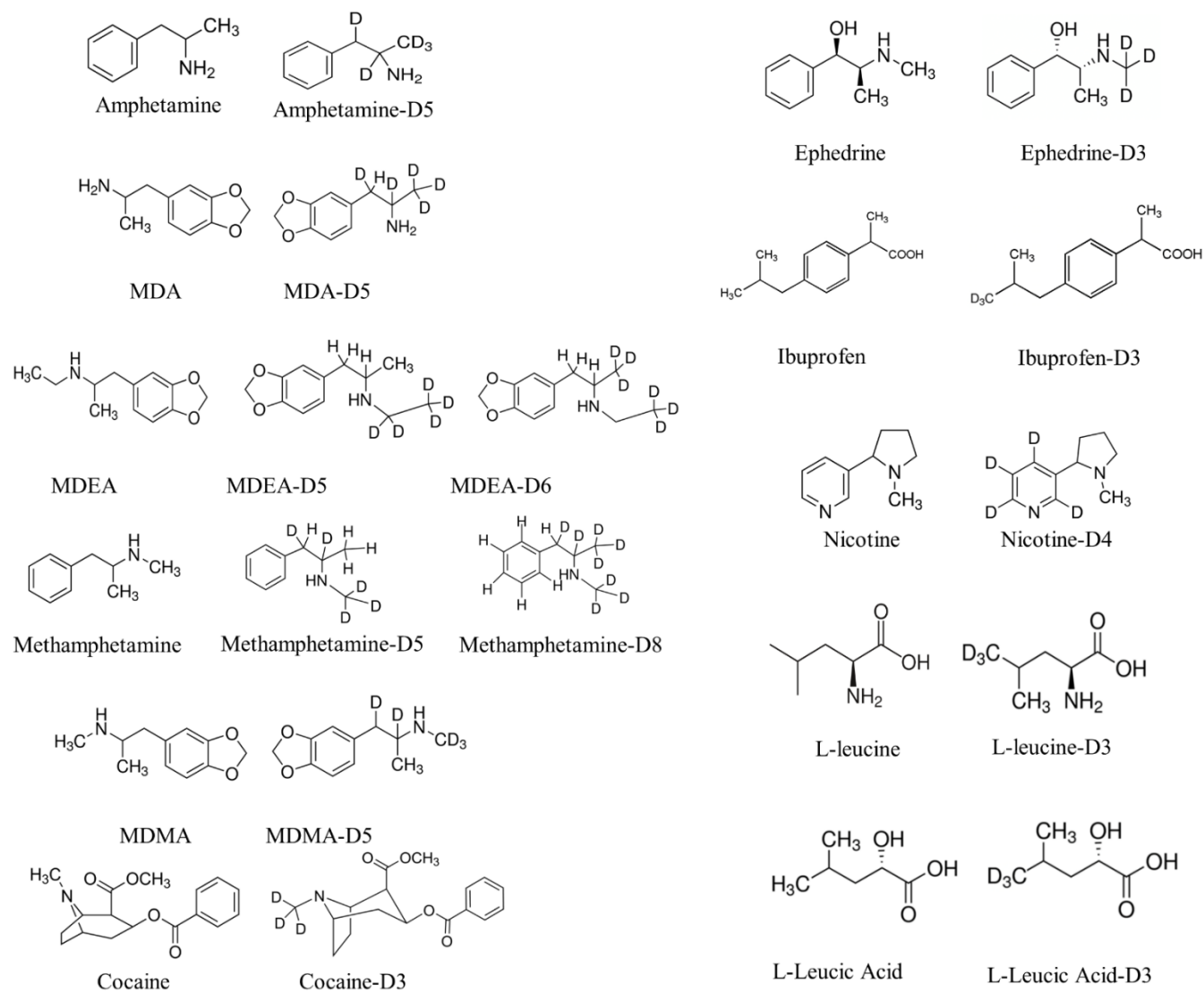


Figure 2.S2: Chemical structures of the drugs analyzed in the study.

Table 2.S1 Effect of % of phenyl in the stationary phase on retention times of benzyl alcohol-D5 and benzyl alcohol-D2. By increasing the phenyl percentage in stationary phase, polarity of the stationary phase will increase (Table1), and as a result the two peaks elute slightly further from each other)

% of phenyl in the stationary phase	Retention time of benzyl alcohol-D2 t_{R2} (minutes)	Retention time of benzyl alcohol-D5 t_{R5} (minutes)	$t_{R5}-t_{R2}$ (minutes)
0	28.58	28.60	0.011
5	29.36	29.37	0.017
20	48.27	48.30	0.022
35	64.36	64.43	0.070
50	84.19	84.27	0.081

Table 2.S2 Effect of % of phenyl in the stationary phase on chromatographic parameters of separation of phenol and phenol-D5.

%of phenyl in the stationary phase	Efficiency	Resolution	Selectivity
0	8400	0.56	1.009
5	9900	0.69	1.011
20	9200	0.81	1.013
35	4600	0.67	1.015
50	5400	0.7	1.016

Chapter 3

Effect of position of deuterium atoms on gas chromatographic isotope effects

3.1 Abstract

Deuterium substitution provides various benefits in drug molecules, including improvement in pharmacokinetic properties, reduction of toxicity, reduction of epimerization, etc. Also, it has been shown that the position of deuterium substitution affects the properties of drug molecules. Therefore, it is important to study low molecular weight deuterated isotopologues which constitute the deuterated pool and are building blocks of larger deuterated molecules. The effect of the position and number of deuterium atoms on the retention of 23 deuterated isotopologues on two gas chromatography stationary phases of different polarities was evaluated. It was observed that the ratio of calculated chromatographic isotope effect resulting from a deuterium atom connected to an sp^2 vs. an sp^3 hybridized carbon is more on the polar IL-111i stationary phase compared to the nonpolar PDMS-5, for each group of isotopologues. Also, a compound with a deuterium atom connected to an sp^2 hybridized carbon always had greater retention than the analogous compared where deuterium was connected to an sp^3 hybridized carbon. The van't Hoff plots for all analytes showed that the effect of entropy is almost negligible in the separation of deuterated vs. protiated isotopologues, thus these separations are enthalpy driven.

3.2. Introduction

Substitution of hydrogen with deuterium can alter the physicochemical properties of the deuterated molecules, including, but not limited to, higher molecular weights, stronger bonds, shorter bond lengths, and altered reaction kinetics. This can result in various benefits for deuterated drugs, including improvements in pharmacokinetic properties [13-15], reduction of toxicities [16-18], reduction of epimerization [19] and increases in drug stability [12, 20]; which can lead to increased efficacy, tolerability or safety [21]. In 2017, Deutetrabenazine (Austedo) was the first FDA approved deuterated drug. It is used for treatment of chorea associated with Huntington's disease [117]. Upon substitution of hydrogen with deuterium, a compound's 3D surface, shape, and steric flexibility remain. Therefore, deuterium-modified compounds usually retain biochemical potency and selectivity. Changes in selectivity are usually minor. However, there are some cases like Sildenafil-D5, which is two to three fold more selective than the protiated compound for phosphodiesterase V versus II and VI [12, 118]. It should be considered that the position of deuterium atom may affect drug safety in some cases, for example, with dapagliflozin, substitution of three deuterium atoms in the D3 analogue, lowers the production of a quinone methine metabolite, which is a side product with hepatotoxicity. However, having even more deuterium atom substitutions, i.e., the D5 analogue of dapagliflozin, did not lower the amount of the toxic metabolite compared to the D3 analogue [12, 119].

Deuterium labeled compounds are used to study reaction mechanisms through kinetic isotope effects, which are defined as the ratio of the reaction rate constants for C-H versus C-D bond cleavage. The kinetic isotope effects are categorized into primary and secondary effects. In primary kinetic isotope effects, the cleavage of C-D or C-H covalent bonds occurs during the rate limiting step [120]. The secondary kinetic isotope effect is produced upon changes in hybridization

(e.g., sp^3 to sp^2) or through involvement of hyperconjugation which might be favored or hindered by substitution of deuterium [121, 122].

There are two main approaches for the synthesis of deuterated compounds. First is the isotope exchange approach in which deuterium is inserted directly to the target molecule or on a late synthetic intermediate [12, 22]. The second approach involves conventional multistep syntheses that utilizes the “deuterated pool”, which consists of a collection of simple low molecular weight deuterium-labelled compounds that are used to synthesize the larger target analytes through a multistep route [12, 22]. Hence, it is important to develop separation methods for analysis of these deuterated building blocks.

The first separation of a deuterated hydrocarbon and its protiated counterpart (cyclohexane and cyclohexane-d12) using gas chromatography was published in 1957 [3].

Subsequently, additional studies were done on the separation of very limited numbers of deuterated compounds [4-8]. The most recent and comprehensive investigation was done by Thakur et al., which provided a guide for separation of 47 pairs of isotopologues on 12 different stationary phases. This study also investigated chromatographic isotope effects (CIEs), which are referred to as the change in the chromatographic retention order resulting from differences in the isotopic content of molecules [9].

One previous study discussed the apparent separation differences between deuterium substitutions on aliphatic vs. aromatic hydrocarbons [4]. Herein, we examine the CIE resulting from a deuterium atom connected to sp^2 hybridized carbon (sp^2 -CIE) versus the isotope effect resulting from a deuterium atom connected to sp^3 hybridized carbon (sp^3 -CIE) to show that the observed CIE is more generally, a function of carbon hybridization (e.g. aliphatic aldehydes, amides, etc.) and not directly the result of a compound's aromaticity.

In all, 23 deuterated isotopologues were investigated, with deuterium at different positions to evaluate the effect of deuterium substitution on chromatographic isotope effects. The effects of stationary phases' polarity and interaction parameters were investigated as well. An empirical approach to evaluate a compound's chromatographic isotope effects was devised.

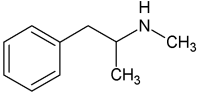
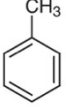
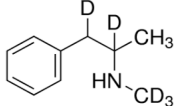
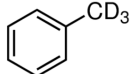
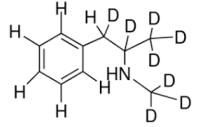
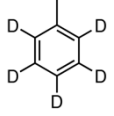
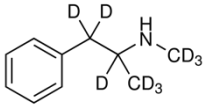
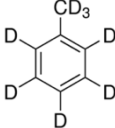
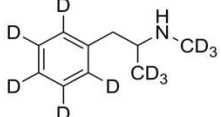
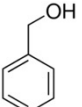
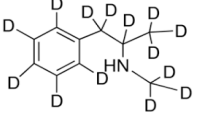
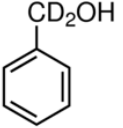
3.3 Experimental

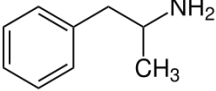
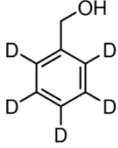
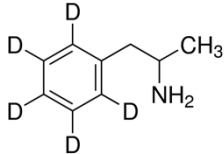
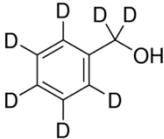
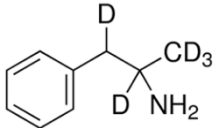
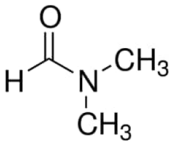
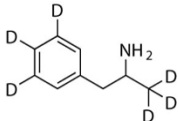
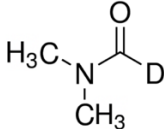
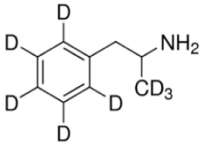
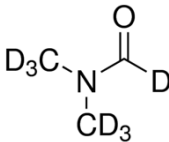
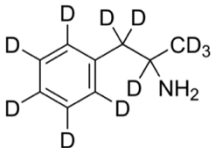
3.3.1. Reagents and materials

The non-deuterated and deuterated benzyl alcohol and N, N-dimethylformamide samples (listed in Table 3.1), and trifluoroacetic anhydride were purchased from MilliporeSigma (formerly Sigma- Aldrich, St. Louis, MO). The non-deuterated and deuterated amphetamine, methamphetamine, and toluene samples were purchased from Cambridge Isotope Laboratories, Inc. as 1 mg/ mL solutions (see Table 3.1 for structures). GC columns (PDMS-5 and IL111i) were provided by MilliporeSigma (Bellefonte, PA, USA). The PDMS-5 stationary phase is a bonded poly (5% diphenyl/95% dimethyl siloxane) phase (PDMS-5). The IL-111i stationary phase is a non-bonded 1,5-di(2,3-dimethylimidazolium) pentane bis (trifluoromethanesulfonyl) imide phase. The IL-111i stationary phase was picked since it has the highest polarity among commercial columns and it provides a wide variety of molecular interactions [123]. The stationary phases with lowest polarity were PDMS-5, PDMS-1 and squalane [123, 124]. PDMS5 was picked since it showed higher chromatographic resolution for separation of deuterated isotopologues in our previous study [9].

Table 3.1

List of compounds used in this study

Compound's name	Compound's structure	Compound's name	Compound's structure
1 Methamphetamine*		13 Toluene	
2 Methamphetamine-D5*		14 Toluene-D3	
3 Methamphetamine-D8*		15 Toluene-D5	
4 Methamphetamine-D9*		16 Toluene-D8	
5 Methamphetamine-D11*		17 Benzyl alcohol*	
6 Methamphetamine-D14*		18 Benzyl alcohol-D2*	

7	Amphetamine*		19	Benzyl alcohol-D5*	
8	Amphetamine-D5-sp ² *		20	Benzyl alcohol-D7*	
9	Amphetamine-D5-sp ³ *		21	N, N-Dimethylformamide	
10	Amphetamine-D6*		22	N, N-Dimethylformamide-D	
11	Amphetamine-D8*		23	N, N-Dimethylformamide-D7	
12	Amphetamine-D11*				

* Trifluoroacetylated

3.3.2 Derivatization experiments

Amphetamine, methamphetamine, and benzyl alcohol compounds were derivatized prior to analysis. For synthesis of trifluoroacetylated analytes, the methanol in 1 ml of 1000 ppm solution of analyte was evaporated. Then the sample was dissolved in 1 mL dichloromethane and 100 μ L of trifluoroacetic anhydride was added to the solution. The mixture was heated at 60 °C for 20 min. Afterwards, the solvent and excess reagent were evaporated with a stream of nitrogen gas and 1 mL of dichloromethane was added to make a ~100 ppm solution.

3.3.3 Methods

The samples were prepared in dichloromethane at ~100 ppm for analysis. Each group of isotopologues were injected in five different temperatures in triplicate. The temperature ranges were picked to give the minimum of 4 for partition coefficient values. The gas chromatographic analyses were performed on an Agilent 6850 (Agilent, Palo Alto, CA, USA) gas chromatograph equipped with a flame ionization detector. Analysis conditions were as follows: carrier gas: He, average velocity 30 cm/sec, split ratio: 20:1, inlet temperature: 250 °C, Detector (FID) temperature: 250 °C, injection volume: 1 μ L, column dimensions: 30 m x 0.25 mm x 0.25 μ m. The temperature settings are provided in Supplementary material (Table 3.S1). An Agilent ChemStation data processing unit was used for processing and storing the chromatograms.

3.4. Results and discussion

3.4.1 Isotope effects

Vapor pressure isotope effects (VPIEs) are determined by the ratio of the vapor pressures of two isotopic substances at a given temperature (or the logarithm of this ratio) [29, 125].

The VPIEs can be normal ($P_{\text{light}}/P_{\text{Heavy}} > 1$) or inverse ($P_{\text{light}}/P_{\text{Heavy}} < 1$) [30]. If the masses are equal, the less symmetrical substance is assigned to the numerator and the more symmetrical to the denominator [29]. Vapor pressure is determined mainly by energy of sublimation of the solid-like molecule, and secondarily, by its moment of inertia and molecular mass [126]. Therefore, the VPIEs are affected by the mass and the symmetry of the molecules as well as rotational and vibrational degrees of freedom of the bonds which can be affected by isotopic substitution [29, 43, 127, 128].

In chromatography, isotope effects (CIEs) are referred to as the change in the chromatographic retention order due to differences in the isotopic content of molecules [4, 7, 9, 26]. A normal CIE in chromatography refers to the case in which the heavier isotopologue elutes last. The inverse CIE effect occurs when the heavier isotopologue elutes first. The inverse isotope effect is observed for nonpolar stationary phases that interact predominantly via dispersive interactions, such as squalane and nonpolar polydimethyl siloxane-based stationary phases. By increasing the polarity of the stationary phase, which provides additional interactions, normal CIEs are observed. The most polar commercial GC stationary phase is the ionic liquid-based IL-111i, which almost always produces normal CIEs [7, 9, 26, 129]. The magnitudes of CIEs depend both on the analyte properties and the properties of the stationary phase [4, 7, 9, 26].

The question arises as to whether the VPIE can explain or show similar trends to the chromatographic isotope effect (CIE). For various isotopologues of water, the heavier

isotopologues have lower vapor pressures [130]. The measurement of enthalpy of vaporization for a group of isotopic pairs including toluene and toluene-D8 showed that the vapor pressure was more for the deuterated isotopologues (inverse VPIE) [131], while toluene and toluene-D8 show a normal CIE on the IL-111i stationary phase [9]. On the other hand, for benzene vs. benzene-D6, the heavier isotopologue has a higher vapor pressure (inverse VPIE) [126], and this pair showed inverse CIE on PDMS-5 stationary phase [9]. The aforementioned observations indicate that the VPIEs don't necessarily have a direct correlation with CIEs.

The stationary phases utilized in this study are IL-111i and PDMS-5. The PDMS-5, which is a polydimethylsiloxane based stationary phase, primarily relies on dispersive interactions for the separations. The IL-111i stationary phase is an ionic liquid-based stationary phase that has a much higher polarity compared to PDMS-5 [123]. However, a high polarity number cannot fully describe the type and magnitude of individual interactions possible since IL-111i provides a plethora of interactions, including π - π , n - π , dipole-dipole, dipole-induced dipole, hydrogen bond acceptor, hydrogen bond donor, and dispersive interactions. The magnitude of these interactions was determined previously for IL stationary phases using a linear solvation parameter model [9, 52, 132, 133]. In this study five groups of isotopologues were analyzed on IL-111i and PDMS-5 at six temperatures. Normal vs inverse isotope effects were investigated with a focus on the impact of the position of deuterium atoms on the magnitude of isotope effects. Table 3.1 shows the retention orders of analytes on the two different stationary phases. As expected, in almost all cases, compounds analyzed by IL-111i showed normal CIE and compounds analyzed by PDMS-5 showed inverse CIEs. These observations are explored in more detail in Section 3.4.

3.4.2 Effect of the location of deuterium atoms on isotope effects

Deuterium substitution changes the chromatographic retention of compounds. However, it is important to consider that the number of deuterium atoms is not the only factor influencing the retention order of deuterated isotopologues. In addition, the hybridization of the deuterated carbon atom (sp^2 vs. sp^3 hybridization) also has an important effect on CIEs. Figure 3.1 shows the chromatograms of amphetamine- $D5_{sp^2}$ vs amphetamine- $D5_{sp^3}$ which both have the same number of deuterium atoms but at different locations on the molecule, resulting in different elution behaviors. In Figure 3.2-A, the CIE of the amphetamine- $D5_{sp^2}$ is larger compared to amphetamine- $D5_{sp^3}$ with the polar ionic liquid IL-111i stationary phase. The opposite behavior is observed in Figure 3.2-B when a nonpolar polydimethylsiloxane stationary phase (PDMS-5) is used.

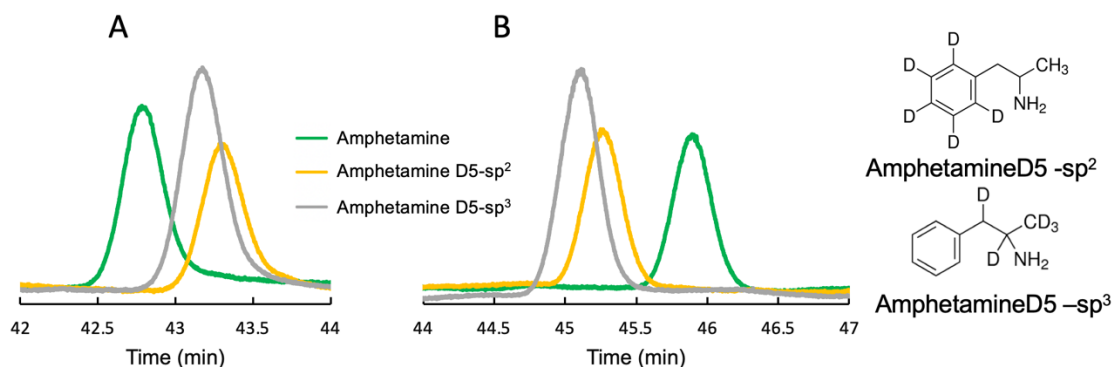


Figure 3.1 Chromatograms of trifluoroacetylated amphetamine isotopologues analyzed with the following conditions : A) Stationary phase: IL-111i, inlet T :250 °C, FID T: 250 °C, oven T: 130 °C, average velocity: 30 cm/sec, split ratio 20:1, injection volume: 1 μ L. B) Stationary phase: PDMS-5, inlet T :250 °C, FID T: 250 °C, oven T : 80 °C, average velocity: 30 cm/sec, split ratio 20:1, injection volume: 1 μ L

In order to understand the effect of the position of deuterium atoms in a variety of analytes, the plots of CIE vs temperature were obtained (see Figure 3.2 and Supplementary Figures 3.S2-3.S5). The isotope effect is presented as the difference between retention factor of each deuterated

isotopologue vs. its protiated counterpart. Figure 3.2 shows that in all cases by increasing the number of deuterium atoms the CIE increased. However, the magnitude of CIE resulting from deuterium substitution on sp^2 hybridized carbon atoms was different than that of deuterium substitution on sp^3 hybridized carbon atoms (sp^2 -CIE vs. sp^3 -CIE). The structures and CIE vs. temperature plots of all other compounds are provided in the Supplementary material (Figures 3.S1-3.S5).

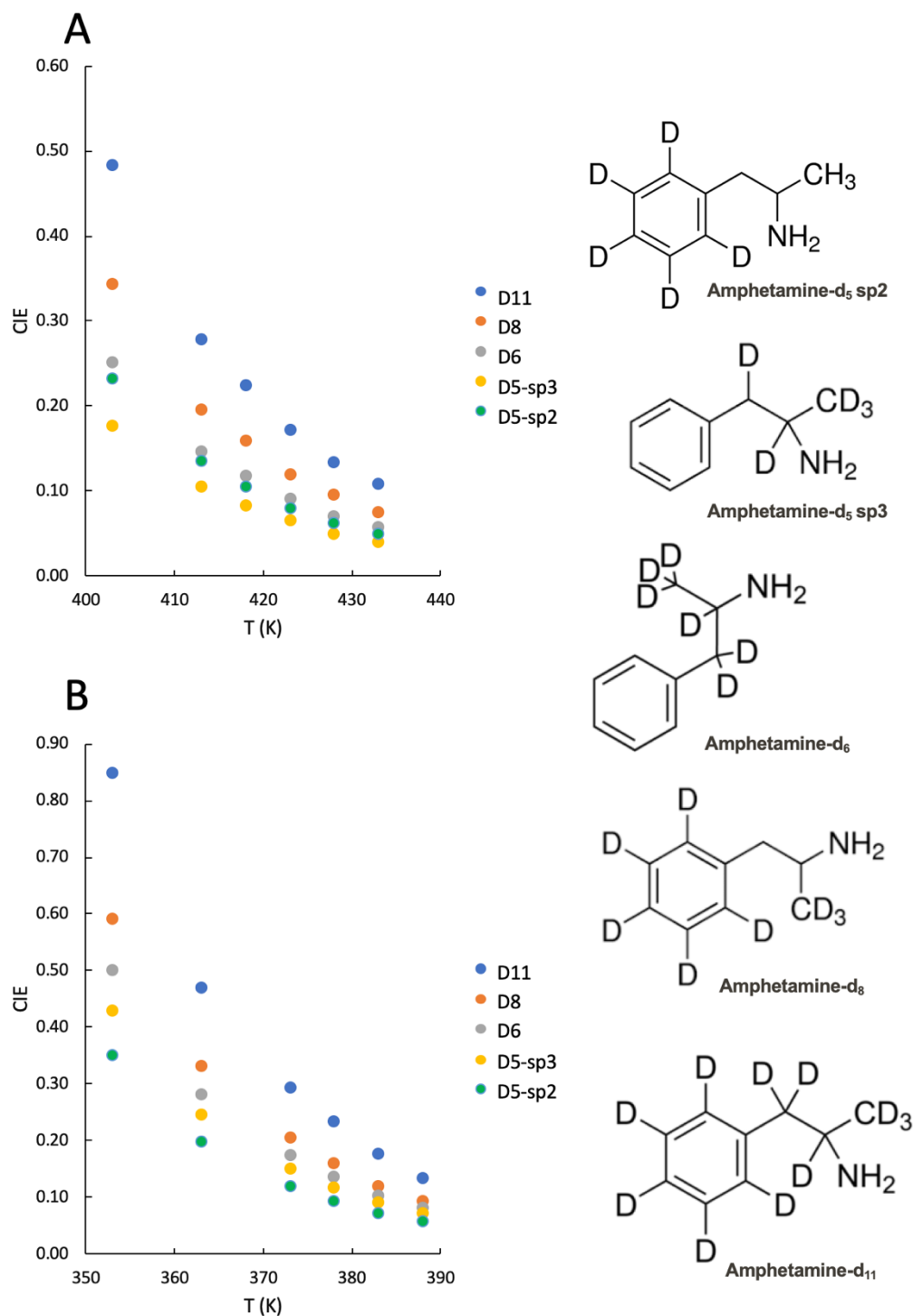


Figure 3.2 Chromatographic isotope effects, CIE (k_D-k_H for normal CIE and k_D-k_H for inverse CIE) vs. temperature plots for trifluoroacetylated amphetamine isotopologues. For chromatographic conditions see Experimental section 2.4. A) IL-111 (normal CIE), B) PDMS5 (inverse CIE)

3.4.3 Additivity of chromatographic isotope effects

Due to difficulties in obtaining and/or synthesizing certain deuterated compounds, the investigation of CIE of all possible iterations of deuterium atoms on different parts of molecules is not possible. For example, methamphetamine with 5 deuterium atoms only on the aromatic ring is not available. In order to calculate the contribution of each type of deuterium atom, we used the additivity of isotope effects, which was shown in 1993 by Shi et al. [4]. They reported that inverse isotope effects are additive, meaning that the summation of CIEs resulting from ethylbenzene-D_{5ring} and ethylbenzene-D_{5aliphatic} was equal to the CIE of ethylbenzene-D₁₀ [4].

In the current study of benzyl alcohol isotopologues, the sum of the CIEs of benzylalcohol-D₂ (two deuterium atoms connected to sp³ carbon) and benzylalcohol-D₅ (five sp² connected deuterium atoms) results in the same CIE value as the CIE of benzylalcohol-D₇ (two sp³ and five sp² connected deuterium atoms). As can be seen in Figure 3.3., this is true for both stationary phases used in this study, i.e., the polar IL-111i, and the nonpolar PDMS-5.

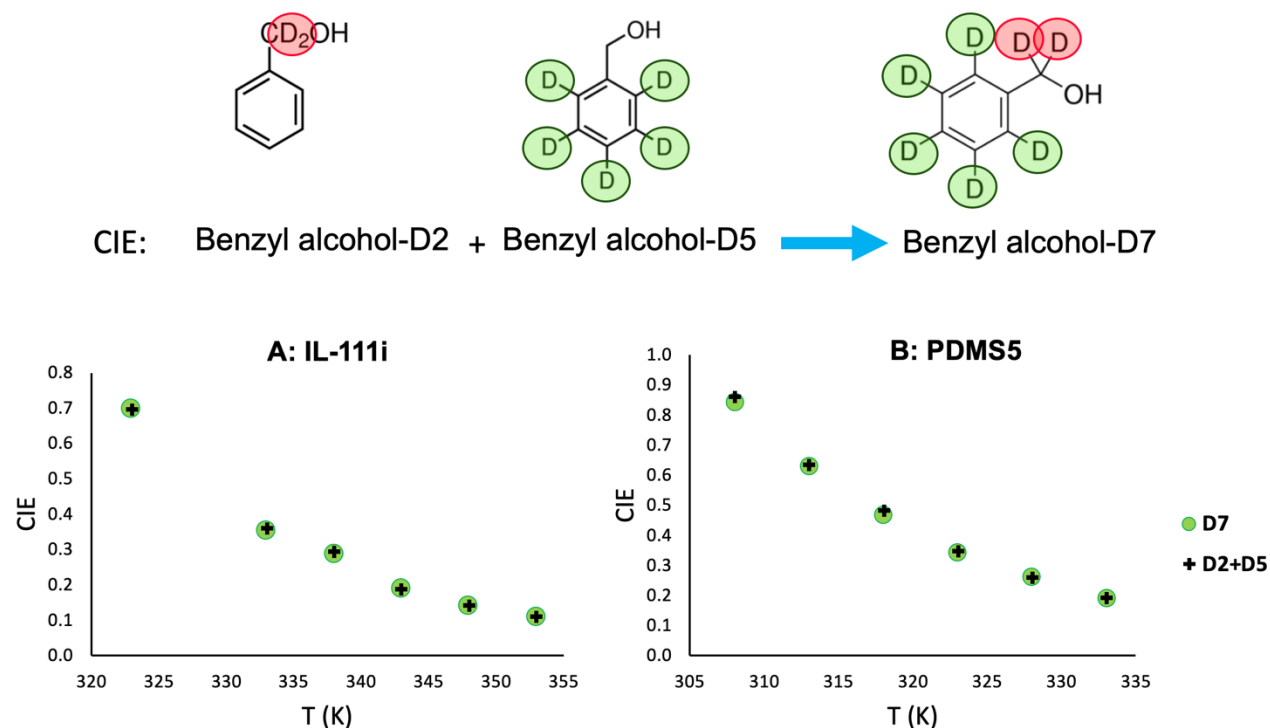


Figure 3.3 CIE vs T plots of benzyl alcohol isotopologues on A) IL-111i stationary phase and B) PDMS-5 stationary phase. The addition of CIEs of benzylalcohol-D2 with two deuterium atoms connected to sp^3 carbon and benzylalcohol-D5 with five sp^2 connected deuterium atoms is the same as the CIE of benzylalcohol-D7 with two sp^3 and five sp^2 connected deuterium atoms. This is true for both stationary phases.

Additionally, the same additive effect was observed for toluene, amphetamine, and methamphetamine isotopologues, see Supplemental Figures 3.S6-3.S8. Using this empirical property of isotope effects, Eq. (1) can be used to calculate the value of sp^2 -CIE for analytes that are not commercially available nor straightforward to synthesize.

$$\text{CIE} = N_{D, sp^2} \cdot X + N_{D, sp^3} \cdot Y \quad (1)$$

Where N_{D, sp^2} is the number of deuterium atoms connected to sp^2 hybridized carbons, N_{D, sp^3} is the number of deuterium atoms connected to sp^3 hybridized carbons, X is the sp^2 -CIE, and Y is the sp^3 -CIE.

For methamphetamine-D14 and methamphetamine-D9 we have the following equations:

$$\text{Methamphetamine D14: CIE} = 5X + 9Y \quad (2)$$

Methamphetamine D9: CIE= 9Y (3)

Therefore, by solving Eq. (3) and Eq. (4), X can be calculated for methamphetamine even though Methamphetamine-D5_{sp2} is not commercially available. The average values for sp²-CIE vs sp³-CIE for each group of compounds on each stationary phase were calculated and listed in Table 3.2. In Table 3.3, the relative magnitudes of the isotope effects are provided for all analytes on PDMS-5 and IL-111i.

Table 3.2

Retention orders and ratios of chromatographic isotope effects for each stationary phase.

Compound group	Stationary phase	Retention order	sp ² -CIE/ sp ³ -CIE (X/Y) ^a
Benzyl alcohol ^b	IL-111i	H<D2<D5<D7	5.0
	SLB 5ms	D7<D2≤D5<H	0.4
Toluene	IL-111i	D3~H <D5<D8	- ^c
	SLB 5ms	D8<D3<D5<H	0.4
DMF	IL-111i	H<D<D7	5.0
	SLB 5ms	- ^c	- ^c
Amphetamine ^b	IL-111i	H<D5sp3<D5sp2<D6<D8<D11	1.3
	SLB 5ms	D11<D8<D6<D5sp3<D5sp2	0.8
Methamphetamine ^b	IL-111i	H<D5<D8<D9<D11<D14	1.7
	SLB 5ms	D14<D11<D9<D8<D5<H	0.8

^a Ratio of calculated chromatographic isotope effect resulting from a deuterium atom connected to an sp² vs sp³ hybridized carbon. X is the sp²-CIE, and Y is sp³-CIE.

^b Derivatized with trifluoroacetic anhydride prior to analysis

^c Not calculated due to coelution.

Table 3.3

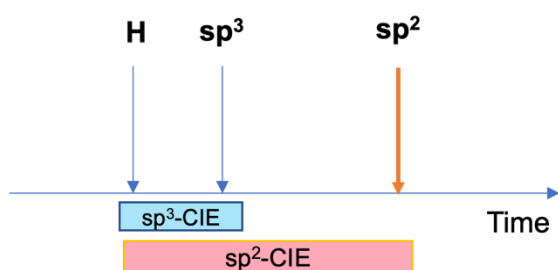
Comparison of magnitudes of isotope effects on PDMS-5 and IL-111i stationary phases.

Compound group	Normal CIE IL-111i	Inverse CIE PDMS-5
Toluene	D8>D5 (D3 shows inverse CIE)	D8>D3>D5
Benzyl alcohol ^a	D7>D5>D2	D7>D5>D2
Amphetamine ^a	D11>D8>D6>D5-sp2>D5-sp3	D11>D8>D6>D5-sp3>D5-sp2
Methamphetamine ^a	D14>D11>D9>D8>D5	D14>D11>D9>D8>D5
DMF	D7>D1	D7>D1

^a Derivatized with trifluoroacetic anhydride prior to analysis

It can be concluded from Tables 3.2 and 3.3 that for the IL-111i stationary phase, the sp²-CIE is more pronounced than the sp³-CIE, while with the PDMS-5 stationary phase, the opposite is true. Figure 3.4 illustrates the general trend for a pair of isotopomers (i.e. compounds with the same isotopic compositions but at different isotopic positions [134]). It shows that in both stationary phases, a compound with a deuterium atom connected to an sp² hybridized carbon retains longer than the analogous compound with a deuterium atom connected to an sp³ hybridized carbon. It also shows that with the polar IL-111i and nonpolar PDMS-5 stationary phases normal and inverse CIEs are observed, respectively.

Normal isotope effect (IL-111i)



Inverse isotope effect (SPB-5)

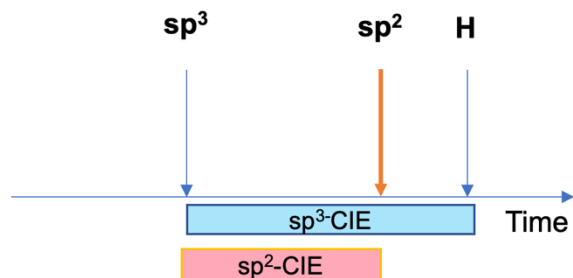


Figure 3.4 The general trend relation between chromatographic isotope effect (CIE) and retention for a pair of isotopomers (i.e. compounds with the same isotopic compositions but different positions of isotopes). Even though the sp^2 -CIE is more on IL-111 and less on PDMS-5 stationary phases, a deuterium connected to an sp^2 carbon (the rigid part of the molecule) results in more retention compared to when connected to an sp^3 carbon with more rotational degrees of freedom.

The results also show that substitution of deuterium on the rigid and planar part of the molecule results in more retention compared to when the deuterium atom is connected to an sp^3 hybridized carbon which have more rotational degrees of freedom. Rotational and vibrational degrees of freedom and the symmetry of a molecule can affect its vapor pressure [29, 43, 127, 128]. However, as mentioned previously, despite the relation of VPIEs and the number and position of deuterium atoms, the CIEs are not directly correlated to the relative vapor pressures, thus more factors are needed to account for chromatographic observations.

3.4.4 Factors that affect deuterated analyte-stationary phase interactions

The location of an isotopic atom (i.e. deuterium in this study) within a compound not only affects its vapor pressure, but also all other solute-stationary phase interactions. These interactions (and thus CIEs) can be influenced through combinations of the following: a) molar volume (C-D bond is shorter than C-H bond), b) inductive influence (D is less electronegative than H), c)

resonance destabilization (C-D bond is stronger and electrons are more difficult to delocalize into its antibonding orbital than for C-H bond) [31-33, 135, 136].

An important factor affecting gas chromatographic interactions is the molar volume effect. The shorter C-D vs. C-H bonds results in lower molar volumes for deuterated compounds compared to their protiated counterparts [31-33]. A lower molar volume results in lower dispersion forces for deuterated compounds. Therefore, deuterated isotopologues are less retained on nonpolar stationary phases such as the polydimethyl siloxane-based phases where dispersion interactions with the stationary phase control retention [4, 7, 9, 26].

When deuterium substitution was on an sp^2 hybridized carbon (e.g. on an aromatic ring or a carbonyl group, as for aldehydes) the reduction of retention relative to protiated compounds (or inverse CIE) was less than that observed for deuteration on an sp^3 part of the molecule for polar and nonpolar stationary phases (see Table 3.2). Deuteration on an aromatic ring leads to an apparent accession of electrons to the ring due to inductive effects [34, 136, 137]. This leads to stronger π - π , dipolar, and dispersive interactions with stationary phases that provide each interaction and longer retention for analytes that have deuteration on the sp^2 part of the molecule. The longer retention of sp^2 -connected deuterium compared to sp^3 -connected deuterium was more prominent for the polar IL-111i stationary phase. This could be due to presence of the strong cation- π interactions, that can have relatively high binding energy (from 10 to 30 kcal/mol) [138]. That is why in Figure 3.4, the sp^2 -CIE is more prominent than sp^3 -CIE in IL-111i (although both provide normal CIEs).

A combination of inductive and resonance effects (reduced hyperconjugative stabilization) has been used to explain the reduced acidity in a group of deuterated aromatic and aliphatic carboxylic acids [34, 136, 139, 140]. It was postulated that the hydrocarbon moiety acquired

substantial negative charge through inductive effects (deuterium being more electropositive than hydrogen) [141]. Also, due to different dipole moments of the C-D vs C-H bonds, deuterium could be an effective electron donor inductively which results in reduced acidity [142, 143]. Also, it was indicated that the difference in dipole moments of the C-D vs C-H bond was 0.0001 Debye and that this small difference could not account for the magnitude of the observed changes in acidity or basicity of the analytes upon deuteration [144-146]. Additionally, since C-D bonds are stronger, the delocalization of lone pairs of electrons into their σ^* orbital is less pronounced leading to poor stabilization of negative charges and reduced acidity [135, 143, 144]. The same effect is responsible for increased basicity of amines that are deuterated in the β position to the nitrogen atom [145, 146]. By changing the electron distribution and dipolarity of a molecule, the dipolar interactions with the stationary phase will change accordingly.

As shown in Figure 3.4 and Tables 3.2 and 3.3, the IL-111i produces normal isotope effects which can be rationalized through increased hydrogen bonding, π - π , and cation- π interactions upon deuteration. These interactions are enhanced through inductive electron donation of deuterium [34]. Deuteration on the side chain also can increase the electron density of the carbonyl through inductive effects and improve hydrogen bonding and π - π interaction of the carbonyl with the IL-111i stationary phase depending on the distance between the deuteration site and the π -system. See Figures 3.S7-3.S11 in Supplementary material.

In our study, when toluene isotopologues were analyzed on the IL-111i stationary phase, toluene-D₃ essentially coeluted with protiated toluene. It was shown that CD₃ lowers the electron accession to the ring due to the accumulative resonance and inductive effects [136, 137, 139, 147, 148]. Therefore, the sp^3 -CIE will manifest as a reduced retention of toluene-D₃ and coelution with protiated toluene due to combination of molar volume effect and hyper conjugative and inductive

effects. For toluene-D5 with the IL-111i, the normal sp^2 -CIE had a bigger magnitude since it results from increased cation- π and π - π interactions. The CIE values for toluene-D5 on PDMS-5 showed that deuteration on the ring resulted in a smaller inverse CIE compared to deuteration on the methyl group in toluene-D3. See Table 3.2.

It should be noted that in Table 3.2, the sp^2 -CIE/ sp^3 -CIE was lower for derivatized amphetamine and methamphetamine isotopologues (which are trifluoroacetamides) compared to DMF isotopologues and derivatized benzyl alcohol isotopologues (which are trifluoroethyl acetates). The ^{13}C NMR chemical shifts support this effect. Amide carbonyls vs ester carbonyls showed that the amide shifts were downfield by 2-3 ppm [149]. Also, ^{13}C NMR chemical shifts showed that the carbonyl carbon's chemical shift is higher for trifluoroacetamide compared to trifluoro ethyl acetate and dimethyl formamide [150]. This indicated that the carbonyl carbon was deshielded and therefore carbonyl oxygen had higher electron density for trifluoroacetamide. This could improve the hydrogen accepting ability of the carbonyl group in the trifluoroacetylated amphetamine and methamphetamine isotopologues to an even greater extent compared to trifluoroacetylated benzyl alcohols.

It should be noted that six deuterium atoms in methyl groups connected to the nitrogen of DMF compounds produced a small normal CIE compared to a single deuterium connected to the carbonyl carbon (see Tables 3.2 and 3.3). The interactions of the sp^2 hybridized part of the molecule with the IL-111i stationary phase are hydrogen bonding, π - π , and cation- π interactions. The deuterium connected to the carbonyl can be inductively electron donating. Also, n - σ^* delocalization (from carbonyl oxygen to σ^* of C-D/C-H bond) is more difficult for a C-D than for a C-H bond [143]. Therefore, the carbonyl bond receives more electron density from CD vs CH bond and interacts more strongly through cation- π and π - π interactions as well as

hydrogen bonding. In the sp^3 hybridized part of the molecule, the CD_3 moieties connected to nitrogen produce a much smaller normal CIE indicating a smaller increase in interactions with the IL-111i stationary phase (see Table 3.2).

3.4.5 van't Hoff studies

In order to understand the thermodynamic effects on isotopic analyte separations, plots of $\ln K$ vs $1/T$ (van't Hoff plots) were done to obtain ΔH° (from the slope of the plots) and ΔS° (from intercept of the plots) as per Eq. (4).

$$\ln K = \frac{-\Delta H^\circ}{RT} + \frac{\Delta S^\circ}{R} \quad (4)$$

The thermodynamic parameters reported in Table 3.2 include $\Delta(\Delta H^\circ)$, which is obtained from the difference between enthalpy values of the protiated analyte versus deuterated analyte ($(\Delta H^\circ)_H - (\Delta H^\circ)_D$) and $\Delta(\Delta S^\circ)$, which is equal to the difference between entropy values of the protiated analyte versus deuterated analyte ($(\Delta S^\circ)_H - (\Delta S^\circ)_D$).

The negative $\Delta(\Delta H^\circ)$ values refer to inverse isotope effects. Therefore, the enthalpy for a deuterated compound is larger compared to the protiated compound ($|(\Delta H^\circ)_H| < |(\Delta H^\circ)_D|$). Consequently, for normal isotope effects $|(\Delta H^\circ)_H| > |(\Delta H^\circ)_D|$. For analytes where the $\Delta(\Delta H^\circ)$ and $\Delta(\Delta S^\circ)$ values do not equal zero and show a temperature dependence, compensation temperatures (T_{iso}) can be defined as the temperature at which the $\Delta(\Delta G^\circ)$ becomes zero which means that the selectivity value will become one (i.e. $\alpha=1$) and no separation will be possible [151]. In enantioselective GC, T_{iso} is the temperature in which enantiomeric resolution becomes zero [109]. T_{iso} can be calculated as follows [109]:

$$\Delta(\Delta G^\circ) = \Delta(\Delta H^\circ) - T(\Delta(\Delta S^\circ)) \quad (6)$$

$$\text{If } \Delta(\Delta G^\circ) = 0; T_{\text{iso}} = \Delta(\Delta H^\circ) / \Delta(\Delta S^\circ) \quad (7)$$

The calculated T_{iso} values for each deuterated analogue vs the protiated counterpart are listed in Table 3.2. DMF-D7 was the only analyte that had T_{iso} within our analysis temperature ranges. For temperature ranges of other analyte groups see Table 3.S1. It was observed that in most cases the effect of entropy on these separations was negligible and the partition equilibria were enthalpy driven (Table 3.4).

Table 3.4

van't Hoff parameters calculated for five groups of isotopologues. $\Delta(\Delta H) = (\Delta H)_{\text{H}} - (\Delta H)_{\text{D}}$ and $\Delta(\Delta S) = (\Delta S)_{\text{H}} - (\Delta S)_{\text{D}}$

Compound Name	IL-111i			PDMS-5		
	$\Delta(\Delta H^\circ)^{a,b}$ cal/mol	$\Delta(\Delta S^\circ)^c$ cal/mol. K	T_{iso} °C	$\Delta(\Delta H^\circ)^{a,b}$ cal/mol	$\Delta(\Delta S^\circ)^c$ cal/mol. K	T_{iso} °C
DMF-D7	330	0.72	183	355	1.14	42
DMF-D1	20	0.00	NA	70	0.20	83
DMF	0	0.00	NA	0.0	0.00	NA
Toluene-D8	45	0.08	281	-30	0.00	NA
Toluene-D5	40	0.06	357	-5	0.00	NA
Toluene-D3	5	0.20	239	-25	0.00	NA
Toluene	0	0.00	NA	0.0	0.00	NA
Benzyl alcohol-D7	40	0.06	321	-20	0.00	NA
Benzyl alcohol-D5	45	0.08	268	-10	0.00	NA
Benzyl alcohol-D2	0	0.00	NA	-15	0.00	NA
Benzyl alcohol	0	0.00	NA	0.0	0.00	NA
Amphetamine-D11	25	0.00	NA	-30	0.00	NA
Amphetamine-D8	30	0.00	NA	-25	0.00	NA
Amphetamine-D6	15	0.00	NA	-15	0.00	NA
Amphetamine-D5A	15	0.00	NA	-11	0.00	NA
Amphetamine-D5R	25	0.00	NA	-11	0.00	NA
Amphetamine	0.0	0.00	NA	0.0	0.00	NA

Methamphetamine-D14	65	0.10	396	-35	0.00	NA
Methamphetamine-D11	50	0.08	396	-35	0.00	NA
Methamphetamine-D9	35	0.06	396	-35	0.00	NA
Methamphetamine-D8	25	0.02	375	-30	0.00	NA
Methamphetamine-D5	15	0.00	NA	-20	0.00	NA
Methamphetamine	0	0.00	NA	0.0	0.00	NA

^a The negative $\Delta(\Delta H^\circ)$ values refer to inverse isotope effect. Therefore, $|(\Delta H^\circ)_H| < |(\Delta H^\circ)_D|$ (since ΔH° values were always negative). Accordingly, for normal isotope effects: $|(\Delta H^\circ)_H| > |(\Delta H^\circ)_D|$.

^b The experimental error for $\Delta(\Delta H^\circ)$ values was 5 cal/mol.

^c The experimental error for $\Delta(\Delta S^\circ)$ values was 0.02 cal/mol.K.

3.5 Conclusions

The position of deuterium atoms on isotopologue separations is of importance because it can change the properties of a deuterated analyte, e.g. safety of deuterated drugs. The position of deuterium atom on a deuterated compound can also affect its chromatographic retention. The observed chromatographic isotope effects on IL-111i and PDMS-5 stationary phases were normal and inverse, respectively in almost all cases. It was observed that the deuterium atom connected to sp^2 hybridized carbon resulted in larger chromatographic isotope effects as compared to when connected to an sp^3 hybridized carbon on a polar stationary phase like IL-111i. On the other hand, compared with sp^2 -connected deuterium atoms results in a smaller isotope effect than a deuterium atom connected to an sp^3 hybridized carbon on a non-polar stationary phase like PDMS-5. On both stationary phases, the compound with sp^2 -connected deuterium atoms was retained longer than the analogous compound with sp^3 -connected deuterium atoms. The thermodynamic studies showed that the separations of these deuterated isotopologues seem to be mostly enthalpy driven.

3.6 Supporting information

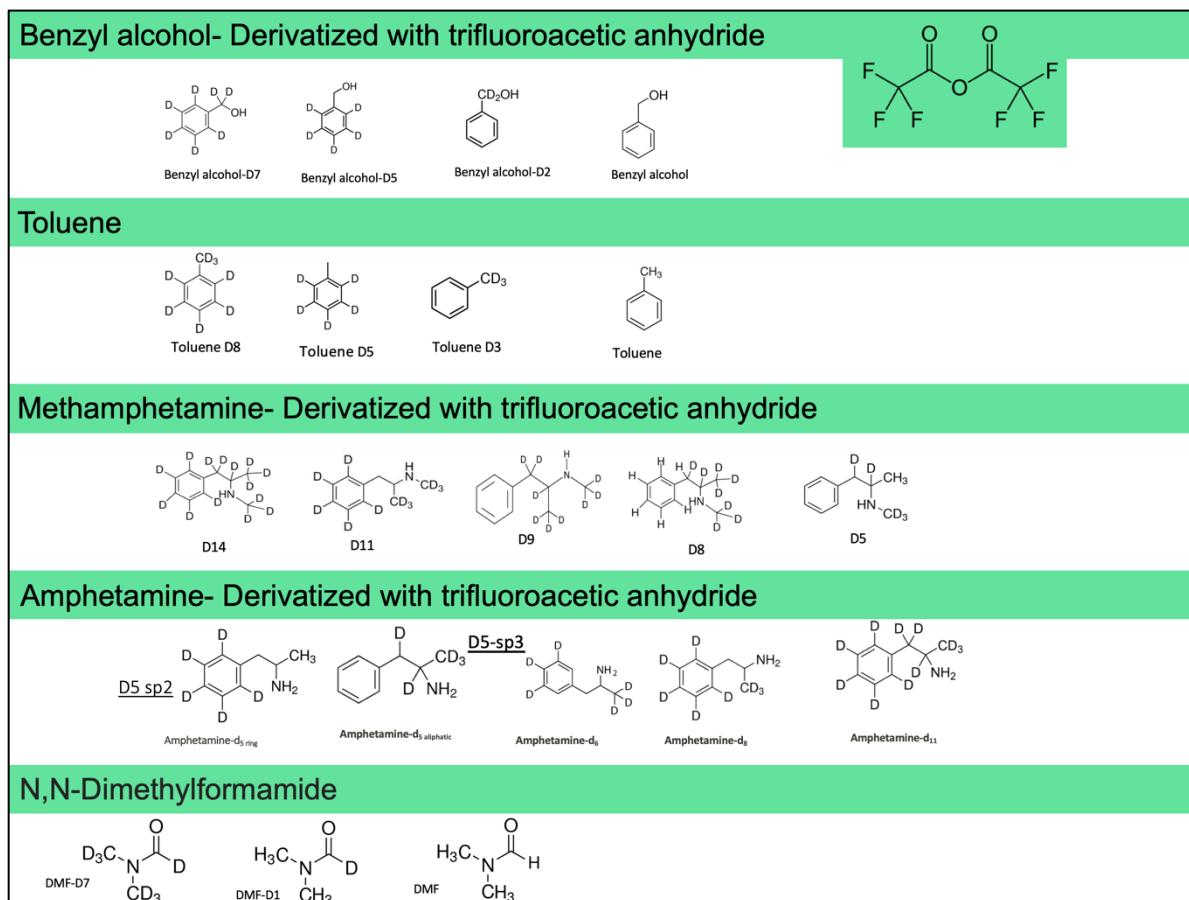


Figure 3.S1 Structure of the analytes

Table 3.S1 Temperature settings

Compound group	Temperatures tested (° C)	
	IL-111	SLB-5ms
Benzyl alcohol	50,60,65,70,75,80	35,40,45,50,55,60
Toluene	30,35,40,45,50,55	25,30,35,45,55,65
N,N-Dimethylformamide	85,90,95,100,105,110	25,30,35,40,45,50
Amphetamine	130,140,145,150,155,160	80,90,100,105,110,115
Methamphetamine	120,130,135,140,145,150	90,100,105,110,115,120

Isotope effect vs T plots (Figures S2-S5)
IE shown in IL-111 is normal and is inversed in PDMS-5

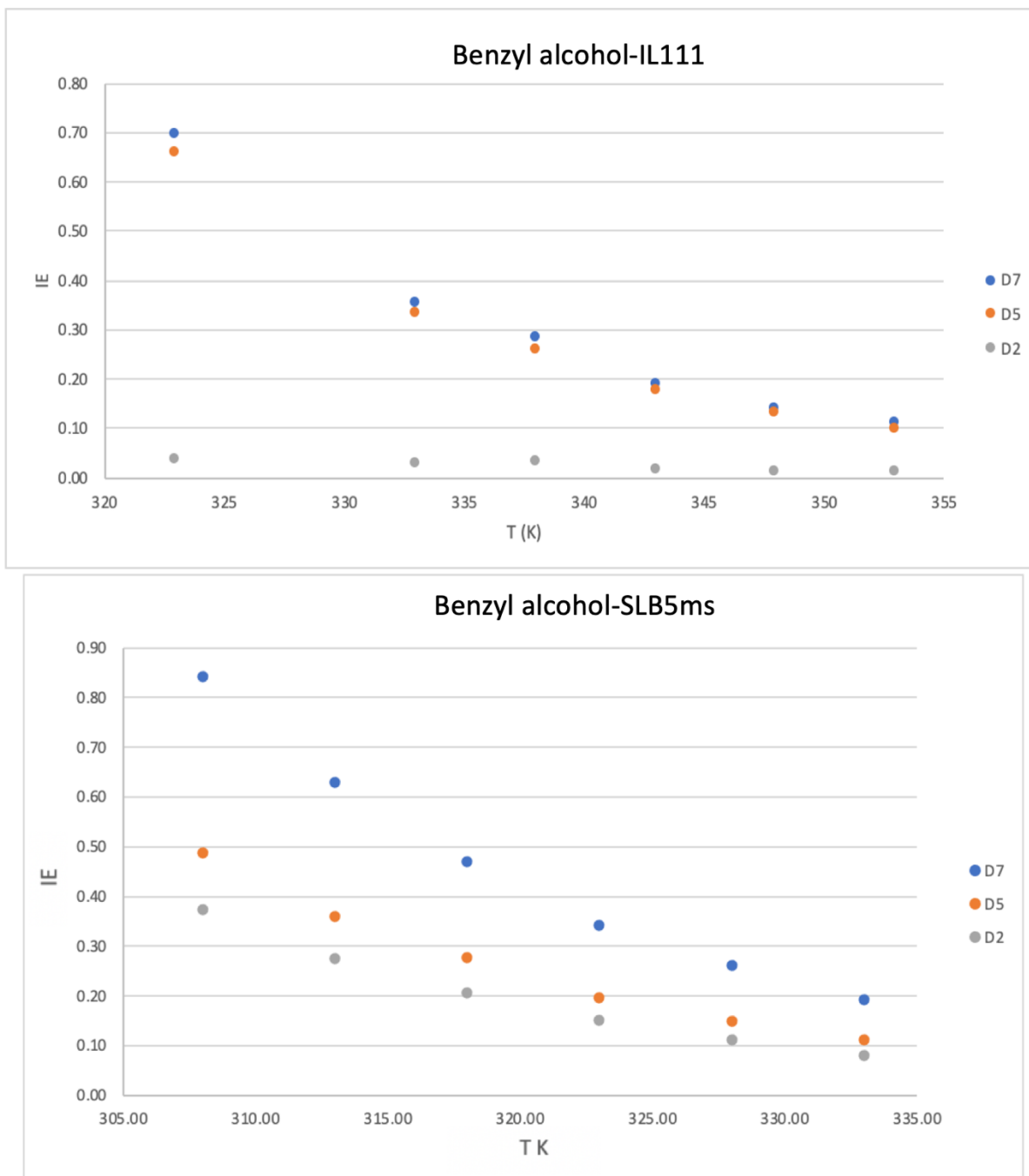


Figure 3.S2

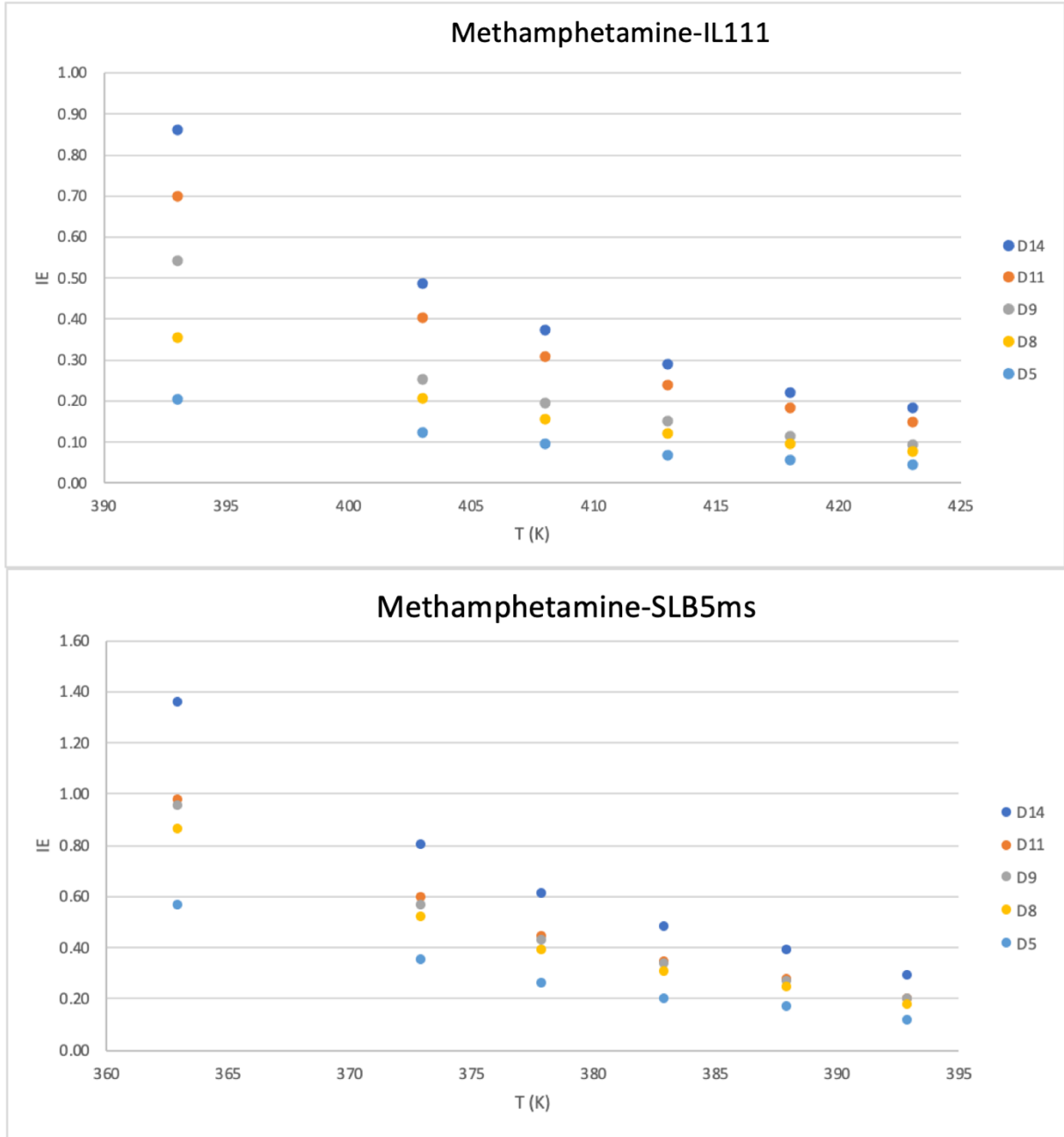


Figure 3.S3

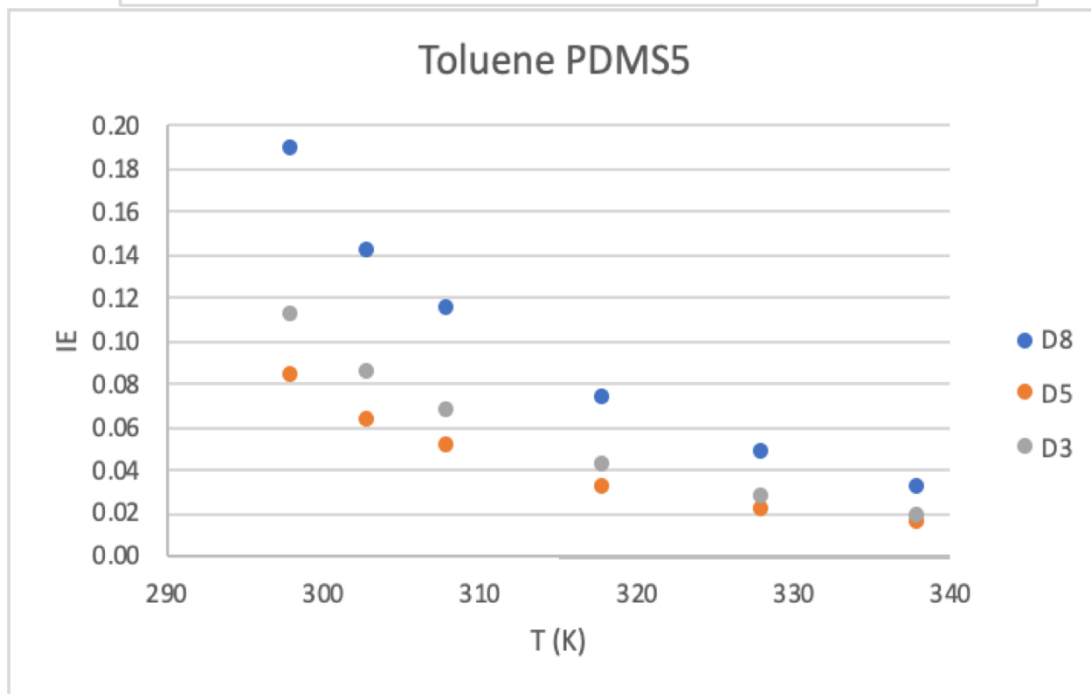
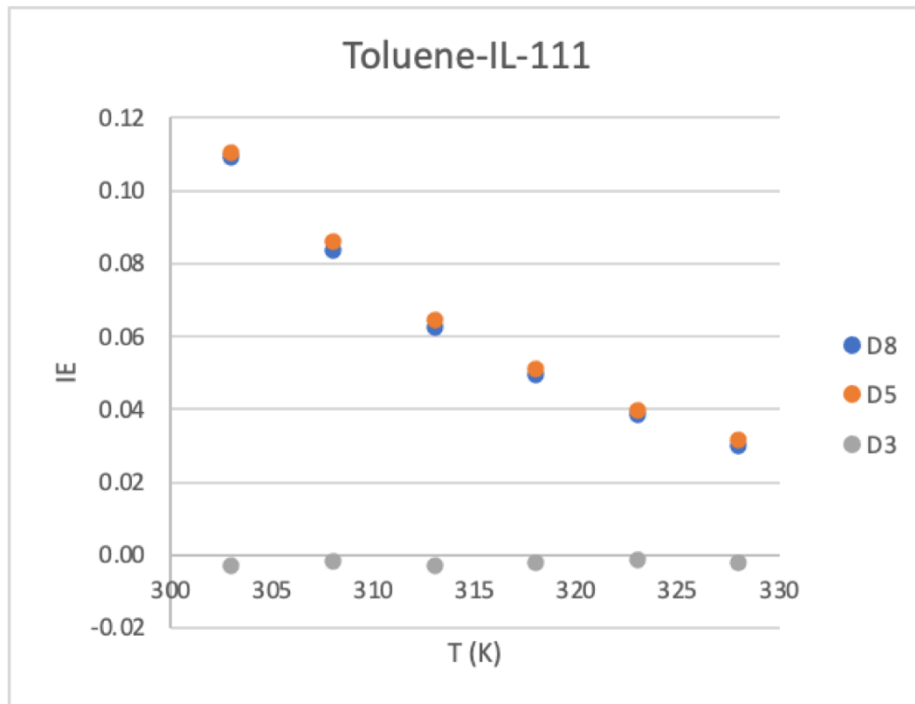


Figure 3.S4

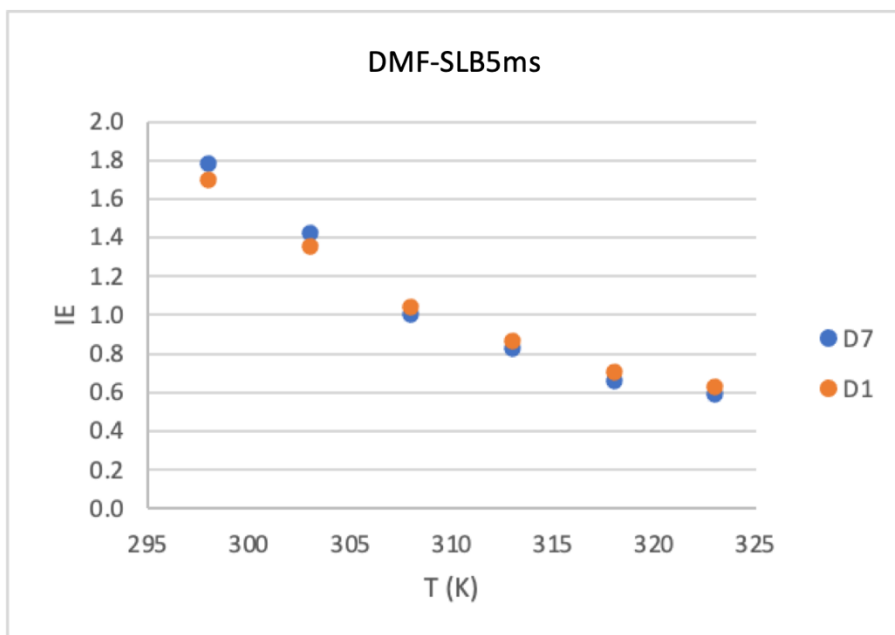
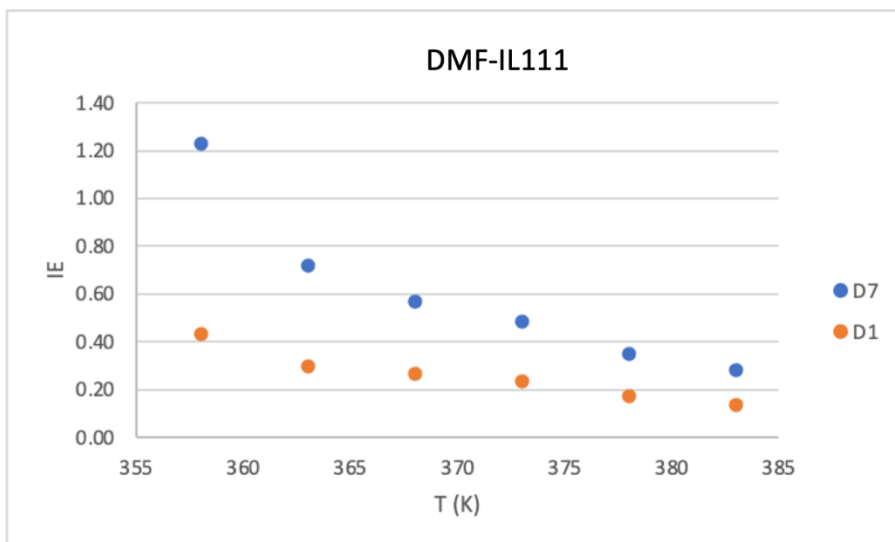


Figure 3.S5

Additivity plots (Figures S6-S8)

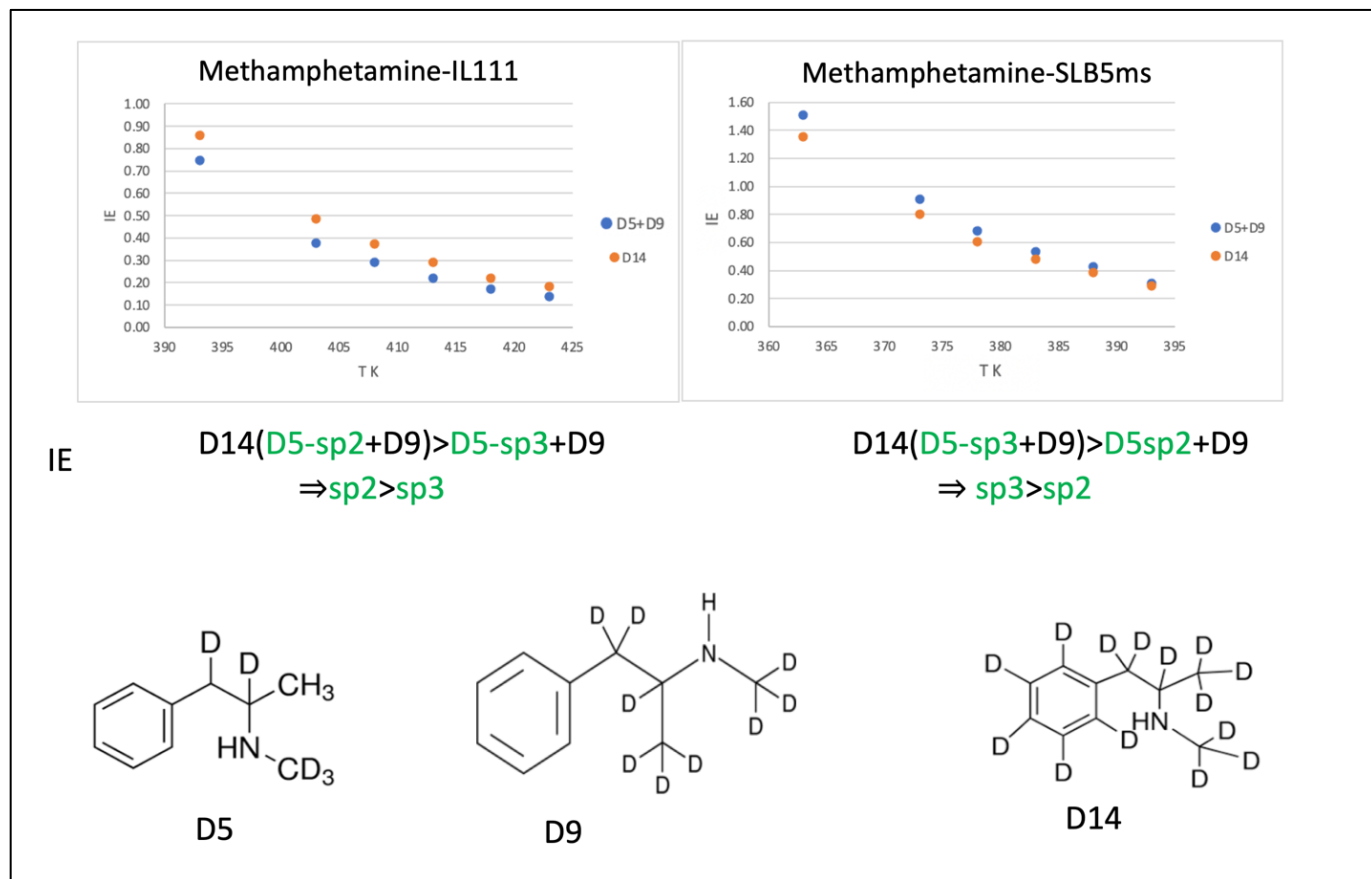


Figure 3.S6

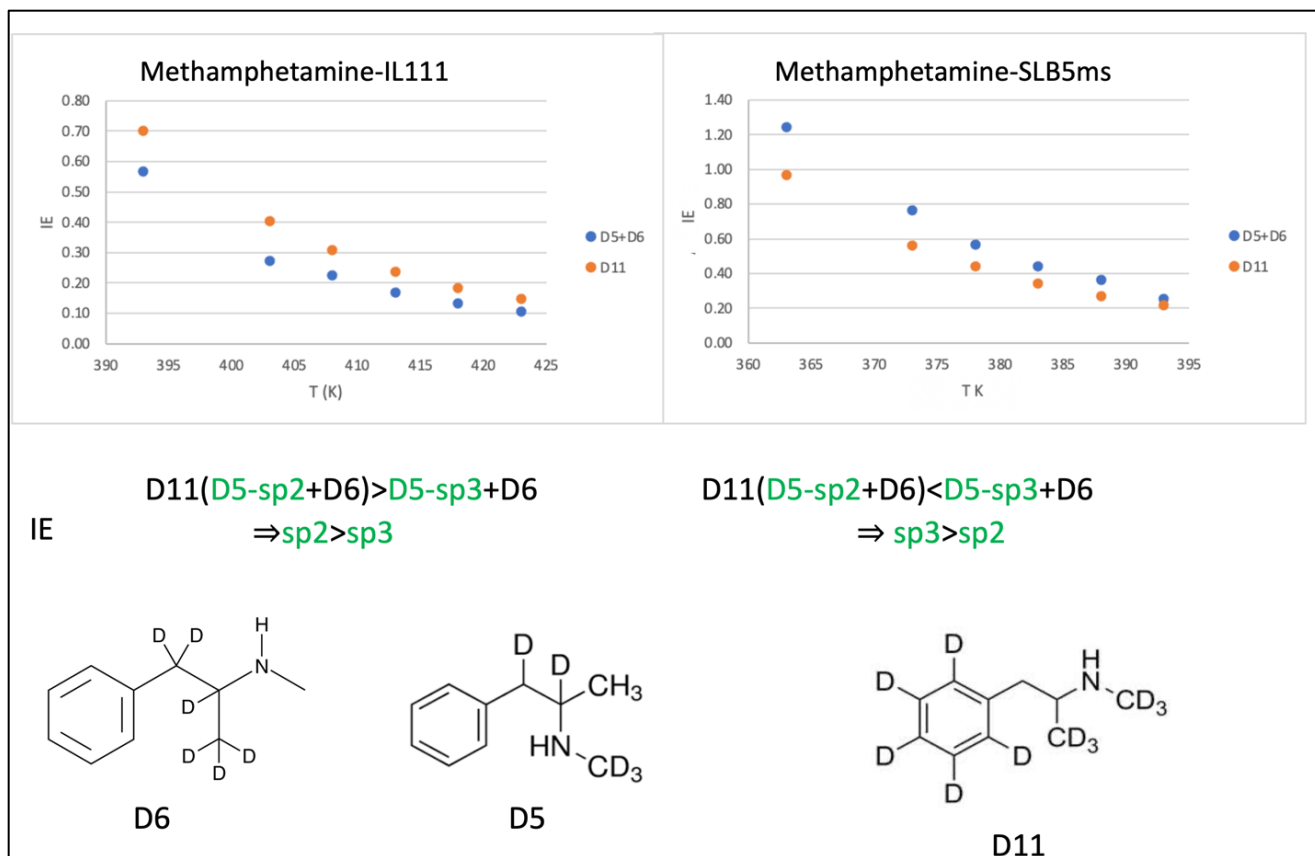


Figure 3.S7

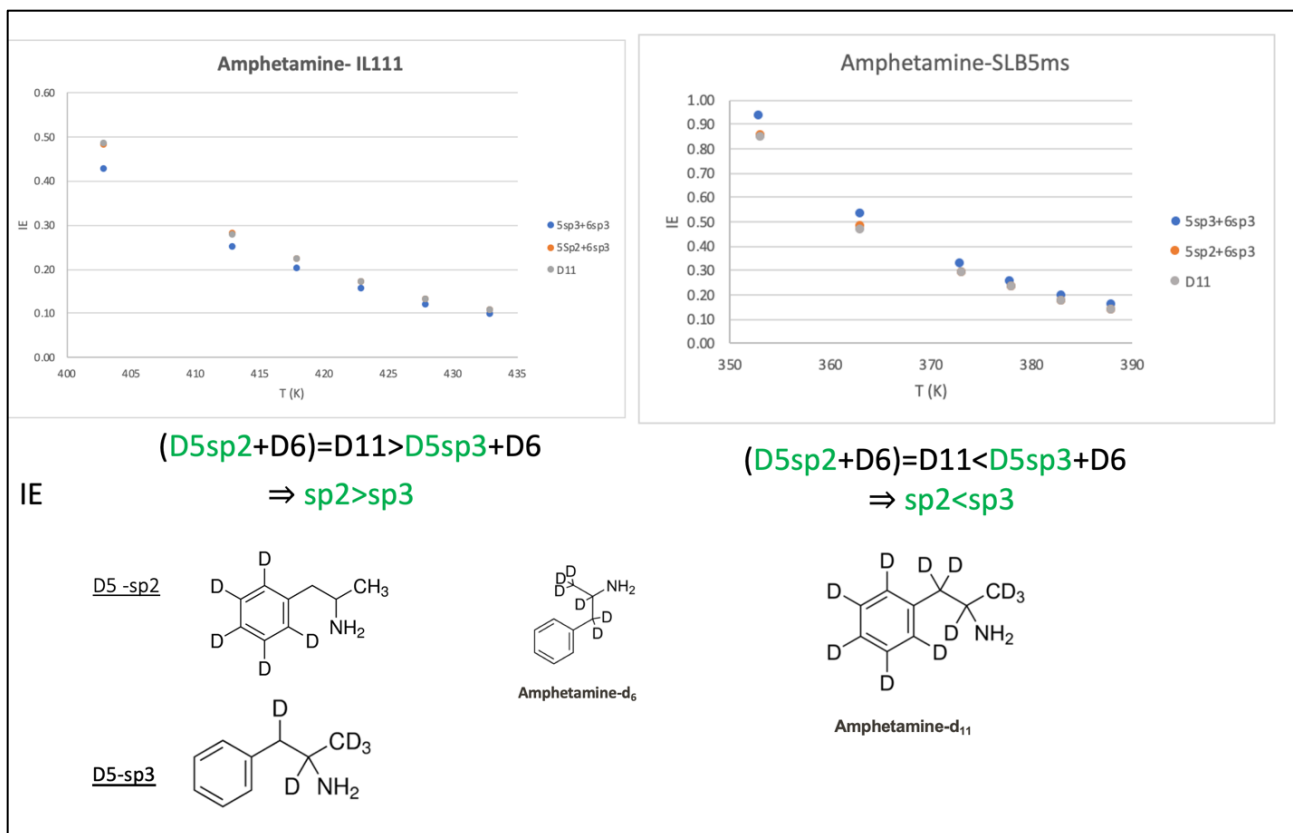


Figure 3.S8

Table 3.S2 Inverse isotope effect of amphetamine isotopologues on PDMS5.

Analyte Amphetamine	Temperature °C	k Average	kH	IE kH-kD	(IE/k)%
D11	80	23.64	24.49	0.85	3.59
	90	13.72	14.19	0.47	3.42
	100	8.53	8.82	0.29	3.43
	105	6.86	7.09	0.23	3.40
	110	5.32	5.50	0.18	3.30
	115	4.37	4.50	0.13	3.09
D8	80	23.90	24.49	0.59	2.47
	90	13.86	14.19	0.33	2.39
	100	8.62	8.82	0.20	2.37
	105	6.93	7.09	0.16	2.31
	110	5.38	5.50	0.12	2.23
	115	4.41	4.50	0.09	2.14
D6	80	23.99	24.49	0.50	2.09
	90	13.91	14.19	0.28	2.03
	100	8.65	8.82	0.17	2.01
	105	6.96	7.09	0.14	1.97
	110	5.40	5.50	0.10	1.93
	115	4.42	4.50	0.08	1.87
D5-chain	80	24.06	24.49	0.43	1.78
	90	13.95	14.19	0.25	1.76
	100	8.67	8.82	0.15	1.72
	105	6.98	7.09	0.12	1.69
	110	5.41	5.50	0.09	1.66
	115	4.43	4.50	0.07	1.63
D5ring	80	24.14	24.49	0.35	1.46
	90	13.99	14.19	0.20	1.42
	100	8.70	8.82	0.12	1.39
	105	7.00	7.09	0.09	1.35
	110	5.43	5.50	0.07	1.32
	115	4.45	4.50	0.06	1.31

Table 3.S3 Inverse isotope effect of methamphetamine isotopologues on PDMS5

Analyte Methamphetamine	Temperature °C	kAverage	kH	IE kH-kD	(IE/k)%
D14	90	27.75	29.10	1.36	4.88
	100	16.43	17.23	0.80	4.87
	105	12.79	13.40	0.61	4.75
	110	10.06	10.54	0.48	4.76
	115	8.15	8.53	0.38	4.69
	120	6.50	6.79	0.29	4.42
D11	90	28.13	29.10	0.97	3.46
	100	16.61	17.23	0.62	3.73
	105	12.96	13.40	0.44	3.40
	110	10.20	10.54	0.34	3.35
	115	8.26	8.53	0.27	3.28
	120	6.60	6.79	0.20	2.97
D9	90	28.16	29.10	0.95	3.36
	100	16.67	17.23	0.56	3.36
	105	12.98	13.40	0.42	3.26
	110	10.20	10.54	0.33	3.26
	115	8.27	8.53	0.26	3.19
	120	6.60	6.79	0.19	2.95
D8	90	28.24	29.10	0.86	3.04
	100	16.71	17.23	0.52	3.11
	105	13.01	13.40	0.39	2.99
	110	10.23	10.54	0.31	2.99
	115	8.29	8.53	0.24	2.95
	120	6.62	6.79	0.18	2.67
D5	90	28.54	29.10	0.56	1.98
	100	16.89	17.23	0.35	2.06
	105	13.14	13.40	0.26	1.96
	110	10.34	10.54	0.20	1.93
	115	8.37	8.53	0.17	1.97
	120	6.68	6.79	0.12	1.73

Table 3.S4 Inverse isotope effect of benzyl alcohol isotopologues on PDMS 5

Analyte Benzyl alcohol	Temperature °C	kAverage	kH	IE kH-kD	(IE/k)%
D7	35	28.29	29.13	0.84	2.97
	40	21.01	21.64	0.63	3.00
	45	15.58	16.04	0.47	3.01
	50	12.00	12.34	0.34	2.86
	55	9.11	9.37	0.26	2.87
	60	6.97	7.16	0.19	2.76
D5	35	28.65	29.13	0.49	1.70
	40	21.28	21.64	0.36	1.69
	45	15.77	16.04	0.28	1.75
	50	12.14	12.34	0.20	1.62
	55	9.22	9.37	0.15	1.62
	60	7.05	7.16	0.11	1.58
D2	35	28.76	29.13	0.37	1.30
	40	21.37	21.64	0.27	1.28
	45	15.84	16.04	0.21	1.30
	50	12.19	12.34	0.15	1.23
	55	9.26	9.37	0.11	1.21
	60	7.08	7.16	0.08	1.14

Table 3.S5 Inverse isotope effect of toluene isotopologues on PDMS 5

Analyte Toluene	Temperature °C	kAverage	kH	IE kH-kD	(IE/k)%
D8	25	4.85	5.04	0.19	3.90
	30	3.80	3.94	0.14	3.70
	35	3.09	3.21	0.11	3.70
	45	2.00	2.07	0.07	3.62
	55	1.41	1.46	0.05	3.35
	65	0.98	1.01	0.03	3.18
D5	25	4.95	5.04	0.19	3.81
	30	3.88	3.94	0.14	3.62
	35	3.16	3.21	0.11	3.62
	45	2.04	2.07	0.07	3.55
	55	1.44	1.46	0.05	3.29
	65	0.99	1.01	0.03	3.13
D3	25	4.92	5.04	0.19	3.84
	30	3.86	3.94	0.14	3.64
	35	3.14	3.21	0.11	3.64
	45	2.03	2.07	0.07	3.57
	55	1.44	1.46	0.05	3.30
	65	0.99	1.01	0.03	3.14

Table 3.S6 Inverse isotope effect of N,N-dimethylformamide isotopologues on PDMS 5

Analyte DMF	Temperature °C	kAverage	kH	IE kH-kD	(IE/k)%
D7	25	7.07	6.86	0.21	3.00
	30	5.41	5.23	0.18	3.35
	35	3.91	3.88	0.03	0.66
	40	3.14	3.14	0.00	-0.06
	45	2.44	2.48	-0.04	-1.62
	50	1.97	1.98	-0.01	-0.26
D1	25	6.99	6.86	0.13	1.84
	30	5.34	5.23	0.11	2.11
	35	3.95	3.88	0.06	1.57
	40	3.18	3.14	0.04	1.23
	45	2.49	2.48	0.01	0.50
	50	2.01	1.98	0.03	1.61

Table 3.S7 Normal isotope effect of amphetamine isotopologues on IL-111

Analyte Amphetamine	Temperature °C	kAverage	kH	IE kD-kH	(IE/k)%
D11	130	18.93	18.45	0.48	2.56
	140	11.51	11.23	0.28	2.42
	145	9.27	9.05	0.22	2.42
	150	7.37	7.20	0.17	2.32
	155	5.92	5.77	0.14	2.43
	160	4.76	4.65	0.11	2.29
D8	130	18.79	18.45	0.34	1.83
	140	11.43	11.23	0.20	1.72
	145	9.21	9.05	0.16	1.72
	150	7.32	7.20	0.12	1.63
	155	5.87	5.77	0.10	1.62
	160	4.72	4.65	0.08	1.59
D6	130	18.70	18.45	0.25	1.34
	140	11.38	11.23	0.15	1.29
	145	9.17	9.05	0.12	1.29
	150	7.29	7.20	0.09	1.25
	155	5.84	5.77	0.07	1.20
	160	4.70	4.65	0.06	1.21
D5-chain	130	18.63	18.45	0.18	0.95
	140	11.34	11.23	0.11	0.93
	145	9.13	9.05	0.08	0.91
	150	7.27	7.20	0.07	0.90
	155	5.82	5.77	0.05	0.84
	160	4.69	4.65	0.04	0.86
D5-ring	130	18.68	18.45	0.23	1.24
	140	11.37	11.23	0.14	1.20
	145	9.15	9.05	0.10	1.15
	150	7.28	7.20	0.08	1.11
	155	5.83	5.77	0.06	1.06
	160	4.70	4.65	0.05	1.06

Table 3.S8 Normal isotope effect of methamphetamine isotopologues on IL-111

Analyte Methamphetamine	Temperature °C	kAverage	kH	IE kD-kH	(IE/k)%
D14	120	25.36	24.50	0.86	3.40
	130	15.37	14.88	0.49	3.17
	135	12.34	11.96	0.37	3.03
	140	9.79	9.50	0.29	2.96
	145	7.83	7.61	0.22	2.82
	150	6.31	6.12	0.18	2.90
D11	120	25.20	24.50	0.70	2.78
	130	15.28	14.88	0.40	2.64
	135	12.27	11.96	0.31	2.52
	140	9.74	9.50	0.24	2.44
	145	7.79	7.61	0.18	2.35
	150	6.27	6.12	0.15	2.36
D9	120	24.95	24.50	0.45	1.80
	130	15.13	14.88	0.25	1.67
	135	12.16	11.96	0.20	1.61
	140	9.66	9.50	0.15	1.56
	145	7.72	7.61	0.12	1.49
	150	6.22	6.12	0.09	1.51
D8	120	24.85	24.50	0.35	1.43
	130	15.09	14.88	0.21	1.37
	135	12.12	11.96	0.16	1.29
	140	9.63	9.50	0.12	1.26
	145	7.70	7.61	0.10	1.24
	150	6.20	6.12	0.08	1.23
D5	120	24.70	24.50	0.21	0.83
	130	15.00	14.88	0.12	0.82
	135	12.06	11.96	0.10	0.79
	140	9.57	9.50	0.07	0.72
	145	7.66	7.61	0.06	0.73
	150	6.17	6.12	0.04	0.71

Table 3.S9 Normal isotope effect of benzyl alcohol isotopologues on IL-111

Analyte Benzyl alcohol	Temperature °C	kAverage	kH	IE kD-kH	(IE/k)%
D7	50	24.09	23.39	0.70	2.89
	60	12.96	12.61	0.35	2.72
	65	9.95	9.67	0.28	2.86
	70	7.49	7.30	0.19	2.53
	75	5.71	5.57	0.14	2.44
	80	4.51	4.41	0.11	2.39
D5	50	24.05	23.39	0.66	2.74
	60	12.94	12.61	0.33	2.58
	65	9.93	9.67	0.26	2.61
	70	7.47	7.30	0.17	2.34
	75	5.70	5.57	0.13	2.27
	80	4.51	4.41	0.10	2.21
D2	50	23.43	23.39	0.04	0.15
	60	12.63	12.61	0.03	0.21
	65	9.70	9.67	0.03	0.34
	70	7.31	7.30	0.01	0.18
	75	5.58	5.57	0.01	0.18
	80	4.42	4.41	0.01	0.21

Table 3.S10 Normal isotope effect of toluene isotopologues on IL-111

Analyte Toluene	Temperature °C	kAverage	kH	IE kD-kH	(IE/k)%
D8	30	2.63	2.54	0.09	3.32
	35	2.10	2.03	0.07	3.19
	40	1.65	1.60	0.05	3.03
	45	1.34	1.30	0.04	2.95
	50	1.07	1.04	0.03	2.90
	55	0.86	0.83	0.02	2.82
D5	30	2.63	2.54	0.09	3.36
	35	2.10	2.03	0.07	3.28
	40	1.65	1.60	0.05	3.14
	45	1.34	1.30	0.04	3.05
	50	1.07	1.04	0.03	2.98
	55	0.86	0.83	0.03	2.95
D3	30	2.54	2.54	0.00	-0.09
	35	2.03	2.03	0.00	-0.06
	40	1.59	1.60	0.00	-0.15
	45	1.30	1.30	0.00	-0.13
	50	1.04	1.04	0.00	-0.09
	55	0.83	0.83	0.00	-0.20

Table 3.S11 Normal isotope effect of N, N-dimethylformamide isotopologues on IL-111

Analyte DMF	Temperature °C	kAverage	kH	IE kD-kH	(IE/k)%
D7	85	11.77	10.54	1.23	10.43
	90	9.19	8.47	0.72	7.83
	95	7.40	6.83	0.57	7.67
	100	6.00	5.52	0.49	8.08
	105	4.84	4.49	0.35	7.26
	110	4.12	3.83	0.28	6.87
D1	85	10.98	10.54	0.43	3.96
	90	8.77	8.47	0.30	3.39
	95	7.09	6.83	0.27	3.75
	100	5.75	5.52	0.24	4.09
	105	4.66	4.49	0.17	3.73
	110	3.97	3.83	0.14	3.45

Chapter 4

Enhancing Sensitivity for High Selectivity Gas Chromatography Molecular Rotational Resonance Spectroscopy

4.1 Abstract

A next-generation gas chromatograph-molecular rotational resonance (MRR) spectrometer (GC-MRR) with instrumental improvements and higher sensitivity is described. MRR serves as a structural information-rich detector for GC with extremely narrow line widths, surpassing the resolution of gas-phase $^1\text{H-NMR/FTIR/MS}$ signals and offering unparalleled specificity in regard to a molecule's three-dimensional structure. With a Fabry-Perot cavity and supersonic jet incorporated into a GC-MRR, dramatic improvements in sensitivity for molecules up to 244 Da were achieved in the microwave region compared to the only prior work, which demonstrated the GC-MRR idea for the first time with millimeter waves. The supersonic jet cools the analytes to ~ 2 K, resulting in a limited number of molecular rotational and vibrational levels and enabled us to obtain stronger GC-MRR signals. This has allowed the limits of detection of GC-MRR to be comparable to a GC thermal conductivity detector with an optimized choice of gases. The performance of this GC-MRR system is reported for a range of molecules with permanent dipole moments, including alcohols, nitrogen heterocyclics, halogenated compounds, dioxins, and nitro compounds in the molecular mass range of 46-244 Da. The lowest amount of any substance yet detected by MRR in terms of mass is reported in this work. A theoretically unexpected finding is reported for the first time about the effect of the GC carrier gas (He, Ne, N_2) on the sensitivity of the analysis in the presence of the gas driving the supersonic jet (He, Ne, N_2) in GC-MRR. Finally, the idea of total molecule monitoring in GC-MRR analogous to selected ion-monitoring in GC-MS is illustrated. Structural isomers and isotopologues of bromobutanes and bromonitrobenzenes are used to demonstrate this concept.

4.2 Introduction

Robust analytical methodologies often utilize a high efficiency separation method coupled with a sensitive and information-rich detector. Among the most broadly applicable of such devices are gas chromatography- and high performance liquid chromatography-mass spectrometry (GC/HPLC-MS) systems.[152-155] In 2019, the GC-MS invention was designated as a "National Historic Chemical Landmark" by the American Chemical Society.[156] Still, even the best available GC-MS can show significant spectrum overlap from structural isomers, isotopomers, isotopologues, and enantiomers. In the past, GCs have been hyphenated with Fourier transform infrared spectrometers (GC-FTIR),[157-159] nuclear magnetic resonance spectrometers (GC-NMR),[160, 161] supersonic jet expansion fluorescence spectrometers,[162] and vacuum ultraviolet spectrometers (GC-VUV),[163-165] all of which provide varying degrees of structural information for analytes. However, efforts are still needed to develop complementary information-rich and structure specific detection technologies to gain an ever-greater insight into the complex analytical problems that GC can be used to investigate.

Gas phase molecular rotational resonance (MRR) spectroscopy offers some exceptional advantages over other information-rich GC detectors in terms of its molecular structural selectivity because the rotational spectrum is extremely sensitive to the 3D mass distribution of the molecule.[166, 167] The 3D mass distribution is characterized by its moments of inertia in a three-dimensional coordinate system. MRR measures pure rotational energy transitions in the microwave (1-40 GHz) or millimeter-wave (approx. 30-1000 GHz) regions with an extremely narrow linewidth (< 1 MHz) under low-pressure conditions. Thus, once a molecule is fingerprinted by rotational spectroscopy, no other molecule can *ever* match it, save enantiomers.

Figure 4.1 shows the coordinate system for 2-chloropyridine. In the principal axis system (axes designated by a , b , and c), only the diagonal tensor components, called the moments of inertia (I_{aa} , I_{bb} and I_{cc}), survive, whereas the products of inertia vanish when the origin is taken as the center of mass.[168] In a polyatomic molecule, the moments of inertia are given by $I_a = \sum_i m_i(b_i^2 + c_i^2)$, $I_b = \sum_i m_i(a_i^2 + c_i^2)$, and $I_c = \sum_i m_i(a_i^2 + b_i^2)$, where m_i are the masses of the atoms and (a_i, b_i, c_i) are the atomic coordinates with respect to the center of mass. Qualitatively, in Figure 4.1, one can visualize that rotating the 2-chloropyridine molecule around the c -axis requires the spatial movement of the relatively heavy Cl and N atoms, whereas rotating along a -axis requires the least energy. The dipole moment μ in Figure 4.1 is oriented in the ab plane. The projections (μ_a , μ_b and μ_c) on the a , b , and c coordinate system determines the type of microwave spectrum which will be observed (a -, b - and c -type, or, more often, a combination). Constructing a Hamiltonian with angular momentum and moments of inertia allows calculating highly accurate rotational transition energies for a given compound. Additionally, the moments of inertia (which depend only on the ground-state electronic structure of the molecule) can be accurately calculated with modern quantum chemical methods, thereby allowing the comparison of computed and experimentally derived values. Consequently, compound structures and identities (including isomeric compounds) can be unambiguously determined.[37, 169] Finally, the response factor for a given molecule can be accurately calculated so that compounds can be quantified even without reference standards [170].

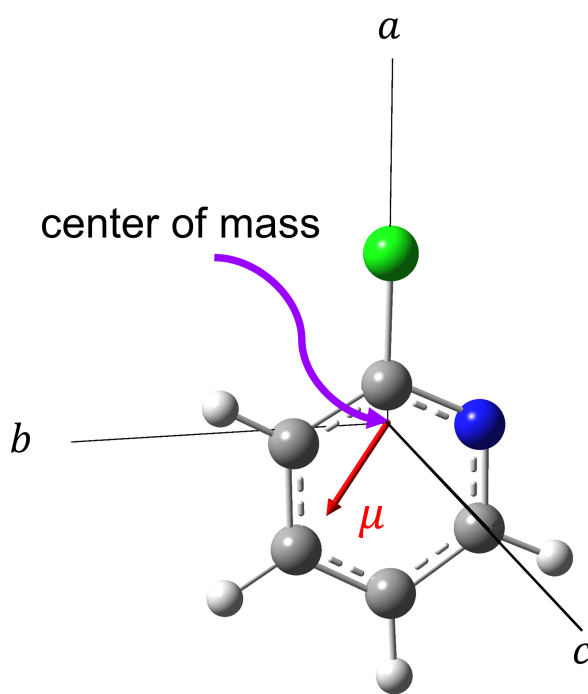


Figure 4.1 Depiction of a 3D coordinate system of an asymmetric rotor, 2-chloropyridine, with the origin at the center of mass of the molecule (N=blue, Cl =green, C=grey, and H=white). The dipole moment vector μ does not lie on any axes for asymmetric rotors (oriented in the ab plane). The asymmetry is assigned based on the magnitudes of three principal moments of inertia (I_c , I_b and I_a), not on the molecular geometry.

Even though MRR signatures are unique to a molecule, and the narrow linewidths allow for direct resolution of mixtures, separation is still highly valuable for complex mixtures because unscrambling and assigning a large number of rotational lines is challenging.[171] The GC-MRR hyphenation addresses this problem and provides three advantages over MS detection: (i) MRR is highly sensitive to differences in molecular structure and so can conclusively identify isomeric compounds of all types, unlike MS; (ii) MRR can resolve and quantify co-eluting compounds without a loss of accuracy; and (iii) both qualitative identification and absolute quantification can be achieved without the need for reference standards. In 2020, we demonstrated a GC system coupled with a millimeter-wave MRR spectrometer with a room-temperature flow cell.[172] This proof-of-concept GC-MRR module allowed the separation and unequivocal identification of a

microliter sample containing 24 isotopologues and isotopomeric compounds, along with accurate isotopic abundances, which could never be separated by any GC column.[172] Such selectivity and molecular information could not be obtained by either direct GC-MS, GC-FTIR, or GC-NMR systems.[172]

The first generation millimeter-wave GC-MRR was limited to small molecules (≤ 120 Da) with very low sensitivity compared to conventional GC detectors. This was due to a combination of factors, including a) the broad mm wave (75-110 GHz) excitation source, b) room temperature to 80 °C operation range of the flow cell, and c) direct coupling of the GC column end into the microwave flow cell. Herein, we report a newly designed, more broadly applicable, more sensitive, and practical, targeted mode GC-MRR instrument utilizing a pulsed jet mechanism and the 9-18 GHz frequency range to account for larger molecules. The minimum detectable sample quantity for this spectrometer is far lower than both the previous GC-MRR instrument and what has been demonstrated in the field of molecular rotational spectroscopy.

4.3 Experimental Section

4.3.1 Materials

All the analytes listed in Table 4.1 were purchased from Millipore Sigma (formerly Sigma-Aldrich, St. Louis, MO). 1-bromobutane, 2-bromobutane and positional isomers of bromonitrobenzene and their deuterated analogs were purchased from Toronto Research Chemicals (Toronto, ON, Canada). Absolute ethanol was purchased from Decon Laboratories (King of Prussia, PA, USA). Hydrogen, helium, neon, nitrogen for GC were obtained from Airgas, Randor, PA, USA. An SLB-5ms capillary GC column ($L \times I.D.$ 30 m \times 0.25 mm, $d_f = 0.25 \mu\text{m}$) was utilized to analyze the mixtures on GC-TCD, millimeter wave GC-MRR, and targeted band GC-MRR. The GC analytical conditions are listed in Table 4.S1, S2, and S3, respectively.

4.3.2 Microwave Library Spectrum Measurements

The microwave spectrum of the analyte was required to select the intense lines of the molecules before using the GC-MRR. The rotational spectra of ethanol,[173] pyridine,[174] thiophene,[175] 2-chloropyridine,[176] nitrobenzene,[177], and quinoline[178] were already available. For the remaining molecules in Table 4.1, the microwave broadband MRR spectra were first taken and used to determine the optimal line frequencies for the targeted study. A 2-8 GHz, chirped-pulse Fourier transform microwave spectrometer was used for this purpose.[47] A small amount (typically 10-20 mg) of each pure compound was loaded into pulsed supersonic nozzles equipped with a heating reservoir, and neon gas (99.999%) was used as carrier gas at a typical backing pressure of +15 psi. The reservoir temperature was adjusted to give optimal signals for each compound (vapor pressure dependency). The spectrum was recorded for approximately an hour for each compound to provide a high signal-to-noise reference spectrum of the pure compound. Final spectrum fits were performed using Pickett's SPFIT/SPCAT program suite.[179]

4.3.3 Millimeter-Wave GC-MRR

Analytes were dissolved in acetonitrile or methanol depending on the solubility in the range of 0.4 to 12 wt. % for the millimeter-wave GC-MRR). Separations were performed on a Hewlett Packard- HP 6890 series gas chromatograph equipped with a split/splitless injection port coupled with a BrightSpec W-band chirped-pulse molecular rotational resonance (MRR) spectrometer (75 to 110 GHz). Hydrogen was used as carrier gas with a constant linear average velocity of 40 cm/sec for all analyses. The MRR initial chamber pressure was 6-8 mTorr, and the chamber temperature was set at 50 °C. The injection volume was 2 μ L with a split ratio of 50:1. The injection temperature was set at 250 °C. Other analyte-specific details are provided in the Supporting Information Table 4.S2.

4.3.4 Microwave GC-MRR with Supersonic Jet Expansion and Fabry Perot Cavity (Targeted band GC-MRR)

A separate Hewlett Packard- HP 6890 series gas chromatograph was connected to a supersonic jet expansion system, fed by the GC's effluent and another make-up gas (Ne, He, or N₂). A pair of spherical mirrors made of 6061 aluminum alloy, held under high vacuum ($\sim 10^{-5}$ - 10^{-6} torr), are coupled to a microwave generator that produces pulses with a frequency that is resonant with the cavity mode. The vacuum was generated by a 6-in. diffusion pump (Agilent/Varian VHS-6) with a rotary vane backing pump. When the microwave pulse is resonant with a molecular rotational transition of an analyte, the sample emits a free induction decay (FID) signal, which is coupled out of the cavity, digitized, and Fourier transformed to yield the MRR spectrum line. The typical stagnant pressure behind the nozzle is +5 psi, and the total flow rate into the chamber during operation (10 Hz repetition rate) was 30 mL/min. Five FID spectra are recorded on each nozzle pulse. More details on this MRR spectrometer can be found elsewhere.[37, 169]

The raw GC-MRR data takes the form of free induction decay (FID) signals saved to disk. In the present instrument, the data from 10 gas pulses are first signal-averaged in the time domain on the instrument's digitizer. Five FID signals are measured during each gas pulse, so there are 50 co-averaged time traces in each data set. The throughput rate is currently limited by the time it takes to save each file to disk (~ 250 ms), a limitation we are improving in the next design. In the current study, this means that a new spectrum is saved approximately every 1.25 s. The raw, co-added FID traces are then gated (i.e., a portion of this time data are selected for Fourier transformation). The signal intensity is highest at the early part of the spectrum, but a higher resolution can be obtained by choosing a longer gate. Fortunately, the user can set all of these

parameters in post-processing and therefore visualize the same data set under different processing conditions. This gated data has an apodization window applied to improve the line shape (a Kaiser-Bessel window with $b=8$) and is then Fourier transformed to yield the final frequency spectrum.

In this work, we present data in the form of both spectra and chromatograms. For the spectra, a single time point, or, for peak integration, a series of consecutive time data are co-added and processed as in the previous paragraph. The data are then presented with a frequency x-axis. For chromatograms, a series of spectra are processed under the same conditions, and the intensity at a single frequency in the spectrum is plotted as a function of the time where the spectrum was acquired. Unless otherwise specified, the resonant frequency of each analyte in Table 4.1 was used for that chromatogram. The targeted band GC-MRR experiments for the detection limit have been conducted with Ne as the carrier and make-up gas unless noted otherwise. Bromobutanes and bromonitrobenzenes (Figure 4.5b) were analyzed by targeted band GC-MRR and Ne carrier gas/make-up gas. The exact analytical details are listed in Table 4.S4. Note that current GCs do not have parameters for neon. The chromatograms in Figure 4.5 were de-noised (Savitsky-Golay) and upsampled in MATLAB 2019a (The MathWorks Inc. USA).

4.3.5 Estimation of Limits of Detection

The limits of detection (LOD) were estimated using a method outlined by Wenzl *et al.*[180] The LODs can be estimated $x_{LOD} = 3.9 \sigma_{blank}/b$. In this equation x_{LOD} is the limit of detection, b is the slope of the calibration curve at concentration levels close to the expected LOD and σ_{blank} is the standard deviation of the blank signals. Homoscedasticity is implicit and assumed in this formula. A minimum of 10 analyses of the blank/pseudo-blank sample under identical conditions is required, and its standard deviation is taken as $\sigma_{psblank}$. Pseudo-blank samples (a

sample with a concentration close to the expected LOD, $\sigma_{psblank}$) may be used instead of blank samples if the blank samples are not available. The complete derivation of this equation is provided by Wenzl *et al.*[180] The amount of analyte reaching the detector was estimated in nanograms (Table 1). Each point on the calibration curve (Supporting Information) corresponds to three runs of a single standard.

$$LOD(ppm) \times \text{solvent density} (mg.\mu L^{-1}) \times \text{injection volume}(\mu L)/\text{split ratio}$$

4.4 Results & Discussion

In the first generation millimeter-wave GC-MRR system, the detector flow cell operated at or above room temperature (< 80 °C) to avoid analyte condensation on the cell walls.[172] However, room temperature microwave/millimeter spectroscopy suffers from severe sensitivity losses for compounds above a molecular mass of approximately > 120 due to a large number of thermally populated vibrational/torsional modes that are present, each with a slightly different spectrum. This results in spectra with a considerable number of very weak transitions. The effect of spectroscopic temperature on intensity is illustrated in Figure 4.2 for the conformational isomer with strongest signals of 1-(2,3-dihydro-1,4-benzodioxin-6-yl)propan-1-one (192.21 Da), using the common microwave region of 6-18 GHz to compare the spectrum intensities. Almost in all cases, the conformer that produces the strong signals also is the lowest energy conformer, unless the lowest energy conformer lacks a dipole moment. This figure shows that the room-temperature spectrum intensity for this molecule is extremely low compared to the 1 K and 10 K spectra. Thus, the lower spectroscopic temperatures produce far fewer transitions with much greater intensities, shifting rotational lines to lower frequencies (Figure 4.2). These low temperatures were selected because the pulsed-jet device,[162, 181, 182] and buffer-gas cooling techniques,[183] can routinely achieve such temperatures. In addition to "cooling out" nearly all vibrational satellites

for most molecules, the rotational partition function scales with approximately $T_{\text{rot}}^{3/2}$, so cooling reduces the number of populated energy levels and increases the microwave spectrum signal levels by a significant factor.[184] The room-temperature transition intensity for this molecule is higher by approximately two orders of magnitude at 75-110 GHz than at 6-18 GHz, but it still falls far short of the sensitivity that can be achieved through cooling. In addition, this effect gets even more pronounced as the molecular mass continues to increase.

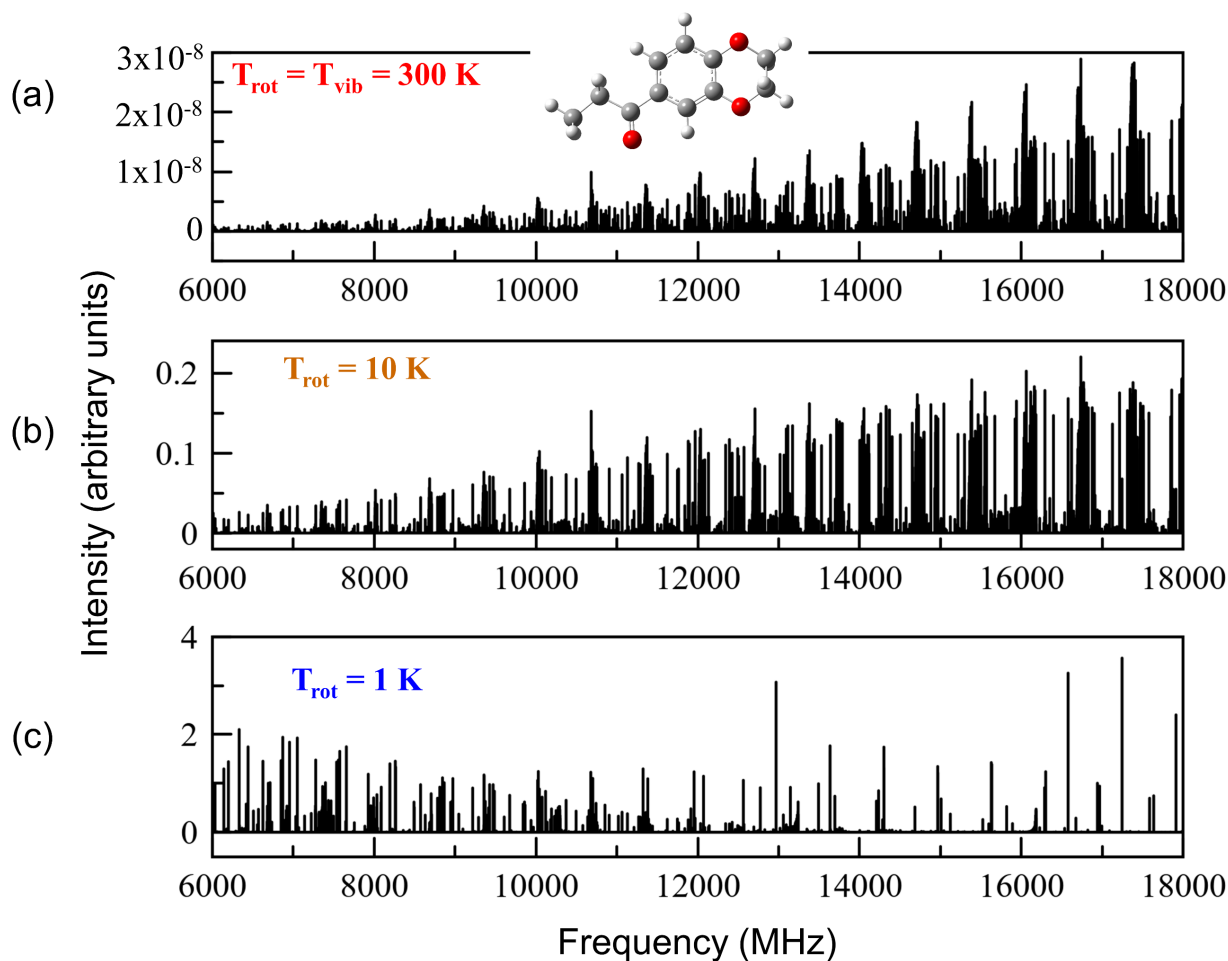


Figure 4.2 Simulation of rotational cooling effect on the microwave rotational resonance (MRR) spectrum of the observed conformational isomer with strongest signals of 1-(2,3-dihydrobenzo[b][1,4]dioxin-6-yl)propan-1-one (192.21 Da) plotted in the 6-18 GHz of the microwave spectrum. Red circles indicate oxygen in the molecule. Microwave spectrum at (a) ambient temperature 300 K, (b) rotationally cooled spectrum at 10 K, and at (c) rotational temperature of 1 K. The simulations use experimental rotational constants measured in this study ($A = 1804.97$, $B = 361.32$, $C = 305.18$ MHz) and computed dipole moments ($\mu_a = 3.34$, $\mu_b = 2.37$, $\mu_c = 0.16$ Debye). For panel (a), the vibrational partition function was estimated by the

harmonic oscillator approximation. Only the spectrum of the ground vibrational state was simulated.

4.4.1 Incorporation of Supersonic Jet Expansion Unit in GC-MRR

One of the simplest ways to realize molecular cooling to cryogenic temperatures while avoiding analyte condensation is to employ a pulsed-jet supersonic expansion valve connected to a high vacuum chamber. Using an adiabatic expansion of gases in a high vacuum ($\sim 10^{-5}$ Torr) yields a supersonic jet of molecules at very low rotational temperatures, significantly reducing the partition function and enormously improving the molecular rotational signal.[182] An additional advantage of a supersonic jet expansion for GC-MRR is that the injected analytes travel through the chamber and go to the exhaust very quickly (<1 ms), and so an essentially fresh sample can be injected with every gas pulse, preventing post-column band-broadening effects that can be observed with a large flow cell. Otherwise, the post-column broadening would have appeared as severely tailing effects arising from the slow sweeping of the analyte from the MRR flow cell. Expansions with rare carrier gases (Ne, He, or Ar) with 1 mm pinholes achieve typical rotational temperatures of 1-2 K.[181]

Figure 4.3 shows the coupling of the GC with a targeted band MRR. The jet expansion unit can operate at rates ranging from 1 to 10 Hz. However, the jet cannot function at typical flow rates encountered in GC carrier gas, requiring typical flow rates of 30-50 mL/min (for a 10 Hz pulse rate); therefore, a make-up gas is necessary, as is commonly required in many GC detectors such as thermal conductivity detectors (TCD) and flame ionization detectors (GC-FID). As reported in a previous investigation, neon was generally found to provide the best sensitivity in pulsed-jet microwave spectroscopy.[185] Preliminary experiments showed that pulsing the jet at 10 Hz when coupled with the GC gave the optimum signal-to-noise ratio. The tradeoff of using supersonic

expansion sources is that they require larger vacuum chambers to allow for the expansion. However, the instrument size is still comparable to that of a high-end mass spectrometer.

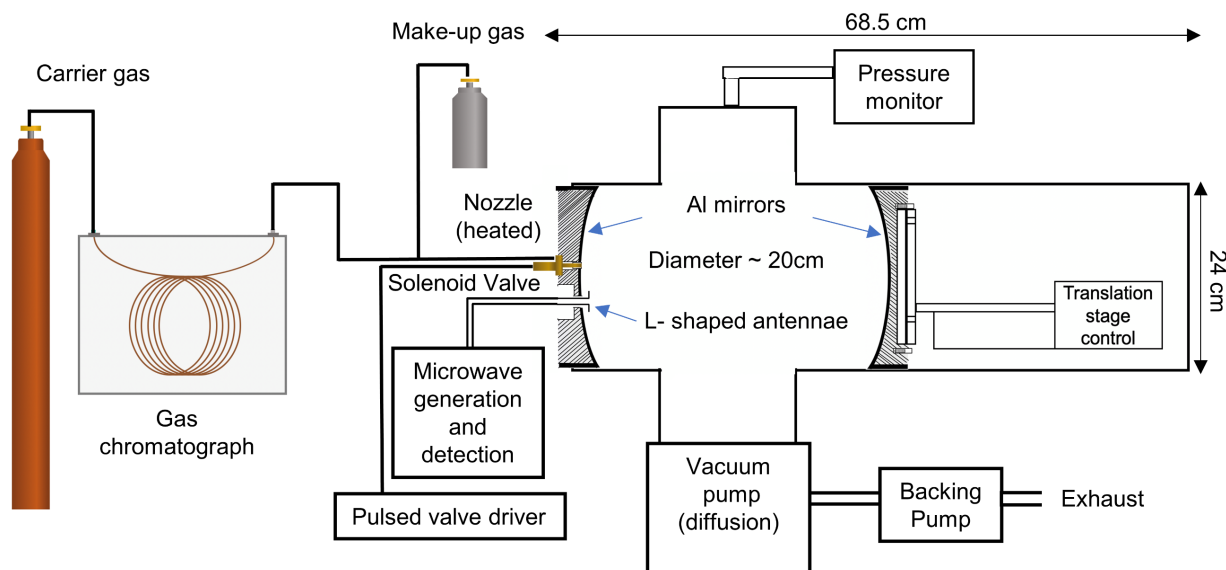


Figure 4.3 The interfacing of gas chromatography with a microwave Fabry-Perot cavity using a supersonic jet expansion system (GC-MRR). The supersonic jet system is operated by a pulsed valve driver operating at 10 Hz with neon as the make-up gas flow. The pressure in the chamber is maintained at 10^{-4} Torr when the nozzle is on.

4.4.2 Fabry-Perot Microwave Cavity in Targeted Mode GC-MRR

The supersonic jet plays a significant role in enhancing signal strength. To further increase the higher detection sensitivity, a resonant cavity incorporated in rotational spectroscopy as depicted in Figure 4.3.[47] This cavity is modeled on the MRR design of Suenram *et al.*[185] In this targeted mode, a narrow frequency range (<1 MHz) resonant with a mode of a Fabry-Perot resonator is excited, and the free induction decay response is collected, followed by a Fourier transform to obtain the targeted rotational line. This targeted band MRR measures a single rotational frequency between 6-18 GHz, which is suitable for the rotational spectrum of small and medium-sized molecules. The microwave pulse makes several thousand reflection rounds (cycles) between two Al mirrors (Figure 4.3) within this cavity, thus enhancing the molecule's interaction

with microwave radiation. This chamber's size is dictated by the size of the mirrors, which is determined by the Fresnel diffraction limit conditions of microwave radiation.[182] In this instrument, the mirror size is 19.5 cm in diameter, allowing stable modes to be achieved at frequencies down to 9 GHz, and the Q value of the cavity (defined as the energy in the cavity divided by the energy lost in making a complete reflection round)[182] is ~ 4000 . Radiation is coupled into and out of the cavity via two L-shaped antennas located in one of the two mirrors (Figure 4.3). Both L-shaped antennae serve as transmitters and detectors. The length of bent wire of the antenna corresponds to approximately $\lambda_{min}/2$, where λ_{min} is the shortest wavelength of the spectrometer.[182] The other mirror is on a motorized stage to bring the cavity in resonance with the chosen frequency.

Table 1 lists the analytes studied in this work, their molecular mass, total dipole moment, and selected rotational transition within the spectrometer bandwidth with the highest intensity rotational transition. All these molecules have a non-zero permanent electric dipole moment, which is a fundamental requirement of microwave spectroscopy. Many small molecules that do not have a permanent dipole, e.g., alkanes or benzene, are not detectable by microwave spectroscopy. Molecules with a wide range of total dipole moments were selected, as shown in Table 4.1. Note that there is no general trend in the molecular mass of the analyte and the rotational frequency with the highest intensity in the microwave spectrum. Generally, as the molecular mass increases, the MRR spectrum shifts to lower frequencies (heavier molecules rotating slowly). These precise wavelengths of maximum intensity have to be chosen from the full MRR spectrum obtained of the pure compound, hence the need for library spectra akin to the mass spectra library. Similar steps are required in selected ion-monitoring mode (SIM) in GC-MS or LC-MS of selected

analytes. Finally, building broadband and targeted measurement capabilities into the same instrument is possible by exciting the sample along orthogonal axes [186].

4.4.3 Performance Comparison of GC-TCD, Millimeter Wave GC-MRR, and Targeted Band GC-MRR

In order to have a broad acceptance of GC-MRR applications, the sensitivity of the targeted band GC-MRR system should be brought close to existing technologies such as thermal conductivity detectors. Table 4.1 shows various structural features and classes of molecules, including alcohols, nitrogen heterocyclics, halogenated compounds, dioxins, and nitro compounds as probes for the GC-MRR. Most organic compounds have a significantly different thermal conductivity than helium; thus, TCD is considered a universal GC detector, making it appropriate for comparative purposes. Neon was used as the carrier gas as well as a make-up gas in the initial investigation. Table 4.1 lists the method limits of detection for the first generation millimeter-wave GC-MRR,[172] versus targeted band GC-MRR with Fabry Perot cavity and GC-TCD. Note that the LODs are conservative toward larger values because the calculation assumes noise homoscedasticity, whereas, in reality, experimental data is invariably heteroscedastic, i.e., the standard deviation of the signal increases with the concentration.[187] The room-temperature millimeter MRR data clearly shows that it is severely limited in sensitivity and has a molecular mass limit. The LOD, for small molecules like ethanol, is on the order of >3000 ppm, whereas when the molecular mass increases for molecules like thiophene or 2-chloropyridine, the LODs are even higher (>10,000 ppm). Molecules above 120 Da are not detectable at room temperature (Table 1, 3rd column). Incorporating the supersonic jet expansion as GC interface and targeted

band MRR detector with lower frequency ranges shows dramatic improvements in sensitivity. Ethanol's LOD is now reduced to 85 from 3900 ppm, and thiophene's LOD is now reduced to 65 from 84,500 ppm. Large molecules that were not measurable on the room temperature millimeter-wave GC-MRR system are easily analyzable using targeted GC-MRR detection with reasonable detection limits.

For fifty years of microwave rotational spectroscopy has been limited to very small and simple molecules. The ease with which a dioxin such as 1-(2,3-dihydro-1,4-benzodioxin-6-yl)propan-1-one (192 Da) or 2,2'-dinitrobiphenyl (244 Da) is now readily detectable is a significant achievement on its own. Therefore, the GC-TCD values provide a fair comparison for smaller molecules. The LOD concentrations also are converted to mass reaching the GC-MRR detector (Table 1) are the smallest amounts ever detected by rotational spectroscopy for any molecule. The following section shows that the combined effect of carrier and make-up gases provide even lower values.

4.4.4 Synergistic Effects of Different Carrier and Supersonic Jet Expansion Gases

Previous investigations have clearly shown that noble gases are best for supersonic jet systems, with neon having the best rotational cooling effects in MRR.[37, 169, 185] We investigated the role of various combinations of monoatomic inert gases (He, Ne) and a diatomic gas (N₂) with 1% pyridine as a probe. First direct targeted MRR measurements (without GC) were made using different expansion gases, as shown in Figure 4.4. Then, the supersonic jet nozzle had to be optimized independently for each gas in terms of nozzle pulse width, nozzle pulse delay, and nozzle tension (level of tightening of the nozzle). Finally, the nozzle parameters were optimized using the three gases individually with pyridine as a probe molecule, and their results are shown in Figure 4.4(a-c). Note that the hole size and its shape in the supersonic jets also are important

parameters.[188] For MRR work using neon, it was found that a 1 mm hole size is a good compromise between good cooling and enough gas to give high signal intensity. On the other hand, small hole sizes tend to favor gas-analyte complexes, which are undesirable for broadband and target band GC-MRR.

The main line in Figures 4.4(a-c) are centered at 14902.95 MHz (note that the peak width at half maximum is a fraction of a MHz). It clearly shows that monoatomic noble gases, neon, and helium, give comparable signal-to-noise ratios (SNRs); however, pure nitrogen gives the weakest direct MRR signal than He or Ne. Using nitrogen (a diatomic gas) reduces the SNR from 28000 to 2800 for a 20-second measurement in direct MRR. The small peak marked with an asterisk to the right of the principal peak is due to the hyperfine splitting from the spin of the ^{14}N nucleus. These results agree with those obtained by the portable microwave instrumentation developed by the National Institute of Science & Technology chemical analysis with acrolein as a probe molecule.[185]

For targeted band GC-MRR, with a typical flow rate of ~ 1 mL/min from the GC column, most of the gas to the expansion is provided by the make-up gas, and therefore the cooling should be dominated by its selection well. Suenram *et al.* showed previously that up to $\sim 25\%$ of a neon carrier gas mix could be replaced by nitrogen without compromising the signal. Therefore, we explored independently changing the carrier gas type supplied to the column and the make-up gas. The fact that argon is more abundant than other noble gases and is often used as a GC carrier gas in some applications does not make it a good candidate for MRR studies due to its relatively weaker cooling properties compared to He and Ne in supersonic jets. Additionally, the more polarizable argon tends to form gas-phase van der Waal complexes with many analytes,[189, 190], and this is problematic for collecting broadband microwave spectra of “pure” analytes since the

interest is in collecting the rotational spectra of the pure compounds, not their noble gas-phase complexes. Consequently, binary Ne, He, and N₂ combinations were tested. The results are shown in Figure 4.4(d-f). It can be seen that neon is the best choice for the make-up gas (Figure 4.4(f)) in general. However, independent of the choice of make-up/carrier gas, we find that the best signal intensities are found if *nitrogen* is used as the gas provided to the column and *neon* as the make-up gas. A typical 2-3 improvement factor over neon alone (comparable in performance to helium) is obtained.

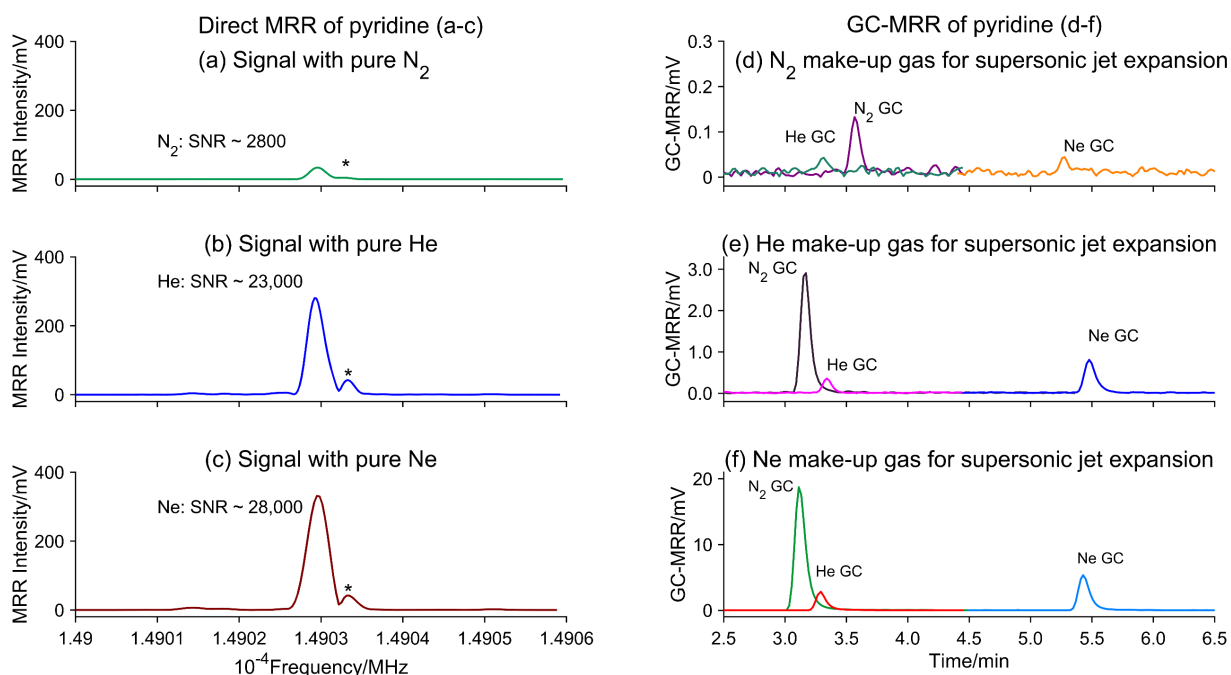
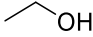
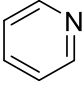

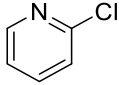
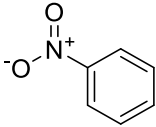
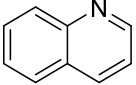
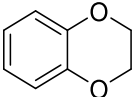
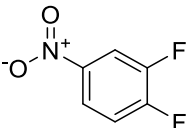
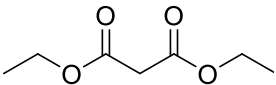
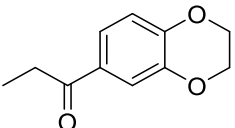
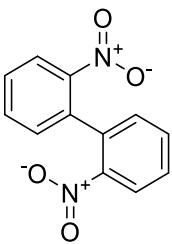


Figure 4.4 Effect of various gases used for supersonic jet expansion in a direct microwave rotational resonance experiment in a Fabry-Perot cavity (without GC). Neat pyridine, as a probe, was directly injected in the supersonic jet Fabry Perot MRR cavity in such a way that the signal became constant with a given gas being used for supersonic jet expansion cooling with pure (a) nitrogen, (b) helium, and (c) neon. Note the very narrow linewidth on the MHz scale. The small shoulder marked with (*) is due to the hyperfine splitting of the rotational transition by nitrogen nucleus. (d-f) Effect of combination of various carrier gases (N₂, He, Ne) in GC vs. make-up gases for supersonic jet expansion system with 1% pyridine injection. For the supersonic jet, (d) nitrogen is a make-up gas, (e) helium is a make-up gas, and (f) neon is a make-up gas.

Low or high pyridine concentration gives a similar enhancement factor (~2.7 fold) with this gas combination. These effects were evaluated for two other analytes, nitrobenzene and 2,3-dihydro-1,4-benzodioxin, and similar results were obtained (Figure 4.S1), with an SNR enhancement factor of 2.4 and 2.3, respectively. Based on the sensitivity gain due to nitrogen as the carrier gas, we should see a 2.7 fold reduction in the Ne-Ne LOD of pyridine. Thus, the amount corresponding to its LOD is $1.2 \text{ ng}/2.7 = 0.44 \text{ ng}$ at the detector (Table 1). Table 4.1 lists the corresponding amounts in nanograms that reach the MRR detector. Note that we do not see significant changes in the chromatographic peak width as different gases are used. Further investigations regarding this exciting and unexpected phenomenon will be addressed in the future.

Table 4.1 A comparison of detection limits of conventional GC-TCD with millimeter-wave GC-MRR and microwave targeted band GC-MRR with supersonic jet expansion cooling and Fabry-Perot cavity (Ne carrier/make-up gas). All methods utilized 2 μL injections with 50:1 split ratio (see SI for method details).

Name (Molecular mass/ Da) μ/Debye^a	Structure	Millimeter wave GC-MRR LOD/ppm	Targeted rotational frequency (MHz)	Targeted GC-MRR LOD/ppm (Amount/ ng°)	GC-TCD LOD/ppm
Ethanol (46.07) $\mu=1.44$ (trans), $\mu=1.13$ (gauche)		8500	9388.25	85 (2.7)	17
Pyridine (79.10) $\mu=2.215$		8600	14902.95	38 (1.2) 14 ^b (0.4)	24
Thiophene (84.14) $\mu=0.53$		91000	15125.6	65 (2.1)	28
2-Chloropyridine (113.54) $\mu=3.81$		17200	14180.75	370 (12)	37
Nitrobenzene (123.11) $\mu=4.22$		Not measurable	10823.65	97 (3.1) 40 ^b (1.3)	24

Quinoline (129.16) $\mu=2.01$		Not measurable	13488.1	565 (18)	39
2,3-Dihydro-1,4-benzodioxin (136.15) $\mu=1.60$		Not measurable	13296.25	380 (12) 160 ^b (5.1)	33
3,4-Difluoronitrobenzene (159.09) $\mu=2.79$		Not measurable	15489.45	420 (13)	33
Diethyl malonate (160.17) $\mu=2.20$ (Conformer 1) $\mu=2.39$ (Conformer 2)		Not measurable	15573.2	890 (28)	11
1-(2,3-Dihydrobenzo[b][1,4]dioxin-6-yl)propan-1-one (192.21) $\mu=3.80$ (Conformer 1) $\mu=4.63$ (Conformer 2)		Not measurable	15405.9	1640 (51)	18
2,2'-Dinitrophenyl (244.20) $\mu=6.30$		Not measurable	10129.5	3920 (123)	37

- a. Calculated from the dipole moment projections as a resultant vector, $\mu = \sqrt{\mu_a^2 + \mu_b^2 + \mu_c^2}$, from the SI Table 4.S5.
- b. These numbers indicate the effect of nitrogen as a GC carrier gas in the targeted band GC-MRR with neon as a make-up gas. See SI Figure 4.S4 to estimate the LOD scaling factor based on the signal enhancement factor.
- c. Amount in nanograms reaching the targeted band GC-MRR detector based on the LOD value (see Experimental section for the equation)

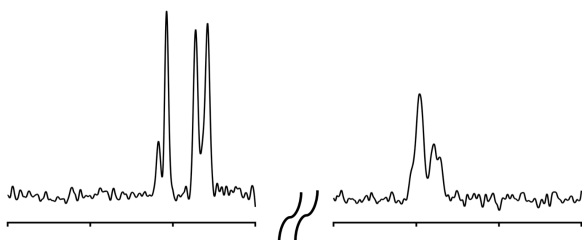
4.4.5 GC-MRR of Isomers and Isotopologues

Most gas chromatography units utilize single-channel detectors such as GC-FID and GC-TCD. On the other hand, a multichannel GC detector produces a characteristic spectrum of the eluent that enables deconvolution of partially overlapping chromatographic peaks without making any assumptions about the chromatographic peak shape as with GC-MS or GC-FTIR. Therefore, MRR is also a multichannel detector, depending on its broadband or targeted mode operation. In the latter approach, a characteristic frequency is chosen for each analyte for high sensitivity analysis.

Figure 4.5 shows that the targeted GC-MRR with a Fabry-Perot cavity can provide selected molecule monitoring analogous to the selected ion monitoring of an MS detector. Further, MRR selectivity often exceeds that of mass spectrometers allowing unambiguous discrimination among closely related compounds (Figure 4.S2-S3). Once the broadband microwave spectrum of a given isomer or isotopomers is experimentally determined or theoretically calculated,[170, 171] the Fabry-Perot cavity can remarkably precisely tune only one rotation line for that particular isomer without any chance of overlap. Figure 4.5(a) shows a typical total molecule GC trace of a mixture of partially resolved isotopomer and structural isomers of 1- and 2-bromobutanes and bromonitrobenzenes. There is a complete overlap of isotopologue peaks, especially for all ^{79}Br vs. ^{81}Br containing compounds. Since each compound has a unique MRR spectrum, specific lines can be monitored for each analyte to provide a chromatogram with no interference from any/all other compounds (Figure 4.5(b)). Table 4.S4 shows the exact frequency of each analyte used for monitoring the bromobutanes and bromonitrobenzenes. Furthermore, an overlapping analyte will not cause a suppression of another compound signal as happens in MS due to ionization suppression.[172] Figure 4.5b shows that the partially co-eluting peaks consist of the signals from

18 isotopically distinct compounds and their structural isomers. Thus, targeted band GC-MRR can provide convenient and unequivocal detection and quantitation of closely related molecules in complex mixtures.

(a) Total molecule chromatogram



(b) Extracted molecule chromatogram

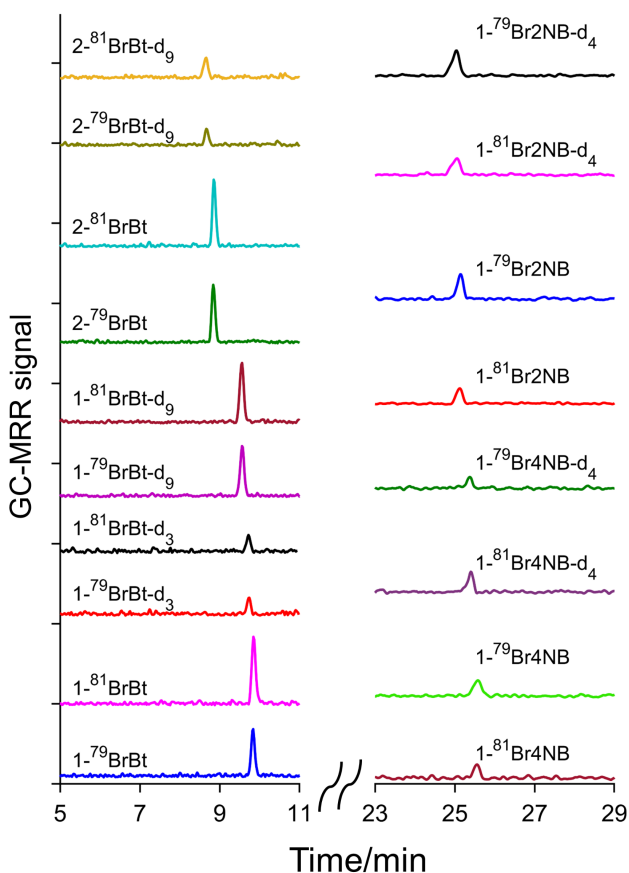


Figure 4.5. Illustration of the concept of a (a) total molecular chromatogram and (b) an extracted molecular chromatogram of various deuterated and structural isomers of bromobutanes (BrBt) and bromonitrobenzenes (BrNB) on an SLB-5ms capillary GC column with Ne as a carrier and make-up gas. The numbers indicate the position of substitution of bromine and the nitro group on

the bromobutane and the benzene ring. See Table 4.S4 for the run conditions of targeted band GC-MRR.

4.5 Conclusions

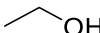
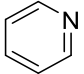
The molecular information and spectrum resolution obtainable from the GC-MRR system were well beyond what can be proffered by GC-FTIR, GC-NMR, GC-VUV, and GC-MS systems, including high-resolution MS or combinations thereof. There are no background signals encountered in GC-MRR because the precisely tuned rotational frequency in the Fabry-Perot cavity is highly specific for a given molecule. Microwave spectroscopy was limited to very simple small molecules with a permanent dipole moment of astronomical interest. This work established the promising character of a targeted MRR as a detector for GC for various small and larger molecules. It was shown that the hot GC effluent must be cooled with a supersonic jet expansion system. In addition, a deeper insight into the instrument design requirements was gained by coupling a microwave spectrometer with a Fabry-Perot microwave cavity for sensitivity enhancement. These developments led to a GC-MRR system with sensitivity close to that of standard thermal conductivity detectors. The added advantage is its superior molecular selectivity as compared to GC-FTIR, GC-MS, or GC-NMR. In addition to unequivocally resolving isomers, isobars, isotopologues, isotopomers, and co-eluting compounds in general, the new GC-MRR developments could also have several practical consequences for the industrial analysis of online reaction monitoring of regioisomers in crude mixtures. The limits of detection reported for these compounds are the smallest known in microwave rotational spectrometer used as a flow cell, i.e., nanogram levels with optimized gases. Total molecule chromatograms can be generated as can


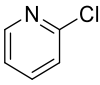
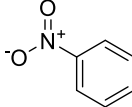
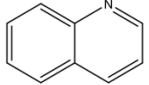
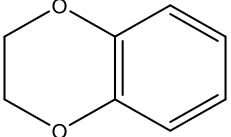
select molecule chromatograms in a process akin to MS detection, which provides total and selected ion chromatograms. Further efforts are underway to understand the nature of mixed gases (N₂ and Ne) and their synergistic effects on signal strength. Additional improvements in signal processing are being expanded, including higher data sampling rates, faster data processing, a user-friendly interface, and digital processing for a commercial product. A library of rotational spectra will be incorporated in the future.

4.6 Supporting Information

Table 4.S1: Summary of GC-TCD Methods

The GC separations were performed on an Agilent 6890N (Agilent, Palo Alto, CA, USA) gas chromatograph equipped with a thermal conductivity detector employing an SLB-5ms capillary GC column (L × I.D. 30 m × 0.25 mm, d_f = 0.25 μm). The inlet and detector temperatures were set at 250 °C. The injection volume was 2 μL with a split ratio of 50:1. The data sampling rate for the thermal conductivity detector was 5 Hz.

Name	Structure	TCD Methods	Solvent
Ethanol		Column name: SLB-5ms 30 m x 0.25 mmx0.25 μm Inlet temp: 250 C Detector temp: 250 C Oven temperature: 25 C Average linear velocity: 25 cm/s Carrier gas: Helium Injection volume: 2 μL Split ratio: 50:1	ACN
Pyridine		Column name: SLB-5ms 30 m x 0.25 mmx0.25 μm Inlet temp: 250 C Detector temp: 250 C Oven temperature: 85 C Average linear velocity: 30 cm/s Carrier gas: Helium Injection volume: 2 μL Split ratio: 50:1	ACN

Thiophene		<p>Column name: SLB-5ms 30 m x 0.25 mmx0.25 μm Inlet temp: 150 C Detector temp: 250 C Oven temperature: 30 C Average linear velocity: 30 cm/s Carrier gas: Helium Injection volume: 1 μL Split ratio: 50:1</p>	MeOH
2-chloropyridine		<p>Column name: SLB-5ms 30 m x 0.25 mmx0.25 μm Inlet temp: 250 C Detector temp: 250 C Oven temperature: 85 C Average linear velocity: 30 cm/s Carrier gas: Helium Injection volume: 2 μL Split ratio: 50:1</p>	ACN
Nitrobenzene		<p>Column name: SLB-5ms 30 m x 0.25 mmx0.25 μm Inlet temp: 250 C Detector temp: 250 C Oven temperature: 95 C Average linear velocity: 30 cm/s Carrier gas: Helium Injection volume: 2 μL Split ratio: 50:1</p>	ACN
Quinoline		<p>Column name: SLB-5ms 30 m x 0.25 mmx0.25 μm Inlet temp: 250 C Detector temp: 250 C Oven temperature: 117 C Average linear velocity: 30 cm/s Carrier gas: Helium Injection volume: 2 μL Split ratio: 50:1</p>	ACN
2,3-Dihydro-1,4-benzodioxin		<p>Column name: SLB-5ms 30 m x 0.25 mmx0.25 μm Inlet temp: 250 C Detector temp: 250 C Oven temperature: 106 C Average linear velocity: 30 cm/s Carrier gas: Helium Injection volume: 2 μL Split ratio: 50:1</p>	ACN

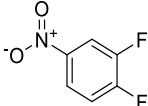
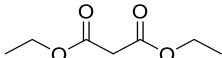
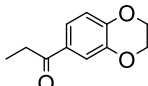
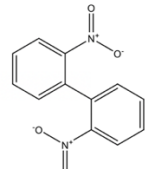
<p>3,4-Difluoronitrobenzene</p>		<p>Column name: SLB-5ms 30 m x 0.25 mmx0.25 μm Inlet temp: 250 C Detector temp: 250 C Oven temperature: 95 C Average linear velocity: 30 cm/s Carrier gas: Helium Injection volume: 2 μL Split ratio: 50:1</p>	<p>ACN</p>
<p>Diethylmalonate</p>		<p>Column name: SLB-5ms 30 m x 0.25 mmx0.25 μm Inlet temp: 250 C Detector temp: 250 C Oven temperature: 87 C Average linear velocity: 30 cm/s Carrier gas: Helium Injection volume: 2 μL Split ratio: 50:1</p>	<p>ACN</p>
<p>1-(2,3-Dihydrobenzo[b][1,4]dioxin-7-yl)propan-1-one</p>		<p>Column name: SLB-5ms 30 m x 0.25 mmx0.25 μm Inlet temp: 250 C Detector temp: 250 C Oven temperature: 250 C Average linear velocity: 30 cm/s Carrier gas: Helium Injection volume: 2 μL Split ratio: 50:1</p>	<p>ACN</p>
<p>2,2'-Dinitrobiphenyl</p>		<p>Column name: SLB-5ms 30 m x 0.25 mmx0.25 μm Inlet temp: 250 C Detector temp: 250 C Oven temperature: 213 C Average linear velocity: 30 cm/s Carrier gas: Helium Injection volume: 2 μL Split ratio: 50:1</p>	<p>ACN</p>

Table 4.S2. Millimeter-wave room temperature broadband GC-MRR conditions

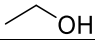
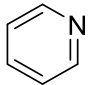
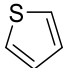
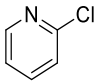
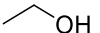
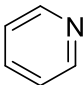
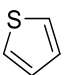
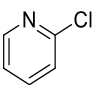
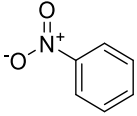
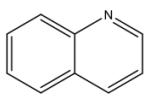
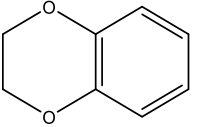
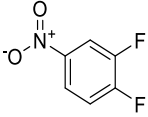
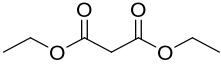
Name	Structure	Room temperature GC-MRR conditions	Solvent
Ethanol		Column name: SLB-5ms 30 m x 0.25 mmx0.25 μm Inlet temp: 250 C Flow cell temp: 50 C Oven temperature: 25 C Average linear velocity: 40 cm/s Carrier gas: Hydrogen Injection volume: 2 μL Split ratio: 50:1	ACN
Pyridine		Column name: SLB-5ms 30 m x 0.25 mmx0.25 μm Inlet temp: 250 C Flow cell temp: 50 C Oven temperature: 85 C Average linear velocity: 40 cm/s Carrier gas: Hydrogen Injection volume: 2 μL Split ratio: 50:1	ACN
Thiophene		Column name: SLB-5ms 30 m x 0.25 mmx0.25 μm Inlet temp: 250 C Flow cell temp: 50 C Oven temperature: 30 C Average linear velocity: 40 cm/s Carrier gas: Hydrogen Injection volume: 2 μL Split ratio: 50:1	MeOH
2-chloropyridine		Column name: SLB-5ms 30 m x 0.25 mmx0.25 μm Inlet temp: 250 C Flow cell temp: 50 C Oven temperature: 85 C Average linear velocity: 40 cm/s Carrier gas: Hydrogen Injection volume: 2 μL Split ratio: 50:1	ACN

Table 4.S3. Supersonic jet targeted band GC-MRR conditions. Neon carrier gas (GC) with neon makeup gas (MRR). GC nominal settings are given as if helium gas was used (as there is no neon option in GC software).

Name	Structure	Targeted band GC-MRR conditions	Solvent
Ethanol		Column name: SLB-5ms 30 m x 0.25 mmx0.25 μ m Inlet temp: 250 C Oven temperature: 45 C Interface and nozzle temp: 65 C Carrier gas: Neon Linear velocity: 40 cm/s (as if for He) Makeup gas pressure: 0.5 psi Injection volume: 2 μ L Split ratio: 50:1	ACN
Pyridine		Column name: SLB-5ms 30 m x 0.25 mmx0.25 μ m Inlet temp: 250 C Oven temperature: 85 C Interface and nozzle temp: 105 C Carrier gas: Neon Linear velocity: 50 cm/s (as if for He) Makeup gas pressure: 0.5 psi Injection volume: 2 μ L Split ratio: 50:1	ACN
Thiophene		Column name: SLB-5ms 30 m x 0.25 mmx0.25 μ m Inlet temp: 250 C Oven temperature: 85 C Interface and nozzle temp: 105 C Carrier gas: Neon Linear velocity: 28 cm/s (as if He) Makeup gas pressure: 0.5 psi Injection volume: 2 μ L Split ratio: 50:1	MeOH
2-chloropyridine		Column name: SLB-5ms 30 m x 0.25 mmx0.25 μ m Inlet temp: 250 C Oven temperature: 85 C Interface and nozzle temp: 105 C Carrier gas: Neon Linear velocity: 35 cm/s (as if He) Makeup gas pressure: 0.5 psi Injection volume: 2 μ L Split ratio: 50:1	ACN

Nitrobenzene		<p>Column name: SLB-5ms 30 m x 0.25 mmx0.25 μm Inlet temp: 250 C Oven temperature: 95 C Interface and nozzle temp: 105 C Carrier gas: Neon Linear velocity: 50 cm/s (as if He) Makeup gas pressure: 0.5 psi Injection volume: 2 μL Split ratio: 50:1</p>	ACN
Quinoline		<p>Column name: SLB-5ms 30 m x 0.25 mmx0.25 μm Inlet temp: 250 C Oven temperature: 150 C Interface and nozzle temp: 170 C Carrier gas: Neon Linear velocity: 35 cm/s (as if He) Makeup gas pressure: 0.5 psi Injection volume: 2 μL Split ratio: 50:1</p>	ACN
2,3-Dihydro-1,4-benzodioxin		<p>Column name: SLB-5ms 30 m x 0.25 mmx0.25 μm Inlet temp: 250 C Oven temperature: 170 C Interface and nozzle: 190 and 175 C Carrier gas: Neon Linear velocity: 36 cm/s (as if He) Makeup gas pressure: 0.5 psi Injection volume: 2 μL Split ratio: 50:1</p>	ACN
3,4-Difluoronitrobenzene		<p>Column name: SLB-5ms 30 m x 0.25 mmx0.25 μm Inlet temp: 250 C Oven temperature: 95 C Interface and nozzle temp: 95 C Carrier gas: Neon Linear velocity: 47 cm/s (as if He) Makeup gas pressure: 0.5 psi Injection volume: 2 μL Split ratio: 50:1</p>	ACN
Diethylmalonate		<p>Column name: SLB-5ms 30 m x 0.25 mmx0.25 μm Inlet temp: 250 C Oven temperature: 170 C Interface and nozzle: 190 and 175 C Carrier gas: Neon</p>	ACN

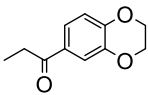
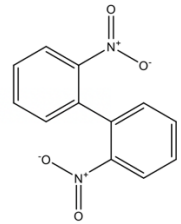
		<p>Linear velocity: 36 cm/s (as if He) Makeup gas pressure: 0.5 psi Injection volume: 2 μL Split ratio: 50:1</p>	
<p>1-(2,3-Dihydrobenzo[b][1,4]dioxin-7-yl)propan-1-one</p>		<p>Column name: SLB-5ms 30 m x 0.25 mmx0.25 μm Inlet temp: 320 C Oven temperature: 300 C Interface and nozzle: 300 and 220 C Carrier gas: Neon Linear velocity: 40 cm/s (as if He) Makeup gas pressure: 0.5 psi Injection volume: 2 μL Split ratio: 50:1</p>	ACN
<p>2,2'-Dinitrobiphenyl</p>		<p>Column name: SLB-5ms 30 m x 0.25 mmx0.25 μm Inlet temp: 320 C Oven temperature: 300 C Interface and nozzle: 300 and 220 C Carrier gas: Neon Linear velocity: 37 cm/s (as if He) Makeup gas pressure: 0.5 psi Injection volume: 2 μL Split ratio: 50:1</p>	ACN

Figure 4.S1. Carrier and makeup gas effects on GC-SJ-MRR: N₂ (GC) + Ne (MRR) signal enhancement near the corresponding limits of quantitation (LOQ) for three chemicals.

Chemical (concentration)	Avg. Signal Enhancement in N ₂ (GC) + Ne (MRR) near LOQ
Pyridine (150 ppm)	~2.7-fold
Nitrobenzene (300 ppm)	~2.4-fold
2,3-Dihydro-1,4-Benzodioxin (1200 ppm)	~2.3-fold

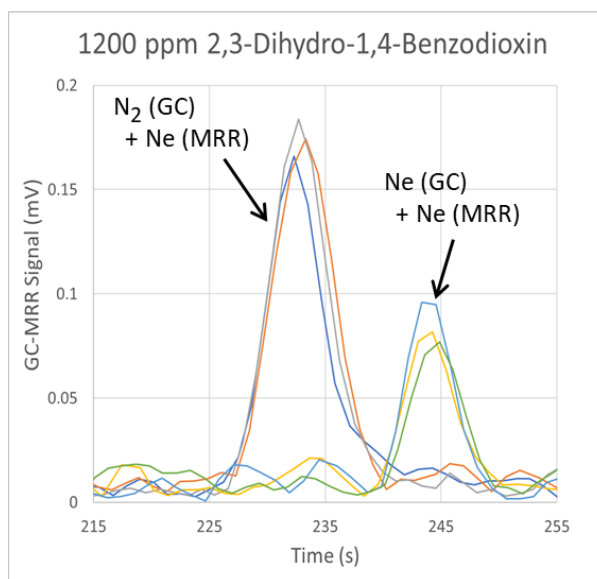
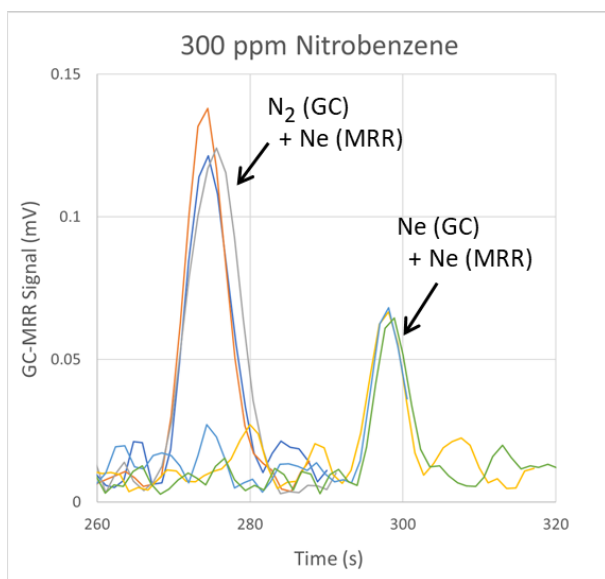
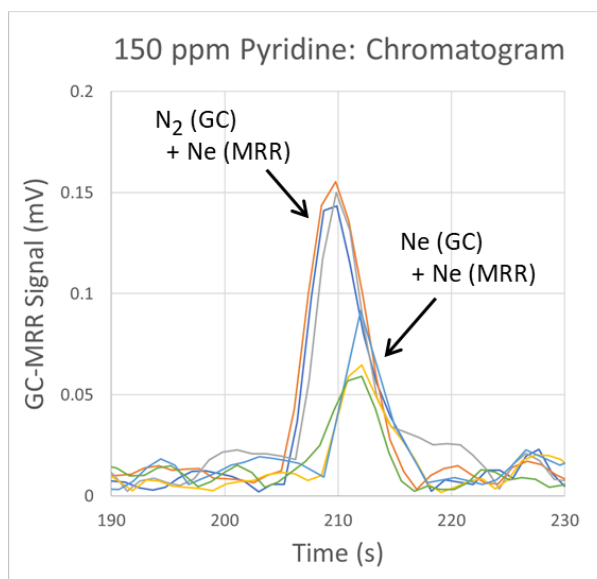


Figure 4.S2 MRR enables unambiguous discrimination between all listed bromonitrobenzene isomers and isotopologues.

Fit MRR spectra: #1. 1-bromo-2-nitrobenzene-⁷⁹Br, #2. 1-bromo-2-nitrobenzene-⁸¹Br, #3. 1-bromo-2-nitrobenzene-⁷⁹Br-d₄, #4. 1-bromo-2-nitrobenzene-⁸¹Br-d₄, #5. 1-bromo-4-nitrobenzene-⁷⁹Br, #6. 1-bromo-4-nitrobenzene-⁸¹Br, #7. 1-bromo-4-nitrobenzene-⁷⁹Br-d₄, #8. 1-bromo-4-nitrobenzene-⁸¹Br-d₄.

Top panel: zoomed to 7500 – 12500 MHz. Bottom panel: zoomed to 9300 – 9500 MHz.

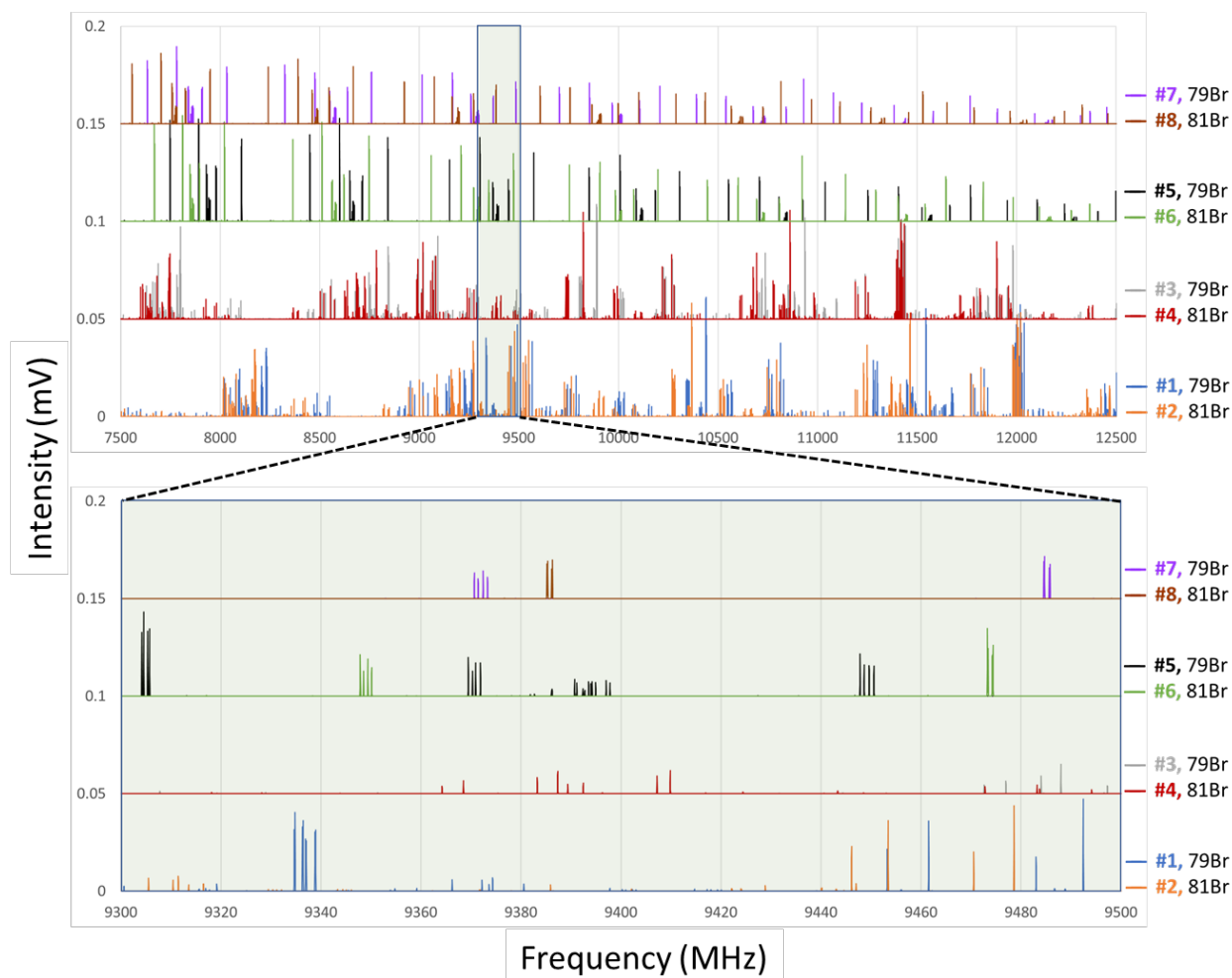


Figure 4.S3 MRR selectivity often exceeds that of mass spectrometry. Highly similar mass spectra (left plots, NIST chemistry webbook) versus remarkably different MRR spectra (right plots, this work) of 1-bromo-4-nitrobenzene and 1-bromo-2-nitrobenzene.

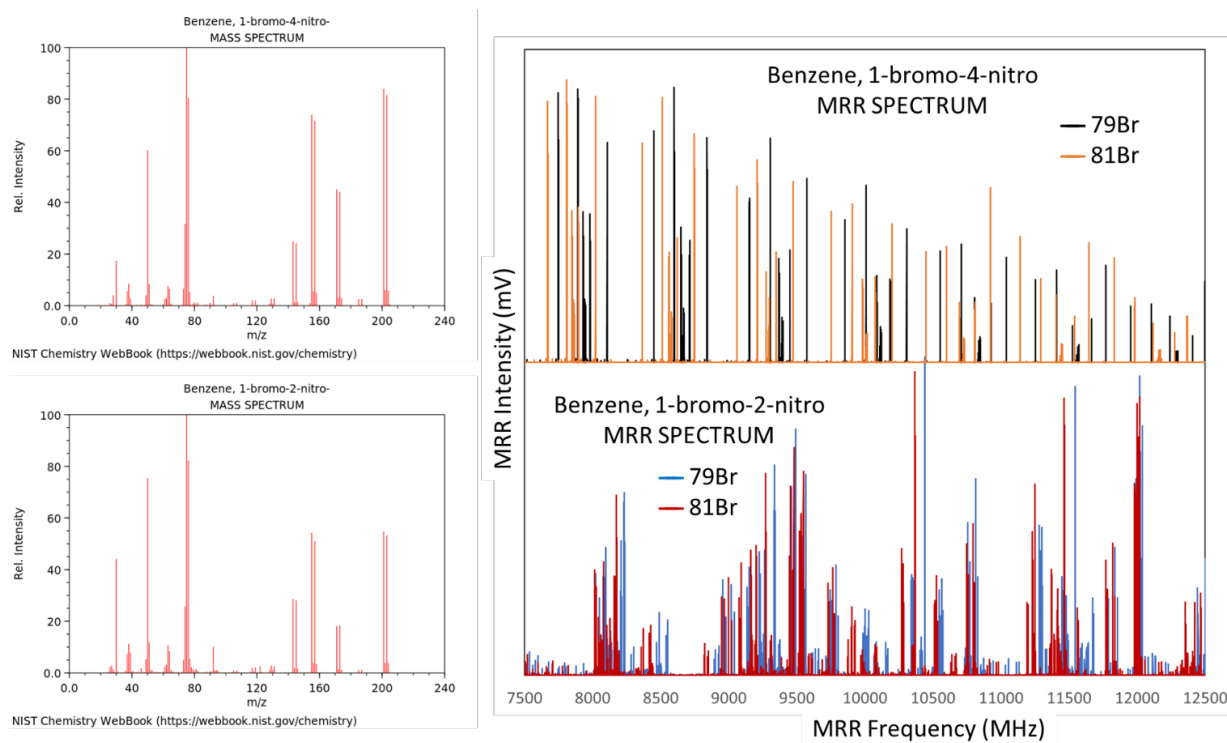
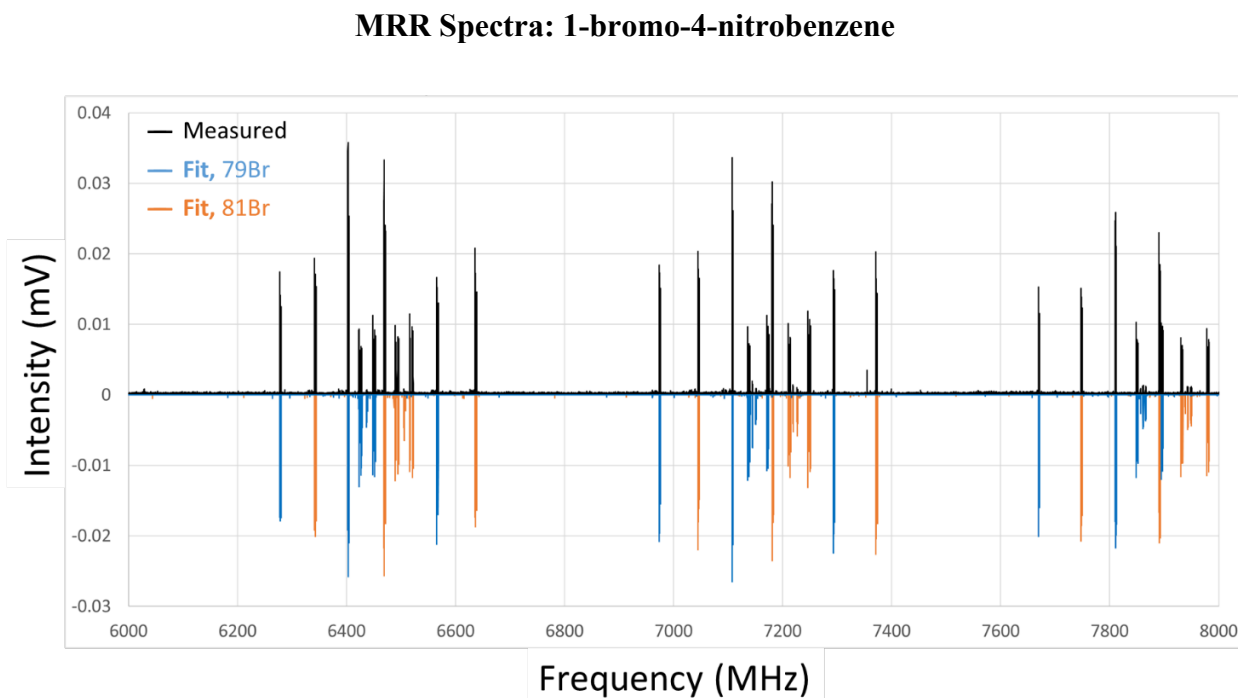


Figure 4.S4. MRR spectra fit utilized in this work: 1-bromo-4-nitrobenzene example.

Black: measured spectrum (zoomed to 6000 – 8000 MHz)

Blue and Orange: Fit spectra for ^{79}Br and ^{81}Br species, respectively. Please note that fit spectra are artificially made negative for visual appearance purpose.



Chapter 5

A metal organic framework - ionic liquid pseudophase system as a gas chromatography stationary phase

5.1 Abstract

Ionic liquids (ILs) containing colloidal metal organic frameworks (MOFs) have been used as gas chromatography stationary phases to provide distinct separation properties. The behavior of four different organic frameworks in 18 ionic liquids was investigated. Metal organic frameworks flocculated, degraded, or formed a colloidal dispersion in ionic liquids. The newly developed stationary phase consisted of colloidal ZIF-8 uniformly dispersed in an imidazolium-based dicationic ionic liquid which provided the first separation of permanent gases via hybrid gas-liquid chromatography. In addition, various groups of alkanes, ketones, alcohols, ethers, and Rohrschneider-McReynolds compounds were separated on this newly developed hybrid stationary phase. Equations for the three-phase model were derived to determine the behavior of solutes with this pseudophase system. Using this model, the distribution constants between all three phases were calculated. It was shown that the metal organic framework had a large contribution to solute partitioning to the stationary phase.

5.2 Introduction

Two of the more high-impact materials involving separations in the last decade are ionic liquids (ILs) and metal organic frameworks (MOFs). Each can be used to produce distinct gas chromatography stationary phases which can be complementary to one another [51, 55, 66, 123, 191-195]. One obvious difference is their state, MOFs are solids and ILs are liquids. Hence, the types of materials separated and the separation mechanism, as well as the thermodynamics and kinetics of the separation processes can differ considerably [192].

First introduced in the 1990s, metal-organic frameworks are a class of porous solid materials that have garnered interest for a variety of prospective applications. These organic-inorganic hybrid solids are built from organic linkers and inorganic metal nodes. The tunability of their synthesis gives these materials structural flexibility, variety and designability for use in various applications [192]. These porous materials are known to have large surface areas, a high propensity for crystallization, diverse structures, and tunable pores, all of which can be varied through synthetic procedures [196].

Many applications have focused on using MOFs as stationary phases in chromatography. In gas-solid chromatography (GSC), MOFs have been used as stationary phases in packed and open tubular columns for the separation of alkanes, xylenes and ethylbenzene, polychlorinated biphenyls, and chiral mixtures [66, 192, 196-198]. The advantages of using GC capillary coated columns are that only very small amounts of stationary phase (MOFs) are required, which allows the use of more expensive materials. It also allows the use of synthesized materials that have unique interactions between various analytes and the stationary phases, due to the diverse structures and unique properties of MOFs [66].

Importantly, metal organic frameworks have been utilized as stationary phases in gas solid chromatography for the separation of gases [191, 192]. MOFs possess the highest surface area per gram and large internal cavity volumes, accessible through pores, as compared to other available materials. MOFs have been used to adsorb and store gases [199, 200]. Membranes consisting of MOFs have been used to separate gases through a molecular sieving effect [191]. Also, MOFs that are used in GSC, often produce poor peak shapes, broadening, tailing, and poor efficiencies for vaporized liquid samples [66, 67, 192]. This is common for GSC regardless of the nature of the

stationary phase. Hence, GSC is most often used for gases, light hydrocarbons and a few other highly volatile compounds that are gases at standard temperature and pressure.

Ionic liquids (IL) are salts which have relatively low melting points. ILs with melting points below 25°C are known as room temperature ionic liquids (RTILs). These salts are generally composed of organic cations and an organic or inorganic anion. ILs have properties that make them favorable as GC stationary phases [51, 55, 193-195]. Desired properties can be enhanced by modifying the IL structure [201]. The advantage of ILs is that they have higher thermal stabilities compared to traditional molecular GC stationary phases in the same polarity range [55, 193, 201, 202]. ILs have a dual nature, meaning that they act like nonpolar stationary phases for the separation of nonpolar analytes while retaining and separating polar analytes like a polar stationary phase [51]. Often, dispersion forces are among the top two or three most important associative interactions between analytes and ILs [132]. This enables them to separate mixtures of compounds with diverse polarities and properties [51]. When measuring the polarity of ILs using common empirical solvent polarity methods, the polarity range of all ionic liquids appears to be similar and close to that of short-chain alcohols [108, 203, 204]. However, it has been found that such simple single parameter measurements cannot adequately describe ILs. When used as solvents for organic reactions or in gas-liquid chromatography, unique individual interactions (i.e., dispersion, π - π , n- π , hydrogen bonding, dipolar, columbic) can all have profound effects on reaction products, kinetics, and distribution constants respectively [132]. These types of multiple solvation interactions can be investigated through linear free energy approaches [132, 205, 206]. Many ionic liquids also have high thermal stabilities which is a necessity for a GC stationary phase. The decomposition of an IL often occurs via nucleophilic attack of its anion on the cation [207]. Reducing the nucleophilicity of the anion usually increases the stability of the IL stationary phase.

Therefore, less nucleophilic anions like bis[(trifluoromethyl)sulfonyl]imide (NTf_2^-) provides more stable ILs compared to chloride or bromide anion containing ILs. Also, dicationic imidazolium-based or phosphonium-based ILs often have higher thermal stabilities [52, 207, 208]. The melting points of ILs can be affected by variations in the linkage chain length [52, 209]. The viscosities of ionic liquids are usually high due to interionic interactions. However, the selection of cation and anion and the size of IL can greatly affect the viscosity [57, 209-212]. Thus, dicationic liquids typically have higher viscosities and thermal stabilities as well as a broader range of physical and chemical properties compared to most conventional monocationic ILs [209].

A stationary phase that can utilize MOFs and mimic the properties of gas-liquid chromatography (GLC) could be highly beneficial and more widely applicable. Thus, a novel stationary phase of colloidal MOFs dispersed in ionic liquids would provide the motif of gas-liquid chromatography that can be utilized for both volatile molecules and gases. Herein, we introduce the first use of metal organic framework dispersions in an ionic liquid as a stationary phase for use in gas chromatography.

5.3 Materials and Methods

5.3.1 Chemicals and reagents

All analytes (dichloromethane, decane, methanol, undecane, 1-propanol, tridecane, 1-butanol, 2-butanol, tetradecane, 1-pentanol, *tert*-butyl methyl ether, 2-pentanone, 2-octanone, 3-hexanone, 2-heptanone, glycidyl methyl ether, pyridine, nitropropane, glycidyl isopropyl ether, cyclopentanone, hexadecane, cyclohexanone) and metal organic frameworks (ZIF-8, HKUST-1, MOF-177, Fe-BTC) were purchased from MilliporeSigma (formerly Sigma-Aldrich, St. Louis, MO).

5.3.2 GC columns

The Gas Chromatography capillary columns (30 m x 0.25 mm i.d x 0.20 μm df) were coated at Supelco using the static method [213]. For IL + MOF [DMIMC9 NTf₂ (1,9-di(3-methylimidazolium)nonane bis[(trifluoromethyl)sulfonyl]imide) + ZIF-8 [Zn(mIM)₂, mIM = 2-methylimidazolate]) column, a saturated solution of MOF in ionic liquid (synthesized in lab) was diluted to 0.2% w/v solution (MOF in IL/ dichloromethane) to coat capillary columns. For the neat IL column, DMIMC9 NTf₂ was diluted to 0.2% w/v solution (IL/dichloromethane) to coat capillary columns. The stationary phase film thickness was 0.12 μm in all columns. It has been shown that immobilized MOF particles have column bleeding, long retentions, poor peak shapes for non-permanent gases when separated isothermally [214]. Five different columns were coated from two batches of IL + MOF saturated mixtures and no significant differences in retention factors and efficiencies were observed.

5.3.3 Experimental

All analyte mixtures were prepared in dichloromethane at 1 mg/mL. Butane, propane, and CO₂ were sampled from the headspace.

5.3.4 Apparatus and instrument

The gas chromatographic analyses were performed on an Agilent 6850 (Agilent, Palo Alto, CA, USA) gas chromatograph equipped with a flame ionization detector and thermal conductivity detector. For all mixture separations helium was used as the carrier gas with the average velocity of 30 cm/sec. The detector and injection port temperatures were both set at 250 °C. The oven temperature was set at 75 °C. The injection volumes were 1 μL and the split ratio was 100:1. For

gas analysis studies, the helium average velocity was 30 cm/sec. The detector and injection port temperature were both set at 250 °C. The oven temperature was set at 12 °C with an injection volume of 3 µL and split ratio of 100:1. An Agilent ChemStation data processing unit was used for processing and storing the chromatograms. Particle size and distributions were measured using a digital microscope (Keyence VHX-7000 series Digital Microscope, Dual-light High-magnification zoom lens (250 x to 2500 x)).

5.3.5 Synthesis of Ionic liquids

The synthesis of dicationic liquids was conducted in two steps. In the first step, 1 molar equivalent of 1,9-dibromononane was reacted with 2 molar equivalents of 1-methylimidazole. The reaction was carried out in acetonitrile in a heavy wall round bottom flask with reflux at 80°C for 72 hours. The solvent was evaporated using rotary evaporation. The resulting liquid was extracted through liquid-liquid extraction using water/dichloromethane (50:50) to remove unreacted materials. The dibromo salt produced through the nucleophilic reaction was collected in the aqueous layer. In the second step, 1 molar equivalent of the dibromo salt was reacted with 2 molar equivalents of bis(trifluoromethane)sulfonamide lithium salt (LiNTf₂) in water for 12 hours. Dichloromethane was added to the reaction mixture to extract the NTf₂⁻ ionic liquid salt. The Dichloromethane layer was collected and washed multiple times with water to remove unreacted lithium bromide and excess NTf₂⁻. Dicationic ionic liquid was extracted through rotary evaporation of dichloromethane. The resulting liquid was dried over phosphorus pentoxide at 40 °C for 24 hours to produce the pure dicationic liquid with NTf₂⁻ counter anion. Refer to Talebi et al. for the synthetic procedures of the ionic liquids mentioned herein [210]. Ionic liquids were characterized per literature [210].

5.3.6 Determination of Behaviors of MOFs in ILs

MOFs were added at 0.06% w/w in ILs after which they were vortexed and sonicated for 2 minutes, each. Their behavior (see Results and Discussion) was observed over course of 72 hours, no significant aggregation of particles was observed.

5.3.7 Partial Specific Volume

Using a pycnometer, the partial specific volume of ZIF-8 was determined. At room temperature (22°C), a measured amount of ZIF-8 is added to the pycnometer then filled to the mark with hexane. To calculate the partial specific volume, the difference in weight between the pycnometer filled with known volume of pure hexane and with ZIF-8 in the same volume is used.

5.4 Results and Discussion

When mixing ILs and MOFs (see Experimental) three different behaviors were observed: 1) the MOFs degraded, 2) they flocculated, or 3) they formed colloidal dispersions. MOFs that are degraded in ILs dissociate into their constituent ions and are no longer viable entities. The flocculation of MOFs produces macroscopic inhomogeneous mixtures which tend to sediment, clog capillaries and results in poor chromatographic separations. Therefore, the only pertinent combinations of MOFs and ILs are those mixtures in which microscopic MOFs are dispersed throughout the ILs as a uniform, stable and homogenous colloidal phase. As summarized in Table 5.1, four different MOFs were dispersed into eighteen different ILs. Determination of behaviors for all combinations of ILs and MOFs were done visually. Degradation was determined through the presence of a clear solution and/or a colored solution, i.e., IL 7 and MOF B produced a purple color associated with free copper ions in solution. In Table 5.1, the green color indicates a homogenous colloidal dispersion, gray indicates flocculation, purple indicates degradation, and

black indicates the mixture was not tested due to a lack of material. Of the four MOFs, ZIF-8 showed the highest dispersion and amongst the various ILs. Imidazolium based ionic liquids dispersed a greater number of MOFs (Table 5.1).

Table 5.1. List of ionic liquids and MOFs with their behavior indicated by green for dispersion, gray for flocculation, purple for degradation, and black for not tested. A: ZIF-8, B: HKUST-1, C: MOF-177, D: Fe-BTC.

#	Ionic Liquid	A	B	C	D
1		Green	Gray	Gray	Gray
2		Green	Gray	Green	Gray
3		Green	Gray	Gray	Gray
4		Green	Gray	Gray	Gray
5		Green	Gray	Gray	Black
6		Green	Green	Gray	Gray
7		Green	Purple	Black	Black
8		Green	Gray	Gray	Gray
9		Green	Gray	Gray	Gray
10		Gray	Gray	Black	Black
11		Green	Gray	Gray	Gray
12		Green	Gray	Gray	Gray
13		Green	Green	Black	Black
14		Green	Green	Green	Black

Out of all the dispersions of IL which met the criteria, the IL best fit for gas chromatography stationary phase, was chosen. Ionic liquids with halogens as anions have low thermal stability (120 °C) while NTf₂ has higher thermal stability (up to 400°C) [52, 209]. Dicationic ILs are more viscous compared to monocationic ILs, which is beneficial in coating uniform thin film on capillary columns [26,25,36,37]. Methyl-based imidazolium cations are preferable to butyl-based imidazolium cations as they are more polar – a useful property in dispersing polar MOFs [209]. Branched chain ILs are difficult to synthesize, while a quick straightforward synthesis of DMIM-C9 is more feasible to produce in bulk quantities [209].

Zeolitic imidazolate frameworks (ZIFs) are a subtype of MOF with structures analogous to zeolites. ZIF-8 has been examined for H₂ storage, CO₂ adsorption, [215] as well as the separation of alkane/alkenes and various other mixtures [216]. These MOFs exhibit a cubic architecture consisting of Zn²⁺ ions and 2-methylimidazole ligands. The structure contains 11.6 Å (1.16 nm) large cages connected through small apertures of 3.4 Å (0.34 nm) that are flexible upon guest adsorption [66] with a surface area of 1250–1600 m² g⁻¹ [216]. For this specific study, the combination of ZIF-8 and DMIMC9 NTf₂ was utilized as it provided a uniform and stable dispersion which may be a consequence of the fact that they share an imidazolium moiety in their structures. X-ray diffraction analysis of dilute MOFs dispersed in an IL has not been nor can be accomplished, to our knowledge.

Optical microscopy was used to determine the particle size of the ZIF-8 MOF dispersed in the IL (DMIM-C9) (0.06% w/w) (see Materials and Methods). The measured particles averaged 1.5 μm, as shown in Figure 5.1. The stable dispersion subsequently was coated onto capillary columns as the stationary phase (see Materials and Methods). It should be noted that the IL + MOF

mixture can't be characterized using scanning electron microscope (SEM) or transmission electron microscope (TEM) because it is a liquid sample.

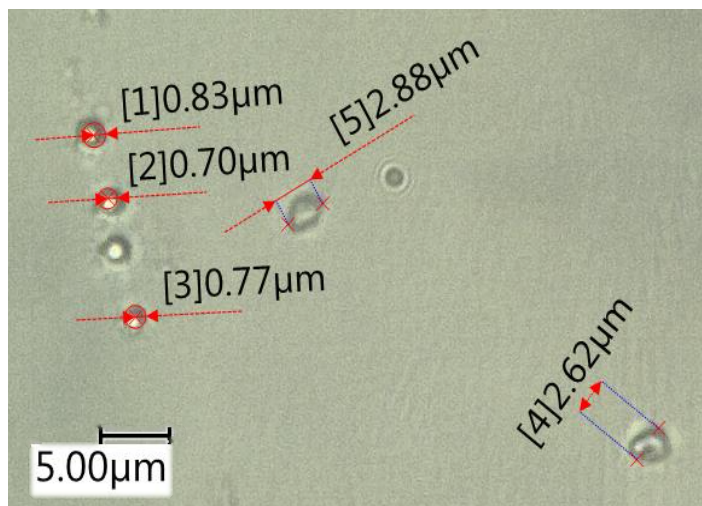


Figure 5.1 Digital microscopic picture of metal ZIF-8 (brown spots) dispersed in DMIM-C9 obtained using a Keyence VHX-7000 series Digital Microscope.

Three different mixtures of compounds were separated on two different stationary phases (i.e., the neat IL vs. the IL + MOF). The mixtures consisting of various alkanes, ketones, alcohols, ethers, and Rohrschneider compounds were used to evaluate the selectivity of the stationary phase for these analytes. The separations of the group of compounds were reproducible after 12 months, and over 300 injections. For three different analyte mixtures separated on both stationary phases, longer retention times were always observed on the ZIF-8 DMIMC9 NTf₂ compared to the neat IL (DMIMC9 NTf₂) stationary phase for all analytes.

Figure 5.2a shows the chromatogram for the separation on a neat IL stationary phase vs. Figure 5.2b which shows the same separation under identical conditions on the IL + MOF stationary phase for an alkane and alcohol mixture. Retention order changes were seen for tridecane (6), 1-butanol (7), tetradecane (8), and 1-pentanol (9). The alkanes (tridecane (6),

tetradecane (8)) retained longer on the IL + MOF column compared to 1-butanol (7) and 1-pentanol (9) resulting in the retention order shifts.

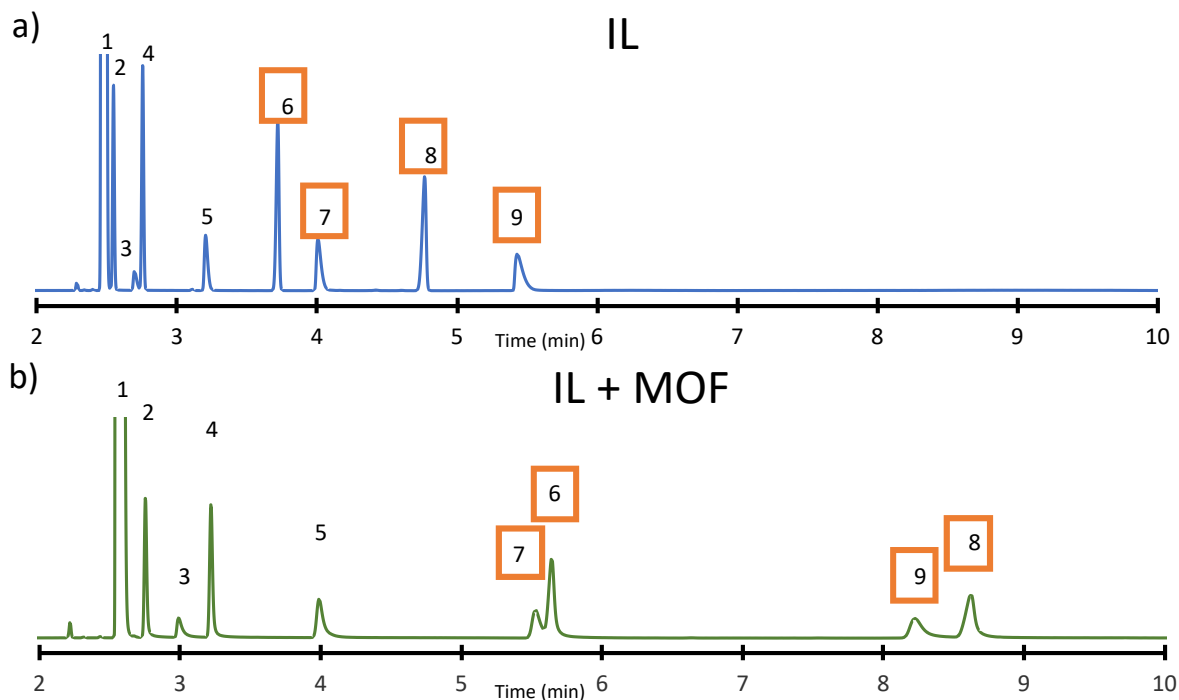


Figure 5.2. Chromatograms of separation of alkane and alcohol compounds on two stationary phases (IL and IL+MOF). 30m x 0.25mm x 0.25 μ m, oven temp: 70 $^{\circ}$ C, average velocity: 30cm/s, carrier gas: He, split ratio 100:1, injection volume: 1 μ l, flame ionization detector. Dichloromethane (1), decane (2), methanol (3), undecane (4), 1-propanol (5), tridecane (6), 1-butanol (7), tetradecane (8), 1-pentanol (9). The chromatographic parameters are listed in Table 5.S1, in supplementary information.

Another change in selectivity was seen in Figure 5.3a in contrast to 3b where the retention of pyridine (20) significantly increases on the IL + MOF stationary phase, where it eluted last. Pyridine (compound 20) changes retention order with nitropropane (21), and glycidyl isopropyl ether (22), eluting much later than on the IL + MOF stationary phase and also showing greater peak tailing (see Supplementary Tables 5.S1 to 5.S3 for chromatographic parameters of all

separations). Again, all compounds in this separation were retained longer on the IL + MOF stationary phase.

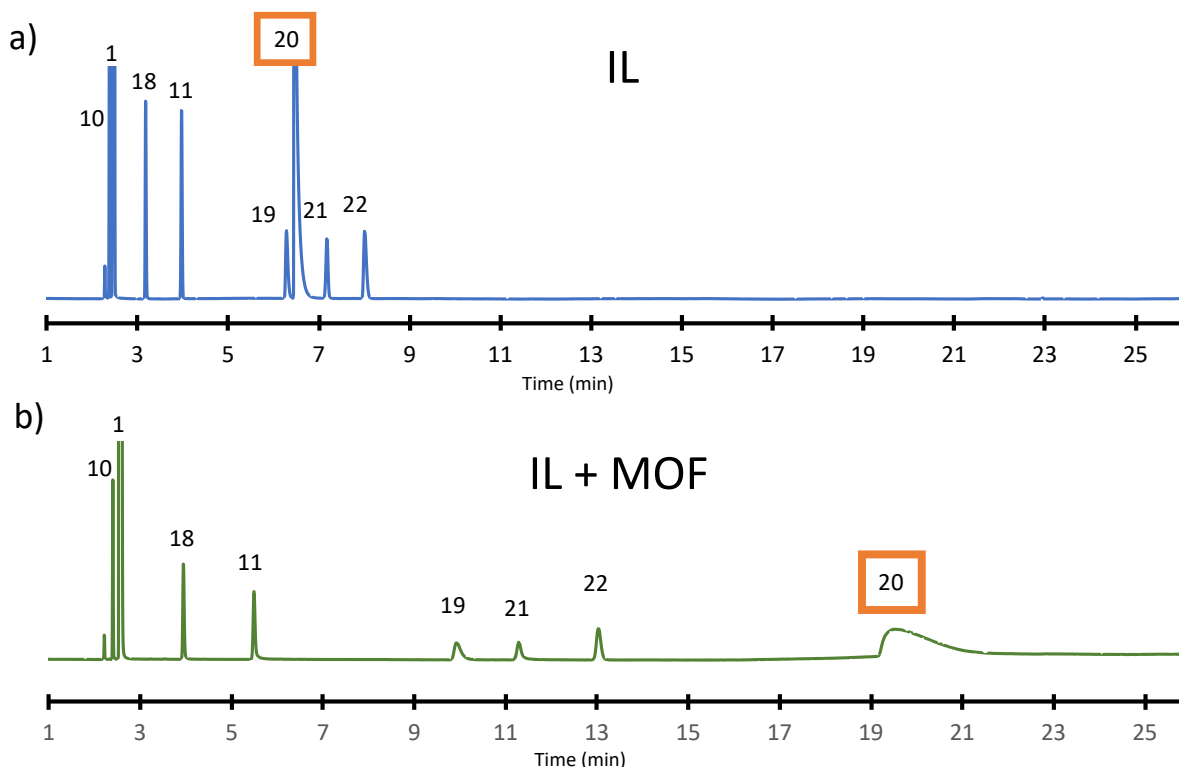


Figure 5.3. Chromatograms of separation of Rohrschneider compounds and ether compounds on two stationary phases (IL and IL+MOF). 30m x 0.25mm x 0.25 μ m, oven temp: 70 $^{\circ}$ C, average velocity: 30cm/s, carrier gas: He, split ratio 100:1, injection volume: 1 μ l, flame ionization detector. Dichloromethane (1), *tert*-butyl methyl ether (10), 2-pentanone (11), 2-butanol (18), glycidyl methyl ether (19), pyridine (20), nitropropane (21), glycidyl isopropyl ether (22). The chromatographic parameters are listed in Table 5.S2, in supplementary information.

In an analogous absorption behavior trend to those discussed previously, Figures 4a and 4b demonstrate changes in selectivity on the ZIF-8 + DMIMC9 NTf₂ (i.e., IL + MOF phase) compared to the neat IL, DMIMC9 NTf₂. A more prominent increase in the retention of alkanes (tridecane (6), tetradecane (8), hexadecane (15)) was seen relative to the ketones (2-pentanone (11) and 3-hexanone (12)). Somewhat lower resolution was seen for tridecane (6) and 2-pentanone (11) on

the IL + MOF phase. The resolution was improved for compounds tetradecane (8) and 3-hexanone (12), where baseline resolution was not observed on the neat IL stationary phase.

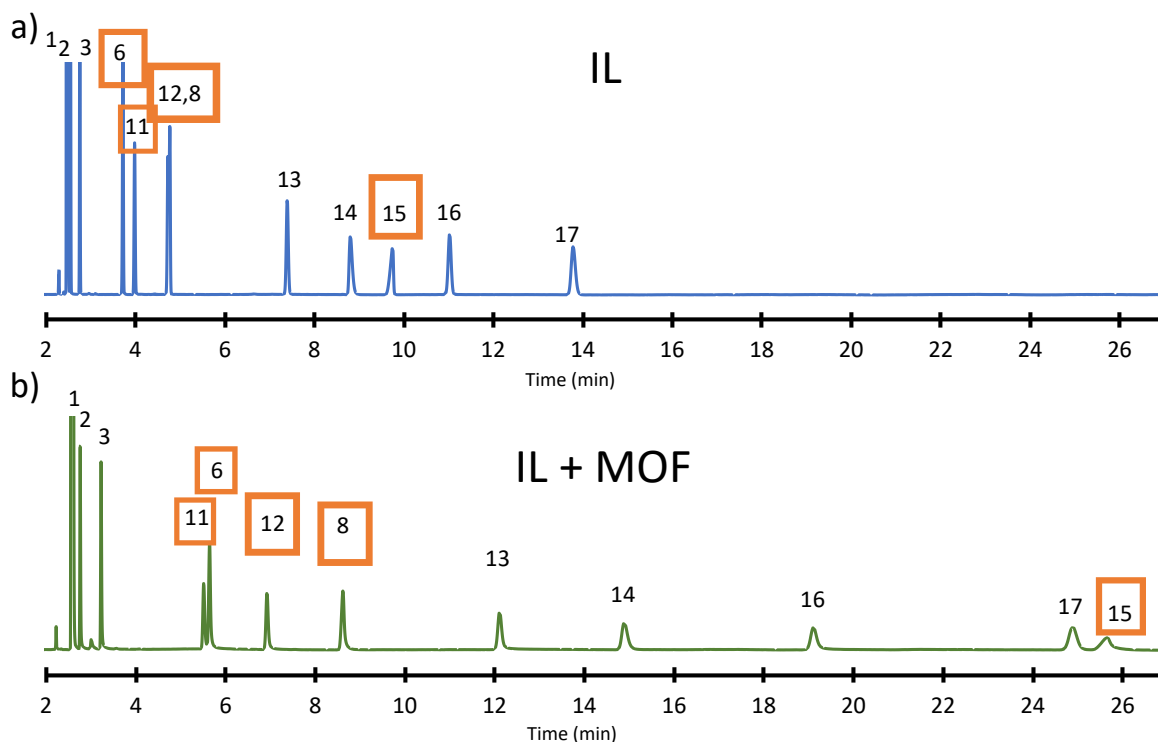


Figure 5.4. Chromatograms showing separations of ketone and alkane compounds on two stationary phases (IL and IL+MOF). 30m x 0.25mm x 0.25 μ m, oven temp: 70 $^{\circ}$ C, average velocity: 30cm/s, carrier gas: He, split ratio 100:1, injection volume: 1 μ l, flame ionization detector. Dichloromethane (1), decane (2), methanol (3), tridecane (6), tetradecane (8), 2-pentanone (11), 3-hexanone (12), 2-heptanone (13), cyclopentanone (14), hexadecane (15), 2-octanone (16), cyclohexanone (17). The chromatographic parameters are listed in Table 5.S3, in supplementary information.

Three gases were analyzed with molecular sizes of 3.3 \AA (CO_2), 4.3 \AA (propane), and 4.7 \AA (butane). Figure 5.5 shows the separation of CO_2 from air on the IL + MOF stationary phase. Under the same conditions the IL column produced a single co-eluting peak at the dead volume. The separations of gases seen here are occurring on a stationary phase that is consisted largely of liquid.

With the addition of MOF, CO₂ was consistently separated from the air peak and the precision was verified with multiple injections.

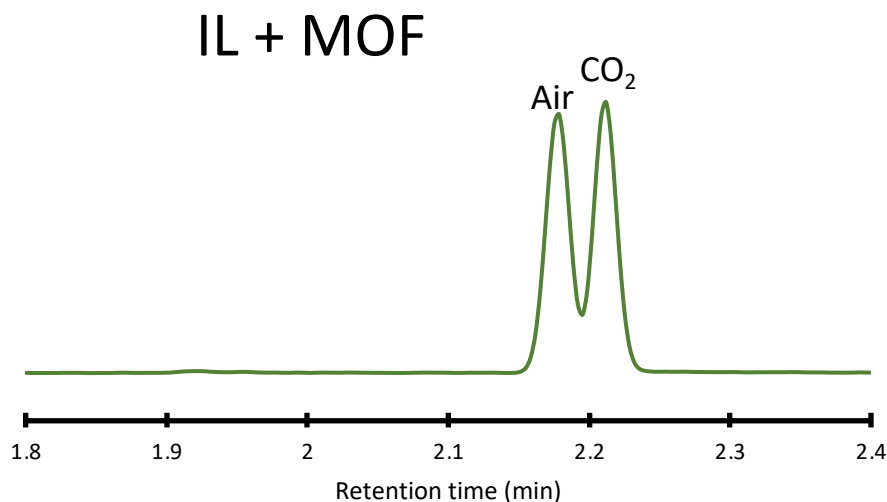


Figure 5.5. Separation of CO₂ from air on ZIF-8 DMIMC9 NTf₂ stationary phase. 30m x 0.25mm x 0.25 μ m, Oven temp: 12 °C, avg. velocity: 30cm/s, Carrier gas: He, Split ratio 50:1, injection volume: 4 μ l, thermal conductivity detector.

Similarly, air and butane were separated on the IL + MOF column (Figure 5.6), whereas they co-eluted at the dead volume on the IL column. These results indicate the possibility of conducting gas separations on GLC with IL + MOF columns. Propane eluted between butane and the air peak under these conditions. Further investigations are underway for optimization and enhancing selectivity to gases with IL + MOF columns.

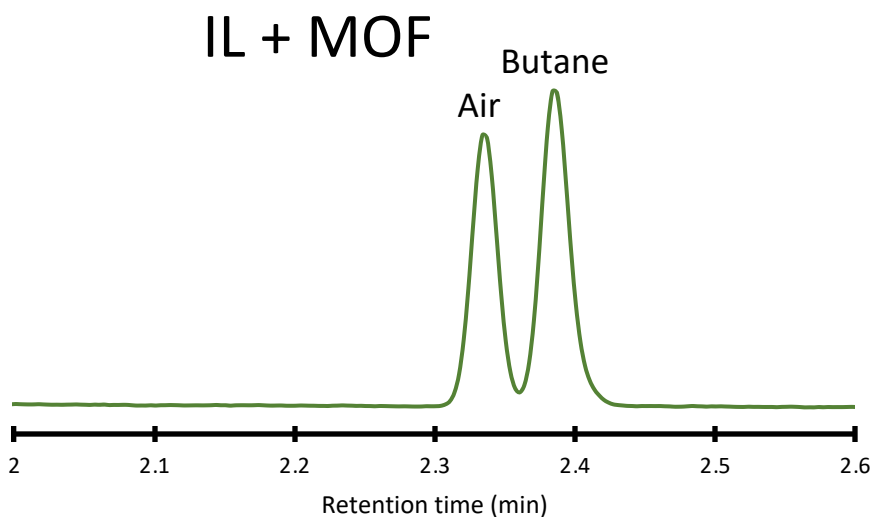


Figure 5.6. Separation of butane from air on ZIF-8 DMIMC9 NTf₂ stationary phase. 30m x 0.25mm x 0.25 μ m, Oven temp: 12 °C, avg. velocity: 30cm/s, Carrier gas: He, Split ratio 100:1, injection volume: 4 μ l, thermal conductivity detector.

There are a few ways to further improve gas separations using the IL + MOF motif. One is to increase the concentrations of the MOF in the IL. Unfortunately, the ZIF-8 concentration cannot be further increased in this particular IL (i.e., DMIMC9 NTf₂). Consequently, either the nature of the IL or a different MOF must be utilized. These approaches are being actively investigated, currently.

5.4.1 The Three Phase Model Theory and Mechanism

The 3-phase or pseudophase model of separations is an extension of the classic phase partitioning model of Martin and Synge [217]. To describe the separation of components in gas-liquid chromatography using MOFs dispersed in ionic liquid stationary-phase, the three phase (aka pseudophase) model can be utilized. The three-phase model has been used to describe and evaluate separations in liquid chromatography [218], liquid-liquid extraction [219], gas chromatography

[220, 221], and capillary electrophoresis [222] to characterize achiral and chiral separations. In this GC study, the three partition equilibria are those between the bulk IL and the metal organic framework (K_{LM}), the bulk ionic liquid and the gas phase (K_{GL}), and between the metal organic framework and gas phase (K_{GM}) (see Figure 5.7).

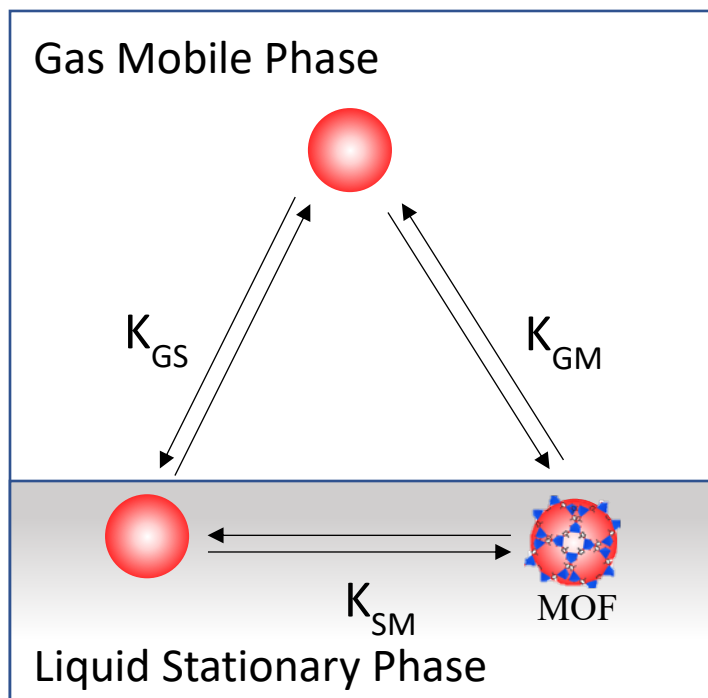


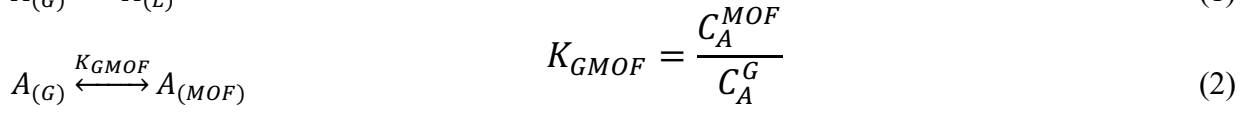
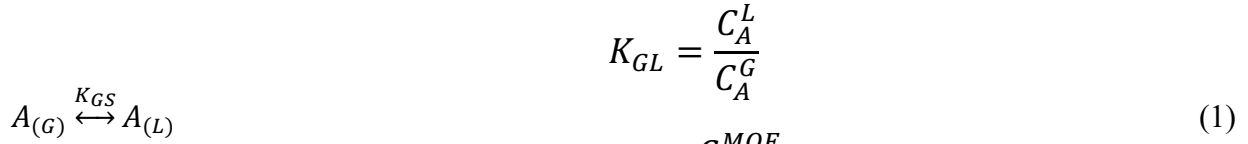
Figure 5.7. Three-phase model showing the partitioning equilibria of an analyte (red ball) in the IL + MOF system when used as a stationary phase in gas chromatography.

As seen, the partitioning of the analytes between the stationary phase and mobile phase occurs either with the neat IL or the metal organic framework exposed at the gas-liquid interface. Upon absorption, the analyte will distribute itself throughout the volume of the stationary phase including cavities or the external surface of the MOFs [220]. There are three ways in which the analyte can interact with the stationary phase. First, external adsorption on the MOF, second internal adsorption within the MOF cavity, and third adsorption to the bulk IL.

The imidazolium based organic linkers found in the metal organic framework provide competing $\pi - \pi$ interactions with the analytes which introduces another host-guest interaction for separation [66]. Molecules that are smaller than the pore size of the MOF cavity can enter and be absorbed within the cavity. Additionally, longer, linear molecules (e.g., containing n-alkane moieties) can partially absorb internally into the MOF cavity. Adsorption to the bulk ionic liquid comes from five interactions, which can be categorized via dispersion forces associated with the carbon linkage chain and polar interactions with imidazolium cation and NTf_2^- anion as outlined in the introduction [132, 201]. It should be noted that in its simplest form the 3-phase (or pseudophase) model only considers the total volume of the pseudophase. Thus, a dimensionless distribution constant is determined (see Theory section). If desired, this can be converted to an adsorption coefficient if the total surface area of the pseudophase is known. Such adsorption coefficients would have dimensions of length or length^{-1} .

5.4.2 Theory

The equations and theory outlined herein for a MOF pseudophase are analogous to those used previously for cyclodextrin GLC, micellar GLC, and micellar liquid chromatography [218-221]. The association of large molecules to a MOF can only be to external surface and while small molecules can associate with the inner surface, inner bulk solvent and outer surface [109]. A distribution constant considers the total volume of the MOF pseudophase and as mentioned adsorption distribution coefficients can be found using the surface area, if known. The three distribution constants indicated in Fig. 7 are defined as follows:



Where A is the analyte in the gas phase (G) and the ionic liquid phase (L) or metal organic framework (MOF) pseudophases. C_A^G , C_A^L , C_A^{MOF} are the concentrations of the analyte in the gas and bulk ionic liquid phases and metal organic framework pseudophase, respectively. The respective distribution constants are: K_{GL} , K_{GMOF} , K_{LMOF} . Based on these equations, the relationship between all three distribution constants is as follows:

$$K_{GMOF} = K_{GL}K_{LMOF} \quad (4)$$

The measured apparent distribution constant (K) obtained through experimental gas-chromatography can be calculated from:

$$K = \frac{(m_A^L + m_A^{MOF}) / (V_L + V_{MOF})}{m_A^G / V_G} \quad (5)$$

where m_A is the mass of the analyte in each respective phase and V is the volume of each phase.

Through substitution of Eq. (1), Eq. (3), and the relationship between concentration of metal organic frameworks to the volume of MOF and ionic liquid phases ($C_{MOF}v_p = V_{MOF} / (V_{MOF} + V_L)$) into Eq. (5), the following expression is obtained:

$$K = v_p K_{GL} (K_{LMOF} - 1) C_{MOF} + K_{GL} \quad (6)$$

Where v_p is the partial specific volume of the metal organic framework and C_{MOF} is the concentration of the metal organic framework. By plotting the values of K versus C_{MOF} all three distribution constants can be extracted. Using the linear fit of data, K_{GL} can be found from the y-

intercept, while K_{LMOF} can be calculated through $K_{LMOF} = \frac{slope}{y-int.v_p} + 1$. Using these values and

Eq. 4, K_{GMOF} can be calculated.

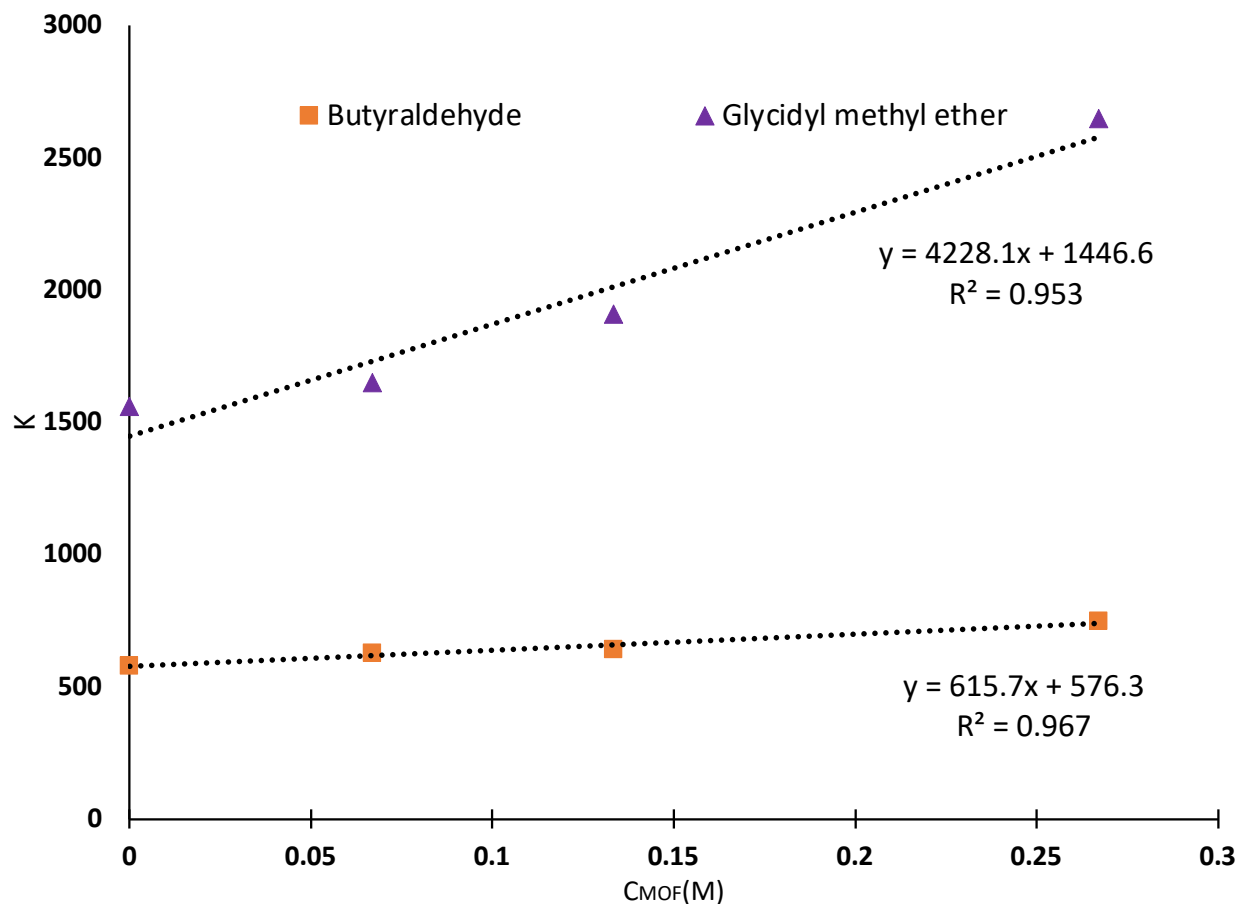


Figure 5.8. Plots of equation 6 ($K = v_p K_{GL} (K_{LMOF} - 1) C_{MOF} + K_{GL}$) for butyraldehyde and tetradecane along with their linear fit.

Using eq. 6, the apparent distribution constant (K) plotted against metal organic framework concentration in the stationary phase is seen in Figure 5.8 for the analytes butyraldehyde and glycidyl methyl ether. Correlations of $R^2 > 0.95$ were obtained, which is quite a good correlation considering each point corresponds to a separate column with a different concentration of dispersed colloidal metal organic framework within the stationary phase.

The calculated distribution constants are as following for butyraldehyde: $K_{GL} = 576$, $K_{GMOF} = 4703$, $K_{LMOF} = 8$ and for glycidyl methyl ether: $K_{GL} = 1447$, $K_{GMOF} = 29785$, $K_{LMOF} = 21$. The analytes have the largest distribution constant between the gas mobile phase and metal organic framework in the stationary phase, while the smaller distribution constants are found between the bulk ionic liquid in the stationary phase and the metal organic framework pseudophase. However, it should be noted that the absolute amount of the IL far exceeds that of the MOF. Analogous trends were found in a cyclodextrin based chiral stationary phase treated using an analogous three-phase model [219]. Hence the retention of the compounds is greatly affected by the presence of the MOF in the stationary phase.

Using the three-phase model and the calculated distribution constants, it can be seen that MOFs in the stationary phase have a large effect on partitioning of analytes. This feature can be further explored to fine tune specific separations by optimizing the concentrations of MOFs in stationary phase. Additionally, the customizability of ILs and the variety of MOFs available means that the number of possible permutations of metal organic framework dispersions in ionic liquids are numerous.

5.5 Conclusions

The first GC stationary phase consisting of a colloidal MOF dispersed in an ionic liquid was devised and evaluated. The colloidal MOF greatly altered the retention and selectivity of the IL stationary phase and vice versa. In general, longer retention times were observed for all the analytes and retention order shifts were seen for analytes from various classes of compounds with the IL + MOF stationary phase. Retention and separation of some gases from air (i.e., CO₂, propane, and butane) also was accomplished with the IL + MOF stationary phase. Solutes that are

strongly retained on gas solid chromatography can be eluted with good peak shapes and notable retention factors were seen with the hybrid IL-MOF stationary phase. The new stationary phase containing MOF can be characterized using the “three-phase” or pseudophase model. The solute partitioning was largely affected by the partition of analytes from the mobile phase to the MOF in the stationary phase. Further, the nature and amount of the MOF in the IL can be altered/tuned to optimize any particular separation.

5.7 Supporting Information

Table 5.S1. Chromatographic parameters for IL and IL + MOF columns for Figure 5.2.

Name	Stationary Phase	Retention time	N(efficiency)	Symmetry	USP tailing factor
			Plates		
Dichloromethane	IL + MOF	2.55	40000	0.28	3.07
Decane	IL + MOF	2.75	125000	0.95	1.25
Methanol	IL + MOF	2.99	37000	0.42	2.69
Undecane	IL + MOF	3.22	113000	0.89	1.28
1-Propanol	IL + MOF	3.99	42000	0.53	2.03
1-Butanol	IL + MOF	5.53	56000	1.00	1.27
Tridecane	IL + MOF	5.64	104000	1.04	0.97
1-Pentanol	IL + MOF	8.22	42000	0.59	2.20
Tetradecane	IL + MOF	8.62	88000	1.19	1.10

Name	Stationary Phase	Retention time	N(efficiency)	Symmetry	USP tailing factor
			Plates		
Dichloromethane	IL	2.47	88000	0.40	1.97
Decane	IL	2.55	187000	0.95	1.03
Methanol	IL	2.70	66000	0.65	1.55
Undecane	IL	2.76	183000	1.08	1.00
1-Propanol	IL	3.21	83000	0.63	1.45
Tridecane	IL	3.72	155000	1.24	0.88

1-Butanol	IL	4.01	69000	0.48	1.85
Tetradecane	IL	4.77	132000	1.62	0.77
1-Pentanol	IL	5.43	49000	0.38	2.52

Table 5.S2. Chromatographic parameters for IL and IL + MOF columns for Figure 5.3.

Name	Stationary Phase	Retention time	N(efficiency)	Symmetry	USP tailing factor
			Plates		
Dichloromethane	IL + MOF	2.56	49000	0.29	3.44
Decane	IL + MOF	2.76	138000	0.67	1.29
Methanol	IL + MOF	3.22	118000	0.74	1.32
2-Pentanone	IL + MOF	5.51	85000	1.01	1.23
Tridecane	IL + MOF	5.64	102000	0.91	1.15
3-Hexanone	IL + MOF	6.92	88000	0.79	1.29
Tetradecane	IL + MOF	8.62	93000	0.97	1.27
2-Heptanone	IL + MOF	12.11	92000	0.69	1.37
Cyclopentanone	IL + MOF	14.89	64000	0.77	1.33
2-Octanone	IL + MOF	19.11	95000	0.76	1.55
Cyclohexanone	IL + MOF	24.89	90000	0.96	1.09
Hexadecane	IL + MOF	25.65	76000	1.08	1.26

Name	Stationary Phase	Retention time	N(efficiency)	Symmetry	USP tailing factor
			Plates		
Dichloromethane	IL	2.46	68000	0.27	2.65
Decane	IL	2.55	179000	0.94	1.03
Methanol	IL	2.76	177000	0.95	1.01
Tridecane	IL	3.72	152000	0.19	0.90
2-Pentanone	IL	3.98	119000	0.99	1.03
3-Hexanone	IL	4.73	170000	1.74	1.10

Tetradecane	IL	4.77	175000	0.98	0.77
2-Heptanone	IL	7.39	119000	0.96	1.03
Cyclopentanone	IL	8.81	75000	0.63	1.44
Hexadecane	IL	9.75	86000	2.72	0.66
2-Octanone	IL	11.02	125000	0.97	1.02
Cyclohexanone	IL	13.78	99000	0.83	1.13

Table 5.S3. Chromatographic parameters for IL and IL + MOF columns for Figure 5.4.

Name	Stationary Phase	Retention time	N(efficiency)	Symmetry	USP tailing factor
			Plates		
Tert-butyl methyl ether	IL + MOF	2.40	124000	0.93	1.03
Dichloromethane	IL + MOF	2.53	32000	0.21	3.75
2-Butanol	IL + MOF	3.94	80000	0.97	1.17
2-Pentanone	IL + MOF	5.49	82000	0.88	1.30
Glycidyl methyl ether	IL + MOF	9.93	24000	0.54	1.78
Nitropropane	IL + MOF	11.29	76000	0.73	1.75
Glycidyl isopropyl ether	IL + MOF	13.03	84000	0.82	1.17
Pyridine	IL + MOF	19.53	1500	0.28	4.27

Name	Stationary Phase	Retention time	N(efficiency)	Symmetry	USP tailing factor
			Plates		
Tert-butyl methyl ether	IL	2.38	157000	0.99	1.04
Dichloromethane	IL	2.45	54000	0.30	3.26
2-Butanol	IL	3.18	105000	0.75	1.13
2-Pentanone	IL	3.97	120000	0.89	1.03
Glycidyl methyl ether	IL	6.28	76000	0.61	1.57
Pyridine	IL	6.46	68000	0.18	6.50
Nitropropane	IL	7.18	112000	1.06	1.00
Glycidyl isopropyl ether	IL	8.01	82000	0.69	1.41

Chapter 6

An Examination of the Effects of Water on Normal Phase Enantioseparations

6.1 Abstract

Superficially porous silica bonded with macrocyclic glycopeptides can separate enantiomers in various chromatographic formats, including normal phase liquid chromatography (NPLC). The conventional wisdom in NPLC is to avoid intentionally adding water in the eluents. Herein we examine the effects of small quantities of water as an additive on chiral separations in NPLC with the n-hexane-ethanol system. A phase diagram (n-hexane-ethanol-water) is used to analyze the physicochemical properties of the mobile phase. The relative polarity change of solvents upon adding water was determined by using bathochromic shifts of dissolved Nile Red dye. The effectiveness of chiral NPLC with water traces is demonstrated for various pharmaceutically relevant enantiomeric compounds. It is postulated that water molecules weaken stationary phase-solute interactions, resulting in lower retention times for both enantiomers in addition to significantly higher efficiencies. Gibbs free energy changes provided an understanding of the different enantioselectivity shifts caused by water addition. Some interesting kinetic effects also were observed. Classical van Deemter curves are not observed on macrocyclic glycopeptide stationary phases due to slow mass transfer kinetics and thermal effects at high flow rates. The most significant advantage of adding water in NPLC is reducing mass transfer kinetics and altering the mass overloading properties which is highly beneficial on macrocyclic glycopeptide phases. By overloading a 10x0.46-cm column with up to 0.6 mg alprenolol, it was found that the relative adsorption isotherm of the first eluting enantiomer was switched from Langmuir to anti-Langmuir type by water addition. The peak shape tuning effect demonstrated the strong influence of water

on specific interaction sites of the chiral stationary phases. Water addition effects were most beneficial for enantiomeric and preparative separations in NP mode.

6.2 Introduction

Normal-phase liquid chromatography (NPLC) is a widely used technique in synthetic organic research where relatively polar nonvolatilizable molecules of research or medicinal value are to be separated, quantified, or subjected to preparative separations [81]. Conventional chiral NPLC employs coated, or immobilized derivatized cellulose or amylose on wide-pore silica supports with alkane/alcohol mixtures as eluents [223]. One of the drawbacks of NPLC is poor reproducibility of the retention times; soon, it was found that this is due to the presence of adventitious water or adsorption of water by the solvents from the ambient atmosphere, which in turn is adsorbed onto the silica supports [81, 224-226]. Hexane/heptane bottles sitting in the laboratory environment may have a different normal phase chromatographic behavior than a freshly opened bottled due to adventitious water. Consequently, a long-accepted practice in NPLC is to minimize the water content of the mobile phase and likewise its adsorption on the stationary phase. Molecular sieves are often added to the mobile phase to dry and maintain retention reproducibility [227]. Molecular sieves, on the other hand, introduce their own set of undesirable impurities, which are often detected in offline NPLC-MS [228]. Undoubtedly, these issues are among major practical hurdles in implementing NPLC separations for routine analysis.

There are reports on the effects of water in NPLC mobile phases on chiral separations with polysaccharide-based chiral stationary phases (CSPs) [81, 82, 229, 230]. One study concluded that the addition of a small amount of water in the normal phase solvent had little effect, causing only a slight decrease in retention and little change in selectivity [229]. Another study observed an improvement in resolution for a selected application in the presence of water [79]. For instance, in

the case of the Chiralpak AD column with 2-propanol, adding as low an amount of water as 0.2% increased retention, whereas the Chiral IA column and ethanol always showed a decrease in retention [229]. More importantly, undesirable “memory effects” have been reported with derivatized amylose columns in the presence of water [231, 232] which points to hysteresis once the stationary phase has been exposed to water. It seems that the effect of water in normal phase separations varies with the stationary phase, the nature of analyte and various types of other mobile phase additives.

Unlike derivatized polysaccharides with hydrophobic aromatic groups, macrocyclic glycopeptides such as vancomycin and teicoplanin bonded to silica are highly polar stationary phases and thus also are suitable as chiral NPLC stationary phases using hexane/heptane and ethanol/2-propanol systems. It was postulated to apply a counterintuitive approach of intentionally "wetting" the NP mobile phase with a known amount of water and investigate its effects systematically. Due to the hydrophilic nature of macrocyclic glycopeptide-based stationary phases, they might show more significant changes in enantioseparations with water addition. Also, vancomycin, teicoplanin, and other modified macrocyclic glycopeptides are commercially available on superficially porous particles, thereby offering high-efficiency chiral separations in conventional NPLC [233]. Recent studies, using these CSPs in supercritical fluid chromatography (SFC), showed that trace amounts of water added to the SFC CO₂-methanol system could have dramatic effects on enhancing chiral and achiral separations [83, 234]. Since SFC mobile phases have some similarities with NP mobile phases, it will be informative to systematically study the effect of water in the enantioseparation of different classes of pharmaceutically important molecules on macrocyclic glycopeptide CSPs.

A phase diagram of n-hexane-ethanol-water is used to analyze the physicochemical properties of the mobile phase. Changes in the solvent polarity due to added water were evaluated via bathochromic shift in the absorption maximum of Nile Red dye. Additionally, we show that the addition of water can tune the overloading peak shape behavior from tailing to fronting and one tailing peak for some enantiomers. Fundamental thermodynamic and kinetic (plate height versus flow rate) studies were performed and evaluated. It is shown that the A-term in the classical van Deemter expression likely encodes additional parameters in such a simple treatment.

6.3 Material and methods

6.3.1. Chemicals

All chiral compounds and Nile red dye were obtained from Sigma-Aldrich (Millipore, St. Louis, MO, USA). n-hexane 97% (Mol.wt. 86.2; $d = 0.655$ g/mL; water content lower than 50 ppm) was from VWR chemicals (Radnor, PA, USA). Ethanol 200 proof (m.w. 46.1; $d = 0.787$ g/mL; water content is typically < 250 ppm) [234] came from Decon Labs, Inc (King of Prussia, PA, USA). This ethanol contains no methanol nor benzene, as per the manufacturer's quality assurance sheet. Distilled and deionized water was purified using a Thermo Scientific GenPure Pro Milli-Q water purification system giving 18 M Ω water (Thermo Fisher, Waltham, MA, USA).

6.3.2 Chromatography

Superficially porous 2.7- μ m columns (TeicoShell, VancoShell, NicoShell, 5 or 10 \times 0.46 cm i.d.) were synthesized by AZYP, LLC (Arlington, TX, USA). These phases consist of bonded teicoplanin, vancomycin and vancomycin derivative. All liquid chromatography separations were performed on an Agilent 1220 LC system with a UV-2075 detector (Agilent, Santa Clara, CA, USA). The degassers were bypassed, and mobile phases were degassed by vacuum sonication

before use. The HPLC thermostat also was bypassed. The enantiomeric separations at ambient temperature were done using three 10-cm, 4.6 mm internal diameter columns packed with 2.7 μm SPP particles. The plate height vs. flow rate experiments were done on three shorter 5x0.46 cm columns with the same stationary phases at ambient temperature. The efficiency values reported in this paper are calculated from the peak width at half height. These stationary phases are bonded with teicoplanin, vancomycin, and another derived macrocyclic glycopeptide selector, respectively. The mobile phases were prepared using graduated cylinders, and water was added by a class-A burette as needed after mixing the nominal volumes of n-hexane and ethanol. For example, n-hexane/ethanol, 80:20 %v/v with 0.8 %v/v water, was made by mixing 800 mL of n-hexane, 200 mL of 200-proof ethanol, and 8.0 mL of water. The solutes were dissolved n-hexane, ethanol mixtures. Methanol was used in cases where sample solubility was limited.

Gas chromatography was used to measure the water content in normal mobile phases. An Agilent 6890N gas chromatograph was used with a thermal conductivity detector and a 30 m x 250 μm i.d. x 0.2 μm film thickness WatercolTM capillary column (Millipore, Sigma-Aldrich). 1 μL of normal mobile phase was injected with a 1:100 split ratio and eluted by helium 30 cm/s at an isothermal temperature of 160 $^{\circ}\text{C}$ giving three well-separated peaks: hexane at 2.25 min ($k = 0.35$), ethanol at 2.35 min ($k = 0.41$ min) and water at 2.63 min ($k = 0.57$).

6.3.3 Spectroscopic measurements

A Shimadzu UV-2600 spectrometer was used to measure the absorbance maximum of a Nile red solution, at a step size of 0.1 nm to capture small changes in peak shifts, in the different mobile phases at room temperature (Shimadzu, Kyoto, Japan). The pathlength of the cuvette was 10 mm.

6.4 Results and discussion

6.4.1 The water-hexane-ethanol ternary system

Liquid-liquid equilibration data has been reported for water-alkane-ethanol mixtures in mole fractions at 20°C, 30°C, and 35°C [235]. The results were compared to the compositions calculated by UNIQUAC software by the authors. Figure 6.1 shows the ternary phase diagram obtained using the experimental mole fraction values listed in [235] with green points and lines. These values were converted to volumes using solvents' molecular weights and densities. Assuming an ideal behavior of solvents so that all volumes can be added, the magenta lines show the volume fraction of the ternary phase diagram at 20°C. Ethanol and water do not mix ideally; for example, the maximum volume contraction at 60:40 % v/v composition is only 4% (60 mL of ethanol mixed with 40 mL water makes 96 mL) [236]. Since the NP studies presented in this work use hexane-rich mobile phases with small amounts of added water, the water-ethanol volume contraction can be neglected. The dashed lines in Figure 6.1 correspond to the tie lines linking the upper organic phase composition (right side) to the lower aqueous phase composition (left side) when two liquid phases are in equilibrium.

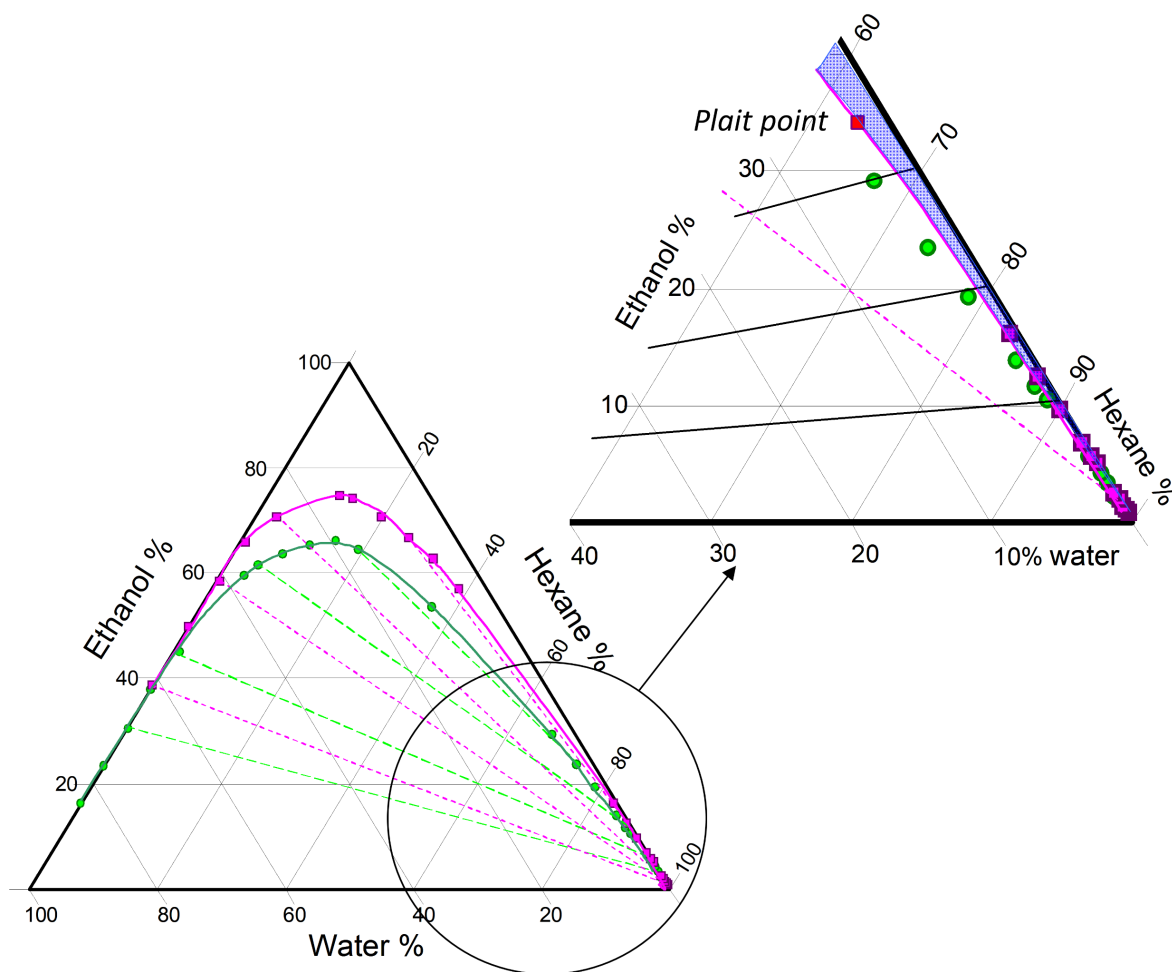


Figure 6.1 Ternary phase diagram of the hexane-water-ethanol system at 20°C. The green lines correspond to the solid binodal and dashed tie lines expressed in molar fractions (data from [235]); the purple lines are the same data expressed in volume fractions. The upper partial diagram is an enlargement of the hexane apex corner showing in blue the monophasic area usable for the mobile phase compositions used in this work.

The hexane apex area of the water-hexane-ethanol phase diagram is enlarged in Figure 6.1 to show the plait point, corresponding to the shortest tie line where the two liquid phases have the closest possible compositions. It also shows the NP normal phase compositions (solid black lines) that were used in the chromatographic separations in this work. The blue area is the monophasic area showing that the maximum water amount possible in a monophasic hexane/ethanol NP mobile phase is minimal and significantly dependent on the ethanol content. For example, the maximum amounts of water in the hexane/ethanol 90:10, 80:20, 70:30, and 60:40 % v/v mixtures forming a single monophasic area at room temperature were respectively 0.33, 0.85, 1.8, and 3.9 % v/v (blue area and solid black lines in Figure 6.1). To avoid these phase separation problems, no more than 80% of these maximum amounts of water were added to the prepared NP mobile phases with different ethanol contents.

6.4.2 Water effect on normal phase chiral separations

Previously, trace amounts of water added to NP mobile phases were found to enhance some enantiomeric separations performed on polysaccharide-based CSPs [81, 82, 229, 230]. These enantiomeric pairs were mostly non-ionizable compounds such as flavanone, chalcone, cyclohexanone [81], pyrrolidinones [229], or paroxetine analogs [230]. Macrocyclic glycopeptides CSP can separate ionizable basic or acidic enantiomers as well as non-ionizable compounds [79, 237, 238].

6.4.3 Water in NPLC makes enantioseparation possible

It was observed that several basic chiral compounds could not be enantiomerically separated in the NP mode on macrocyclic glycopeptide CSPs without trace amounts of water added to the mobile phase. Figure 6.2 (top) shows three racemic cathinone derivatives, listed as controlled drugs, that could not be enantioresolved in the classic NP mode by the NicoShell CSP (this which

is derived from vancomycin). Note that this CSP works best with trace additives such as 0.06% v/v acetic acid (AA) and triethylamine (TEA) added to the hexane/ethanol 70:30 v/v NP mobile phase. Adding equal volumes of AA and TEA produces about the same molar amounts of TEA acetate and excess AA that can ionize basic compounds. The three racemic drugs were baseline resolved when 1.4% water was added to the hexane/ethanol 70:30 v/v mobile phase with added AA and TEA (Figure 6.2 bottom). The solute retention times were always reduced. These experimental observations can be due to a substantial increase in mobile phase polarity, a significant stationary phase modification, or a combination of these factors. The mobile phase polarity can be evaluated by spectroscopy (*vide infra*). Since peak retention is related to the thermodynamics of the solute-stationary phase interactions and peak efficiency is related to kinetic factors, the effect of water on both of these was examined.

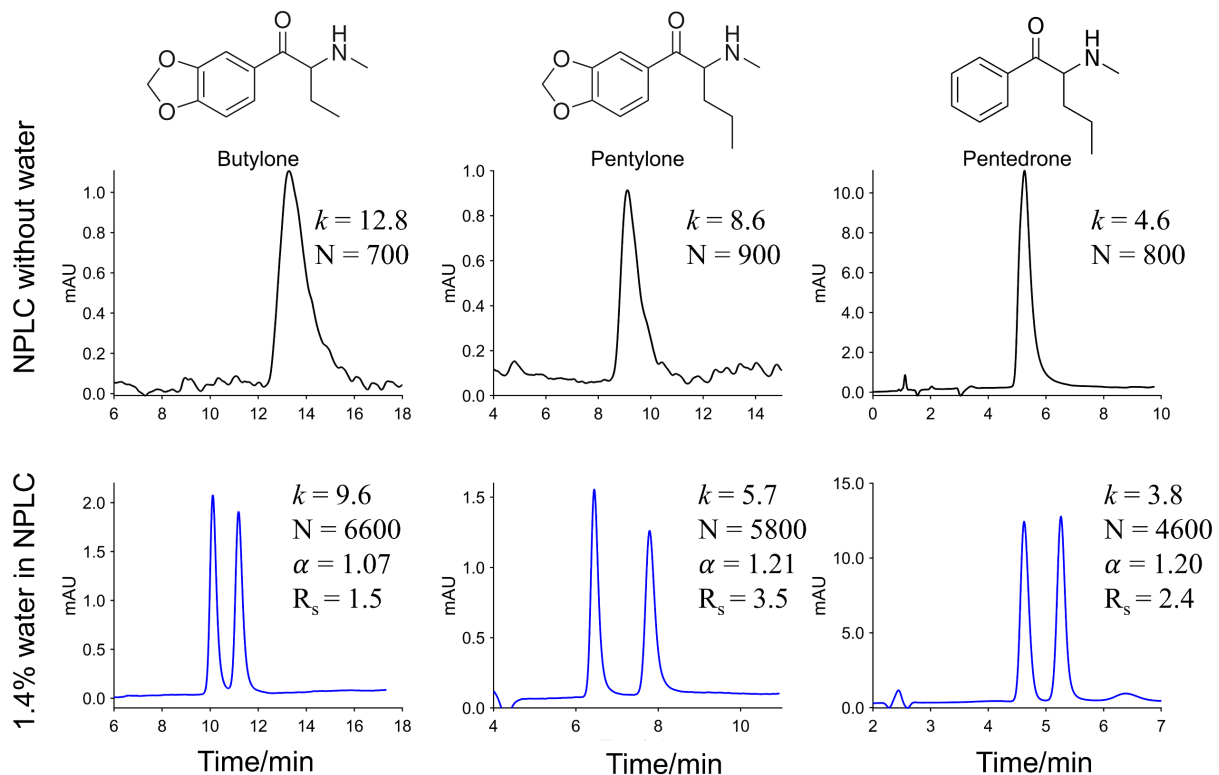


Figure 6.2 Effect of water on the separation of three chiral cathinones. Top chromatograms: NPLC without added water. Mobile phase: hexane/ethanol 70:30 % v/v with 0.06 % v/v added AA and TEA, 1 mL/min. Bottom chromatograms: same mobile phase with 1.4% v/v added water. The k values correspond to the first eluting enantiomers. Column: NicoShell 10 cm x 4.6 mm, 2.7 μ m SPP particle diameter. Detection UV 254 nm.

6.4.4 Water effects on normal phase solvent polarity studied by solvatochromism

Evaluation of solvent polarities using dye absorbance maxima was developed by Kosower [239]. A Z-scale was built based on E , the transition energy corresponding to the absorbance maximum of the salt N-ethyl-4-methoxycarbonyl-pyridinium iodide in different solvents. This energy is expressed per mole as:

$$E = N_A h \nu = N_A h \frac{c}{\lambda} \quad (1)$$

where N_A is the Avogadro's number, h is the Planck's constant, ν is the frequency, c , is the speed of light, and λ , is the absorption wavelength. Using the values of the three constants, Eq. 1 can be simply expressed as $E = 119510/\lambda$ kJ. Unlike Kosower's dye, which is too polar to dissolve in normal phase solvent mixture, Nile red dye, $C_{20}H_{18}N_2O_2$ (Mol. wt. 318.1), was used instead in this work. The Nile red dye has a bathochromic absorption shift from 548.3 nm (purple appearance) in ethanol to 484.4 nm (yellow appearance) in hexane.

Table 6.1 lists the absorbance maxima and energies obtained in different mobile phase mixtures. Arbitrarily assigning the value of 0 for the apolar hexane transition energy and 100 to the more polar ethanol transition energy, the values obtained in the hexane/ethanol mixtures gave a clear idea of the mobile phase polarity changes. In this scale, an eleven unit change from 63 to 74 is produced by the addition of 0.8% water in the hexane/ethanol mixture. The increase from 0.2 to 0.4 percent water induced a 6.2 polarity increment, while the increase from 0.4% to 0.8% water induced only 2.7 polarity increment (Table 6.1). The effect of the additives, acetic acid, and triethylamine was measured in all mobile phases and produced only minor polarity changes (Table

6.1). Clearly, the spectroscopically derived polarity increases cannot fully explain the retention time shifts and efficiency gains produced by adding small amounts of water to NP mobile phases.

Table 6.1. Solvatochromic data of Nile red in different hexane/ethanol mobile phases

Medium^a	Absorption maximum λ /nm	Transition energy kJ/mol	Relative polarity
Hexane	484.4	246.9	0
Hex/EtOH 80:20	522.6	228.7	63.0
Hex/EtOH 80:20 + 0.2% H ₂ O	526.6	226.9	69.2
Hex/EtOH 80:20 + 0.4% H ₂ O	528.0	226.3	71.3
Hex/EtOH 80:20 + 0.8% H ₂ O	530.0	225.5	74.0
Hex/EtOH 80:20 + 0.8% H ₂ O + 0.06% AA + 0.06% TEA	530.9	225.1	75.4
Ethanol	548.3	218.0	100

^a All numbers correspond to volume percentages. AA is acetic acid; TEA is triethylamine.

6.4.5 How much is water hydrating the stationary phase?

Following the work of Irgum determining how much water was hydrating HILIC stationary phases, the amount of water hydrating the macrocyclic glycopeptides SPP stationary phases was determined [240]. First, a weighed amount of dried (>24 h, 50 °C) bulk stationary phase was placed in a headspace vial, and then 1 mL of normal phase solvent was transferred to the vial. Next, the vial was sealed and allowed to equilibrate for 30 min with occasional vortex agitation. After which, the supernatant solvent phase was analyzed for water content, taking 1 μ L aliquot for GC analysis. The difference in water content before and after exposure of the normal phase solvent gives the amount of water adsorbed by the solid SPP phase. Figure 6.3 shows the results in terms of μ g (or nL) of water adsorbed per mg of stationary phase versus the 80:20 hexane/ethanol-water content.

The TeicoShell SPP absorbs slightly more water than the two other SPP at 0.8% water content without reaching an apparent plateau. It is impossible to add more water into the 80:20 hexane/ethanol phase since it breaks into two liquid phases, as shown by the phase diagram (Figure 6.1). Taking into account the SPP pore volume of about 0.32 cm³/g or 0.32 μ L/mg [83], for the TeicoShell SPP phase exposed to the solvent containing 0.8% water (Figure 6.3), the 17 μ g of water per SPP mg corresponds to a water concentration of 5.3%, seven times higher than the water content in the hexane/ethanol solvent. Considering the 10 μ g of water adsorbed by the NicoShell SPP equilibrated by hexane/ethanol containing only 0.4% water, the water concentration in the solid NicoShell phase is 3.1 %, almost 8 times higher than that in the solvent phase. Using Irgum's presentation expressing adsorbed water in mg/m² and the specific SPP area of 120 m²/g, the TeicoShell 17 μ g/mg and NicoShell 10 μ g/mg adsorbed water correspond respectively to 0.14 and 0.083 mg/m² of adsorbed water. These values are perfectly coherent with the values obtained in

the HILIC study with polar-bonded or bare silica packings and 0.8 or 0.4% water in acetonitrile [240]. The SPP solid phases adsorb and concentrate water in their porous structure, changing their polarity and chromatographic performances comparable to the water behavior described in the HILIC case [240].

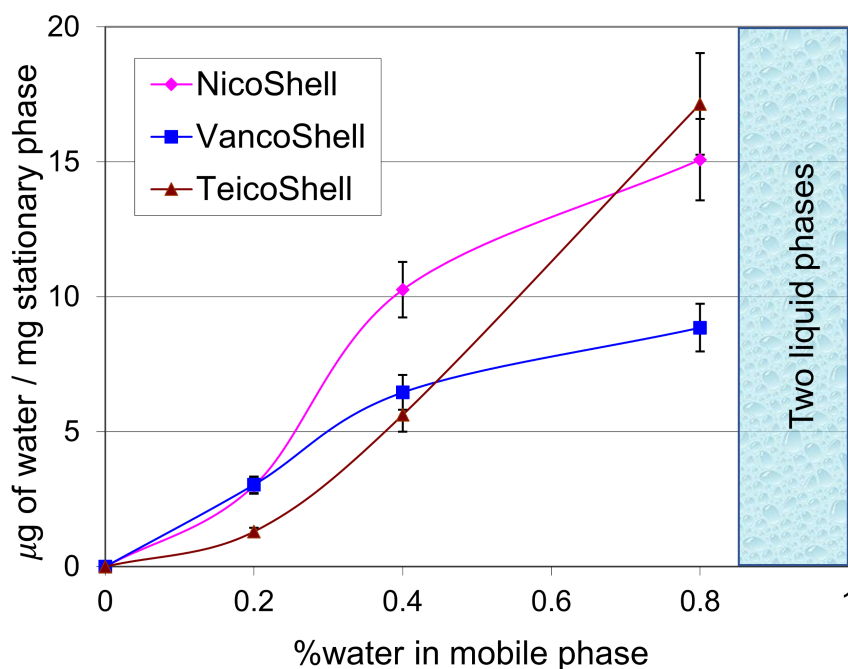


Figure 6.3 Water adsorption by the macrocyclic glycopeptide SPP stationary phases exposed to the hexane/ethanol 80:20 v/v solvent containing the indicated amount of water. The vertical blue line indicates the maximum amount of water maintaining a single phase. The blue area corresponds to phase separation (see Figure 6.1).

6.4.6 Thermodynamic study of water's influence on solute-stationary phase interactions

The solute interaction between phases can be studied through the Gibbs free energy of transfer change, ΔG^o of the solute moving from the mobile to the stationary phase. ΔG^o is expressed by [241]:

$$\Delta G^o = -RT \ln \left(\frac{k}{\phi} \right) \quad (2)$$

where k is the solute retention factor, and ϕ is the column phase ratio (stationary phase volume over the mobile phase volume). This expression can be rewritten expressing the Gibbs energy using the enthalpy, ΔH^o , and entropy, ΔS^o , as:

$$\ln k = - \left(\frac{\Delta H^o}{RT} \right) + \left(\frac{\Delta S^o}{R} \right) + \ln \phi \quad (3)$$

In chromatography, van't Hoff plots of $\ln k$ versus $1/T$ are commonly prepared to obtain the ΔH and ΔS thermodynamic parameters making experiments at different temperatures. In this study at constant temperature and for each enantiomer, different k_w values were obtained for different water amounts in the mobile phase, so the term $\ln \phi$ cancels providing:

$$\ln k_{w1} - \ln k_{w2} = \frac{-\Delta(\Delta G^o)}{RT} \quad (4)$$

The $\Delta(\Delta G^o)$ values quantify the effect of added water on each of the enantiomers in specific chromatographic systems. These $\Delta(\Delta G^o)$ values were calculated for several enantiomeric pair separations performed with increasing amounts of water. As a result, three different cases can be described as follows: (i) the water effect is greater on the first eluting enantiomer, (ii) the water effect is greater on the last eluting enantiomer, and (iii) the water effect is initially greater on one enantiomer and becomes more prominent on the other enantiomer when more water is added.

Figure 6.4 illustrates these three different situations that resulted in a substantial increase in enantioselectivity. For case (i) the first enantiomers saw a sharp decrease of retention time and the second enantiomers only a moderate decrease. Consequently, the selectivity factor increases (pentylone, Figure 6.4a and chromatograms Figure 6.5). A sharp decrease in enantioselectivity is observed in case (ii) since the second enantiomers elutes closer to the first one as more water is added (cis-4,5-diphenyl-2-oxazolidinone, Figure 6.4b and chromatograms in Figure 6.5). Case (iii) is associated with moderate enantioselectivity variation since the water effect on both enantiomers has a similar magnitude. Figure 6.4c shows the case of alprenolol on NicoShell CSP with an increasing water effect. Figure 6.4d shows the case of ethylone on the VancoShell CSP with a decreasing water effect. In Figure 6.4c and 4d, the enantioselectivity factor shows a moderate maximum near the $\Delta(\Delta G^\circ)$ crossing point. Also, the initial small amount of water effect was stronger on the first enantiomer, increasing selectivity, and the effect reversed as more water was added, thereby decreasing selectivity (Figs. 4c and 4d). In all three cases, as more water is added, it may increase the slope of the $\Delta(\Delta G^\circ)$ vs. %water, (Figure 6.4c) or decrease the slopes, as shown in Figs. 4a, 4b, and 4d.

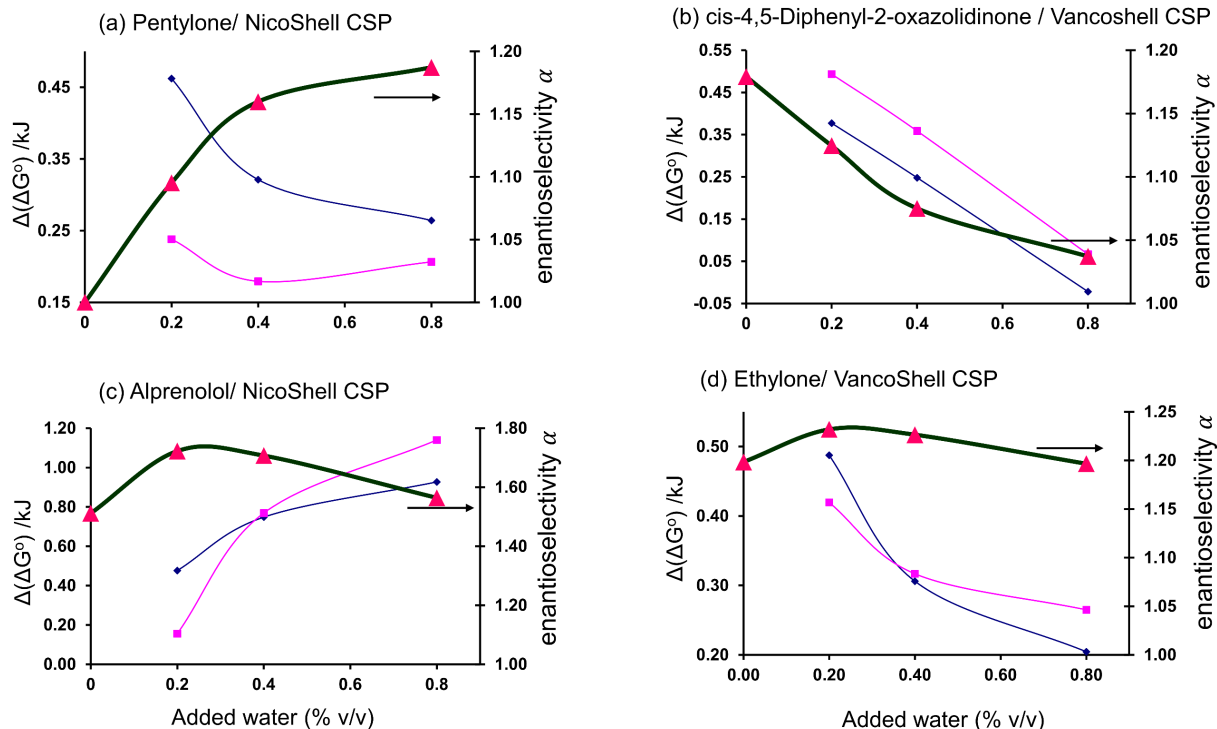


Figure 6.4 Variation of the water effect expressed in terms of Gibbs energy variation, $\Delta(\Delta G^\circ)$, versus the amount of added water in hexane/ethanol 70:30 %v/v mobile phase with 0.06% AA and 0.06 % v/v TEA for the indicated compounds and chiral stationary phases. Dark triangles and thick lines: enantioselectivity factor α (right axis); blue lozenges and line: first eluting enantiomer; pink squares and line: second eluting enantiomer. The three cases, noted (i), (ii) and (iii), are discussed in the text. Figs. 4a and 4b correspond to cases a and b; Figs. 4c and 4d both correspond to case (iii).

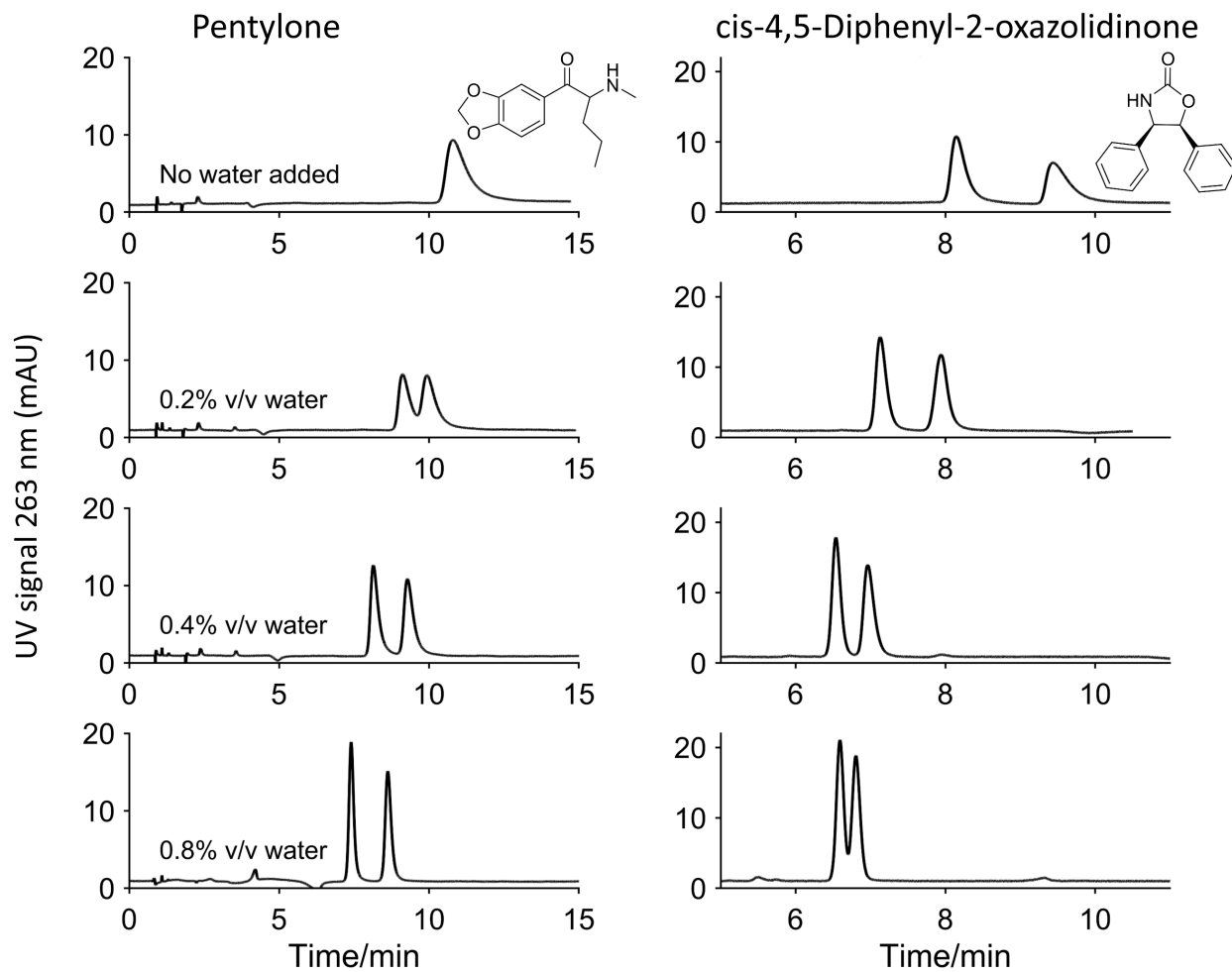


Figure 6.5 Effect of water addition to hexane/ethanol 80:20 v/v mobile phase with 0.06 % v/v of acetic acid and triethylamine on the chromatography of pentylone on 2.7 μm NicoShell 10x0.46 cm (left) and cis-4,5-Diphenyl-2-oxazolidinone on 2.7 μm VancoShell 10x0.46 cm (right). Flow rate: 1 mL/min; room temperature; UV detection at 263 nm.

Table 6.2 provides the chromatographic data obtained on three different CSPs with hexane/ethanol 70:30% v/v and 80:20% v/v mobile phases. The label "wet" corresponds to 1.4 or 0.8% added water for 70:30% v/v and 80:20% v/v respectively. A variety of chiral neutral or basic compounds were analyzed. Only two compounds were acidic: mecoprop and trans-4-cotinine carboxylic acid. In all cases, a decrease in retention time was associated with a significant increase in efficiency. These results are consistent with those obtained with carbohydrate-based CSPs [81, 82, 229, 230] in similar NP conditions. They also are comparable to the results presented in a recent study on the water effect in chiral separations by SFC using macrocyclic glycopeptide CSPs [83]. The acidic mecoprop compound shows minimal changes in retention by adding water to NP solvents on the TeicoShell CSP: the retention time of the first enantiomer decreased by a mere 0.2 min or -3.7%, and the retention of the last eluting enantiomer increased by the same 0.2 min or +3.2% (Table 6.2). This was the only increase in retention time observed upon water addition producing a very small negative $\Delta(\Delta G^{\circ})$ energy change (-0.09 kJ, Table 6.2). All $\Delta(\Delta G^{\circ})$ variations produced by the addition of water in the NP mobile phase were positive, meaning that the solute-stationary phase interaction, hence the retention times, were reduced. The enantioselectivity was altered depending on the relative effect of water on each enantiomer, as detailed above (Figure 6.4). It is clear that water molecules accumulated in the stationary phase (Figure 6.3) will decrease strong solute-stationary phase interactions. Considering the macrocyclic glycopeptides structure [242], these bonds can be H-bonds that firmly hold both enantiomers but differ from coulombic interactions having different strengths after hydration. The peak shapes were always improved, which implies changes in kinetics.

Table 6.2: Chromatographic retention parameter changes induced by addition of water to mobile phase.

Compound and chiral phase	Retention factor		Efficiency plates		$\Delta(\Delta G^\circ)$ kJ	Enantio selectivity		Resolution	
	<i>k</i> w/o water	<i>k</i> wet	N w/o water	N wet		α w/o water	α wet	R_s w/o water	R_s wet
VancoShell 4-(Diphenylmethyl)-2-oxazolidinone	1.98	1.08	4200	12300	1.47	1.23	1.09	2.1	1.2
	2.44	1.18	2700	10100	1.78				
5-Ethyl-5-methylhydantoin	5.53	2.16	1700	10700	2.30	1.17	1.10	1.5	1.6
	6.47	2.37	2100	8050	2.46				
cis-4,5-Diphenyl-2-oxazolidinone	7.53	5.84	8000	18000	0.58	1.18	1.04	2.8	1.1
	8.89	6.05	4500	16800	0.90				
Nicardipine	0.97	0.76	3500	12900	0.60	1.43	1.18	1.8	1.8
	1.39	0.89	830	6400	1.08				
Fluoxetine	23.74	6.68	900	8000	3.10	1.26	1.52	1.8	7.4
	29.95	10.16	1100	5000	2.65				
Ethylone	9.95	7.00	960	8000	0.96	1.17	1.21	1.2	3.5
	11.70	8.47	1100	6100	0.88				
Chlorophedianol	6.05	3.95	900	5600	1.05	1.12	1.13	0.7	1.8
	6.79	4.47	590	4600	1.02				
TeicoShell	<i>k</i> w/o water	<i>k</i> wet	N w/o water	N wet	$\Delta(\Delta G^\circ)$ kJ	α w/o water	α wet	R_s w/o water	R_s wet
4-(Diphenylmethyl)-2-Oxazolidinone	4.26	1.75	700	7550	2.19	1.25	1.11	1.2	1.8
	5.32	1.95	760	12500	2.46				
4-Benzyl-5,5-dimethyl-2-oxazolidinone	2.89	1.42	970	10100	1.74	1.84	1.37	3.0	4.0
	5.32	1.95	320	3200	2.46				
5-Ethyl-5-methylhydantoin	3.21	2.05	1760	10400	1.10	1.30	1.10	1.7	1.7
	4.16	2.26	450	9300	1.49				
5-Methyl-5-phenylhydantoin	3.42	2.16	1060	13000	1.13	2.11	1.39	4.3	5.8
	7.21	3.00	550	6400	2.15				
Lorazepam	3.00	1.53	2450	9300	1.66	4.65	2.59	12.1	13.0
	13.95	3.95	1030	3600	3.09				
Mecoprop	4.68	4.47	2180	11600	0.11	1.16	1.26	1.4	3.5
	5.42	5.63	3500	9600	-0.09				

Compound and chiral phase	Retention factor		Efficiency plates		$\Delta(\Delta G^\circ)$	Enantio selectivity		Resolution	
	<i>k</i> w/o water	<i>k</i> wet	N w/o water	N wet	$\Delta(\Delta G^\circ)$ kJ	α w/o water	α wet	R_s w/o water	R_s wet
Eutylone	6.37	5.21	900	7400	0.49	1.15	1.16	0.9	2.6
	7.32	6.05	800	6500	0.46				
Propafenone	55.11	18.68	1900	9200	2.65	1.82	1.75	5.8	12.0
	100.47	32.79	1300	7300	2.74				
Propanolol	43.32	17.74	1500	8400	2.19	1.54	1.64	3.8	9.9
	66.89	29.00	1100	6300	2.05				
trans-4-Cotinine carboxylic acid	8.47	6.37	1100	8300	0.70	1.29	1.21	1.8	3.8
	10.89	7.74	1000	8020	0.84				
Butylone	12.79	9.63	700	6600	0.69	1.00	1.12	0.0	1.5
	12.79	10.79	700	6630	0.42				
Pentdrone	4.58	3.84	800	4600	0.43	1.00	1.19	0.0	2.4
	4.58	4.58	800	6500	0.00				
Pentylone	8.58	5.74	900	5800	0.99	1.00	1.26	0.0	3.5
	8.58	7.21	900	5200	0.43				
Alprenolol	24.26	10.16	2900	11300	2.13	1.52	1.56	5.0	10.5
	36.79	15.84	2100	10100	2.06				
Tulbuterol	10.47	7.11	1700	9700	0.95	1.62	1.34	4.1	6.1
	17.00	9.53	1100	8000	1.42				

$\Delta(\Delta G^\circ)$: Gibbs energy change between without water (w/o water) and wet mobile phases calculated for each enantiomer using Eq. 4. For each compound: first line = first eluting enantiomer; second line = last eluting enantiomer. The ratio of hexane to ethanol in the mobile phase was 70:30 (with the maximum added water % of 1.4) for all cases except for alprenolol, cis-4,5-Diphenyl-2-oxazolidinone, mecoprop, and chlorophedianol in which the ratio was 80:20 with the maximum water % of 0.8). The additives, acetic acid and triethylamine were added at 0.06 % v/v each. In the case of trans-4-Cotinine carboxylic acid only 0.1% TFA was used.

6.4.7 Kinetic study of water influence on solute-stationary phase interaction

The kinetics of solute-stationary phase interactions are commonly studied by preparing plate height ($H = L/N$) curves against mobile phase flow rate (F) or linear velocity (u). Short 5 cm columns were chosen for this work to have a reasonable retention time at low flow rates and stay within the pressure limits (< 400 bar on HPLC) at high flow rates with $2.7 \mu\text{m}$ SPPs. Figure 6.6 shows three such curves in NPLC without added water and with 2.2 % v/v water for alprenolol, 5-methyl-5-phenylhydantoin, and lorazepam with 60:40 n-hexane/ethanol. Several remarkable features exist in these curves. The first thing to be noted is that there is a significant reduction in the H values at "all" flow rates in the presence of water for both enantiomers of the three analytes. Secondly, the curves tend to bend over at higher flow rates (> 1 mL/min). Also, there is an absence of a clear-cut minimum for 5-methyl-5-phenylhydantoin and lorazepam. Consequently, the curves do not fit the classical van Deemter equation ($H = A + B/F + CF$) or the Knox equation ($H = AF^{1/3} + B/F + CF$).

The downward vertical translation of the kinetic plots to lower H for all analytes in the presence of water in NPLC is rather striking because it "apparently" indicates a change in the A -term or the eddy diffusion term of the classical van Deemter equation. By fitting the raw data to the van Deemter equation, the translation of the curves will be lumped into the A term. However, the model will be meaningless since the A -term of the traditional van Deemter equation is a factor that embodies particle size, d_p , and the packing factor λ . In this study, the same column was used for each analyte, and there is no change in packing quality or the particle size when limited amounts water were added to the mobile phases. This critical point implies that for these separations the constant $A = 2\lambda d_p$ is not causing this shift. Also, the longitudinal diffusion, B term, should not

change significantly because there should be no considerable change in the mobile phase viscosity by the addition of trace amounts of water. If the A and B values were to be independently measured and constrained to remain constant, the mathematical fitting process would force all these effects into the C term. It is the mass transfer C term (sorption-desorption kinetics) is the main cause of the downward shift of the curves. A detailed discussion of the fallacies associated with interpreting van Deemter terms is discussed elsewhere [243].

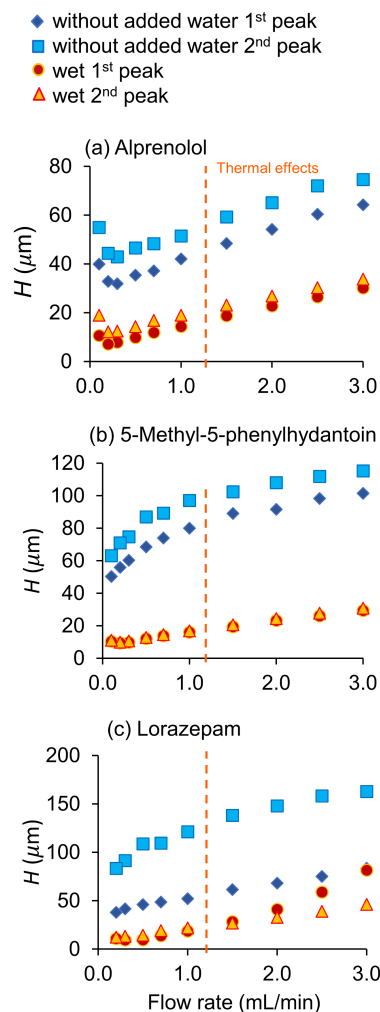


Figure 6.6 Evolution of H , the height equivalent to a theoretical plate, with the mobile phase flow rate. Experimental data obtained with hexane/ethanol 60:40 %v/v mobile phases with 0.06 % v/v of acetic acid and triethylamine (light blue squares and lozenges) and with 2.2% added water (red circles and yellow triangles), (a): NicoShell (alprenolol) and (b) VancoShell (5-Methyl-5-phenyl hydantoin), and (c) TeicoShell (lorazepam) 5-cm x 4.6 mm i.d. columns.

A detailed 1978 study on liquid chromatography band spreading by Horvath and Lin [244] relates the A -term to particle size and six packing parameters, namely, the porous tortuosity factor, the ratio of intraparticulate to interstitial void volume, and four structural packing parameters. Figure 6.7a shows the interactions considered (orange circles). The significant amount of water adsorbed by the stationary phases is likely to adsorb on the polar silica or polar ligand surfaces, changing these interactions. Furthermore, with SPP particles, Figure 6.7b is an oversimplified cartoon of the entire shell loaded with more water than in the mobile phase, as seen by the water adsorption study. As seen by analytes, the diffusion layer is different in the mobile phase without water and the "wet" mobile phase. The shell layer thickness may also be seen differently. As expected, the classical van Deemter and the Knox equation do not fit the data of the three analytes reliably in Figure 6.6(a-c). The fitting of the convex plots with Knox observed with 5-methyl-5-phenyl hydantoin and lorazepam (Figure 6.6a, blue lines) spurious (negative) A , B , and C values for the two enantiomers meaning that the cubic root of F on the first Knox term was already too high with the A -terms.

At high flow rates, the H vs. F curves show a flatter rise than seen in "well behaved" van Deemter curves. This observation indicates that the efficiencies of the analyte do not degrade as fast as they should at high flow rates when the separation temperature is not controlled. This unexpected effect in NPLC is a consequence of thermal effects arising from viscous frictional heating and compression of the mobile phase at higher flow rate and pressure, respectively [245-248]. Usually, efficiency decreases due to radial temperature gradients in reversed-phase achiral separation, whereas axial temperature gradients improve efficiency. In these chiral separations, the gain in plate count from axial temperature gradient outweighs any radial temperature gradients. However, with no exception, the chromatographic kinetics of the separation observed on the three

macrocyclic glycopeptides CSPs was significantly improved by adding small amounts of water to the NPs (Table 6.1). Others have also reported unusual van Deemter curves in chiral chromatography [249, 250].

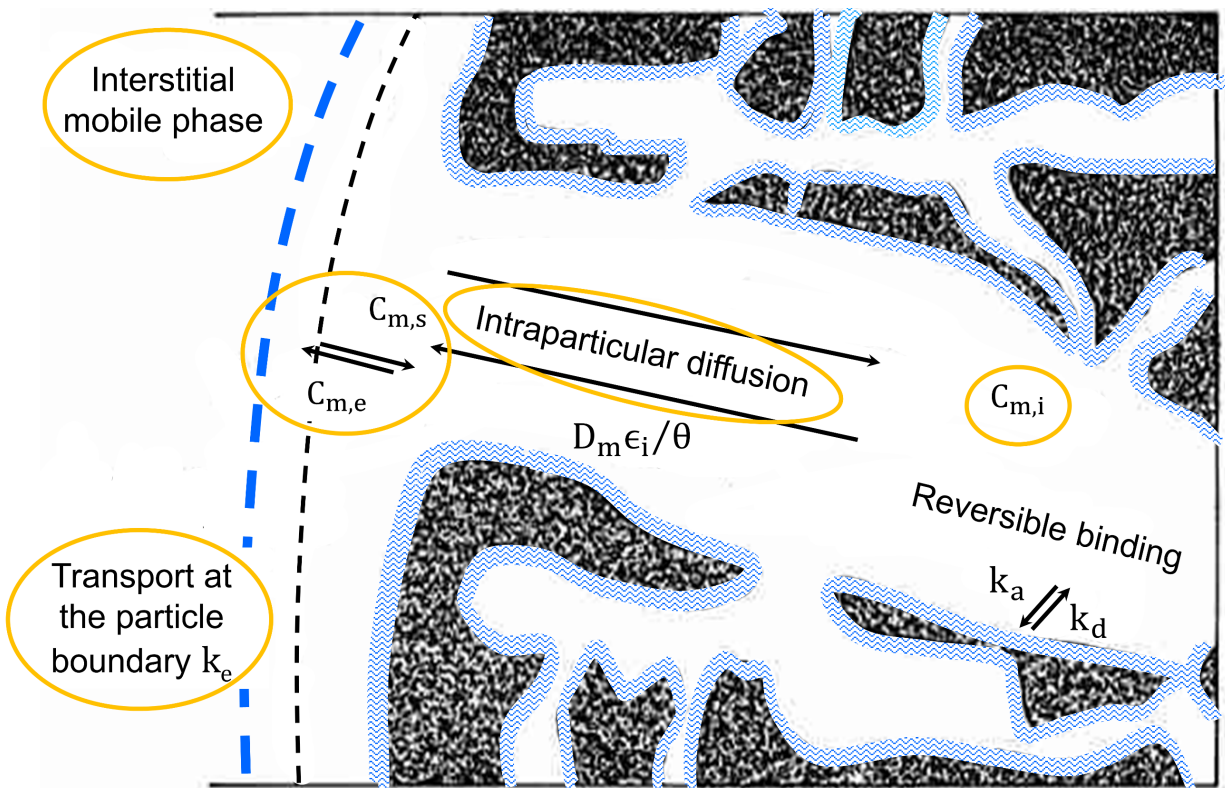


Figure 6.7 Six possible solute-stationary phase exchanges as described by Horvath and Lin [244]. The blue layer represents adsorbed water on the polar silica or polar bonded macrocyclic glycopeptides selector surfaces changing all solute-stationary phase interactions. The dashed lines show the hypothetical particle boundaries in dry NP (black, [244]) and water containing NP (blue). was adapted from [244]. The symbol θ shows "the tortuosity factor for the porous particles, D_m is the diffusivity of the unretained analyte in the bulk mobile phase, ϵ_i the appropriate intraparticle porosities, k_a and k_d the rate constants for the association and the dissociation processes, C_s denotes the surface concentration of the bound elute, C_m the concentration of the free elute in the mobile phase, $C_{m,i}$ the elute concentration in the stagnant mobile phase inside the particle, $C_{m,s}$ is the elute concentration at the outer surface of the particles $C_{m,e}$ denotes the elute concentration in the bulk mobile phase, k_e the mass transfer coefficient.

6.4.8 Water effects on adsorption isotherms

Adsorption isotherms are critically required in preparative chromatography to predict the elution behavior of large amounts of material loaded on the column [251]. The most commonly used isotherm representation was developed by Langmuir [252]. It relates Q , the solute concentration in the stationary phase, to C , the solute concentration in the mobile phase as:

$$Q = \frac{aC}{(1 + bC)} \quad (5)$$

in which a and b are the coefficients related respectively to the solute affinity for the stationary phase and to the isotherm curvature. The solute retention factor, k , is related to the isotherm by [253]:

$$k = \Phi \frac{dQ}{dC} \quad (6)$$

in which Φ is the column phase ratio (noted as F in the cited articles [244, 251]). When a reduced amount of solute is injected, the limit of Eq. 6 is the analytical retention factor k_0 giving the a term as [251]:

$$\lim_{C \rightarrow 0} \left(\Phi \frac{dQ}{dC} \right) = k_0 = \Phi a \quad (7)$$

Having a limited number of experiments, we will work on finite differences with Eq. 6 modified for the "overloaded" retention factor, k_i obtained injecting the concentration C_i , as:

$$k_i = \Phi \frac{\Delta Q}{\Delta C} = \Phi \frac{Q_i - Q_{i-1}}{C_i - C_{i-1}} \quad (8)$$

and the initial conditions: $Q_0 = C_0 = 0$ giving $Q_1 = k_1 C_1 / \Phi$. The successive Q_i can be iteratively obtained as $Q_i = k_i C_i / \Phi$. Since we do not know the column phase ratio, Φ , the relative Q'_i values can be defined as:

$$Q'_i = Q_i / \Phi \quad (9)$$

Plots of the relative concentration of analyte in stationary phase (Q'_i), vs. C_i (the relative adsorption isotherms), will follow the same trends as the real isotherms however, the slopes will be higher by a factor of Φ .

Figs. 8a and 8b show the increasingly asymmetrical chromatograms as greater amounts of alprenolol were injected (up to 0.588 mg corresponding to a 7 μ L injection) on a 10 x 0.46 i.d. cm SPP NicoShell column and eluted either by a hexane/ethanol 80:20 v/v NP mobile phase (Figure 6.8a) or with the same mobile phase containing 0.8% v/v added water (Figure 6.8b). With water, the change in the isotherm type is evident for the first eluting alprenolol peak showing slightly fronting peaks when tailing peaks were observed in all other situations. Figure 6.8c shows that the first eluting peak is related to a concave anti-Langmuirian isotherm (negative b in Eq. 8) while its isotherm was a classical convex Langmuir isotherm eluted without water in the NP solvent. Also, comparing the isotherms of the last eluting alprenolol enantiomer (Figure 6.8c), it is clear that the b term is reduced in water-containing NP solvents. The enthalpy changes observed (Figure 6.4) are due to changes induced by adsorbed water molecules competing for existing adsorption sites or creating different sites on the CSP. The first eluting enantiomer has necessarily fewer and/or weaker interactions than the most retained enantiomer, and water molecules interact with one important alprenolol enantiospecific binding site, completely changing the first enantiomer isotherm. These "water interactions" are very beneficial in preparative chromatography. Figure 6.8a shows that enantiomer overlap starts as soon as 0.25 mg alprenolol is loaded on the 10 cm

column. Figure 6.8b shows that there was no overlap when 0.588 mg was injected; more than twice that amount could be loaded with "wet" NPs with the added benefit of halving the retention times.

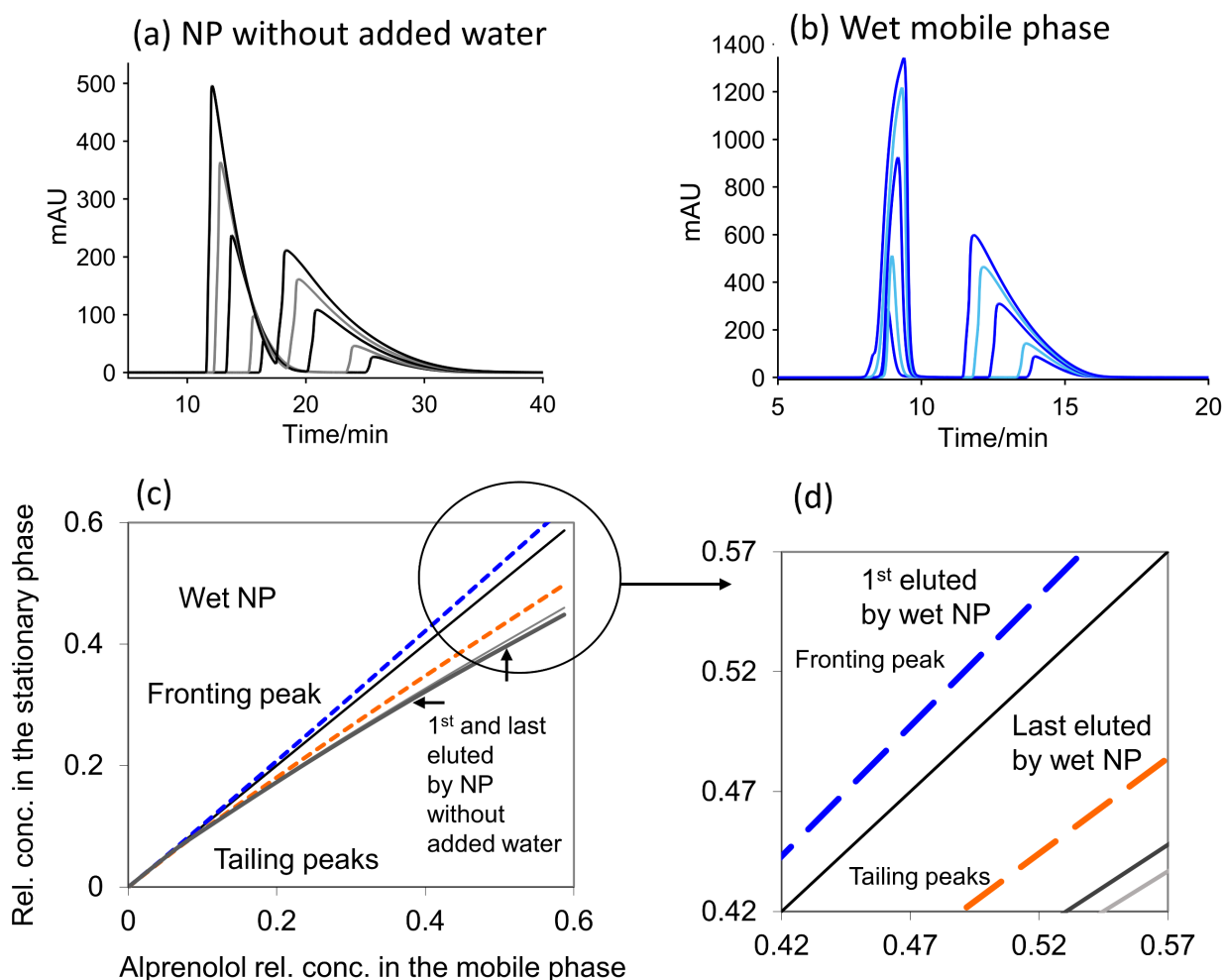


Figure 6.8 Effect of water addition in semi-preparative conditions. a) Chromatograms of alprenolol separated on the NicoShell CSP by hexane/ethanol 80:20 %v/v mobile phases with 0.06 % v/v of acetic acid and triethylamine; b) Same but 0.8% water was added to the mobile phase; Injection volumes are 0.5, 1, 3, 5, and 7 μL corresponding to 42, 84, 252, 420 and 587 μg respectively c) Reduced adsorption isotherms obtained with the (a) and (b) chromatograms as indicated in text. Injected solution is 84 mg/mL of alprenolol in ethanol.

6.5 Conclusions

This work showed that in NPLC, adding small amounts of water to the hexane/ethanol mobile phase reduced retention times significantly with an added advantage of substantial efficiency gains for enantioseparations. This effect was observed with ionizable and semi-polar chiral compounds on macrocyclic glycopeptides bonded to superficially porous particles. The water effect on one enantiomer interaction with the CSP may be very different from that of the other enantiomer, which in turn can enhance or lower the enantioselectivity. Very polar water molecules change the overall mobile phase polarity measured by the bathochromic shift of Nile red. The major water effect is due to modified adsorption sites on the chiral stationary phase. These changes modify the adsorption isotherms up to the point of changing a convex Langmuir-type into a concave anti-Langmuir type. Also, water interactions with the stationary phase always increase the solute-stationary phase kinetic parameters, drastically reducing the simplified A -term of H vs. F curves. The causal mechanism appears to be related to the heavily hydrated pores within the core-shell CSP particles. It seems that it is beneficial to add small amounts of water when working in normal phase mode with macrocyclic glycopeptides CSPs either for analytical enantiomer identification or for preparative purification.

Chapter 7 Conclusions

Chapter 2 provided optimum separation conditions for separation of 47 pairs of isotopologues. It was concluded that the three stationary phases that provided the highest number of separations were: a) polydimethyl siloxane with 20% diphenyl, b) IL-111i, and c) PAG (polyalkylene glycol). This chapter is the single most comprehensive study on the GC separation of isotopic isomers. Chromatographic isotope effects were reported for all stationary phases.

Chapter 3 investigated the effect of the location of deuterium atom on gas chromatographic isotope effects. Deuterium isotope effects can result from the difference in electron distribution for deuterated vs. protiated analytes. The magnitude of the isotope effect depends on number of deuterium atoms, location of deuterium atoms, and the nature of the stationary phase.

Chapter 4 introduced the second-generation GC-MRR, which can provide the greatest amount of structural information. It was shown how the sensitivity of MRR instrument was improved to the levels surpassing those of the thermal conductivity detector. Implementing supersonic jet expansion and effective cooling in addition to heated transfer line, Fabry-Perot cavity, and more effective transmitting and detecting the microwaves with L-shaped antennae are the main factors resulting in improved sensitivity in the second-generation MRR.

Chapter 5 showed how the new stationary phase developed by dispersion of metal organic frameworks in ionic liquids provided unique selectivities in the separation of different groups of alkanes, alcohols, ethers, and ketones and provided the first separation of permanent gases with gas liquid chromatography.

In chapter 6, the effects of trace, but controlled amounts of added water in stationary phase were studied. The presence of water almost always increased the efficiency and reduced the retention of peaks in enantioselective NPLC. In most cases it led to increased enantioselectivity as well. The solvatochromic studies showed that addition of small amounts of water can lead to small changes in the polarity of the mobile phase. However, the hydration of glycopeptide-based chiral stationary phases and the increasing concentration of water in the pore, can provide a better explanation for observations involving efficiency and enantioselectivity.

Appendix A

Publication information of the dissertation

Chapter 2

Thakur, Nimisha, Saba Aslani, and Daniel W. Armstrong. "Evaluation of gas chromatography for the separation of a broad range of isotopic compounds." *Analytica Chimica Acta* 1165 (2021): 338490.

Chapter 3

Saba Aslani and Daniel W. Armstrong. Submitted to *Talanta* August 2023.

Chapter 4

Wahab, M. Farooq, et al. "Enhancing sensitivity for high-selectivity gas chromatography-molecular rotational resonance spectroscopy." *Analytical Chemistry* 93.46 (2021): 15525-15533.

Chapter 5


Patel, Arzoo, et al. "A Metal Organic Framework+ Ionic Liquid Pseudophase System as a Gas Chromatography Stationary Phase." *Chromatographia* (2023): 1-10.


Chapter 6

Aslani, Saba, et al. "An examination of the effects of water on normal phase enantioseparations." *Analytica Chimica Acta* 1200 (2022): 339608.

Appendix B Rights and Permissions

Chapter 2

Home Help Live Chat Sign in Create Account




Evaluation of gas chromatography for the separation of a broad range of isotopic compounds
Author: Nimisha Thakur, Saba Aslani, Daniel W. Armstrong
Publication: Analytica Chimica Acta
Publisher: Elsevier
Date: 22 June 2021
© 2021 Elsevier B.V. All rights reserved.


Journal Author Rights

Please note that, as the author of this Elsevier article, you retain the right to include it in a thesis or dissertation, provided it is not published commercially. Permission is not required, but please ensure that you reference the journal as the original source. For more information on this and on your other retained rights, please visit: <https://www.elsevier.com/about/our-business/policies/copyright#Author-rights>

[BACK](#) [CLOSE WINDOW](#)

Chapter 4

Home Help Live Chat Sign in Create Account



Enhancing Sensitivity for High-Selectivity Gas Chromatography-Molecular Rotational Resonance Spectroscopy
Author: M. Farooq Wahab, Saba Aslani, Alexander V. Mikhonin, et al
Publication: Analytical Chemistry
Publisher: American Chemical Society
Date: Nov 1, 2021
Copyright © 2021, American Chemical Society

PERMISSION/LICENSE IS GRANTED FOR YOUR ORDER AT NO CHARGE

This type of permission/license, instead of the standard Terms and Conditions, is sent to you because no fee is being charged for your order. Please note the following:

- Permission is granted for your request in both print and electronic formats, and translations.
- If figures and/or tables were requested, they may be adapted or used in part.
- Please print this page for your records and send a copy of it to your publisher/graduate school.
- Appropriate credit for the requested material should be given as follows: "Reprinted (adapted) with permission from {COMPLETE REFERENCE CITATION}. Copyright {YEAR} American Chemical Society." Insert appropriate information in place of the capitalized words.
- One-time permission is granted only for the use specified in your RightsLink request. No additional uses are granted (such as derivative works or other editions). For any uses, please submit a new request.

If credit is given to another source for the material you requested from RightsLink, permission must be obtained from that source.

[BACK](#) [CLOSE WINDOW](#)

Chapter 5

A Metal Organic Framework Ionic Liquid Pseudophase System as a Gas Chromatography Stationary Phase

SPRINGER NATURE

Author: Arzoo Patel et al
Publication: Chromatographia
Publisher: Springer Nature
Date: May 2, 2023

Copyright © 2023, The Author(s), under exclusive licence to Springer-Verlag GmbH Germany, part of Springer Nature

Order Completed

Thank you for your order.

This Agreement between University of Texas at Arlington -- Saba Aslani ("You") and Springer Nature ("Springer Nature") consists of your license details and the terms and conditions provided by Springer Nature and Copyright Clearance Center.

Chapter 6



An examination of the effects of water on normal phase enantioseparations

Author: Saba Aslani, M. Farooq Wahab, Marziyeh Eshaghi Kenari, Alain Berthod, Daniel W. Armstrong
Publication: Analytica Chimica Acta
Publisher: Elsevier
Date: 1 April 2022

© 2022 Elsevier B.V. All rights reserved.

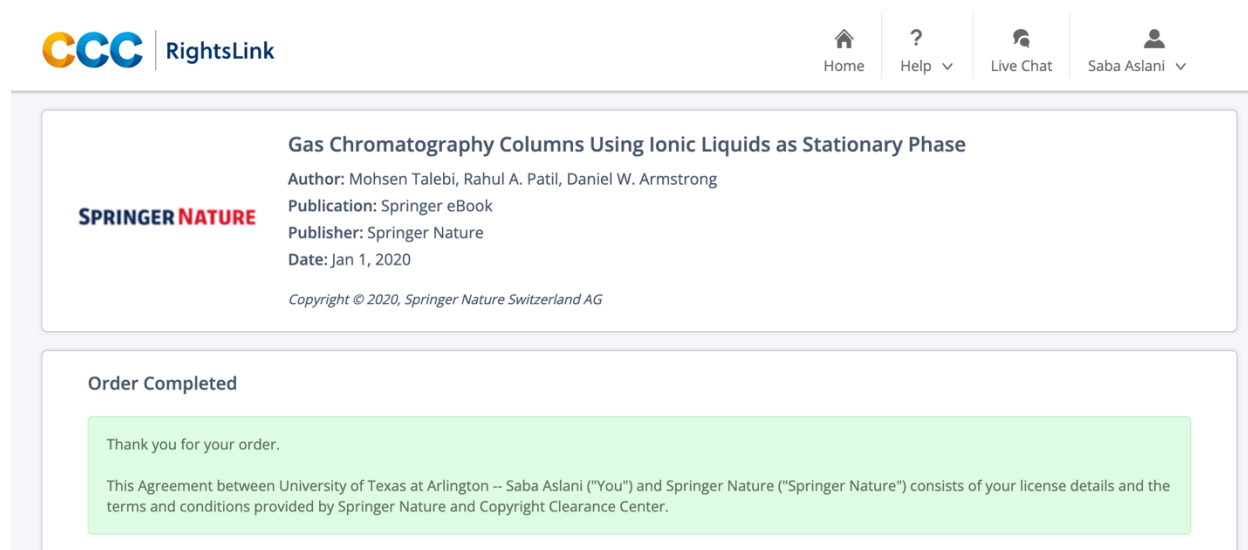
Journal Author Rights

Please note that, as the author of this Elsevier article, you retain the right to include it in a thesis or dissertation, provided it is not published commercially. Permission is not required, but please ensure that you reference the journal as the original source. For more information on this and on your other retained rights, please visit: <https://www.elsevier.com/about/our-business/policies/copyright#Author-rights>

BACK

CLOSE WINDOW

Table 1.1



The screenshot shows the top navigation bar with the CCC RightsLink logo and user options: Home, Help, Live Chat, and Saba Aslani. The main content area displays the title "Gas Chromatography Columns Using Ionic Liquids as Stationary Phase" by Mohsen Talebi, Rahul A. Patil, and Daniel W. Armstrong. It lists the publication as Springer eBook, published by Springer Nature on Jan 1, 2020. A copyright notice for 2020 is also present. Below this, a green box titled "Order Completed" contains a thank-you message and a link to the license agreement between the University of Texas at Arlington and Springer Nature.

CCC RightsLink Home Help Live Chat Saba Aslani

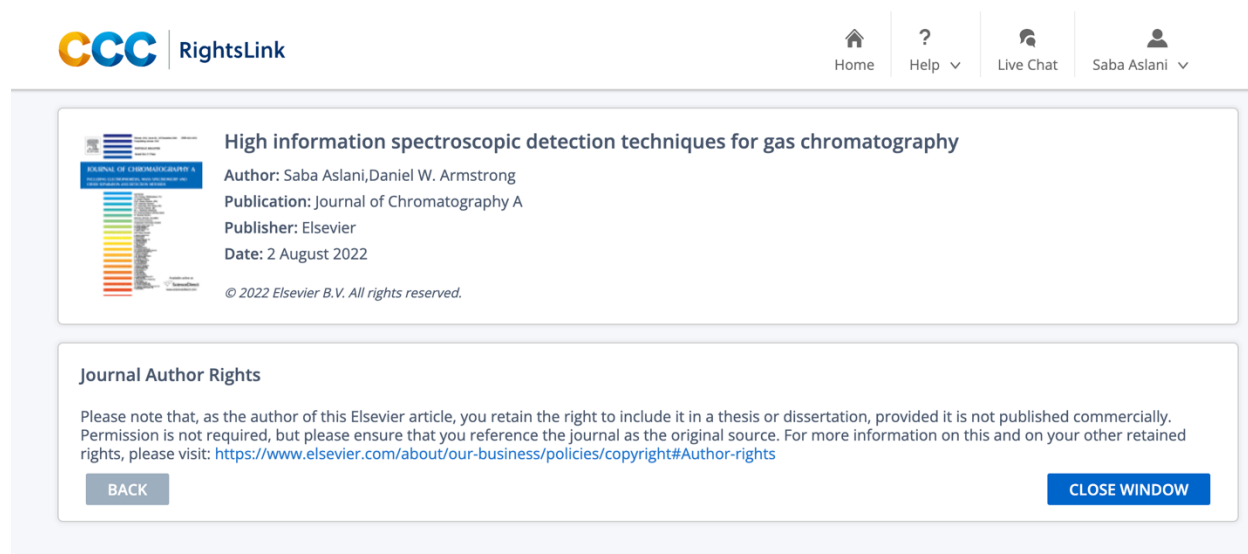
SPRINGER NATURE **Gas Chromatography Columns Using Ionic Liquids as Stationary Phase**
Author: Mohsen Talebi, Rahul A. Patil, Daniel W. Armstrong
Publication: Springer eBook
Publisher: Springer Nature
Date: Jan 1, 2020
Copyright © 2020, Springer Nature Switzerland AG

Order Completed

Thank you for your order.

This Agreement between University of Texas at Arlington -- Saba Aslani ("You") and Springer Nature ("Springer Nature") consists of your license details and the terms and conditions provided by Springer Nature and Copyright Clearance Center.

Figure 1.1



The screenshot shows the top navigation bar with the CCC RightsLink logo and user options: Home, Help, Live Chat, and Saba Aslani. The main content area displays the title "High information spectroscopic detection techniques for gas chromatography" by Saba Aslani and Daniel W. Armstrong. It lists the publication as Journal of Chromatography A, published by Elsevier on 2 August 2022. A copyright notice for 2022 Elsevier B.V. is also present. Below this, a section titled "Journal Author Rights" provides a disclaimer and a link to Elsevier's author rights policy. At the bottom, there are "BACK" and "CLOSE WINDOW" buttons.

CCC RightsLink Home Help Live Chat Saba Aslani

High information spectroscopic detection techniques for gas chromatography
Author: Saba Aslani, Daniel W. Armstrong
Publication: Journal of Chromatography A
Publisher: Elsevier
Date: 2 August 2022
© 2022 Elsevier B.V. All rights reserved.

Journal Author Rights


Please note that, as the author of this Elsevier article, you retain the right to include it in a thesis or dissertation, provided it is not published commercially. Permission is not required, but please ensure that you reference the journal as the original source. For more information on this and on your other retained rights, please visit: <https://www.elsevier.com/about/our-business/policies/copyright#Author-rights>

BACK CLOSE WINDOW

Figure 1.2

CCC | RightsLink

Home ? Help Live Chat Saba Aslani

 **A Gas Chromatography-Molecular Rotational Resonance Spectroscopy Based System of Singular Specificity**
Author: Justin L. Neill, Matt T. Muckle, Alexander V. Mikhonin, et al
Publication: Angewandte Chemie
Publisher: John Wiley and Sons
Date: Nov 19, 2019
© 2020 Wiley-VCH Verlag GmbH & Co. KGaA, Weinheim

Order Completed

Thank you for your order.

This Agreement between University of Texas at Arlington -- Saba Aslani ("You") and John Wiley and Sons ("John Wiley and Sons") consists of your license details and the terms and conditions provided by John Wiley and Sons and Copyright Clearance Center.

References

- [1] <https://goldbook.iupac.org/terms/view/I03351>,
- [2] <https://goldbook.iupac.org/terms/view/I03352>,
- [3] K.E. Wilzbach, P. Riesz, Isotope effects in gas-liquid chromatography, *Science* 126(3277) (1957) 748-749 [10.1126/science.126.3277.748](https://doi.org/10.1126/science.126.3277.748)
- [4] B. Shi, B.H. Davis, Gas chromatographic separation of pairs of isotopic molecules, *Journal of Chromatography A* 654(2) (1993) 319-325 [https://doi.org/10.1016/0021-9673\(93\)83377-5](https://doi.org/10.1016/0021-9673(93)83377-5)
- [5] R. Bentley, N.C. Saha, C.C. Sweeley, Separation of Protium and Deuterium Forms of Carbohydrates by Gas Chromatography, *Analytical Chemistry* 37(9) (1965) 1118-1122 <https://doi.org/10.1021/ac60228a012>
- [6] F. Bruner, G.P. Carloni, M. Possanzini, Separation of isotopic methanes by gas chromatography, *Analytical Chemistry* 41(8) (1969) 1122-1124 <https://doi.org/10.1021/ac60277a043>
- [7] H.-G. Schmarr, P. Slabizki, S. Müntrich, C. Metzger, E. Gracia-Moreno, Ionic liquids as novel stationary phases in gas liquid chromatography: Inverse or normal isotope effect?, *Journal of Chromatography A* 1270 (2012) 310-317 <https://doi.org/10.1016/j.chroma.2012.11.010>
- [8] G. Carloni, A. Liberti, A. Pela, Gas chromatographic separation of polar isotopic molecules, *Analytical Chemistry* 39(13) (1967) 1618-1622 <https://doi.org/10.1021/ac50156a037>
- [9] N. Thakur, S. Aslani, D.W. Armstrong, Evaluation of gas chromatography for the separation of a broad range of isotopic compounds, *Analytica Chimica Acta* 1165 (2021) 338490 <https://doi.org/10.1016/j.aca.2021.338490>
- [10] C. Schmidt, First deuterated drug approved, *Nature Biotechnology* 35(6) (2017) 493-494 [10.1038/nbt0617-493](https://doi.org/10.1038/nbt0617-493)
- [11] D.O. Claassen, B. Carroll, L.M. De Boer, E. Wu, R. Ayyagari, S. Gandhi, D. Stamler, Indirect tolerability comparison of Deutetrabenazine and Tetrabenazine for Huntington disease, *Journal of clinical movement disorders* 4 (2017) 1-11
- [12] T. Pirali, M. Serafini, S. Cargnin, A.A. Genazzani, Applications of deuterium in medicinal chemistry, *Journal of medicinal chemistry* 62(11) (2019) 5276-5297
- [13] X. Pang, Y. Wang, Y. Chen, Design, synthesis, and biological evaluation of deuterated apalutamide with improved pharmacokinetic profiles, *Bioorganic & medicinal chemistry letters* 27(12) (2017) 2803-2806 <https://doi.org/10.1016/j.bmcl.2017.04.071>
- [14] X. Pang, L. Peng, Y. Chen, Effect of N-methyl deuteration on pharmacokinetics and pharmacodynamics of enzalutamide, *Journal of Labelled Compounds and Radiopharmaceuticals* 60(9) (2017) 401-409 <https://doi.org/10.1002/jlcr.3516>
- [15] S.L. Harbeson, A.J. Morgan, J.F. Liu, A.M. Aslanian, S. Nguyen, G.W. Bridson, C.L. Brummel, L. Wu, R.D. Tung, L. Pilja, Altering metabolic profiles of drugs by precision deuteration 2: discovery of a deuterated analog of ivacaftor with differentiated pharmacokinetics for clinical development, *Journal of Pharmacology and Experimental Therapeutics* 362(2) (2017) 359-367 <https://doi.org/10.1124/jpet.117.241497>

- [16] D.H. Phillips, G.A. Potter, M.N. Horton, A. Hewker, C. Crofton-Sleigh, M. Jarman, S. Venitt, Reduced genotoxicity of [D5-ethyl]-tamoxifen implicates α -hydroxylation of the ethyl group as a major pathway of tamoxifen activation to a liver carcinogen, *Carcinogenesis* 15(8) (1994) 1487-1492 <https://doi.org/10.1093/carcin/15.8.1487>
- [17] D.M. Calinski, H. Zhang, S. Ludeman, M.E. Dolan, P.F. Hollenberg, Hydroxylation and N-dechloroethylation of Ifosfamide and deuterated Ifosfamide by the human cytochrome p450s and their commonly occurring polymorphisms, *Drug Metabolism and Disposition* 43(7) (2015) 1084-1090 <https://doi.org/10.1124/dmd.115.063628>
- [18] H. Jia, G. Dai, J. Weng, Z. Zhang, Q. Wang, F. Zhou, L. Jiao, Y. Cui, Y. Ren, S. Fan, Discovery of (S)-1-(1-(Imidazo [1, 2-a] pyridin-6-yl) ethyl)-6-(1-methyl-1 H-pyrazol-4-yl)-1 H-[1, 2, 3] triazolo [4, 5-b] pyrazine (Volitinib) as a Highly Potent and Selective Mesenchymal–Epithelial Transition Factor (c-Met) Inhibitor in Clinical Development for Treatment of Cancer, *Journal of medicinal chemistry* 57(18) (2014) 7577-7589 <https://doi.org/10.1021/jm500510f>
- [19] Y. Zhu, J. Zhou, B. Jiao, Deuterated clopidogrel analogues as a new generation of antiplatelet agents, *ACS medicinal chemistry letters* 4(3) (2013) 349-352 <https://doi.org/10.1021/ml300460t>
- [20] T. Yamamoto, E. Tokunaga, S. Nakamura, N. Shibata, T. Toru, Synthesis and configurational stability of (S)-and (R)-deuteriothalidomides, *Chemical and pharmaceutical bulletin* 58(1) (2010) 110-112 <https://doi.org/10.1248/cpb.58.110>
- [21] S.L. Harbeson, R.D. Tung, Chapter 24 - Deuterium in Drug Discovery and Development, in: J.E. Macor (Ed.), *Annual Reports in Medicinal Chemistry*, Academic Press 2011, pp. 403-417 <https://doi.org/10.1016/B978-0-12-386009-5.00003-5>
- [22] X. Yang, H. Ben, A.J. Ragauskas, Recent Advances in the Synthesis of Deuterium-Labeled Compounds, *Asian Journal of Organic Chemistry* 10(10) (2021) 2473-2485 <https://doi.org/10.1002/ajoc.202100381>
- [23] J. Bigeleisen, M.G. Mayer, Calculation of equilibrium constants for isotopic exchange reactions, *The Journal of Chemical Physics* 15(5) (1947) 261-267
- [24] R.M. O'Ferrall, A pictorial representation of zero-point energy and tunnelling contributions to primary hydrogen isotope effects, *Journal of Physical Organic Chemistry* 23(7) (2010) 572-579
- [25] J. Atzrodt, V. Derdau, W.J. Kerr, M. Reid, Deuterium-and tritium-labelled compounds: applications in the life sciences, *Angewandte Chemie International Edition* 57(7) (2018) 1758-1784
- [26] M. Matucha, W. Jockisch, P. Verner, G. Anders, Isotope effect in gas—liquid chromatography of labelled compounds, *Journal of Chromatography A* 588(1-2) (1991) 251-258 [https://doi.org/10.1016/0021-9673\(91\)85030-J](https://doi.org/10.1016/0021-9673(91)85030-J)
- [27] J. Mráz, P. Jheeta, A. Gescher, M.D. Threadgill, Unusual deuterium isotope effect on the retention of formamides in gas—liquid chromatography, *Journal of Chromatography A* 641(1) (1993) 194-198 [https://doi.org/10.1016/0021-9673\(93\)83476-9](https://doi.org/10.1016/0021-9673(93)83476-9)
- [28] P. Atkins, J. De Paula, *Atkins' physical chemistry*, Oxford university press 2006,

- [29] A. Höpfner, Vapor pressure isotope effects, *Angewandte Chemie International Edition in English* 8(10) (1969) 689-699
- [30] I. Kiss, G. Jákli, G. Jancsó, H. Illy, Vapor Pressures of Some Deuterated Alcohols and Amines, *The Journal of Chemical Physics* 47(11) (1967) 4851-4852 [10.1063/1.1701711](https://doi.org/10.1063/1.1701711)
- [31] D.J. Lacks, Origins of molar volume isotope effects in hydrocarbon systems, *The Journal of Chemical Physics* 103(12) (1995) 5085-5090 [10.1063/1.470595](https://doi.org/10.1063/1.470595)
- [32] W.A.V. Hook, Isotope effects in condensed phases, the benzene example. Influence of anharmonicity; harmonic and anharmonic potential surfaces and their isotope independence. Molar volume effects in isotopic benzenes, *The Journal of Chemical Physics* 83(8) (1985) 4107-4117 [10.1063/1.449842](https://doi.org/10.1063/1.449842)
- [33] L.S. Bartell, R.R. Roskos, Isotope Effects on Molar Volume and Surface Tension: Simple Theoretical Model and Experimental Data for Hydrocarbons, *The Journal of Chemical Physics* 44(2) (1966) 457-463 [10.1063/1.1726709](https://doi.org/10.1063/1.1726709)
- [34] E. Halevi, Secondary isotope effects, *Progress in physical organic chemistry* (1963) 109-221
- [35] C.N. Banwell, E.M. McCash, *Fundamentals of molecular spectroscopy*, Indian Edition 2017
- [36] R.L. Cook, Microwave molecular spectroscopy, in: R.A. Meyers (Ed.), *Encyclopedia of Physical Science and Technology* (Third Edition), Academic Press, New York, 2003, pp. 799-852 <https://doi.org/10.1016/B0-12-227410-5/00447-6>
- [37] J.L. Neill, A.V. Mikhonin, T. Chen, R.E. Sonstrom, B.H. Pate, Rapid quantification of isomeric and dehalogenated impurities in pharmaceutical raw materials using MRR spectroscopy, *Journal of Pharmaceutical and Biomedical Analysis* 189 (2020) 113474 <https://doi.org/10.1016/j.jpba.2020.113474>
- [38] J.L. Neill, Y. Yang, M.T. Muckle, R.L. Reynolds, L. Evangelisti, R.E. Sonstrom, B.H. Pate, B.F. Gupton, Online Stereochemical Process Monitoring by Molecular Rotational Resonance Spectroscopy, *Organic Process Research & Development* 23(5) (2019) 1046-1051 <https://doi.org/10.1021/acs.oprd.9b00089>
- [39] M.F. Wahab, S. Aslani, A.V. Mikhonin, J.L. Neill, D.W. Armstrong, Enhancing Sensitivity for High-Selectivity Gas Chromatography-Molecular Rotational Resonance Spectroscopy, *Analytical Chemistry* (2021) <https://doi.org/10.1021/acs.analchem.1c03710>
- [40] L.A. Joyce, D.M. Schultz, E.C. Sherer, J.L. Neill, R.E. Sonstrom, B.H. Pate, Direct regioisomer analysis of crude reaction mixtures via molecular rotational resonance (MRR) spectroscopy, *Chemical science* 11(24) (2020) 6332-6338 <https://doi.org/10.1039/D0SC01853H>
- [41] P.F. Bernath, *Spectra of atoms and molecules*, fourth ed., Oxford university press, New York, 2020
- [42] D.C. Harris, M.D. Bertolucci, *Symmetry and spectroscopy: an introduction to vibrational and electronic spectroscopy*, first ed., Dover Publications, New York, USA, 1989

- [43] D.W. Armstrong, M. Talebi, N. Thakur, M.F. Wahab, A.V. Mikhonin, M.T. Muckle, J.L. Neill, A Gas Chromatography-Molecular Rotational Resonance Spectroscopy Based System of Singular Specificity, *Angewandte Chemie* 132(1) (2020) 198-202 <https://doi.org/10.1002/ange.201910507>
- [44] J.L.N. B. J. Harris, R. L. Pulliam, M. T. Muckle, Fourier transform molecular rotational resonance spectroscopy for reprogrammable chemical sensing, *LC_GC* (33) (2015) 18 – 24. <https://doi.org/10.1117/12.2080101>
- [45] J.E. Szulejko, T. Solouki, Potential Analytical Applications of Interfacing a GC to an FT-ICR MS: Fingerprinting Complex Sample Matrixes, *Analytical Chemistry* 74(14) (2002) 3434-3442 <https://doi.org/10.1021/ac011192z>
- [46] A.L. Rockwood, M.M. Kushnir, N.J. Clarke, 2 - Mass Spectrometry, in: N. Rifai, A.R. Horvath, C.T. Wittwer (Eds.), *Principles and Applications of Clinical Mass Spectrometry*, Elsevier2018, pp. 33-65 <https://doi.org/10.1016/B978-0-12-816063-3.00002-5>
- [47] G.G. Brown, B.C. Dian, K.O. Douglass, S.M. Geyer, S.T. Shipman, B.H. Pate, A broadband Fourier transform microwave spectrometer based on chirped pulse excitation, *Review of Scientific Instruments* 79(5) (2008) 053103 <https://doi.org/10.1063/1.2919120>
- [48] G.B. Park, R.W. Field, Perspective: The first ten years of broadband chirped pulse Fourier transform microwave spectroscopy, *The Journal of chemical physics* 144(20) (2016) 200901 <https://doi.org/10.1063/1.4952762>
- [49] S. Aslani, D.W. Armstrong, High information spectroscopic detection techniques for gas chromatography, *Journal of Chromatography A* (2022) 463255
- [50] T. Balle, W. Flygare, Fabry–Perot cavity pulsed Fourier transform microwave spectrometer with a pulsed nozzle particle source, *Review of Scientific Instruments* 52(1) (1981) 33-45 <https://doi.org/10.1063/1.1136443>
- [51] D.W. Armstrong, L. He, Y.-S. Liu, Examination of ionic liquids and their interaction with molecules, when used as stationary phases in gas chromatography, *Analytical chemistry* 71(17) (1999) 3873-3876
- [52] J.L. Anderson, R. Ding, A. Ellern, D.W. Armstrong, Structure and properties of high stability geminal dicationic ionic liquids, *Journal of the American Chemical Society* 127(2) (2005) 593-604
- [53] Z.S. Breitbach, D.W. Armstrong, Characterization of phosphonium ionic liquids through a linear solvation energy relationship and their use as GLC stationary phases, *Analytical and bioanalytical chemistry* 390(6) (2008) 1605-1617 <https://doi.org/10.1007/s00216-008-1877-3>
- [54] P. Sun, D.W. Armstrong, Ionic liquids in analytical chemistry, *Analytica Chimica Acta* 661(1) (2010) 1-16 <https://doi.org/10.1016/j.aca.2009.12.007>
- [55] X. Han, D.W. Armstrong, Ionic Liquids in Separations, *Accounts of Chemical Research* 40(11) (2007) 1079-1086 <https://doi.org/10.1021/ar700044y>
- [56] K. Huang, X. Han, X. Zhang, D.W. Armstrong, PEG-linked geminal dicationic ionic liquids as selective, high-stability gas chromatographic stationary phases, *Analytical and Bioanalytical Chemistry* 389(7) (2007) 2265-2275 <https://doi.org/10.1007/s00216-007-1625-0>

- [57] T. Payagala, J. Huang, Z.S. Breitbach, P.S. Sharma, D.W. Armstrong, Unsymmetrical dicationic ionic liquids: manipulation of physicochemical properties using specific structural architectures, *Chemistry of Materials* 19(24) (2007) 5848-5850
- [58] K.G. Furton, R. Morales, Effect of anion chain length on the solvent properties of liquid tetrabutylammonium alkylsulfonate salts studied by gas—liquid chromatography, *Analytica chimica acta* 246(1) (1991) 171-179 [https://doi.org/10.1016/S0003-2670\(00\)80674-1](https://doi.org/10.1016/S0003-2670(00)80674-1)
- [59] A. Berthod, J.J. Kozak, J.L. Anderson, J. Ding, D.W. Armstrong, Ionic liquid-alkane association in dilute solutions, *Theoretical Chemistry Accounts* 117(1) (2007) 127-135 <https://doi.org/10.1007/s00214-006-0155-8>
- [60] R. Hayes, G.G. Warr, R. Atkin, Structure and Nanostructure in Ionic Liquids, *Chemical Reviews* 115(13) (2015) 6357-6426 <https://doi.org/10.1021/cr500411q>
- [61] T. Payagala, Y. Zhang, E. Wanigasekara, K. Huang, Z.S. Breitbach, P.S. Sharma, L.M. Sidisky, D.W. Armstrong, Trigonal Tricationic Ionic Liquids: A Generation of Gas Chromatographic Stationary Phases, *Analytical Chemistry* 81(1) (2009) 160-173 <https://doi.org/10.1021/ac8016949>
- [62] E. Wanigasekara, X. Zhang, Y. Nanayakkara, T. Payagala, H. Moon, D.W. Armstrong, Linear Tricationic Room-Temperature Ionic Liquids: Synthesis, Physicochemical Properties, and Electrowetting Properties, *ACS Applied Materials & Interfaces* 1(10) (2009) 2126-2133 <https://doi.org/10.1021/am900519j>
- [63] P.S. Sharma, T. Payagala, E. Wanigasekara, A.B. Wijeratne, J. Huang, D.W. Armstrong, Trigonal Tricationic Ionic Liquids: Molecular Engineering of Trications to Control Physicochemical Properties, *Chemistry of Materials* 20(13) (2008) 4182-4184 <https://doi.org/10.1021/cm800830v>
- [64] M. Talebi, R.A. Patil, D.W. Armstrong, Gas Chromatography Columns Using Ionic Liquids as Stationary Phase, *Commercial Applications of Ionic Liquids*, Springer International Publishing 2020, pp. 131-165 [10.1007/978-3-030-35245-5_6](https://doi.org/10.1007/978-3-030-35245-5_6)
- [65] P.A. Shinde, M.A. Abdelkareem, E.T. Sayed, K. Elsaid, A.-G. Olabi, Metal Organic Frameworks (MOFs) in Supercapacitors, in: A.-G. Olabi (Ed.), *Encyclopedia of Smart Materials*, Elsevier, Oxford, 2022, pp. 414-423 <https://doi.org/10.1016/B978-0-12-815732-9.00152-2>
- [66] A.A. Kotova, D. Thiebaut, J. Vial, A. Tissot, C. Serre, Metal-organic frameworks as stationary phases for chromatography and solid phase extraction: A review, *Coordination Chemistry Reviews* 455 (2022) 214364 <https://doi.org/10.1016/j.ccr.2021.214364>
- [67] L. Fan, X.-P. Yan, Evaluation of isostructural metal—organic frameworks coated capillary columns for the gas chromatographic separation of alkane isomers, *Talanta* 99 (2012) 944-950 <https://doi.org/10.1016/j.talanta.2012.07.063>
- [68] N. Chang, X.-P. Yan, Exploring reverse shape selectivity and molecular sieving effect of metal-organic framework UIO-66 coated capillary column for gas chromatographic separation, *Journal of Chromatography A* 1257 (2012) 116-124 <https://doi.org/10.1016/j.chroma.2012.07.097>

- [69] Z.Y. Gu, X.P. Yan, Metal–organic framework MIL-101 for high-resolution gas-chromatographic separation of xylene isomers and ethylbenzene, *Angewandte Chemie* 122(8) (2010) 1519-1522
- [70] N. Vargesson, Thalidomide-induced teratogenesis: History and mechanisms, *Birth Defects Research Part C: Embryo Today: Reviews* 105(2) (2015) 140-156
- [71] J. McConathy, M.J. Owens, Stereochemistry in Drug Action, *Prim Care Companion J Clin Psychiatry* 5(2) (2003) 70-73 [10.4088/pcc.v05n0202](https://doi.org/10.4088/pcc.v05n0202)
- [72] F. Policy, Statements for the Development of New Stereoisomeric Drugs Rockville, MD: US Food & Drug Administration (1992)
- [73] M.E. Andersson, D. Aslan, A. Clarke, J. Roeraade, G. Hagman, Evaluation of generic chiral liquid chromatography screens for pharmaceutical analysis, *Journal of Chromatography A* 1005(1) (2003) 83-101 [https://doi.org/10.1016/S0021-9673\(03\)00888-4](https://doi.org/10.1016/S0021-9673(03)00888-4)
- [74] C.J. Welch, Chiral chromatography in support of pharmaceutical process research, *Preparative enantioselective chromatography* (2005) 1
- [75] S. Ahuja, Chiral separation methods for pharmaceutical and biotechnological products, John Wiley & Sons 2011
- [76] T. Toyooka, Resolution of chiral drugs by liquid chromatography based upon diastereomer formation with chiral derivatization reagents, *Journal of Biochemical and Biophysical Methods* 54(1) (2002) 25-56 [https://doi.org/10.1016/S0165-022X\(02\)00127-6](https://doi.org/10.1016/S0165-022X(02)00127-6)
- [77] A. Karlsson, C. Pettersson, S. Björkman, Determination of (R)- and (S)-propranolol in plasma by high-performance liquid chromatography using N-benzoxycarbonylglycyl-L-proline as chiral selector in the mobile phase, *Journal of Chromatography B: Biomedical Sciences and Applications* 494 (1989) 157-171
- [78] J. Zhuang, S. Kumar, A. Rustum, Development and Validation of a Normal Phase Chiral HPLC Method for Analysis of Afoxolaner Using a Chiralpak® AD-3 Column, *Journal of Chromatographic Science* 54(10) (2016) 1813-1819 [10.1093/chromsci/bmw162](https://doi.org/10.1093/chromsci/bmw162)
- [79] D.W. Armstrong, Y. Tang, S. Chen, Y. Zhou, C. Bagwill, J.-R. Chen, Macrocyclic antibiotics as a new class of chiral selectors for liquid chromatography, *Analytical Chemistry* 66(9) (1994) 1473-1484 <https://doi.org/10.1021/ac00081a019>
- [80] S. Aslani, M.F. Wahab, M.E. Kenari, A. Berthod, D.W. Armstrong, An examination of the effects of water on normal phase enantioseparations, *Analytica Chimica Acta* 1200 (2022) 339608
- [81] L. Hintermann, Peak separation by adventitious or added water in normal-phase chiral HPLC, *The Journal of Organic Chemistry* 72(25) (2007) 9790-9793 <https://doi.org/10.1021/jo7019256>
- [82] J. Lu, A.M. Rustum, Effect of trace amounts of water in the mobile phase of normal-phase enantioselective high-performance liquid chromatography on selectivity and resolution of optical isomers, *Journal of Chromatographic Science* 47(4) (2009) 320-323 <https://doi.org/10.1093/chromsci/47.4.320>

- [83] D. Roy, M.F. Wahab, T.A. Berger, D.W. Armstrong, Ramifications and insights on the role of water in chiral sub/supercritical fluid chromatography, *Analytical chemistry* 91(22) (2019) 14672-14680
- [84] S.L. Harbeson, R.D. Tung, Deuterium in drug discovery and development, *Annual Reports in Medicinal Chemistry*, Elsevier 2011, pp. 403-417
- [85] J. Yang, *Deuterium: discovery and applications in organic chemistry*, Elsevier, Amsterdam Netherlands, 2016
- [86] J. Liu, X. Liu, *Application of Deuterated Compounds, Deuteride Materials*, Springer, Singapore, 2019 pp. 231-285 https://doi.org/10.1007/978-981-13-6962-9_6
- [87] E.M. Russak, E.M. Bednarczyk, Impact of deuterium substitution on the pharmacokinetics of pharmaceuticals, *Annals of Pharmacotherapy* 53(2) (2019) 211-216
- [88] S. Cargnin, M. Serafini, T. Pirali, A primer of deuterium in drug design, *Future Medicinal Chemistry*, 2019, pp. 2039–2042 10.4155/fmc-2019-0183
- [89] C. Schmidt, First deuterated drug approved, *Nature Publishing Group*, 2017, pp. 493-494
- [90] H.-W. Chen, J.-H. Lee, B.-Y. Lin, S. Chen, S.-T. Wu, Liquid crystal display and organic light-emitting diode display: present status and future perspectives, *Light: Science & Applications* 7(3) (2018) 17168-17168
- [91] H. Tsuji, C. Mitsui, E. Nakamura, The hydrogen/deuterium isotope effect of the host material on the lifetime of organic light-emitting diodes, *Chemical Communications* 50(94) (2014) 14870-14872
- [92] K. Hiruma-Shimizu, H. Shimizu, G.S. Thompson, A.P. Kalverda, S.G. Patching, Deuterated detergents for structural and functional studies of membrane proteins: Properties, chemical synthesis and applications, *Molecular membrane biology* 32(5-8) (2015) 139-155
- [93] M. Rychlik, S. Asam, Stable isotope dilution assays in mycotoxin analysis, *Analytical and Bioanalytical Chemistry* 390(2) (2008) 617-628
- [94] C. Bicchi, C.E.I. Cordero, E. Liberto, B. Sgorbini, P. Rubiolo, *Headspace Sampling in Flavor and Fragrance Field*, 4.01 (2012) 1-25 10.1016/B978-0-12-381373-2.00125-3
- [95] S. Ohkoshi, Y. Fujita, T. Kwan, Gas Chromatographic Separation of Hydrogen Isotopes D2 and HD, *Bulletin of the Chemical Society of Japan* 31(6) (1958) 770-771
- [96] F. Bruner, G. Cartoni, A. Liberti, Gas Chromatography of Isotopic Molecules on Open Tubular Columns, *Analytical Chemistry* 38(2) (1966) 298-303
- [97] H.-G. Schmarr, M. Wacker, M. Mathes, Isotopic separation of acetaldehyde and methanol from their deuterated isotopologues on a porous layer open tubular column allows quantification by stable isotope dilution without mass spectrometric detection, *Journal of Chromatography A* 1481 (2017) 111-115
- [98] C.D. Tran, I. Mejac, J. Rebek, R.J. Hooley, Gas Chromatographic Separation of Isotopic Molecules Using a Cavitand-Impregnated Ionic Liquid Stationary Phase, *Analytical Chemistry* 81(3) (2009) 1244-1254 10.1021/ac8021423
- [99] <https://www.sigmaaldrich.com/content/dam/sigma-aldrich/migrationresource4/Derivatization%20Rgts%20brochure.pdf>.

[https://www.sigmaaldrich.com/content/dam/sigma-](https://www.sigmaaldrich.com/content/dam/sigma-aldrich/migrationresource4/Derivatization%20Rgts%20brochure.pdf)

[aldrich/migrationresource4/Derivatization%20Rgts%20brochure.pdf](https://www.sigmaaldrich.com/content/dam/sigma-aldrich/migrationresource4/Derivatization%20Rgts%20brochure.pdf). (Accessed 12/17/2020

- [100] S. Misra, M.F. Wahab, D.C. Patel, D.W. Armstrong, The utility of statistical moments in chromatography using trapezoidal and Simpson's rules of peak integration, *Journal of separation science* 42(8) (2019) 1644-1657
- [101] A. Berthod, E.Y. Zhou, K. Le, D.W. Armstrong, Determination and use of Rohrschneider-McReynolds constants for chiral stationary phases used in capillary gas chromatography, *Analytical chemistry* 67(5) (1995) 849-857
- [102] M.D. Joshi, J.L. Anderson, Recent advances of ionic liquids in separation science and mass spectrometry, *Rsc Advances* 2(13) (2012) 5470-5484
- [103] R.A. Patil, M. Talebi, L.M. Sidisky, D.W. Armstrong, Examination of selectivities of thermally stable geminal dicationic ionic liquids by structural modification, *Chromatographia* 80(10) (2017) 1563-1574
- [104] Y. Xiao, S.-C. Ng, T.T.Y. Tan, Y. Wang, Recent development of cyclodextrin chiral stationary phases and their applications in chromatography, *Journal of Chromatography A* 1269 (2012) 52-68
- [105] W.-Y. Li, H. Jin, D. Armstrong, 2, 6-Di-O-pentyl-3-O-trifluoroacetyl cyclodextrin liquid stationary phases for capillary gas chromatographic separation of enantiomers, *Journal of Chromatography A* 509(2) (1990) 303-324
- [106] D.W. Armstrong, W. Li, J. Pitha, Reversing enantioselectivity in capillary gas chromatography with polar and nonpolar cyclodextrin derivative phases, *Analytical Chemistry* 62(2) (1990) 214-217
- [107] D.W. Armstrong, C.D. Chang, W.Y. Li, Relevance of enantiomeric separations in food and beverage analyses, *Journal of Agricultural and Food Chemistry* 38(8) (1990) 1674-1677
- [108] C. Reichardt, Solvatochromic dyes as solvent polarity indicators, *Chemical reviews* 94(8) (1994) 2319-2358
- [109] A. Berthod, W. Li, D.W. Armstrong, Multiple enantioselective retention mechanisms on derivatized cyclodextrin gas chromatographic chiral stationary phases, *Analytical chemistry* 64(8) (1992) 873-879
- [110] A. Andrews, Z. Wu, A. Zlatkis, The separation of hydrogen and deuterium homologues by inclusion gas chromatography, *Chromatographia* 34(9-10) (1992) 457-460
- [111] J.F. Buchanan, C.R. Brown, Designer drugs, *Medical toxicology and adverse drug experience* 3(1) (1988) 1-17
- [112] J.L. Zimmerman, Cocaine intoxication, *Critical care clinics* 28(4) (2012) 517-526
- [113] S. Valtier, J.T. Cody, Evaluation of internal standards for the analysis of amphetamine and methamphetamine, *Journal of analytical toxicology* 19(6) (1995) 375-380
- [114] D.-L. Lin, H.-C. Liu, R.-M. Yin, D.-T. Chen, S.-J. Soong, R.H. Liu, Effectiveness of multiple internal standards: deuterated analogues of methylenedioxymethamphetamine, methylenedioxyamphetamine, methamphetamine, and amphetamine, *Journal of analytical toxicology* 28(8) (2004) 650-654
- [115] D.-L. Lin, W.-T. Chang, T.-L. Kuo, R.H. Liu, Chemical derivatization and the selection of deuterated internal standard for quantitative determination—Methamphetamine example, *Journal of analytical toxicology* 24(4) (2000) 275-280
- [116] L. Bartell, H. Higginbotham, Electron diffraction study of the structures of ethane and deuterioethane, *The Journal of Chemical Physics* 42(3) (1965) 851-856

- [117] M. Dean, V.W. Sung, Review of deutetrabenazine: a novel treatment for chorea associated with Huntington's disease, *Drug Des Devel Ther* 12 (2018) 313-319 10.2147/DDDT.S138828
- [118] F. Schneider, E. Mattern-Dogru, M. Hillgenberg, R.-G. Alken, Changed phosphodiesterase selectivity and enhanced in vitro efficacy by selective deuteration of sildenafil, *Arzneimittelforschung* 57(06) (2007) 293-298 10.1055/s-0031-1296622
- [119] G. Xu, B. Lv, J.Y. Roberge, B. Xu, J. Du, J. Dong, Y. Chen, K. Peng, L. Zhang, X. Tang, Y. Feng, M. Xu, W. Fu, W. Zhang, L. Zhu, Z. Deng, Z. Sheng, A. Welihinda, X. Sun, Design, Synthesis, and Biological Evaluation of Deuterated C-Aryl Glycoside as a Potent and Long-Acting Renal Sodium-Dependent Glucose Cotransporter 2 Inhibitor for the Treatment of Type 2 Diabetes, *Journal of Medicinal Chemistry* 57(4) (2014) 1236-1251
<https://doi.org/10.1021/jm401780b>
- [120] R.A.M. O'Ferrall, A pictorial representation of zero-point energy and tunnelling contributions to primary hydrogen isotope effects, *Journal of Physical Organic Chemistry* 23(7) (2009) 572-579 <https://doi.org/10.1002/poc.1738>
- [121] J. Atzrodt, V. Derdau, W.J. Kerr, M. Reid, Deuterium- and Tritium-Labelled Compounds: Applications in the Life Sciences, *Angewandte Chemie International Edition* 57(7) (2018) 1758-1784 <https://doi.org/10.1002/anie.201704146>
- [122] K. Houk, S.M. Gustafson, K.A. Black, Theoretical secondary kinetic isotope effects and the interpretation of transition state geometries. 1. The Cope rearrangement, *Journal of the American Chemical Society* 114(22) (1992) 8565-8572 <https://doi.org/10.1021/ja00048a032>
- [123] C. Ragonese, D. Sciarrone, P.Q. Tranchida, P. Dugo, L. Mondello, Use of ionic liquids as stationary phases in hyphenated gas chromatography techniques, *Journal of Chromatography A* 1255 (2012) 130-144 <https://doi.org/10.1016/j.chroma.2012.04.069>
- [124] M.M. Rahman, A.M. Abd El-Aty, J.-H. Choi, H.-C. Shin, S.C. Shin, J.-H. Shim, Basic Overview on Gas Chromatography Columns, *Analytical Separation Science*, pp. 823-834
<https://doi.org/10.1002/9783527678129.assep024>
- [125] W.A. VAN HOOK, Isotope separation by gas chromatography, ACS Publications 1969, 10.1021/ba-1969-0089.ch007
- [126] J. Grosh, M.S. Jhon, T. Ree, H. Eyring, Significant Structure Theory of Isotope Effect, *Proceedings of the National Academy of Sciences* 58(6) (1967) 2196-2203
doi:10.1073/pnas.58.6.2196
- [127] S. Aslani, D.W. Armstrong, High information spectroscopic detection techniques for gas chromatography, *Journal of Chromatography A* 1676 (2022) 463255
<https://doi.org/10.1016/j.chroma.2022.463255>
- [128] M.F. Wahab, S. Aslani, A.V. Mikhonin, J.L. Neill, D.W. Armstrong, Enhancing Sensitivity for High-Selectivity Gas Chromatography-Molecular Rotational Resonance Spectroscopy, *Analytical Chemistry* 93(46) (2021) 15525-15533 10.1021/acs.analchem.1c03710

- [129] J. Bermejo, C.G. Blanco, M.D. Guillén, Gas chromatography of deuterated and protiated chloro derivatives of 1,4-dimethylbenzene, *Journal of Chromatography A* 351 (1986) 425-432 [https://doi.org/10.1016/S0021-9673\(01\)83520-2](https://doi.org/10.1016/S0021-9673(01)83520-2)
- [130] M.H. Wahl, H.C. Urey, The vapor pressures of the isotopic forms of water, *The Journal of Chemical Physics* 3(7) (1935) 411-414
- [131] H. Zhao, P. Unhannant, W. Hanshaw, J.S. Chickos, Enthalpies of Vaporization and Vapor Pressures of Some Deuterated Hydrocarbons. Liquid–Vapor Pressure Isotope Effects, *Journal of Chemical & Engineering Data* 53(7) (2008) 1545-1556 10.1021/jc800091s
- [132] J.L. Anderson, J. Ding, T. Welton, D.W. Armstrong, Characterizing Ionic Liquids On the Basis of Multiple Solvation Interactions, *Journal of the American Chemical Society* 124(47) (2002) 14247-14254 <https://doi.org/10.1021/ja028156h>
- [133] S. Aslani, D.W. Armstrong, Chapter SIX - Ionic liquids as gas chromatography stationary phases, in: S. Carda-Broch, M. Ruiz-Angel (Eds.), *Ionic Liquids in Analytical Chemistry*, Elsevier2022, pp. 171-202 <https://doi.org/10.1016/B978-0-12-823334-4.00011-4>
- [134] IUPAC. Compendium of Chemical Terminology, 2nd ed. (the "Gold Book"). Compiled by A. D. McNaught and A. Wilkinson. Blackwell Scientific Publications, Oxford (1997). Online version (2019-) created by S. J. Chalk. ISBN 0-9678550-9-8., <https://doi.org/10.1351/goldbook>
- [135] E.S. Lewis, Isotope effects and hyperconjugation, *Tetrahedron* 5(2) (1959) 143-148 [https://doi.org/10.1016/0040-4020\(59\)80100-9](https://doi.org/10.1016/0040-4020(59)80100-9)
- [136] E.A. Halevi, B. Ravid, Secondary isotope effects on pi-complex formation, *Pure and Applied Chemistry* 8(3-4) (1964) 339-346 doi:10.1351/pac196408030339
- [137] E.A. Halevi, The secondary hydrogen isotope effect, *The International Journal of Applied Radiation and Isotopes* 7(3) (1960) 192-197 [https://doi.org/10.1016/0020-708X\(60\)90039-9](https://doi.org/10.1016/0020-708X(60)90039-9)
- [138] T. Gutel, C.C. Santini, A.A.H. Pádua, B. Fenet, Y. Chauvin, J.N. Canongia Lopes, F. Bayard, M.F. Costa Gomes, A.S. Pensado, Interaction between the π -System of Toluene and the Imidazolium Ring of Ionic Liquids: A Combined NMR and Molecular Simulation Study, *The Journal of Physical Chemistry B* 113(1) (2009) 170-177 10.1021/jp805573t
- [139] E.A. Halevi, M. Nussim, 162. Secondary hydrogen isotope effects. Part II. Association constants between methylbenzenes and chloranil, *Journal of the Chemical Society (Resumed)* (0) (1963) 876-880 10.1039/JR9630000876
- [140] E.A. Halevi, M. Nussim, A. Ron, 161. Secondary hydrogen isotope effects. Part I. Strengths of α -deuterated carboxylic acids and amines, *Journal of the Chemical Society (Resumed)* (0) (1963) 866-875 10.1039/JR9630000866
- [141] A. Streitwieser, D. Van Sickle, Acidity of hydrocarbons. IV. Secondary deuterium isotope effects in exchange reactions of toluene and ethylbenzene with lithium cyclohexylamide, *Journal of the American Chemical Society* 84(2) (1962) 254-258
- [142] S. Toyota, M. Oki, Dynamic NMR as a Nondestructive Method for the Determination of Rates of Dissociation. XX. Secondary Isotope Effect on Kinetic Basicity of Amine Ligands in Boronate–Amine Complexes and Ammonium Salts, *Bulletin of the Chemical Society of Japan* 65(8) (1992) 2215-2220

- [143] C.L. Perrin, Y. Dong, Secondary Deuterium Isotope Effects on the Acidity of Carboxylic Acids and Phenols, *Journal of the American Chemical Society* 129(14) (2007) 4490-4497
10.1021/ja069103t
- [144] C.L. Perrin, A. Flach, No Contribution of an Inductive Effect to Secondary Deuterium Isotope Effects on Acidity, *Angewandte Chemie International Edition* 50(33) (2011) 7674-7676
<https://doi.org/10.1002/anie.201102125>
- [145] C.L. Perrin, B.K. Ohta, J. Kuperman, β -Deuterium Isotope Effects on Amine Basicity, "Inductive" and Stereochemical, *Journal of the American Chemical Society* 125(49) (2003) 15008-15009 10.1021/ja038343v
- [146] C.L. Perrin, B.K. Ohta, J. Kuperman, J. Liberman, M. Erdélyi, Stereochemistry of β -Deuterium Isotope Effects on Amine Basicity, *Journal of the American Chemical Society* 127(26) (2005) 9641-9647 10.1021/ja0511927
- [147] C.G. Swain, T.E. Knee, A.J. Kresge, Relative reactivities of toluene, toluene- α,α,α -d₃ and toluene- α -t in electrophilic nitration, mercuriation and bromination, *Journal of the American Chemical Society* 79(2) (1957) 505-505 10.1021/ja01559a078
- [148] J.R. Wesener, H. Günther, Deuterium-induced perturbation of hyperconjugation ? - a carbon-13 nmr study, *Tetrahedron Letters* 23(28) (1982) 2845-2848
[https://doi.org/10.1016/S0040-4039\(00\)88429-4](https://doi.org/10.1016/S0040-4039(00)88429-4)
- [149] M.U. Hasan, ¹³C NMR spectra of some amides and imides. Effect of inductive and mesomeric interactions, cyclization and hydrogen bonding on ¹³C NMR chemical shifts, *Organic Magnetic Resonance* 14(6) (1980) 447-450 <https://doi.org/10.1002/mrc.1270140605>
- [150] <https://spectrabase.com/>,
- [151] R.R. Krug, Detection of the compensation effect (θ rule), *Industrial & Engineering Chemistry Fundamentals* 19(1) (1980) 50-59 <https://doi.org/10.1021/i160073a009>
- [152] R.S. Gohlke, Time-of-flight mass spectrometry and gas-liquid partition chromatography, *Analytical Chemistry* 31(4) (1959) 535-541
- [153] R.A. Hites, Development of gas chromatographic mass spectrometry, *Analytical chemistry* 88(14) (2016) 6955-6961
- [154] D.W. Armstrong, T.J. Ward, R.D. Armstrong, T.E. Beesley, Separation of drug stereoisomers by the formation of beta-cyclodextrin inclusion complexes, *Science* 232(4754) (1986) 1132-1135
- [155] S. Wong, C. Meng, J. Fenn, Multiple charging in electrospray ionization of poly (ethylene glycols), *J. Phys. Chem.* 92(2) (1988) 546-550
- [156] Gas Chromatography-Mass Spectrometry A National Historic Chemical Landmark 2019. <https://www.acs.org/content/acs/en/education/whatischemistry/landmarks/gas-chromatography-mass-spectrometry.html> (accessed 22-Aug-21). Feb 16, 2021)
- [157] G. Gachot, S. Grugeon, I. Jimenez-Gordon, G.G. Eshetu, S. Boyanov, A. Lecocq, G. Marlair, S. Pilard, S. Laruelle, Gas chromatography/Fourier transform infrared/mass spectrometry coupling: a tool for Li-ion battery safety field investigation, *Anal. Methods* 6(15) (2014) 6120-6124 10.1039/C4AY00054D

- [158] D.T. Kuehl, P.R. Griffiths, Microcomputer-controlled interface between a high performance liquid chromatograph and a diffuse reflectance infrared Fourier transform spectrometer, *Analytical Chemistry* 52(9) (1980) 1394-1399
- [159] M.J. Low, S.K. Freeman, Measurements of infrared spectra of gas-liquid chromatography fractions using multiple-scan interference spectrometry, *Analytical Chemistry* 39(2) (1967) 194-198
- [160] M.D. Grynbaum, D. Kreidler, J. Rehbein, A. Porea, P. Schuler, W. Schaal, H. Czesla, A. Webb, V. Schurig, K. Albert, Hyphenation of gas chromatography to microcoil ¹H nuclear magnetic resonance spectroscopy, *Analytical chemistry* 79(7) (2007) 2708-2713
- [161] M. Kühnle, D. Kreidler, K. Holtin, H. Czesla, P. Schuler, W. Schaal, V. Schurig, K. Albert, Online Coupling of Gas Chromatography to Nuclear Magnetic Resonance Spectroscopy: Method for the Analysis of Volatile Stereoisomers, *Analytical Chemistry* 80(14) (2008) 5481-5486
10.1021/ac8004023
- [162] T. Imasaka, T. Okamura, N. Ishibashi, High-temperature pulsed nozzle for supersonic jet spectrometry and its application to gas chromatography, *Analytical Chemistry* 58(11) (1986) 2152-2155
- [163] K.A. Schug, I. Sawicki, D.D. Carlton Jr, H. Fan, H.M. McNair, J.P. Nimmo, P. Kroll, J. Smuts, P. Walsh, D. Harrison, Vacuum ultraviolet detector for gas chromatography, *Analytical chemistry* 86(16) (2014) 8329-8335
- [164] A. Lelevic, V. Souchon, M. Moreaud, C. Lorentz, C. Geantet, Gas chromatography vacuum ultraviolet spectroscopy: A review, *Journal of separation science* 43(1) (2020) 150-173
- [165] H. Fan, J. Smuts, L. Bai, P. Walsh, D.W. Armstrong, K.A. Schug, Gas chromatography–vacuum ultraviolet spectroscopy for analysis of fatty acid methyl esters, *Food chemistry* 194 (2016) 265-271
- [166] G.B. Park, R.W. Field, Perspective: The first ten years of broadband chirped pulse Fourier transform microwave spectroscopy, *J. Chem. Phys.* 144(20) (2016) 200901
- [167] E.B. Wilson, Microwave spectroscopy in chemistry, *Science* 162(3849) (1968) 59-66
- [168] P.F. Bernath, *Spectra of atoms and molecules*, 3rd ed., Oxford University Press, New York, 2016, pg. 169-173
- [169] J.L. Neill, Y. Yang, M.T. Muckle, R.L. Reynolds, L. Evangelisti, R.E. Sonstrom, B.H. Pate, B.F. Gupton, Online Stereochemical Process Monitoring by Molecular Rotational Resonance Spectroscopy, *Org. Process Res. Dev.* 23(5) (2019) 1046-1051
10.1021/acs.oprd.9b00089
- [170] L.A. Joyce, D.M. Schultz, E.C. Sherer, J.L. Neill, R.E. Sonstrom, B.H. Pate, Direct regioisomer analysis of crude reaction mixtures via molecular rotational resonance (MRR) spectroscopy, *Chem. Sci.* 11(24) (2020) 6332-6338
- [171] K.N. Crabtree, M.-A. Martin-Drumel, G.G. Brown, S.A. Gaster, T.M. Hall, M.C. McCarthy, Microwave spectral taxonomy: A semi-automated combination of chirped-pulse and cavity Fourier-transform microwave spectroscopy, *J. Chem. Phys.* 144(12) (2016) 124201
10.1063/1.4944072
- [172] D.W. Armstrong, M. Talebi, N. Thakur, M.F. Wahab, A.V. Mikhonin, M.T. Muckle, J.L. Neill, A Gas Chromatography-Molecular Rotational Resonance Spectroscopy Based System of Singular Specificity, *Angewandte Chemie International Edition* 59(1) (2020) 192-196

- [173] M. Takano, Y. Sasada, T. Satoh, Microwave spectrum of ethyl alcohol: The trans rotamer, *Journal of Molecular Spectroscopy* 26(2) (1968) 157-162
- [174] K. McCulloh, G.F. Pollnow, An investigation of the microwave spectrum of pyridine, *J. Chem. Phys.* 22(4) (1954) 681-682
- [175] B. Bak, D. Christensen, J. Rastrup-Andersen, E. Tannenbaum, Microwave Spectra of Thiophene, 2-and 3-Monodeutero, 3, 3'-Dideutero, and Tetradeuterothiophene. Structure of the Thiophene Molecule, *J. Chem. Phys.* 25(5) (1956) 892-896
- [176] R. Walden, R.L. Cook, Microwave spectrum of 2-chloropyridine, *Journal of Molecular Spectroscopy* 52(2) (1974) 244-250
- [177] J. Holg, L. Nygaard, G. Sorensen, Microwave spectra and planarity of benzene, *Journal of Molecular Structure* 7 (1971) 111-121
- [178] Z. Kisiel, O. Desyatnyk, L. Pszczółkowski, S. Charnley, P. Ehrenfreund, Rotational spectra of quinoline and of isoquinoline: spectroscopic constants and electric dipole moments, *Journal of Molecular Spectroscopy* 217(1) (2003) 115-122
- [179] H.M. Pickett, The fitting and prediction of vibration-rotation spectra with spin interactions, *J. Mol. Spectrosc.* 148(2) (1991) 371-377
- [180] J.H. T. Wenzl, A. Schaechtele, P. Robouch, J. Stroka, European Commission, JRC Technical Reports: Guidance Document on the Estimation of LOD and LOQ for Measurements in the Field of Contaminants in Feed and Food, EUR 28099, Publications Office of the European Union, Luxembourg. (2016)
- [181] M.V. Johnston, Supersonic jet expansions in analytical spectroscopy, *TrAC Trends in Analytical Chemistry* 3(2) (1984) 58-61 [https://doi.org/10.1016/0165-9936\(84\)87055-7](https://doi.org/10.1016/0165-9936(84)87055-7)
- [182] J.-U. Grabow, E.S. Palmer, M.C. McCarthy, P. Thaddeus, Supersonic-jet cryogenic-resonator coaxially oriented beam-resonator arrangement Fourier transform microwave spectrometer, *Review of scientific instruments* 76(9) (2005) 093106
- [183] J.P. Porterfield, L. Satterthwaite, S. Eibenberger, D. Patterson, M.C. McCarthy, High sensitivity microwave spectroscopy in a cryogenic buffer gas cell, *Review of Scientific Instruments* 90(5) (2019) 053104
- [184] W. Gordy, R.L. Cook, *Microwave molecular spectra*, John Wiley & Sons, New York, 1984
- [185] R. Suenram, J.U. Grabow, A. Zuban, I. Leonov, A portable, pulsed-molecular-beam, Fourier-transform microwave spectrometer designed for chemical analysis, *Review of scientific instruments* 70(4) (1999) 2127-2135
- [186] M.-A. Martin-Drumel, M.C. McCarthy, D. Patterson, B.A. McGuire, K.N. Crabtree, Automated microwave double resonance spectroscopy: A tool to identify and characterize chemical compounds, *J. Chem. Phys.* 144(12) (2016) 124202
- [187] Analytical Methods Committee, Recommendations for the definition, estimation and use of the detection limit, *Analyst*, The Royal Society of Chemistry, 1987, pp. 199-204
10.1039/AN9871200199
- [188] M. Herman, R. Georges, M. Hepp, D. Hurtmans, High resolution Fourier transform spectroscopy of jet-cooled molecules, *Int. Rev. Phys. Chem.* 19(2) (2000) 277-325
10.1080/01442350050020905

- [189] J.M. Hollas, Determination of molecular conformation from large amplitude vibrations in electronic spectra of organic molecules in a supersonic jet, *Chem. Soc. Rev.* 22(6) (1993) 371-382 10.1039/CS9932200371
- [190] E. Clementi, G. Corongiu, Van der Waals interaction energies of helium, neon, and argon with naphthalene, *J. Phys. Chem. A* 105(45) (2001) 10379-10383
- [191] J.-R. Li, J. Sculley, H.-C. Zhou, Metal–Organic Frameworks for Separations, *Chemical Reviews* 112(2) (2012) 869-932 10.1021/cr200190s
- [192] S.K. Firooz, D.W. Armstrong, Metal-organic frameworks in separations: A review, *Analytica Chimica Acta* 1234 (2022) 340208 <https://doi.org/10.1016/j.aca.2022.340208>
- [193] J.L. Anderson, D.W. Armstrong, G.-T. Wei, Ionic liquids in analytical chemistry, *Analytical Chemistry* 78(9) (2006) 2892-2902
- [194] C.F. Poole, N. Lenca, Gas chromatography on wall-coated open-tubular columns with ionic liquid stationary phases, *Journal of Chromatography A* 1357 (2014) 87-109 <https://doi.org/10.1016/j.chroma.2014.03.029>
- [195] M. Talebi, R.A. Patil, D.W. Armstrong, Gas chromatography columns using ionic liquids as stationary phase, *Commercial Applications of Ionic Liquids* (2020) 131-165
- [196] Z.-L. Fang, S.-R. Zheng, J.-B. Tan, S.-L. Cai, J. Fan, X. Yan, W.-G. Zhang, Tubular metal–organic framework-based capillary gas chromatography column for separation of alkanes and aromatic positional isomers, *Journal of Chromatography A* 1285 (2013) 132-138 <https://doi.org/10.1016/j.chroma.2013.02.024>
- [197] C. Zhang, R.P. Lively, K. Zhang, J.R. Johnson, O. Karvan, W.J. Koros, Unexpected molecular sieving properties of zeolitic imidazolate framework-8, *The journal of physical chemistry letters* 3(16) (2012) 2130-2134
- [198] Z.-Y. Gu, C.-X. Yang, N. Chang, X.-P. Yan, Metal–Organic Frameworks for Analytical Chemistry: From Sample Collection to Chromatographic Separation, *Accounts of Chemical Research* 45(5) (2012) 734-745 10.1021/ar2002599
- [199] S. Ma, H.-C. Zhou, Gas storage in porous metal–organic frameworks for clean energy applications, *Chemical Communications* 46(1) (2010) 44-53 10.1039/B916295J
- [200] J.A. Mason, M. Veenstra, J.R. Long, Evaluating metal–organic frameworks for natural gas storage, *Chemical Science* 5(1) (2014) 32-51 10.1039/C3SC52633J
- [201] S. Aslani, D.W. Armstrong, Ionic liquids as gas chromatography stationary phases, *Ionic Liquids in Analytical Chemistry*, Elsevier2022, pp. 171-202
- [202] GC Column Selection Guide. <https://www.sigmaaldrich.com/US/en/technical-documents/technical-article/analytical-chemistry/gas-chromatography/gc-column-selection-guide>. Accessed 21 Sep 2022,
- [203] A.J. Carmichael, K.R. Seddon, Polarity study of some 1-alkyl-3-methylimidazolium ambient-temperature ionic liquids with the solvatochromic dye, Nile Red, *Journal of Physical Organic Chemistry* 13(10) (2000) 591-595
- [204] P. Bonhôte, A.-P. Dias, N. Papageorgiou, K. Kalyanasundaram, M. Grätzel, Hydrophobic, highly conductive ambient-temperature molten salts, *Inorganic chemistry* 35(5) (1996) 1168-1178

- [205] M.H. Abraham, Scales of solute hydrogen-bonding: their construction and application to physicochemical and biochemical processes, *Chemical Society Reviews* 22(2) (1993) 73-83
10.1039/CS9932200073
- [206] P. Mukherjee, J.A. Crank, P.S. Sharma, A.B. Wijeratne, R. Adhikary, S. Bose, D.W. Armstrong, J.W. Petrich, Dynamic solvation in phosphonium ionic liquids: Comparison of bulk and micellar systems and considerations for the construction of the solvation correlation function, *The Journal of Physical Chemistry B* 112(11) (2008) 3390-3396
- [207] R.A. Patil, M. Talebi, A. Berthod, D.W. Armstrong, Dicationic ionic liquid thermal decomposition pathways, *Analytical and Bioanalytical Chemistry* 410(19) (2018) 4645-4655
10.1007/s00216-018-0878-0
- [208] C. Maton, N. De Vos, C.V. Stevens, Ionic liquid thermal stabilities: decomposition mechanisms and analysis tools, *Chemical Society Reviews* 42(13) (2013) 5963-5977
10.1039/C3CS60071H
- [209] R.A. Patil, M. Talebi, C. Xu, S.S. Bhawal, D.W. Armstrong, Synthesis of thermally stable geminal dicationic ionic liquids and related ionic compounds: an examination of physicochemical properties by structural modification, *Chemistry of Materials* 28(12) (2016) 4315-4323
- [210] M. Talebi, R.A. Patil, D.W. Armstrong, Physicochemical properties of branched-chain dicationic ionic liquids, *Journal of Molecular Liquids* 256 (2018) 247-255
<https://doi.org/10.1016/j.molliq.2018.02.016>
- [211] W. Silva, M. Zanatta, A.S. Ferreira, M.C. Corvo, E.J. Cabrita, Revisiting ionic liquid structure-property relationship: A critical analysis, *International journal of molecular sciences* 21(20) (2020) 7745
- [212] S. Jiang, Y. Hu, Y. Wang, X. Wang, Viscosity of Typical Room-Temperature Ionic Liquids: A Critical Review, *Journal of Physical and Chemical Reference Data* 48(3) (2019) 033101 10.1063/1.5090486
- [213] K. Grob, G. Grob, Static coating: An attempt to optimize a straightforward technique involving mechanical closure of the column, *Journal of High Resolution Chromatography* 5(3) (1982) 119-123 <https://doi.org/10.1002/jhrc.1240050302>
- [214] N. Chang, Z.-Y. Gu, X.-P. Yan, Zeolitic Imidazolate Framework-8 Nanocrystal Coated Capillary for Molecular Sieving of Branched Alkanes from Linear Alkanes along with High-Resolution Chromatographic Separation of Linear Alkanes, *Journal of the American Chemical Society* 132(39) (2010) 13645-13647 10.1021/ja1058229
- [215] K. Sumida, D.L. Rogow, J.A. Mason, T.M. McDonald, E.D. Bloch, Z.R. Herm, T.-H. Bae, J.R. Long, Carbon Dioxide Capture in Metal–Organic Frameworks, *Chemical Reviews* 112(2) (2012) 724-781 10.1021/cr2003272
- [216] Y.-R. Lee, M.-S. Jang, H.-Y. Cho, H.-J. Kwon, S. Kim, W.-S. Ahn, ZIF-8: A comparison of synthesis methods, *Chemical Engineering Journal* 271 (2015) 276-280
<https://doi.org/10.1016/j.cej.2015.02.094>

- [217] A. Martin, R. Synge, A new form of chromatogram employing two liquid phases: 1. A theory of chromatography 2. Application to the micro-determination of the higher monoaminoacids in proteins, *Trends in Biochemical Sciences* 2(11) (1977) N245
- [218] D.W. Armstrong, F. Nome, Partitioning behavior of solutes eluted with micellar mobile phases in liquid chromatography, *Analytical Chemistry* 53(11) (1981) 1662-1666
- [219] R.A. Menges, D.W. Armstrong, Use of a three-phase model with hydroxypropyl- β -cyclodextrin for the direct determination of large octanol-water and cyclodextrin-water partition coefficients, *Analytica chimica acta* 255(1) (1991) 157-162
- [220] V. Pino, A.W. Lantz, J.L. Anderson, A. Berthod, D.W. Armstrong, Theory and Use of the Pseudophase Model in Gas-Liquid Chromatographic Enantiomeric Separations, *Analytical Chemistry* 78(1) (2006) 113-119 [10.1021/ac051289b](https://doi.org/10.1021/ac051289b)
- [221] A.W. Lantz, V. Pino, J.L. Anderson, D.W. Armstrong, Determination of solute partition behavior with room-temperature ionic liquid based micellar gas-liquid chromatography stationary phases using the pseudophase model, *Journal of Chromatography A* 1115(1) (2006) 217-224 <https://doi.org/10.1016/j.chroma.2006.02.064>
- [222] K.-H. Gahm, L.W. Chang, D.W. Armstrong, Chiral separation of monoterpenes using mixtures of sulfated β -cyclodextrins and α -cyclodextrin as chiral additives in the reversed-polarity capillary electrophoresis mode, *Journal of Chromatography A* 759(1) (1997) 149-155 [https://doi.org/10.1016/S0021-9673\(96\)00747-9](https://doi.org/10.1016/S0021-9673(96)00747-9)
- [223] M.F. Wahab, C.A. Weatherly, R.A. Patil, D.W. Armstrong, *Chiral Liquid Chromatography in Chiral analysis: advances in spectroscopy, chromatography and emerging methods* Polavarapu, P. L., Ed.; , Second Edition ed., Elsevier, Cambridge, MA, 2018, pg 507-564
- [224] L. Snyder, J. Ward, The surface structure of porous silicas, *The Journal of Physical Chemistry* 70(12) (1966) 3941-3952 <https://doi.org/10.1021/j100884a034>
- [225] Z. El Rassi, C. Gonnet, J. Rocca, Chromatographic studies of the influence of water and thermal treatment on the activity of silica gel, *Journal of Chromatography A* 125(1) (1976) 179-201 [https://doi.org/10.1016/S0021-9673\(00\)93819-6](https://doi.org/10.1016/S0021-9673(00)93819-6)
- [226] J. Soukup, P. Jandera, Adsorption of water from aqueous acetonitrile on silica-based stationary phases in aqueous normal-phase liquid chromatography, *Journal of Chromatography A* 1374 (2014) 102-111 <https://doi.org/10.1016/j.chroma.2014.11.028>
- [227] P. Jandera, Mechanism and prediction of retention of oligomers in normal-phase and reversed-phase HPLC, *Chromatographia* 26(1) (1988) 417-422 <https://doi.org/10.1007/BF02268192>
- [228] N.E. Oro, R.M. Whittal, C.A. Lucy, Sample handling and contamination encountered when coupling offline normal phase high performance liquid chromatography fraction collection of petroleum samples to Fourier transform ion cyclotron resonance mass spectrometry, *Analytica Chimica Acta* 741 (2012) 70-77 <https://doi.org/10.1016/j.aca.2012.06.047>
- [229] A. Bielejewska, K. Duszczuk, K. Kulig, B. Malawska, M. Miśkiewicz, A. Leś, J. Żukowski, Influence of the mobile phase composition on chiral recognition of some pyrrolidin-2-ones in the liquid chromatographic system with polysaccharide stationary phases, *Journal of Chromatography A* 1173(1-2) (2007) 52-57 <https://doi.org/10.1016/j.chroma.2007.09.070>

- [230] J. Zukowski, M. Brightwell, V. De Biasi, Chiral HPLC method for chiral purity determination of paroxetine drug substance, *Chirality: The Pharmacological, Biological, and Chemical Consequences of Molecular Asymmetry* 15(7) (2003) 600-604
<https://doi.org/10.1002/chir.10250>
- [231] J. Putnam, G. Guiochon, A test to determine the nature and presence of the memory effect columns packed with the amylose tris(3,5-dimethylphenylcarbamate) stationary phase, *Journal of Chromatography A* 1218(37) (2011) 6302-6307 <https://doi.org/10.1016/j.chroma.2011.06.060>
- [232] J. Putnam, G. Guiochon, The influence of water on the memory effect of the amylose tris(3,5-dimethylphenyl carbamate) stationary phase, *Journal of Chromatography A* 1217(52) (2010) 8146-8153 <https://doi.org/10.1016/j.chroma.2010.10.054>
- [233] D.C. Patel, Z.S. Breitbach, M.F. Wahab, C.L. Barhate, D.W. Armstrong, Gone in seconds: praxis, performance, and peculiarities of ultrafast chiral liquid chromatography with superficially porous particles, *Analytical Chemistry* 87(18) (2015) 9137-9148
<https://doi.org/10.1021/acs.analchem.5b00715>
- [234] D. Roy, M.F. Wahab, M. Talebi, D.W. Armstrong, Replacing methanol with azeotropic ethanol as the co-solvent for improved chiral separations with supercritical fluid chromatography (SFC), *Green Chemistry* 22(4) (2020) 1249-1257 <https://doi.org/10.1039/C9GC04207E>
- [235] C.-y. Huang, P.-y. Chung, I.-M. Tseng, L.-s. Lee, Measurements and correlations of liquid-liquid-equilibria of the mixtures consisting of ethanol, water, pentane, hexane, and cyclohexane, *The Open Thermodynamics Journal* 4(1) (2010) 10.2174/1874396X01004010102
- [236] G. Onori, Adiabatic compressibility and structure of aqueous solutions of ethyl alcohol, *The Journal of Chemical Physics* 89(7) (1988) 4325-4332 <https://doi.org/10.1063/1.454816>
- [237] M. da Silva Gonçalves, D.W. Armstrong, L.M. Cabral, E.C. Pinto, V.P. de Sousa, Development and validation of a fast HPLC method for methyl dopa enantiomers using superficially porous particle based macrocyclic glycopeptide stationary phase, *Microchemical Journal* 164 (2021) 105957 <https://doi.org/10.1016/j.microc.2021.105957>
- [238] H. Guo, M.F. Wahab, A. Berthod, D.W. Armstrong, Mass spectrometry detection of basic drugs in fast chiral analyses with vancomycin stationary phases, *Journal of Pharmaceutical Analysis* 8(5) (2018) 324-332 <https://doi.org/10.1016/j.jpha.2018.08.001>
- [239] E.M. Kosower, The effect of solvent on spectra. I. A new empirical measure of solvent polarity: Z-values, *Journal of the American Chemical Society* 80(13) (1958) 3253-3260
<https://doi.org/10.1021/ja01546a020>
- [240] N.P. Dinh, T. Jonsson, K. Irgum, Water uptake on polar stationary phases under conditions for hydrophilic interaction chromatography and its relation to solute retention, *Journal of Chromatography A* 1320 (2013) 33-47 <https://doi.org/10.1016/j.chroma.2013.09.061>
- [241] J.S. Winn, *Physical Chemistry*, HarperCollins College Publishers, New York, USA, 1995
- [242] M.P. Gasper, A. Berthod, U.B. Nair, D.W. Armstrong, Comparison and modeling study of vancomycin, ristocetin A, and teicoplanin for CE enantioseparations, *Analytical Chemistry* 68(15) (1996) 2501-2514 <https://doi.org/10.1021/ac960154q>

- [243] F. Gritti, G. Guiochon, The van Deemter equation: Assumptions, limits, and adjustment to modern high performance liquid chromatography, *Journal of Chromatography A* 1302 (2013) 1-13 <https://doi.org/10.1016/j.chroma.2013.06.032>
- [244] C. Horvath, H.-J. Lin, Band spreading in liquid chromatography: General plate height equation and a method for the evaluation of the individual plate height contributions, *Journal of Chromatography A* 149 (1978) 43-70 [https://doi.org/10.1016/S0021-9673\(00\)80978-4](https://doi.org/10.1016/S0021-9673(00)80978-4)
- [245] H. Poppe, J. Kraak, J. Huber, J. Van den Berg, Temperature gradients in HPLC columns due to viscous heat dissipation, *Chromatographia* 14(9) (1981) 515-523 <https://doi.org/10.1007/BF02265631>
- [246] F. Gritti, M. Martin, G. Guiochon, Influence of viscous friction heating on the efficiency of columns operated under very high pressures, *Analytical Chemistry* 81(9) (2009) 3365-3384 <https://doi.org/10.1021/ac802632x>
- [247] K. Kaczmarek, F. Gritti, G. Guiochon, Prediction of the influence of the heat generated by viscous friction on the efficiency of chromatography columns, *Journal of Chromatography A* 1177(1) (2008) 92-104 <https://doi.org/10.1016/j.chroma.2007.11.009>
- [248] A.A. Makarov, B.F. Mann, E.L. Regalado, G.F. Pirrone, C. Sun, S. Sun, T. Nowak, H. Wang, I. Mangion, Visualizing and studying frictional heating effects in reversed-phase liquid chromatography using infrared thermal imaging, *Analytica Chimica Acta* 1018 (2018) 1-6 <https://doi.org/10.1016/j.aca.2018.02.061>
- [249] L.D. Asnin, A.A. Boteva, O.P. Krasnykh, M.V. Stepanova, I. Ali, Unusual van Deemter plots of optical isomers on a chiral brush-type liquid chromatography column, *Journal of Chromatography A* 1592 (2019) 112-121 <https://doi.org/10.1016/j.chroma.2019.01.048>
- [250] S. Felletti, C. De Luca, G. Lievore, T. Chenet, B. Chankvetadze, T. Farkas, A. Cavazzini, M. Catani, Shedding light on mechanisms leading to convex-upward van Deemter curves on a cellulose tris(4-chloro-3-methylphenylcarbamate)-based chiral stationary phase, *Journal of Chromatography A* 1630 (2020) 461532 <https://doi.org/10.1016/j.chroma.2020.461532>
- [251] S. Golshan-Shirazi, G. Guiochon, Experimental characterization of the elution profiles of high concentration chromatographic bands using the analytical solution of the ideal model, *Analytical Chemistry* 61(5) (1989) 462-467 <https://doi.org/10.1021/ac00180a017>
- [252] I. Langmuir, The adsorption of gases on plane surfaces of glass, mica and platinum, *Journal of the American Chemical Society* 40(9) (1918) 1361-1403 <https://doi.org/10.1021/ja02242a004>
- [253] T. Fornstedt, G. Guiochon, Theoretical study of high-concentration elution profiles and large system peaks in nonlinear chromatography, *Analytical Chemistry* 66(13) (1994) 2116-2128 <https://doi.org/10.1021/ac00085a030>

Biographical information

Saba Aslani was born in Esfahan, Iran. She obtained her Bachelor of Science degree in chemistry from Shahid Beheshti University, Tehran, Iran (August 2017). She started her graduate program at the university of Texas at Arlington in August 2019. She joined Dr. Daniel Armstrong's group and conducted research focusing on gas chromatography, spectroscopy, and chiral liquid chromatography. She interned at AZYP, LLC in 2022 and worked on improving method developments for preparation of HILIC and chiral liquid chromatography stationary phases as well as packing HPLC columns.